EXPLOITING THE SPATIAL INFORMATION
IN HIGH RESOLUTION SATELLITE DATA
AND UTILISING MULTI-SOURCE DATA FOR
TROPICAL MOUNTAIN FOREST AND LAND COVER MAPPING

Dissertation

zur Erlangung des Doktorgrades

der Mathematisch-Naturwissenschaftlichen Fakultäten

der Georg-August-Universität zu Göttingen

vorgelegt von

Anke Gleitsmann, geb. Brötje

aus Braunschweig

Göttingen 2005

Abstract: **Exploiting the Spatial Information in High Resolution Satellite Data and Utilising Multi-Source Data for Tropical Mountain Forest and Land Cover Mapping**

The heterogeneous, fragmented land cover pattern of the upper catchment area of the Río Yaque del Norte, in the Cordillera Central of the Dominican Republic, is typical for many tropical mountain areas. Parts of the catchment area have been colonised in the course of the 20th century, in spite of their marginality for agricultural land use purposes. At the same time, there are still several types of primary mountain forests remaining in this mountain range, among them fragmented cloud forest areas with threatened endemic species. Deforestation and unsustainable land use methods on the steep slopes of the study area have led to erosion and land degradation. There are efforts to foster more sustainable land use practices, to reforest some areas and to protect the threatened ecosystems. Detailed spatial land cover information would be important for improving the basis of the necessary land management decisions.

The study area is challenging for forest and land cover mapping. The usefulness of medium resolution (e.g. Landsat) satellite data for mapping its vegetation types is limited, because the small-scale mix of land cover types leads to a large proportion of mixed pixels in such data. The introduction of a new generation of commercial high spatial resolution satellites like IKONOS has led to new possibilities for more detailed classifications of special interest areas, but the high resolution data also pose new challenges for automated land cover mapping. Single pixels in these data fail to integrate the elements of the target classes (e.g. forest types) and the increased amount of spatial information contained in the data cannot be fully extracted by using the per-pixel multispectral classification approaches which are common for medium resolution satellite data. To make use of the high resolution spatial information contained in the IKONOS panchromatic channel in automated classifications, customised texture parameters were created and used as additional channels in the classification. At the same time, several methods for the spatial integration of the multispectral data were tested and compared, in order to make the spectral signals of the image primitives more representative of the target classes. Both the spatial integration of the multispectral data (especially low pass filtering) and the introduction of texture parameters led to significantly increased classification accuracies. The integration of multi-source data as input for the classifiers (combining additional Landsat multispectral channels or DEM-derived topographic models with the IKONOS data sets) did not lead to significantly improved results, compared to the results which were achieved with IKONOS data alone. However, the elevation data did show some potential to increase the separability of some classes. They could probably have been more useful if a higher resolution DEM had been available. The Maximum-Likelihood-Classifier produced better results than the tested non-parametric classifiers. With the optimised methods, a detailed land cover classification (13 classes, six of which represented forest types) was possible using information derived from the IKONOS data. There were some inherently problematic classes like open pine forest and agroforestry, but for most forest classes, good classification accuracies could be achieved, particularly for the ecologically important cloud forest class.

Acknowledgements

Contents

List of Figures

List of Tables

List of Plates

XIII

List of Abbreviations

ANN: Artificial Neural Network

a.s.l.: above sea level

ASM: Angular Second Moment (GLCM texture feature)

AVHRR: Advanced Very High Resolution Radiometer

BD: Bhattacharyya Distance

C: Celsius

CONT: Contrast (GLCM texture feature)

CORR: Correlation (GLCM texture feature)

CRIES: Comprehensive Resource Inventory and Evaluation System

D: Divergence

DED: Deutscher Entwicklungsdienst (German Development Service)

DEM: Digital Elevation Model

DTM: Digital Terrain Model

DGF: Dirección General de Foresta

DIRENA: Departamento de Inventario de los Recursos Naturales (Department for the Inventory of Natural Resources)

DISS: Dissimilarity (GLCM texture feature)

DN: Digital Number

DNP: Dirección Nationál de Parques

e.g.: for example

ENT: Entropy (GLCM texture feature)

ETM+: Enhanced Thematic Mapper Plus

FAO: Food and Agriculture Organisation of the United Nations

FRA 2000: Global Forest Resources Assessment 2000

GCP: Ground Control Point

GIS: Geographical Information System

GLCM: Grey-Level Co-occurrence Matrix

GLCV: Grey-Level Co-occurrence Vector

GMT: Greenwich Mean Time

GPS: Global Positioning System

GSD: Ground Sample Distance

GTZ: Deutsche Gesellschaft für Technische Zusammenarbeit GmbH

ha: hectare

HOM: Homogeneity (GLCM texture feature)

ICEC: International Classification of Ecological Communities

ICM: Instituto Cartográphico Militar

i.e.: that is

IFOV: Instantaneous Field Of View

IHS: Intensity, Hue, Saturation

INDHRI: Instituto Nacional de Recursos Hidráulicos (National Institute for Water Resources)

IRS: Indian Remote Sensing

ISA: Instituto Superior de Agricultura (in Santiago de los Caballeros, Dominican Republic)

KfW: Kreditanstalt für Wiederaufbau

KIA: Kappa index of agreement

km: kilometre

k-NN: k-Nearest-Neighbour

LAI: Leaf Area Index

m: metre

MLC: Maximum Likelihood Classification

MODIS: Moderate Resolution Imaging Spectroradiometer

ms: multispectral

MSS: Multispectral Scanner

NOAA: National Oceanic and Atmospheric Administration

NGO: Non-Governmental Organisation

NIR: Near Infra-Red

NNC: Neural Network Classification

No.: Number

NP: National Park

OA: Overall Accuracy

OEA (OAS): Organización de los Estados Americanos (Organization of American States)

PROCARYN: Proyecto Maneja y Conservación de la Cuenca Alta Río Yaque del Norte (Project for the Management and Conservation of the Upper Catchment of the Río Yaque del Norte)

RGB: Red, Green, Blue (display colour channels)

RMSE: Root Mean Square Error

SAR: Synthetic Aperture Radar

SD: Standard Deviation (GLCM texture feature)

SEA: Secretaría de Estado de Agricultura (Ministry of Agriculture)

s: second

SEMARENA: Secretaría de Estado de Medio Ambiente y Recursos Naturales (Ministry for Environment)

SPOT HRV XS: SPOT High Resolution Visible Multispectral

SR: Scientific Reserve

StNN: Standard Nearest Neighbour Classification

TD: Transformed Divergence

Tex: Texture

TM: Thematic Mapper

TMCF: Tropical Mountain Cloud Forest

UCRYN: Upper Catchment Area of the Río Yaque del Norte

UNESCO: United Nations Educational, Scientific and Cultural Organization

USAID: United States Agency for International Development

USGS: United States Geological Survey

UTM: Universal Transverse Mercator

VAR: Variance

Abbreviations of Land Cover Class Names

AF: Agroforestry

BG: Bare ground

brn: Burnt areas

BRF: Broadleaved riparian forest

bu: Built-up areas

Cal: *Calimetal* / fern

CF: Cloud forest

Cof: Coffee without shade

Cr: Other crops

GL: Grassland

Mat: Matorral

MF: Mixed forest

PFd: Dense pine forest

PFo: Open pine forest

PmF: Palm dominated forest

SF: Secondary forest

SFd: Dense secondary forest

SFo: Open secondary forest

W: Water

Copyright Notice

1   Introduction

Tropical ecosystems are changing rapidly as a result of human activity. Land cover changes in the tropics include deforestation and landscape fragmentation, often in connection with the colonisation of marginal areas. Achard et al. (2002) state that between 1990 and 1997, 5.8 ± 1.4 million ha of humid tropical forest were lost per year and 2.3 ± 0.7 million ha were visibly degraded. The world-wide loss and degradation of tropical forests has far-ranging ecological and climatic consequences. Tropical mountain forests in particular play a central role in many aspects of sustainable development. They can be linked with soil conservation and the prevention of land degradation, water supply and climate change, biodiversity, and tourism development, apart from providing timber and other forest products (Price & Butt 2000).

The Caribbean islands are a region where the population density is much higher than in many continental tropical countries and the proportion of forests which have survived on these islands is accordingly low (Lugo 1995). The Dominican Republic has seen the destruction of most of its forests in the course of the 20th century, but due to its mountainous relief and historically relatively low population density, some considerable parts of its rich and varied natural vegetation are still remaining – in contrast to its disastrously degraded neighbouring country Haiti.

The problems of deforestation, especially in the mountain areas, are recognized in the Dominican Republic and there are efforts to protect selected areas of natural forests and to reforest mountain areas which are degraded or in danger of further degradation. However, as in many developing countries, there is a lack of information on forest resources. More information would be needed for forest management planning and for monitoring the sustainable development of forests in agreement with Agenda 21 of the Rio Earth Summit 1992 (Lund 1996). According to Saket (2002), most developing countries were unable to provide detailed information to the Global Forest Resources Assessment 2000 (FRA 2000), and only 10 % could provide information on changes in area. None of the countries in Latin America and the Caribbean reported information based on country-wide field sampling, but most could provide area estimates based on remote sensing. The "*Inventario de Cobertura Forestal*" (inventory of forest coverage) published by the Dominican ministry of the environment in 2001 (SEMARENA 2001a) is based mostly on the classification of several Landsat scenes from the 1990s.

Remote sensing is a necessary data source for mapping, spatial analysis and geo-referenced information (Kleinn 2002). Even if remote sensing technologies cannot provide the same information that would be the result of a complete forest inventory based on extensive field sampling as conducted in many developed countries, they can provide information about some core attributes like forest area and area by forest type, among other things. Only remote sensing can provide full-cover, spatially explicit information on the location of forest types, changes of forest

cover and forest fragmentation. The resulting land cover maps can serve as one basis for forest management and protection. They could also help to choose an optimized sample, reducing the necessary intensity of field sampling if further forest inventory efforts were to follow. Land cover maps are also needed as an input for the analysis and modelling of interrelationships of landscape processes.

Classifications based on Landsat or similar medium-resolution satellite data can give a first overview over the spatial distribution of the major vegetation units, but they are often inadequate when dealing with the heterogeneous land cover patterns that are characteristic for many tropical mountain areas due to topographic, climatic, geologic and edaphic variations and land use patterns including subsistence agriculture and shifting cultivation.

The recent introduction of commercially available high spatial resolution satellite imagery has brought about new possibilities and new challenges for the field of satellite remote sensing of the environment. Before the launch of IKONOS-2 in 1999 imagery of a comparable spatial resolution was only available from airborne sensors. Changing the spatial resolution of the measurement changes the information content and statistical properties of image data (Marceau et al. 1994a), and digital image analysis methods used with medium resolution satellite images are not always applicable. Increasing the spatial resolution of an image reduces the integrating effect of larger pixels and thus the homogeneity within land cover classes. High (and very high) spatial resolution imagery such as aerial photographs is traditionally interpreted by manually delineating vegetation boundaries (Coulter et al. 2000). In these cases, the human interpreter does not only use the information of grey levels or colours, but also attributes like texture, patterns, location, form, and size. Correspondingly, automated digital analysis of high spatial resolution images should include methods which use not only the per-pixel spectral information but also the spatial information present in these images.

One way to utilise the spatial information from high resolution imagery is to extract texture parameters which can then be included in the classification process. Texture in digital image analysis is the variability or the spatial relationship of grey levels in a pixel neighbourhood or window. Image texture parameters can be derived from a variety of first- and second-order statistics. Texture is related to the size and distribution of objects in the scene and to the spatial resolution of the imagery. In high resolution cases, where the pixels are smaller than the size of the objects in the image (which is the case for IKONOS images of forest), texture information can be expected to be especially valuable for class discrimination.

The spatial resolution of high resolution imagery may be too high for optimal per-pixel classification results of heterogeneous land cover classes like forest, because the different elements of a class (e.g. illuminated crowns, shaded crown parts and understorey vegetation) are not

integrated in the single pixels. It may thus be necessary to perform some kind of spatial integration before classification, e.g. by reducing the spatial resolution of the imagery or using a low pass filter. Another way to incorporate the spatial context is image segmentation, followed by object oriented image analysis. Image segmentation divides an image into separated, spatially continuous regions which are homogeneous with respect to some characteristic or characteristics. The resulting image objects are more meaningful than single pixels and allow for object-oriented or per-parcel image classification.

Given the influence of elevation and other terrain variables on vegetation, valuable ancillary information for forest classifications in mountainous areas can be derived from digital elevation models (DEM). Appropriate data integration methods are needed to be able to use multi-source data (satellite and DEM-derived), data of different spatial resolutions, as well as spectral and textural data in the classification process. The established maximum likelihood classification method has some limitations as to the types of data it is appropriate for and it is not adapted for using data of different scales. Therefore, other (non-parametric) classification methods or ways to incorporate ancillary data in pre- or post-classification processes have to be considered.

Geographical entities such as forests are not only scale-dependent in their definition, but they are also inherently fuzzy, with indeterminate boundaries (Cheng 2002). Detailed classifications of natural and semi-natural vegetation in particular entail fuzziness in the class definitions and the spatial delineation of class areas. In addition, the occurrence of mixed pixels on class borders can never be completely avoided even in high resolution imagery. Therefore, the concept of fuzziness is important when addressing the unavoidable uncertainties in class definition, classification and the resulting maps.

1.1 Aims and Objectives

This study aims at finding, testing and comparing methods for forest and land cover mapping in tropical mountainous terrain using automated classifications of recent optical satellite data, comparing the usefulness of medium and high resolution satellite data and combining multi-source data in order to improve classification results.

The main objectives are

- to produce a regional land cover base map using Landsat ETM+ data;
- to evaluate high resolution satellite data (IKONOS) for mountain forest and land cover mapping;
- to test the usefulness of spatial information (texture) for improving the discrimination of forest and other land cover classes;

- to test the usefulness of different kinds of spatial integration of high resolution data, including segmentation;

- to produce an integrated data set as a basis for an optimised classification;

- to test and compare suitable classification methods;

- to generate optimised land cover maps of the study area, discriminating forest formations and other physiognomic vegetation units.

1.2 Central Hypothesis

Digital image classification of high spatial resolution satellite data can contribute to improved results in (localised) tropical mountain forest mapping compared to medium resolution satellite data. The successful use of high resolution data for automated land cover classifications requires that the spatial characteristics of these data are taken into consideration and that the spatial information contained in the high resolution data is extracted and used in the classification process as well as the spectral information.

1.3 Outline

In the following chapters, I will present the theoretical framework of this study and then describe the land cover (especially the forests) and the land use in the study area, including the physical and historical basis for the current situation. The next chapter describes the data that were available to me for this study. The first methodological chapters describe the field work and the pre-processing methods used. Chapter 7 explores the possibilities and limitations of a land cover classification without high resolution data. After that, the methods used to extract additional information from high-resolution data are described and, subsequently, the results of the analysed issues (questions of spatial resolution and spatial integration, use of texture, multi-source data integration, classification methods, assessment of results) are described and discussed. The tenth chapter presents the conclusions of this study. It is followed by a summary in German.

2 Methodical Background

2.1 Use of Remote Sensing in Forest Mapping

In many countries outside the tropics, remote sensing is an established tool used in forest mapping and, in combination with ground sampling, in forest inventory (Tomppo 1996, Sutter 1990, Magnussen 1997, Tickle et al. 1998) as well as in forest damage surveys (Thomas 1990). Most of these practical applications involve the use of high spatial resolution remote sensing data, and aerial photographs are still the most common data source used, even though digital air-borne data have gained in importance in recent years (Kayitakire et al. 2002). The analysis of these high resolution images is dominated by manual, non-automated methods (Magnussen 1997, Biggs 1996, Sutter 1990), although this is time-consuming and can lead to inconsistent results (Green 2000). The automatic analysis of aerial imagery is mostly still in the experimental rather than the operational stage (Pouliot et al. 2002, Kadmon & Harari-Kremer 1999, Atzberger & Schlerf 2002).

Until 1999, only airborne sensors and cameras provided high resolution data for forestry applications, while multispectral high resolution satellite data with a repetitive coverage were not commercially available. Since then, a number of high resolution satellites have been put into orbit. Satellites like IKONOS-2 and QuickBird represent a new generation of remote sensing satellites, delivering multispectral imagery with spatial resolutions of 4 m and less. The advent of high resolution satellite data since 1999 provides new incentives to develop automated analysis methods for digital high resolution remote sensing data. Automated methods for forest classification and the mapping of biophysical stand parameters with digital airborne data have been tested for example in North America (Quackenbush et al. 2000, St-Onge & Cavayas 1995, Franklin et al. 2001a, Cosmopoulos & King 2004, Leckie et al. 2003, Kellndorfer et al. 2003) and Europe (Baulies & Pons 1995). IKONOS high resolution satellite data were used by Goetz et al. (2003) to map tree cover and by Hirata et al. (2002) and Franklin et al. (2001b) to test techniques for the extraction of information about coniferous forest stands.

Medium resolution satellite data like Landsat are used in some large area forest inventories for example in Finland (Tomppo 1996), but are not deemed to be suitable information sources for practical forest management purposes by Holmgren & Thuresson (1998) and Pitt et al. (1997). Remote sensing cannot deliver information about all the variables which field sampling produces for a forest inventory, but on the other hand, field sampling cannot produce geo-referenced information with complete coverage for a whole region. Spatially explicit information about the area and distribution of forest and land cover types can only be gained with the help of remotely sensed data (Kleinn 2002). Consequently, Landsat TM (Thematic Mapper) and similar optical satellite data are much used in regional forest type and land cover mapping (e.g. Franklin 1992,

Koch et al. 2002). There are also efforts to estimate parameters like forest age and crown closure from Landsat TM data (Jakubauskas & Price 2000, Franklin et al. 2003, Xu et al. 2003). There are many more studies using satellite data for forest mapping, but an exhaustive review of the use of medium to low resolution optical data (e.g. Latifovic et al. 2004) and synthetic aperture radar (SAR) data (e.g. Dobson et al. 1996, Kellndorfer et al. 1998) for regional to global forest and land cover mapping would go beyond the scope of this overview.

Besides high spatial resolution satellite data, other new data sources for detailed forest information are airborne lidar (light detection and ranging), which can be used to provide measurements of the vertical canopy structure (Means et al. 2000, Hudak et al. 2002, Dubaya & Drake 2000), and airborne and satellite hyperspectral data (Ustin & Trabucco 2000, Martin et al. 1998). Specialized techniques like these, aiming to provide detailed information for forest managers, are usually developed in non-tropical countries like Canada and Finland, but the aims and conditions of boreal and temperate forest mapping and management are in many respects quite different from the situation in the tropics.

Remote sensing of tropical forests

In many tropical developing countries, there is a lack of even very basic forest information which would be needed for effective forest protection and management. For the Global Forest Resources Assessment 2000 (FAO 2001), none of the Latin American and Caribbean countries could provide forest information based on country-wide field sampling, while about half of these countries had mapped their forest resources using aerial photographs or satellite imagery, providing area estimates for more or less detailed or broad forest types (Saket 2002). Terrestrial surveys of tropical forests are usually difficult and expensive due to poor accessibility and the heterogeneous forest structure (Köhl 1996).

Many tropical forest studies using remote sensing are focused on deforestation. Tropical deforestation is typically studied over large areas using medium and low resolution satellite data, most commonly of the Landsat sensors MSS, TM and ETM+ (Skole & Tucker 1993, Sanchez-Azofeifa et al. 2002, Ichii et al. 2003). Deforestation studies are usually multitemporal studies where for a single date, often just the classes 'forest' and 'non-forest' are separated (Millington et al. 2003, Peralta & Mather 2000, Alves et al. 1999). Wang et al. (2003) refine these simple forest/non-forest classifications by trying to estimate the forest canopy cover fraction within Landsat pixels, Herrera et al. (2004) differentiate between forest, non-forest and trees outside forest, and Asner et al. (2003) differentiate between several land cover types in deforested areas, but they all treat the remaining forest as a single class. This is the case in many deforestation and tropical land cover classification studies, despite the large variety of tropical forest types.

Several authors have classified different successional stages of tropical forest regeneration (Thenkabail et al. 2004a, Kimes et al. 1999, Foody et al. 1996). Efforts to differentiate between different mature forest types are rare in comparison to forest/non-forest classifications. Tuomisto et al. (1994) and Paradella et al. (1994) used mainly visual interpretation of Landsat images to distinguish several tropical vegetation types. The statistical spectral separability of ecological forest types was studied by Singh (1987) using Landsat MSS data and by Hill & Foody (1994) and Foody & Hill (1996) using Landsat TM data. They came to the conclusion that between three and four groups of forest types were spectrally separable based on these multispectral data, but not all land cover classes which were identified in the field could be separated. Hill (1999) managed to classify six Amazonian forest types using segmented Landsat data. Riaza et al. (1998), García & Alvarez (1994) and Behera et al. (2001) also classified several tropical forest types on three different continents using medium resolution multispectral satellite data. Country-wide forest type and land cover mappings were conducted for Puerto Rico by Helmer et al. (2002) and for the Dominican Republic by Tolentino & Peña (1998) using Landsat TM and ancillary data, and for Mexico by Mas et al. (2002) using visual interpretations of Landsat ETM+ data. Low spatial resolution data (AVHRR) are used by Ferreira & Huete (2004) to monitor woodland, shrubland and grassland vegetation types in the Brazilian Cerrado.

Medium and low resolution optical satellite data are also used in the estimation of tropical forest biophysical characteristics like leaf area index (LAI) or biomass (Foody et al. 2003, Kalácska et al. 2004, Thenkabail et al. 2004a, Atkinson et al. 2000). Another application for these data is the mapping of burned areas resulting from tropical forest fires (Stibig et al. 2001, Fuller & Fulk 2001).

Newly available hyperspectral satellite data have not yet been used much in tropical forest applications (Thenkabail et al. 2004a), while there are a few examples for the application of the new high spatial resolution satellite data. IKONOS data have been used for the validation of products derived from lower resolution data (Wang et al. 2003, Morisette et al. 2003). They have also been tested for forest land use and land cover classifications as well as for the estimation of forest biomass and the detection of selective logging (Clark et al. 2004, Thenkabail et al. 2004a, Hurtt et al. 2003). High resolution remote sensing data is also needed to resolve the narrow mangrove fringes along tropical coastlines. Wang et al. (2004b) compare IKONOS and Quickbird images for mangrove mapping and achieve slightly better classification results with the IKONOS data. Davis & Jensen (1998) study the correlation between mangrove biophysical variables and airborne high resolution data. There are also examples of traditional aerial photograph interpretation for the mapping of tropical forests (e.g. Hudson 1991).

SAR data is often seen as a solution to the problem of frequent cloud cover in tropical areas which renders much of the optical satellite data unusable. However, the information about moisture and vegetation structure that is contained in radar data (Dobson et al. 1995) is not necessarily suitable

for the separation of ecological forest types. Costa (2004) and Simard et al. (2000), using JERS-1 and Radarsat data, were successful mainly in separating different types of floodplain forest and aquatic vegetation in tropical river basins but did not map more than a single dense upland forest class. In addition, the classification of Simard et al. (2000) worked well only in the low topography region, while the terrain induced geometric and radiometric distortions in the radar data hampered the classification in a more mountainous area.

One of the challenges of tropical forest and land cover mapping is the discrimination of agroforestry (Hurtt et al. 2003). Agroforestry (main land use agriculture) is usually not included in the definition of forest (e.g. FAO 2001), but can look very similar from a remote sensing view point, with a more or less dense tree canopy and sometimes crops in the form of shrubs (e.g. coffee) below. Helmer et al. (2000) could not separate coffee cultivation from moist forest in Puerto Rico using Landsat TM data and ended up with a mixed class. Langford & Bell (1997) also find that their 'coffee' and 'woodland' classes are often confused. Hill (1999) managed to separate six different tropical forest types in segmented Landsat TM data but could not separate agricultural land containing trees from other open-canopied forest classes.

When forest is mapped it needs to be defined first. For the FAO's global forest resources assessment (FRA 2000), forest is defined as "lands of more than 0.5 hectares, with trees able to reach a minimum height of 5 meters maturity *in situ* and with a canopy cover of more than 10 percent, which are not primarily under agricultural or urban land use" while other wooded land includes land with 5 to 10 percent tree crown cover or shrub or bush cover of more than 10 percent (FAO 2001). The International Classification of Ecological Communities (ICEC), which is used by Areces-Mallea et al. (1999) as a standardized classification system for all Caribbean islands, differentiates between 'closed tree canopy' with 60 to 100 percent crown cover and 'open tree canopy' with 25 to 60 percent crown cover, while areas with under 25 percent tree cover and dominated by shrubs (over 25 percent cover) are classified as shrubland. This study will use the ICEC as guideline for the definition of closed forest, open forest (called 'woodland' in the ICEC) and shrubland.

Open forests and other low density woodland account for an important part of tropical forest resources (Matthews & Granger 2002). If a forest stand has an open canopy, a significant proportion of the variance in Landsat spectral data can result from variations in the background (undergrowth, soil, shadows), and the proportion of shadow viewed by the sensor is in turn influenced by slope and aspect (Gemmell 1995, 1999). This weakens the statistical connection between forest properties and the remotely sensed signal and makes it more difficult to monitor open forests by remote sensing techniques than closed forest. Consequently, the accuracy of estimates of open forest and woodland areas is poor (FAO 2001, Matthews & Grainger 2002). Trees outside forest, including trees growing on land with a tree cover below 25 percent, trees on

agricultural land and trees growing along roads and rivers, also fulfill many ecological and economic functions (Herrera et al. 2004, FAO 2001). Nevertheless, there is very little information on these trees available in developing countries (Saket 2002). Helmer et al. (2002) noted that grass-dominated lands with up to 25 percent tree cover are spectrally very similar to grassland without trees in Landsat data. Higher resolution data could make it possible to gain more reliable information on trees outside forest with remote sensing means (Herrera et al. 2004).

Most of the available literature on monitoring neotropical forests is about the relatively homogeneous Amazon basin (e.g. Palubinskas et al. 1995, Foody et al. 1996). Central America, especially the Caribbean islands, has a much more heterogeneous landscape (Castro et al. 2003) with a very varied mosaic of different primary and secondary forest types. The complexity of tropical mountainous landscapes with small scale agriculture and agroforestry and fragmented areas of natural and semi-natural vegetation can be expected to lead to relatively low classification accuracies when using medium resolution satellite data like Landsat TM (Langford & Bell 1997).

On the whole, Landsat TM and ETM+ are the sensors most commonly used in tropical forest applications and remain the standard to which other optical satellite data are usually compared. In contrast, high spatial resolution satellite data has as yet rarely been used for tropical forest mapping.

2.2 The Role of Spatial Resolution in Satellite Remote Sensing, with Particular Regard to Forest Mapping

A remotely sensed image is an abstraction of the real world (scene) and the objects which constitute the scene (Ferro & Warner 2002). The relationship between the scene and the image is substantially controlled by the scale of capture, which (in the case of non-photographic imaging systems) is determined by the sensor's spatial resolution, approximated by its instantaneous field of view (IFOV). The IFOV represents the limit of spatial detail that can be recorded by the sensor. A pixel (picture element) is the square display unit in the remotely sensed digital image to which the sensor's measurement is assigned (Atkinson & Aplin 2004). It cannot carry distinct information about ground areas smaller than the IFOV and it covers the approximate area of an IFOV in most remote sensing products (Zhang 2003). Effectively, remote sensing can be regarded as a case of spatial sampling with complete cover and a regular sampling grid, used to obtain measurements of the geographical entities making up the scene (Marceau et al. 1994a, Hay et al. 2003). Remotely sensed images of a particular satellite sensor have a fixed nominal spatial resolution; in other words, the grid spacing is fixed according to the sensor's properties. Spatial resolution can be defined in different ways. It refers to the smallest resolvable object (or separation between two objects) in an image, and is thus primarily determined by the distance between pixels in a digital image (Atkinson & Aplin 2004). In the following text pixel size will be treated as equivalent to spatial resolution.

Depending on the field of application and the time of writing (state of technology), definitions of 'high resolution' satellite data vary greatly. For current land cover mapping applications, satellite remote sensing data can be classified into low resolution (with a spatial resolution of hundreds of metres to kilometres, for example NOAA AVHRR, MODIS), medium resolution (tens of metres, for example Landsat TM, Landsat ETM+, Spot HRV XS), and high resolution (1 to 10 m, for example IKONOS), with the term 'very high resolution' being reserved for imagery with a spatial resolution finer than 1 m. These definitions will be used in this study.

The information content of an image changes with its spatial resolution (Treitz & Howarth 2000a, Woodcock & Strahler 1987, Marceau et al. 1994a, Treitz 2001, Millington et al. 2003). Every kind of remote sensing acts as a "spatial frequency filter" (Hay et al. 1996: 109), influencing the level and type of information about the scene which can be retrieved from the image (Sampson et al. 2001). On the one hand, patterns with a higher frequency than the spatial resolution are filtered out. On the other hand, patterns with a lower frequency than the spatial extent of the whole image are also filtered out. Every given spatial resolution corresponds to a level of spatial aggregation of the smaller elements within the sample units (pixels) (Marceau et al. 1994a).

Every natural scene contains objects at several levels in what can be described as a hierarchy of scales (Ferro & Warner 2002, Hay et al. 2003). Looking closely at a forested environment, we see leaves and branches, at the next higher level, there are whole trees, shrubs etc., at the next level forest stands, and so on. A forest stand is defined here as a contiguous area or forest that is homogeneous with regard to some of its characteristics (e.g. ecosystem type, density, age/maturity) and can be distinguished from neighbouring forest stands which differ in these characteristics. In a classification, the objects at one level are the target classes (e.g. forest stands of certain types), and the objects at the next finer level (trees etc.) are the base elements of these classes. Different classes can share common elements. A pine tree for example can be part of a pine forest, but also of a mixed forest or it might, as a tree in a garden or park, be part of an urban class. It is usually a combination of elements and their relative frequency that characterises a particular class.

The kinds of targets which can be classified depend on the spatial resolution of the image. According to Puech (1994), each target at a given level has a threshold of homogeneity and a threshold of heterogeneity, with regard to the spatial resolution. At a fine resolution, the elements of the target are resolved separately, so that the target is textured. When the resolution becomes gradually coarser, there comes a point when several elements are aggregated in a single pixel. When the resolution is so coarse that each pixel contains about the same representative mix of base elements, the threshold of homogeneity is reached, i.e. the target object becomes homogeneous in the image. But when the resolution gets even coarser, the pixels eventually become so large that they contain several targets (mixed pixels). Puech (1994) calls the resolution at which the targets

become indistinguishable because of mixed pixels the "threshold of heterogeneity". (This equals the threshold of homogeneity for targets at the superior level.)

Pixels of low resolution images integrate the spectral response of several objects in the scene. In high resolution images, by contrast, the information of one pixel is related not to the character of an object (target land cover class) as a whole, but to components of it (Ehlers et al. 2003). The critical thresholds of resolution depend on the target classes. In a forest type classification, a high resolution image of a forest stand, e.g. an IKONOS image with 4 m resolution, can be a mix of pixels representing illuminated crown parts, shaded crown parts, illuminated background (understorey and/or soil), and shaded background. The resolution here is finer than the threshold of homogeneity and the pixels are not large enough to integrate all the components of the considered land cover class. By contrast, if the target class is an agricultural field or a young forest plantation, the 4 m IKONOS pixels might already be large enough to integrate the constituent elements of these classes (whole small plants and their background). The spatial resolution of Landsat data (30 m) is coarse enough to integrate the elements of most land cover classes including forest (if the forest structure is not very heterogeneous) on the one hand. On the other hand, for small target objects in a fragmented, heterogeneous landscape, it might in many cases already be beyond the threshold of heterogeneity, and thus cause a considerable percentage of mixed pixels.

To emphasize that the properties of an image do not only depend on the absolute spatial resolution but on the relation between the spatial resolution and the size of the objects in the scene, Strahler et al. (1986) differentiate between "H-resolution" cases where the pixels are smaller than the objects (Pixel size/Object size < 1) and "L-resolution" cases where the pixels are larger than the objects (Pixel size/Object size > 1). This definition has been taken up for example by Hay et al. (2003).

The effect of differing spatial resolutions on image statistical properties can be tested by gradually degrading the spatial resolution of high resolution images (upscaling). This can be done using block averaging, i.e. calculating the average of pixel values within a square window and assigning the result to the window which becomes the new coarser resolution pixel. Block averaging is a simple method to approximate the spectral response at different spatial resolutions (Hay et al. 1997), although it does not account for nonlinear relationships between finer and coarser resolutions and is an exact approximation of an image at a coarser resolution only if the pixel values have a normal distribution (Wang et al. 2004a).

Several studies have calculated and compared the statistics of images of the same scene at several spatial resolutions (Chen et al. 2004, Woodcock & Strahler 1987, Marceau et al. 1994a, Cushnie 1987). The overall conclusion is that, while the mean is relatively stable over different resolutions, measures of variability are very resolution dependent. Chen et al. (2004) find that the standard deviation and also the spatial autocorrelation decrease when the spatial resolution of an image of an

urban environment is gradually reduced from 4 m to 24 m. The internal variability within the image of a residential area decreases with reduced spatial resolution (Cushnie 1987). Bruniquel-Pinel & Gastellu-Etchegorry (1998) find that reducing the resolution of simulated forest imagery from 0.5 m to 3 m through block averaging decreases image variance. Treitz (2001) and Song & Woodcock (2002) also observe lower variance of forest reflectance with coarser spatial resolution data.

Contrary to global variance (calculated on the whole image), local variance (calculated using only neighbouring pixels for example in 3×3 pixel windows) does not always monotonically increase with higher spatial resolution. The local variance of simulated forest images is higher for 1 and 4 m resolution data than for 15 m resolution data (Song & Woodcock 2002). For young forest stands it is also higher in 1 m than in 4 m resolution data, but for mature forest stands with larger crowns and fewer trees the 4 m resolution data has a higher local variance than the 1 m data. This can be explained by the fact that in a mature forest, neighbouring 1 m pixels tend to fall within one tree crown. In other words, in very high resolution imagery, most pixel values will be highly correlated with their neighbour's, keeping local variance low. When the resolution gets coarser, the probability of neighbouring pixels covering different objects or class elements (e.g. one pixel representing an illuminated tree crown, its neighbours shadow and undergrowth) rises and so does the local variance. When the pixels become large enough to integrate the different elements in the image, the local variance decreases again (Woodcock & Strahler 1987).

Spectral per-pixel classifiers work under the implicit assumption that the pixels to be classified are large enough for a spatial integration of the elements comprising the classes (Woodcock & Strahler 1987). These traditional automated image analysis techniques developed for lower resolution satellite data may not be appropriate for high resolution imagery (Quackenbush 2000). The statistical class separability with traditional classifiers is reduced for high spatial resolution data because of increased within-class spectral variability (Marceau et al. 1990, Arai 1992). Schlerf et al. (2003) achieved better forest classification results with 30 m resolution data than with 5 m resolution data, concluding that the high small-scale spectral variability in the 5 m data was responsible for misclassifications. It has to be taken into account though that Schlerf et al. (2003) used only central areas of forest stands for their accuracy assessment, excluding the areas close to class boundaries which are most likely to profit from a higher resolution because of a reduction of the proportion of mixed pixels (see also chapter 2.8: Strategies for Accuracy Assessment). On the whole, many studies come to the conclusion that a higher spatial resolution does not necessarily lead to higher per-pixel classification accuracies (Cushnie 1987). Although the information content is inherently higher in high resolution data (Hay et al. 1997), the additional information only acts as noise in such a spectral classification (Markham & Townshend 1981).

Some authors have used low pass filtering as a method to reduce unwanted within-class variability (Arai 1992, Hill 1999, Amarsaikhan & Douglas 2004). Another possibility is image segmentation

(see chapter 2.3) followed by per-object instead of per-pixel classification. A third possibility is a reduction of the spatial resolution through regular pixel aggregation, for example in the form of block averaging. These methods are going to be tested and compared in this study for the case of forest and land cover classification with IKONOS data.

Optimal spatial resolution problem

When the image resolution gets coarser (or the image is smoothed with a low pass filter) the benefits of integrating the elements of the target class and making the class more homogeneous are counteracted by smoothing over class boundaries, leading to an increased percentage of mixed boundary pixels (Cao & Lam 1997, Markham & Townshend 1981). With this trade-off in mind, a number of studies have attempted to find an optimal spatial resolution that "minimizes within-class variability, but maximizes between-class discrimination" (Treitz & Howarth 2000b: 315) for a given set of land cover classes and for a given landscape structure.

To identify and map a particular object (informational class), the pixels need to be smaller than the object but larger than its constituent elements (objects at the next finest level in the hierarchy of scales) (Ferro & Warner 2002, Curran 1988). Several methods have been developed to determine the spatial resolution at which the class elements (objects at the finer level) are optimally integrated: the average local variance method and the semivariogram.

Term	Definition
Lag	distance (and direction in two or more directions) between sampling pairs
Sill	maximum level of semivariance
Range	point on lag axis where semivariance reaches a maximum; places closer than the range are related; places further apart are not
Nugget variance	point where the extrapolated relationship between the two variables intercepts the semivariance axis; represents spatially independent variance
Spatially dependent structural variance	sill minus nugget variance

Figure 1: Variogram (from Treitz & Howarth 2000a, fig. 1).

The semivariogram (or variogram for short) is the key tool in geostatistics, which is the theory of regionalized variables. The variogram measures the spatial dependency of neighbouring

observations. Semivariance is half the average variance between pairs of pixels with a certain spatial separation along a transect. The variogram plots semivariance against spatial separation (Curran 1988). For small distances of separation (lags), semivariance tends to be low and rises as the lag gets larger. The maximum level of semivariance is called the sill and represents the amount of variation in the whole transect. The lag at which a semivariance maximum is reached is called the range. It represents the limit to spatial dependence; at larger separations the observations (pixel values) are statistically independent of each other (Treitz & Howarth 2000a, Atkinson & Aplin 2004). Pixels larger than the range of the variogram (measured at a higher resolution) are expected to average the within-class spectral variability and thus to be suitable representatives of that class for a classification (Curran 1988).

Treitz & Howarth (2000a) derived variograms for a number of boreal forest ecosystem classes from airborne high resolution data. They found that the optimal spatial resolution for forest ecosystem classification varies between about 3 m and 7 m depending on wavelength and forest class. Treitz (2001), studying the same boreal forest classes and using airborne data of two different spatial resolutions, found that the mean variogram range increases with stand complexity and with the spatial resolution of the collected data. The range is also higher for NIR (near infrared) than for visible reflectance data, which Treitz (2001) attributes to multiple scattering of NIR energy, leading to a stronger interaction with understorey components. Overall, the mean ranges for broadleaved and mixed forests are between around 5-6 m (for visible data collected with a spatial resolution of 0.73 m × 5.36 m) and 12-14 m (for NIR data collected with a spatial resolution of 1.39 m × 5.36 m). For pure spruce stands, equivalent mean ranges are between 2-5 m and 8-11 m, showing that the influence of spatial resolution and wavelength of the data is larger than that of the forest type. To avoid the question of wavelength, Sampson et al. (2001) based their mean range estimates on the first principal component of a multispectral image. The estimated mean ranges for a mature broadleaved forest varied between 6 m and 9 m depending on the spatial resolution of the imagery used.

Overall, the range of the variogram really is not a very hard indicator for the optimal spatial resolution. There are some difficulties involved in fitting a continuous curve to an experimental variogram, and resulting range estimates may differ depending on the modelling process (Hese 2001). Besides, a variogram is dependent on the direction of the transect and on the waveband (Curran 1988) and it changes with the resolution of the image from which it is calulated (Treitz 2001).

The average local variance (ALV) method was introduced by Woodcock and Strahler (1987). It involves the calculation of the 'local variance' which is defined as the standard deviation of the nine values in a 3×3 pixel window. The 'average local variance' of an image is the mean of all local variance values, computed in a moving window over the whole image. The image is then gradually

degraded to coarser spatial resolution using block averaging. The average local variance is calculated for every resolution, and a graph of ALV as a function of spatial resolution is plotted. A peak in this graph is reached when the size of the resolution cells approaches the size of the scene objects or the distance between elements on a uniform background (Bøcher et al. 2003), while a minimum in the graph suggests that the threshold of homogeneity (in the terminology of Puech 1994) is reached.

Several authors have used variations of this method to determine an optimum spatial resolution for classifications, calculating the ALV not for the whole image but for the areas of separate forest classes, thus identifying class-specific optimum resolutions. Holopainen & Wang (1998) determined the optimum spatial resolution degrading aerial photographs of a forested area by averaging pixels in windows of growing sizes. Optimum resolution was defined as the window size resulting in minimum intraclass standard deviation. For images with an original resolution of 2.82 m, optimum resolution varied between 8.5 and 36.7 m depending on forest stand classes and spectral bands (red, green, or blue). Marceau et al (1994b) used the same criterion of minimum intraclass variance, plotting the class-specific ALV against resolutions between 0.5 and 29.5 m. They arrived at optimal spatial resolution values for forest classes between 2.5 m and 21.5 m, depending on the forest classes, especially the forest structure (finer for dense homogeneous stands, coarser for less dense or mixed stands).

It has been established that the "optimal spatial resolution" differs from class to class and also depends on the waveband. With the methods described above, it is difficult to determine a single appropriate spatial resolution for general region of interest containing several land cover types (Atkinson & Aplin 2004). However, if the aim is the classification of an image, it is not practical to use a separate optimal resolution for each class, because this would require complete prior knowledge about the location of the classes.

Another empirical method to determine an optimal spatial resolution for a classification is to measure classification accuracies or class separabilities for images at different spatial resolutions. Treitz & Howarth (2000b) thus found that, for a visible to near infrared dataset, 6 m was the optimal resolution to discriminate boreal forest ecosystem classes (compared to 4, 5 and 7 m resolution).

Not only the internal characteristics of the land cover classes but also their spatial arrangement in the landscape (the landscape structure) influence the spatial resolution which will lead to the optimal classification results. Smith et al. (2002) study the influence of land cover heterogeneity and patch size on classification accuracy and come to the conclusion that increased land cover heterogeneity and smaller patch sizes lead to lower accuracies. More fragmented landscapes require finer spatial resolution data to achieve optimized classification accuracies (Chen et al. 2004).

Medium resolution data like Landsat has limitations in heterogeneous landscapes. The percentage of mixed pixels carrying spectral information of more than one informational class can become unacceptably high, like in a Finnish forest management example described by Pekkarinen (2002), where a typical forest stand has a size of 1.5 ha, so that 30 m resolution satellite data consists mostly of mixed pixels. The lack of sensitivity of medium resolution (Landsat ETM+) data to selective logging in tropical forest areas is pointed out by Asner et al. (2002) and Read (2003). Higher resolution data are needed in order to be able to achieve greater classification accuracies when mapping small targets, for example marine environments (Mumby & Edwards 2002) or single forest stands (Kayitakire 2002). It can be hypothesized that in the heterogeneous and fragmented tropical mountain landscape of the study area, the classification possibilities with Landsat data will also be limited and classification results should benefit from the use of higher resolution data. This will be investigated in chapters 7, 8 and 9.

Another aspect of high resolution imagery (compared to medium resolution) is the hugely increased amount of data involved, requiring increased amounts of storage space, calculating capacity and calculating times. This makes it necessary to use efficient analysis techniques and it can, together with the current costs of high resolution satellite imagery, limit the area which can be covered and analysed with this data (Read 2003). This means that high resolution data can only be used for key study sites or sample locations within large study areas (Hurtt et al. 2003).

High spatial resolution satellite data available today also have the limitation that (due to the trade-off between spatial and spectral resolution) the spectral resolution of these data is restricted to no more than four multispectral broadband channels and they do not provide channels in the mid and thermal infrared region of the electromagnetic spectrum. This is a disadvantage for the spectral discrimination of vegetation classes (Mumby & Edwards 2002, Thenkabail et al. 2004b, Goetz et al. 2003). It should be possible, however, to compensate for these spectral deficiencies of the high spatial resolution data (compared to medium or low spatial resolution data with more spectral channels) by incorporating the increased amount of spatial information contained in these data in the classification process.

2.3 Texture and its Role in Land Cover and Forest Classification

Texture is a key element for visual image interpretation, used for example in manual vegetation mapping from aerial photographs. Humans have the innate ability to recognize textural differences in images, being able to identify areas in the image as smooth or rough, coarse or fine. Texture provides structural information to the interpreter. The transfer of this information source into the domain of digital image processing has proven rather difficult, so that in most cases only tone, i.e. the spectral information in a set of image bands, has been used in digital satellite image classification.

Texture in an image is a function of the spatial arrangement of tones or grey levels within an image band, i.e. grey level differences or contrast, the size of the area where change occurs and the degree of directionality or regularity (Hall-Beyer 2002). The latter characteristic is also known as 'pattern' and not included in the narrower definition of texture in visual image interpretation (Campbell 1996), but both elements are usually incorporated in the term texture in digital image processing.

For texture to become useful in image classification, the objects to be classified have to be larger than the size of the pixels (Woodcock & Ryherd 1989), so that each object contains enough pixels to make an analysis of their spatial arrangement feasible. Thus, spatial information in addition to spectral information becomes increasingly useful when the spatial resolution of the imagery is increased (Chen et al. 2004). According to Curran (1988), the range of the variogram, while indicating the minimum pixel size for per-pixel spectral classifications, marks the upper limit of the pixel size if the pixels are to be used to derive a measure of class texture. In order to fully exploit high resolution satellite data like IKONOS, texture information should be incorporated in the image analysis (Dikshit & Roy 1996, Kayitakire et al. 2002) so that the internal spectral variability of the classes is used as a source of information and not discarded as noise.

Several methods have been developed to quantify image texture. They can be assigned to two broad categories: statistical and structural approaches (Haralick 1979, He & Wang 1990). Statistical approaches aim to characterize the stochastic properties of the spatial distribution and relationships of grey-levels in an image. Statistical texture measures can be classified as first order, second order and higher order textures. First order texture measurements are calculated directly from the original digital numbers (DNs) of an image, usually under a moving window. Second order texture measures are based on the relationship between groups of two pixels. Third and higher order texture measures, involving groups of three or more pixels, are also possible. They are, however, connected to an increase in computation time (Anys & He 1995) and interpretation difficulties, so that they are usually not implemented in the context of the classification of remotely sensed images.

Structural approaches regard texture as a repetitive pattern of primitives which can be more complex than grey levels of single pixels. Fourier spectrum analysis is one of the methods used to determine the placement rule responsible for the pattern of primitives. The texture of remotely sensed images, however, is stochastic in nature, with a considerable spatial variation of primitives, hampering the determination of a placement rule (Pizzolato et al. 2003, Hay & Niemann 1994). As a consequence, structural approaches are rarely used in remote sensing.

GLCM texture

A frequently used statistical method for second order texture extraction is based on the Grey-Level Co-Occurrence Matrix (GLCM). The GLCM is a matrix of the relative frequencies $P(i,j)$ with which two neighbouring pixels with a defined spatial relationship and with the combination of grey

levels *i* and *j*, occur in an image window, or more specifically in an image window centred on the pixel for which the texture is calculated (figure 2). Grey-tone co-occurrence statistics were first used for texture discrimination by Julesz (1962). Haralick et al. (1973) proposed 14 different texture measures which can be extracted from the GLCM. Apart from the specific GLCM texture measure, there are several other control variables for this kind of texture analysis: the input channel, the window size, the number of grey levels to which the input data is scaled down for GLCM calculations and the spatial relationship of the neighbouring pixels (offset distance and direction). This leads to a very large number of possible GLCM texture features which can be calculated from one image.

Figure 2: A 5×5 image window and the corresponding Grey-Level Co-Occurrence Matrix (spatial relationship in this case: neighbour pixel is defined as the one directly to the right of the reference pixel). Read: grey level 2 occurs next to grey level 2 one time; grey level 3 occurs next to grey level 2 no time; …

A number of recent Canadian studies have found that the inclusion of GLCM texture features improved forest classifications when using high resolution airborne data (Franklin et al. 2000, 2001a, Treitz & Howarth 2000b) and IKONOS panchromatic data (Franklin et al. 2001b). GLCM texture features derived from IKONOS and higher resolution airborne data, together with spectral data, have also been used to determine forest parameters like leaf area index (Colombo et al. 2003), defoliation severity (Moskal & Franklin 2004) and a forest structure index which included canopy closure, leaf area index and the density of blown down trees and dead stems (Cosmopoulos & King 2004). Franklin et al. (2003) use GLCM texture measures derived from medium resolution data (Landsat TM) to discriminate between conifer height, age and crown closure classes in a relatively homogeneous boreal forest, while Kimes et al. (1999) use secondary forest SPOT HRV and GLCM texture to map secondary forest age in Amazonia.

In the field of more general land use and land cover classifications, GLCM texture has been successfully used in combination with spectral data by Narasimha Rao (2002), using IRS-1D panchromatic data (6 m spatial resolution), Kiema (2002), using SPOT panchromatic data, and

Franklin & Peddle (1990), Gong et al. (1992) and Marceau et al. (1990), using SPOT HRV data. Presutti et al. (2000, quoted in Presutti et al. 2001) found that the inclusion of texture in a land cover classification with RADARSAT and Landsat TM data improved the classification accuracy for forest classes by 25 % and somewhat less for urban and agricultural classes. Fransson et al. (1999), however, did not find an improvement in the identification of clear cut areas when including SAR data derived GLCM texture features.

First-order texture measures

Statistical texture measures calculated from the original pixel values (first-order texture measures) include *local variance*. Here, the variance (or sometimes the standard deviation) of the grey levels in an image window is calculated and assigned to the central pixel of the window, which then continues to move over the whole image.

Local variance in high resolution (IKONOS) imagery, calculated in filter windows of varying sizes, has helped to improve classifications of mangroves (Wang et al. 2004c) and marine habitats (Mumby & Edwards 2002). Ferro & Warner (2002) achieved a slight improvement in land cover classification accuracies when including variance calculated on high resolution airborne imagery. Coops & Culvenor (2000) relate variance to the spatial pattern of trees modelled in simulated high resolution imagery and Zhang (2001) uses variance for the detection of urban tree covered areas in very high resolution airborne data.

The usefulness of local variance decreases when the spatial resolution gets coarser. In the study of Chen et al. (2004), the inclusion of variance improved the classification accuracy for an urban area for imagery of 4, 8 and 12 m spatial resolution, but not significantly if the resolution was 16 m or more. Local variance derived from IKONOS data improves the classification accuracy of marine environments, but is not useful when derived from Landsat data (Mumby & Edwards 2002). Asner et al. (2003) find local variance to be valuable for the delineation of cleared lands from forest with Landsat TM data, while more detailed structural differences within the forest (logging damage) could not be resolved with Landsat ETM+ spectral and textural data, because the spatial resolution was insufficient (Asner et al. 2002).

For land cover classification purposes, local variance has the disadvantage that it also works as an edge detector with high values near the edges of objects so that the differences of texture within different class areas can be outweighed by the effect of the between-class texture (Woodcock & Ryherd 1989).

Other statistical measures which can be calculated in a moving window include the first order measures mean, skewness, kurtosis, minimum and maximum. Debeir et al. (2002) used these first order statistics and auto-correlation measurements to incorporate textural information in Landsat

TM land cover classification. This improved classification results significantly, but it also introduced artefacts leading to misclassifications around the edges of homogeneous spectral zones.

Variograms

Another second order statistical method is to use coefficients of the variogram (e.g. range and sill) as texture parameters. Variogram derived parameters like range and sill estimates have been linked to forest biophysical parameters and stand structure (Colombo et al. 2003, Bruniquel-Pinel & Gastellu-Etchegorry 1998, St-Onge & Cavayas 1997, Hese 2001). Song & Woodcock (2002) studied the relationship between forest age (tree size), spatial resolution and the variogram. Tree size and density affect the range of the variogram (the distance between two pixels at which the observations become independent). St-Onge & Cavayas (1997) regard the variogram range as a good indicator of texture coarseness. Calculating the experimental variogram in a moving window and adjusting a theoretical model variogram to these calculations to derive texture measures for each pixel is computationally expensive, however. In many cases, variogram texture measures are only calculated for some transects in the land cover classes of interest and not directly integrated in image classifications (e.g. Sampson et al. 2001). This approach will also be followed in this study.

Other texture concepts

A method belonging to the structural approach of texture extraction is presented by Hay & Niemann (1994) and Hay et al. (1996) for the analysis of high resolution forest imagery. They use object-oriented image primitives for the discrimination of forest stands of different height, crown diameter and density, with promising results for the classification of these structural parameters in relatively homogeneous forest stands. Other texture measures which have been studied in relation to forest and land cover classification but are not widely used are based on Fourier analysis (Riou & Seyler 1997), Gabor filtering (Pizzato Angelo & Haertel 2003), wavelet transforms (Myint 2001, Simard et al. 2000) and a Markov random field model (Palubinskas et al. 1995).

Comparison of different texture features

Carr & Miranda (1998) compare the co-occurrence matrix to a method based on the variogram for texture classification and conclude that, while for microwave images the variogram method results in improved accuracy, for optical images both textural classifiers yield similar accuracies. Lloyd et al. (2004), however, find statistics derived from the variogram more helpful for the classification of an agricultural area than GLCM texture. Franklin et al. (2001b) find GLCM *homogeneity* more useful for distinguishing between Douglas-fir forest age classes than the first-order texture measure variance. Gong et al. (2002) achieve better results with the GLCM *angular second moment* feature than with first order standard deviation, but they achieve the best results with a combination of both. Coburn & Roberts (2004) compare local variance and GLCM texture for coniferous forest

classification and while both improve classification results compared to spectral data alone, local variance leads to slightly better overall results. Wulder et al. (1998) find that regarding the prediction of the leaf area index, first-order texture measures work best for homogeneous stands, while second-order and semivariance-based texture measures are better for heterogeneous forest stands.

On the whole, the texture in high resolution images is strongly correlated with forest structure, while texture derived from medium resolution imagery is less useful for forest classification (St-Onge & Cavayas 1995). For the classification of relatively heterogeneous natural and semi-natural forest areas using high resolution optical imagery, as it is intended in this study, the use of GLCM texture features or a combination of GLCM and first order local variance appears to be a promising approach.

Problem of optimal window size

Most types of image texture, including GLCM texture measures and local variance, are produced by performing calculations on the DNs (digital numbers) of the pixels in a window centred on the pixel which receives the resulting texture value. In these calculations, the size of the window can be a more important factor than the choice of statistics used as texture measures (Marceau et al. 1990).

For stable texture measures which are representative of the land cover classes in the image, window sizes must not be too small (Franklin et al. 2001b), but large window sizes lead to increasing edge effects (Ferro & Warner 2002). Franklin et al. (2001b) calculate variance and GLCM homogeneity from an IKONOS panchromatic image (1 m resolution) using three different window sizes (5×5, 15×15 and 25×25). The separability of forest age classes increased with window size and was highest when the 25×25 pixel window was used, but the test pixels for this study were all located near the stand centres so that edge effects could not occur.

Ferro & Warner (2002) agree that large window sizes are needed to produce stable texture measures. But when they used the local variance, calculated on 1 m resolution imagery with different variance filter window sizes, they included areas near the edges in the evaluation of the results. Variance in combination with spectral information improves class separability away from class edges, but for pixels near class edges, when the filter window covers more than one class, between-class variance is measured instead of within-class variance, leading to a decrease in class separability for these areas. As the windows get larger, the proportion of pixels being assigned between-class texture values rises (figure 3). This proportion is of course also dependant on the size of the contiguous class areas. In landscapes with small class areas, edge effects may lead to a decrease in the overall classification accuracy when texture is included.

Woodcock & Ryherd (1989) tried to reduce edge effects by using small 3×3 'adaptive windows' to calculate variance. These windows were not necessarily centred on the pixel receiving the texture value but chosen from all 9 windows including the pixel using the criterion of least variance. The resulting texture images were not really satisfactory though because of their blocky appearance, although the edge detection effects of local variance where somewhat reduced (Ryherd & Woodcock 1996, Ferro & Warner 2002).
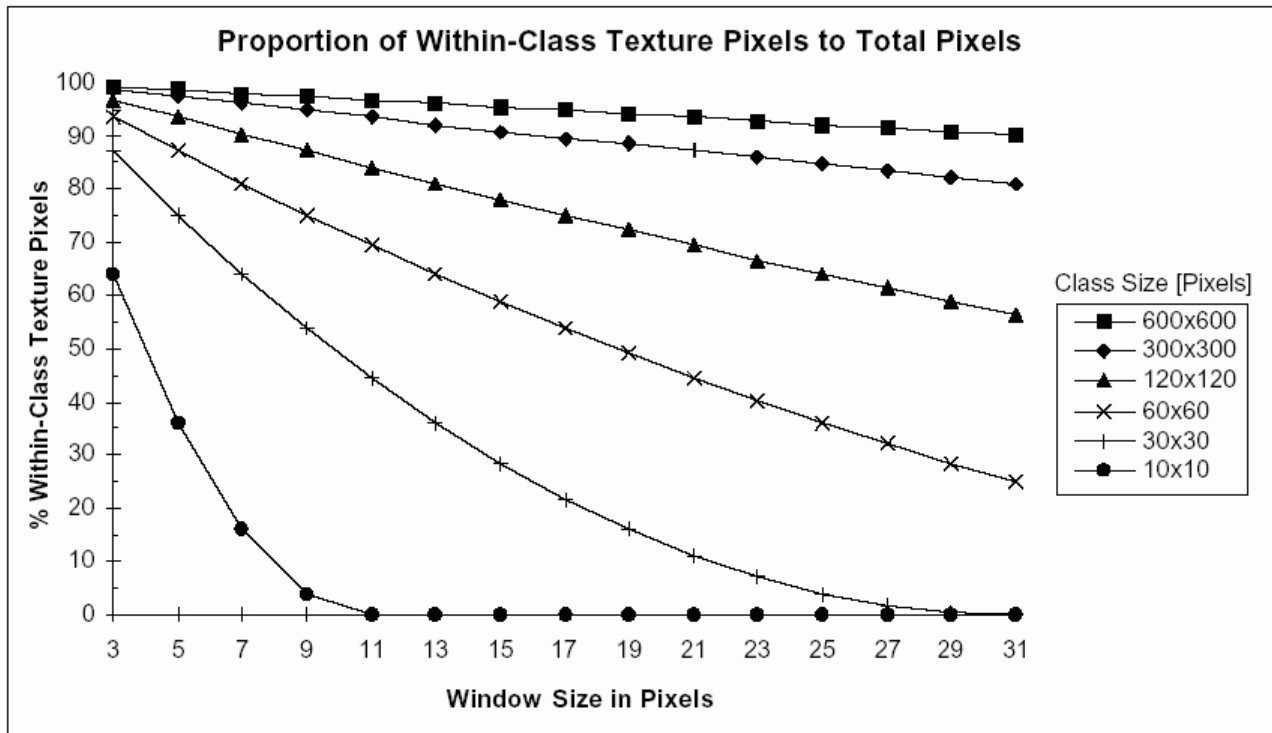
Figure 3: Proportion of within-class texture pixels to total pixels. From: Ferro & Warner (2002).

Chen et al. (2004) use local variance calculated with different window sizes on images with different spatial resolutions for the classification of an urban environment. They find that small window sizes are good for homogeneous classes, while heterogeneous classes need larger texture windows. Larger windows (measured in pixels) are needed for finer resolution images. The best overall results in this case are achieved with 5×5 windows when using 4 m resolution data and 3×3 widows for 8 m resolution data. When deriving texture from medium resolution satellite data, window sizes usually have to be small because most land cover classes do not have large enough contiguous areas to allow for the use of windows covering many pixels. Arai (1992), using Landsat data, takes only window sizes between 2×2 and 4×4 into consideration for the improvement of class separability with first order texture.

Larger windows than that are recommended as a basis for the calculation of second order texture features (PCI Geomatics 2003). Marceau et al. (1990) test seven window sizes between 5×5 and 49×49 for the calculation of GLCM texture measures from SPOT XS data (20 m resolution). They

find that window sizes of 17×17 and 25×25 lead to the best classification results for most land cover classes in their Canadian study site. Wulder et al. (1998) use the variogram range as an indication for the best window size for the calculation of first- and second-order texture measures which are then used as a surrogate for forest structure in leaf area index estimations. Based on 1 m resolution airborne data, the variogram ranges suggest window sizes between 7×7 and 11×11. Coburn & Roberts (2004) compare and combine window sizes between 5×5 and 15×15 for the texture aided classification of coniferous forest stands in a 4 m resolution image. They achieve the best overall results when texture measures calculated from different window sizes are combined, capturing the different scales of information in the image.

Most examples for the use of texture in forest classification which can be found in the literature regard the classification of temperate and boreal forests or simulated forest images. Studies in the tropics, like those of Asner et al. (2003) and Kimes et al. (1999), who use texture derived from medium resolution satellite data for land cover classifications in Amazonia, or that of Wang et al. (2004b), who use IKONOS texture data for mangrove classification, are rare exceptions. This study will use texture derived from high resolution satellite data in the classification of a heterogeneous, partly forested tropical mountain landscape.

2.4 Image Segmentation

Image segmentation aims at dividing an image into a number of spatially continuous, non-overlapping regions which are homogeneous with respect to some characteristic or characteristics (Pal & Pal 1993). Image segmentation followed by per-segment (per-object) classification instead of per-pixel classification is one way to reduce within-class variability and noise in the classification of textured high resolution imagery. Using the statistics of segments (groups of pixels) instead of single pixels can increase class separabilities and classification accuracy (Lobo 1997). In contrast to block averaging, the aggregated groups of pixels which are the result of segmentation processes are intended to be meaningful image units, representing image objects or parts of objects ('object primitives'). This allows the use of object oriented image processing methods, analysing image units which carry more semantic information than single pixels. This method also avoids the reduction of the spatial resolution entailed by block averaging and makes use of the spatial information which is present in the image.

Sometimes the borders between objects are known beforehand, for example in the form of vector data depicting the boundaries of agricultural fields or forest stands in a GIS database, making it possible to use per-field classification techniques on that basis (Aplin et al. 1999, Kayitakire et al. 2002). As long as such vector data is not available, image segmentation is the prerequisite for object oriented image processing.

Image segmentation techniques have long been applied in the field of computer vision and pattern recognition, as segmentation is the foundation of low level vision. Haralick & Shapiro (1985) and Pal & Pal (1993) present reviews of segmentation methods. However, not all of the methods which are developed for the segmentation of e.g. grey tone images or images used in the field of medicine are also suitable for segmenting multi-spectral satellite images of forested areas.

In order to group contiguous pixels in a meaningful way, some kind of homogeneity criterion has to be found which links these pixels, while excluding pixels from neighbouring regions representing different objects of interest. For the purpose of forest type classification, objects of interest are regions of a common forest type covering all the elements of this forest type, so the desired segments may be quite heterogeneous with respect to the spectral properties of the included pixels (Pekkarinen 2002). This makes it more difficult to join pixels to meaningful units and to find the borders between different vegetation types.

The techniques which are used to segment remotely sensed images can be grouped into pixel-, edge- and region-based methods and their combinations.

Pixel-based segmentation methods start by grouping the pixels using thresholding or clustering in the feature space (see also chapter 2.6). This can be regarded as unsupervised classification rather than segmentation, because spatially unconnected areas can end up belonging to the same cluster. Segments are then defined as connected components of the same cluster (Haralick & Shapiro 1985). Such methods, based on the image histogram or multiple-band feature space are not suitable for the segmentation of noisy or textured images (Pal & Pal 1993).

Edge-based segmentation methods employ edge detection algorithms to find the edges of the different regions of an image. Edge operators such as the Sobel filter are used to enhance edges (points of abrupt changes in grey values). Thresholding is employed to determine the edge pixels in the enhanced image and finally, these edge pixels are linked to contours. If these contours surround a region, a segment is created, but there is the problem that there are often gaps in the edges so that the segmentation cannot be completed with this method alone (Pekkarinen 2002, Haralick & Shapiro 1985).

The majority of authors who seek to segment remotely sensed images use region-based methods. These methods involve region growing, region merging, region splitting or combinations thereof. Pure region splitting, where the image is split into successively smaller segments (e.g. by quartering) as long as the resulting segments are not homogeneous enough, are usually not used in practice because of the squarish, artificial looking results (Haralick & Shapiro 1985). Region growing involves the identification of starting points (seed pixels) from which regions are grown in an agglomerative manner by joining similar neighbouring pixels to them. In the case of centroid linkage region growing, each time a new pixel joins a region, the average value of the growing

region is updated. If pixels are rejected because they are not similar enough, they form starting points for new regions. St-Onge & Cavayas (1997) use this method for the segmentation of simulated and real high resolution forest images, based on the similarity of a multidimensional value composed of three texture parameters. They come to the conclusion that precise segmentation is easier for closed than for open forest stands. Hill (1999) uses a combination of edge detection and region growing to segment separate bands of a Landsat TM image with the aim of reducing the spectral overlap between tropical forest types.

Region merging consists of merging adjacent regions if they conform to a homogeneity criterion. Several techniques involving region merging have been developed to deal with textured data. Lobo (1997) starts by repeatedly running an edge preserving smoothing algorithm over the first principal component of his multispectral image, creating small homogeneous regions. Then he employs an iterative region merging technique to merge adjacent regions if they are the most similar neighbours to each other (local mutual best fitting criterion) and if their distance in the multispectral space does not exceed a user-defined threshold. Pekkarinen (2002) suggests a two-phase approach for the segmentation of a high resolution image of a forested landscape. The method consists of a low-level segmentation on a per-pixel basis (clustering and labelling connected components) and a second step using a region merging technique. However, using the derived segments did not significantly improve the results of his tree volume estimations. Fransson et al. (1999) perform a segmentation on a SPOT optical satellite image and transfer the resulting segment boundaries to noisy SAR data in order to be able to extract per-segment information from both optical and radar data. Beaulieu (2004) describes the development of a region merging technique for SAR data with speckle noise which includes a shape criterion favouring merges which produce compact segments.

A similar shape criterion is also part of heterogeneity criterion used to decide which regions to merge in the segmentation technique which is embedded in the 'eCognition' software. This segmentation technique starts with single pixels as the basic regions or image object primitives, and merges neighbouring object primitives in subsequent steps. In order to let regions grow simultaneously in the whole image and to end up with comparable image object primitives of similar sizes, subsequent merges are placed as far as possible from each other in the image, and each region is treated once per cycle, looking for the pair with the 'local mutual best fitting' in the vicinity of each object. Two adjacent regions are thus merged if they fulfil the local mutual best fitting condition and if their degree of fitting (defined as the change in heterogeneity caused by the proposed merge, weighted by the region size) does not exceed a user defined threshold. The user can set a so called 'scale parameter' which defines the threshold and thus influences the size of the resulting image object primitives. It is also possible to construct a hierarchical network of image objects or object primitives at different scales, from the pixel level to large objects (multiresolution segmentation). The degree of fitting, which is calculated for every possible merge, is a combination of the influence this merge would have on the heterogeneity in the feature space ('spectral

heterogeneity') and a criterion describing the change in spatial compactness ('shape heterogeneity'). The heterogeneity values are weighted by the size of the objects, so that smaller regions are favoured for merges. The heterogeneity in feature space is calculated, for a user-defined number of image channels or layers of the source data, as the sum of the standard deviations of the values in each channel, weighted by the channel weights (Baatz & Schäpe 2000, Baatz et al. 2002).

In recent years, this segmentation technique offered by the eCognition software has been tested in a number of studies (e.g. Tufte 2003, Mitri & Gitas 2004). Due to its ability to produce meaningful-looking segments even in textured high resolution data, the software was used for the segmentation of IKONOS data by Giada et al. (2003) to gain information about tents in a refugee camp, by Meinel et al. (2001) for an urban land use classification, by Hay et al. (2003) to extract image-objects from an IKONOS sub-image of a landscape with a mix of forestry and agriculture and by Wang et al. (2004c) for mangrove mapping. Other forest applications are described by Herrera et al. (2004), who segment scanned aerial photographs with 3 m spatial resolution, and by de Kok et al. (2000). Koch et al. (2002, 2003) use eCognition for a segmentation based forest classification using a combination of Landsat ETM+ and IRS pan (5.6 m resolution). They conclude that this is a suitable method for the classification of forest types but that some information is lost due to the generalisation entailed by the treatment of larger objects as a whole. Wang et al. (2004c) also point out that, while segmentation and object-based processing reduce within-class variabilities and increase the spectral separability of the classes, there is the risk of incorporating pixels from different classes into one object primitive, resulting in misclassifications. This 'mixed object' effect could not be avoided in their attempts to separate different mangrove types.

Possible per-segment (object-oriented) classification methods are discussed in chapter 2.6.

2.5 Multi-Source Data Integration and GIS in Vegetation Mapping

Advances in space and computer technology during the last decades and the increased availability of digital geographic information about the Earth's surface entail that in more and more cases, digital land cover classification is based not just on multispectral data from one sensor, but on data sets including data from different sources. The integration of complementary data in order to enhance the information which is extracted from a data set can involve different combinations of data and different integration methods. Possible data combinations include the integration of different kinds of remote sensing data (multispectral, panchromatic, textural), from one or multiple sensors, or the integration of remote sensing data with ancillary geographical data like digital elevation model (DEM) data with the help of GIS (geographical information system) techniques.

Most authors integrate multispectral and textural data at the pixel level by including the texture features as additional channels in the data set (e.g. Treitz & Howarth 2000b). Various methods are

used for the integration of multi-sensor remotely sensed data. They can be fused at the pixel level (e.g. sharpening a multispectral image with a higher resolution panchromatic image), at the feature or object level (e.g. after segmentation) and at the decision level (after first classifying them separately) (Pohl & van Genderen 1998). Especially the data integration at the pixel level requires that the data are precisely co-registered to each other. Scarth et al. (2001) use local variance derived from high resolution video data to optimise a geometric-optical model applied to Landsat TM data for the estimation of forest structure parameters. Kiema (2002) combines SPOT panchromatic, SPOT-derived texture data and multispectral Landsat TM data by simply adding channels, having resampled the Landsat data to 10 m pixel size. Amarsaikhan & Douglas (2004) integrate SPOT XS multispectral optical and SAR data creating new, fused image channels through band ratioing, intensity-hue-saturation transformation, among other techniques. For the integration of remotely sensed data, pixel-based methods like the additional channel concept and the channel fusion for enhancing the resolution of a multispectral image are most common.

Apart from the integration of remotely sensed data and data layers that are directly derived from them (e.g. texture parameters or vegetation indices) there are also other sources of geographic information which can be included in the classification process in the form of ancillary data. Ancillary data can be defined as non-remotely-sensed data, collected independently and used to assist in the analysis or classification of remotely sensed data (Campbell 1996). They may consist of digital elevation data or digitised soil and geological maps, among others. Not all types of ancillary data that may be available for an area are compatible with the remotely sensed data. The additional information should only be used if it is significant for the distribution of the classes which are to be mapped. It must be possible to integrate all the data in a GIS setting, so the ancillary data must be in digital form and in the same reference system, as well as accurately registered to the other data layers. They should also be compatible with respect to scale (level of detail). Some ancillary data derived from thematic maps contain discrete classes, contrary to the continuous nature of the remotely sensed data. In addition, the map derived information may not be metric (quantitative) at all but nominal / qualitative (e.g. soil types). These differences in data types limit the methical possibilities of data integration.

Topographic (DEM derived) data have been used to improve vegetation mapping efforts based on satellite imagery from the early times of satellite remote sensing (e.g. Strahler et al. 1978). The topographic variables elevation, slope and aspect can be seen as surrogates for climatic data such as temperature and moisture conditions (Woodcock et al. 2002). The natural vegetation of an area is directly influenced by the local moisture regime, temperature regime, nutrient availability and solar radiation. These environmental gradients are in turn determined by climate, topography and geology (Franklin 1995). While climatic variables are most important for determining the vegetation patterns of large areas, at landscape scales, the topography modifies the macroclimatic variables. The elevation has an effect on temperature and precipitation and can thus correspond to a vertical

zonation of vegetation. Aspect and slope determine the local insolation regime and slope is also related to hydrology and thus soil moisture. Other topographic variables which can be derived from DEMs and which are related to vegetation patterns include the slope curvature and the specific catchment area (Florinsky 1998, Franklin 1995). It is possible to model the potential vegetation using topographic variables (Felicísimo et al. 2002) and / or other ancillary data, and then to use remotely sensed data only to differentiate between natural vegetation (e.g. forest) on the one hand and disturbed areas or land use types on the other hand. For the purpose of improved vegetation mapping however, it is only practical to use such GIS methods for stratifying the study area into areas of potential vegetation if sufficiently accurate and detailed maps of the controlling environmental variables (or their surrogates) are available or if these variables are easier to map than the vegetation itself (Franklin 1995). Modelling vegetation distributions with GIS also requires extensive knowledge about the relationships between the known environmental variables and the local vegetation types.

There are three stages at which ancillary environmental data can be incorporated with the satellite imagery for vegetation classification (Hutchinson 1982):

- before classification for a stratification of the study area;
- during classification (inclusion as additional variables in a classification or for modifying prior probabilities in a maximum likelihood classification);
- after classification for post-classification sorting.

Stratification divides the study area into smaller areas or strata. Its first aim is to reduce the number of potential classes in any sub-area, making it possible to assign different classes to spectrally similar units depending on which stratum they belong to. The second aim is to reduce the variation within strata, considering that the spectral characteristics of one informational class tend to vary over distance, for example because of varying atmospheric conditions or different substrate (Hutchinson 1982). This is a deterministic approach requiring the creation of strata masks using the ancillary data (Florinsky 1998). The approach is most promising for large study areas. Helmer et al. (2002) stratified the area of Costa Rica into 10 sub-areas based on geoclimatic and geologic maps, before mapping vegetation formations using Landsat TM data. This approach helped in the mapping of forest formations, but the abrupt boundaries between strata also resulted in some misclassifications where the real transition between vegetation formations was more gradual and patchy than predicted by the strata boundaries. Stratification has to be conducted with care, because incorrect stratification criteria will prevent correct classification later on. The separate classification of the strata requires an adequate number of training samples for every class in every sub-area. Inconsistent training sets for classes in neighbouring strata may result in class boundary offsets in the final merged map (Hutchinson 1982).

When including ancillary data in the classification itself, the most straightforward approach is to use the ancillary data as additional variables in a multivariate classification. The new data are simply combined with the remotely sensed data as additional channels. This technique has been called the 'logical channel' or 'stacked vector' approach (e.g. Benediktsson et al. 1990). Dymond & Johnson (2002) use this probabilistic approach for the combination of modelled biophysical data and Landsat TM spectral data, to improve the classification of Canadian mountain forest. Treitz & Howarth (2000b) use terrain variables successfully as additional channels in a linear discriminant analysis. In contrast, Arora & Mathur (2001) find that the inclusion of slope and aspect as additional channels in a maximum likelihood classification (MLC) did not improve the average accuracy in their land cover classification. The additional channel method can introduce new problems in the classification (Florinsky 1998), because of different data types and the difficulty of obtaining sufficient samples to represent the range of all variables for each class. There is the danger that the classification accuracy is decreased for land cover classes which are independent of the additional variables used. These classes may thus need to be treated separately during the classification (Strahler et al. 1978). Another way to include ancillary information during the classification is to modify the prior probabilities in a maximum likelihood classification depending on the ancillary data (Strahler 1980), but this approach has not been widely adopted. Liu et al. (2002b) integrate satellite and ancillary data by assigning conditional probabilities to all data layers in a rule-based expert system classifier using Bayesian probability reasoning.

Both the stacked-vector approach and the prior probabilities method require very intensive sampling to adequately characterise the relationship between the classes and both the spectral and the ancillary data (Hutchinson 1982). Sampling costs can be the limiting factor in studies of tropical mountain forests with difficult access, which may rule out the use of these methods in some cases.

An alternative to these probabilistic approaches are 'artificial neural network' (machine learning) approaches (see chapter 2.6). Using ancillary data as additional input for neural network classifications has the advantage that these systems are non-parametric so that input data can be of any type (Florinsky 1998). This can be a more suitable method for the inclusion of terrain parameters in a classification than the stacked vector approach in MLC (Arora & Mathur 2001), at least if the appropriate neural network models are used and if the training samples are representative (Benediktsson et al. 1990).

After classification, ancillary variables can be used to divide a spectral class into different informational classes according to e.g. elevation or slope (Hutchinson 1982). The sorting technique is derived from GIS overlay analysis. Post-classification sorting, like stratification, is a deterministic approach and requires an understanding of the relationship between the classes of interest and the ancillary data for the formulation of sorting rules. The method can be used to resolve confusion between spectral classes using elevation data (Liu et al. 2002a, Colby & Keating

1998), other topographic variables (Vogelmann et al. 1998, Hutchinson 1982) or other GIS layers providing information about soil types, the location of water bodies, or other features (Sader et al. 1995). Post-classification sorting is a simple, inexpensive way to make use of ancillary data and expert knowledge. It has the additional advantage that, being applied after the classification, it can be confined to deal with 'problem classes' only, and errors made in the construction of sorting rules can be easily undone.

Some authors integrate ancillary data at several stages: Ma et al. (2001) use topographic data both as additional channels during the classification and for post-classification sorting. Ehlers et al. (2003) use a digital surface model for a stratification of their image, as part of a stacked vector during classification and also during post-processing.

2.6 Classification Issues

The partitioning of local observations into classes is a prerequisite for the creation of land cover maps. Digital image classification is the process of allocating image primitives (pixels or groups of pixels) to classes, usually according to their values in several spectral bands (Campbell 1996). Additional (non-spectral) data layers or contextual information can also be used in the classification process. Unsupervised classification methods are used to identify natural homogeneous groups (clusters) within the data. Only afterwards are informational labels assigned to the resulting groups or clusters. These methods have the disadvantage that the interpreter cannot influence the identity and extent of the resulting categories, which may then not correspond to the informational classes of interest. Supervised classification, by contrast, makes use of ground knowledge introduced through training areas (samples of known class identity) and extends it to the entire image with statistical methods (Lobo 1997). Each image primitive is characterised by n observations (the values in n data channels). The training samples are vectors in an n-dimensional space (the feature space). A supervised classifier uses the distribution of the training samples for each class to estimate density functions in the feature space and to divide the space into class regions (Fukunaga 1990).

A basic step in supervised image classification and mapping is the design of a realistic classification scheme, i.e. the definition of discrete informational land cover units which are separable with the available data (Cingolani et al. 2004). Informational classes determined by the interpreter or required by the prospective map user may not correspond to consistent classes in the data. It may be necessary to subdivide an informational class into several subclasses if it belongs to separate clusters in feature space or to merge several informational classes if they are not separable with the data used.

Feature selection and class separability

A second basic step in image classification and mapping is the selection of an appropriate feature combination from the available data set (which may consist of spectral bands, textural features and other data layers) to be used for the separation of the classes. This step is not always necessary if only a small number of channels is available for classification. But having integrated a number of spectral bands and texture features, and perhaps also ancillary data like topographical variables as additional channels, the resulting vector can be too large for the classification algorithm to deal with. The data stack may also contain redundant or unhelpful data layers, making the classification unnecessarily slow. A reduced number of data layers may still contain sufficient information for the classification. Discarding some of the channels can even lead to improved classification results if the classifier used is impaired by high dimensionality data (see discussion of the maximum likelihood classification below) or by the statistical properties of some of the data layers (Peddle 1993) or if the discarded data do not contain information helpful for the separation of the classes.

A simple method to reduce the number of channels before classification is to look at the correlation between pairs of data layers and, in the case of high correlation coefficients, to discard channels which are regarded as redundant. Liu et al. (2002b) use this method to select data layers with small correlation coefficients out of a number of spectral and topographical features. Especially the large number of texture features which can be generated from the spectral data (see chapter 2.3) require the choice of a subset of features. One way to approach this task is correlation analysis. Gong et al. (1992), having generated ten GLCM texture features with partially very high correlation coefficients, choose three relatively little correlated ones for later combination with other features and classification. Correlation analysis is also employed by Narasimha Rao et al. (2002) as a first step during the selection of texture features.

To simply find a set of channels which are not closely related to each other is not always a sufficient criterion for feature selection. If it is the objective to find an optimal subset of m out of n features (channels) for the discrimination of a given set of classes, one needs to apply feature selection methods based on separability measures, e.g. class divergence. The task is to determine the set of m channels which maximises the divergence between the classes for this reduced number of channels. The pairwise class divergence is a measure of statistical separation between two classes as characterised by the means and covariance matrices of the class training samples (Hill & Foody 1994). The class divergence can be calculated relatively easily for Gaussian distributions (Landgrebe 2003). With increasing statistical separability between two classes, the divergence increases without bound. Classification accuracy, by contrast, cannot exceed 100 %. The transformed divergence was developed as a divergence measure which also reaches an asymptote (Singh 1987). It is based on a transformation of the divergence (using the exponent) and limits the transformed divergence to a range of 0 to 2 with larger increments for differences between small

divergence values. A divergence measure for not only two classes but all the pairs of classes can be calculated using averaging methods. Average interclass divergence is simply the average of the divergence for each pair of classes. This leads to a dominance of class pairs with very high divergence in the average value. Using the average transformed divergence instead reduces the dominance of class pairs with the highest divergence and helps to select the features which are best at differentiating even between relatively similar classes.

Dikshit & Roy (1996) use the average transformed divergence as a measure of the relative capability of feature sets with and without textural data for the discrimination of class pairs. Chen et al. (2004) use transformed divergence for the selection of texture features. Singh (1987) and Hill & Foody (1994) use matrices of pairwise transformed divergence to study the separability of tropical forest classes with the help of Landsat data.

Several authors have noted that there is no close correspondence between the average transformed divergence for a feature set and the accuracy achieved when they classified their image using this feature set (Chen et al. 2004, Gong et al. 1992). One of the reasons for that is the fact that separability measures are usually calculated from the training samples only. Therefore they cannot be expected to predict the exact classification accuracy for the whole image, if the training samples are not exactly representative of the whole image including areas of potential edge effects. Also, there is generally no one-to-one relationship between separability measures and classification accuracy. Instead, in the best case, a given value of a separability measure can determine a certain range of possible classification accuracies for the samples under examination (Landgrebe 2003). Separability indices are thus no linear predictors of classification results, but they do give an indication for the potential of a certain set of data layers to discriminate between the classes as represented by their class signatures.

Another criterion for class separability is the Bhattacharyya distance. Like the divergence and transformed divergence, the Bhattacharyya distance in its common form is calculated from the class means and covariance matrices assuming normal distributions (Verbeke et al. 2004). It is possible to derive error bounds (upper and lower bounds on the probability of correct classification) for the Bhattacharyya distance and the related Jeffries-Matusita distance measure (Landgrebe 2003, Fukunaga 1990). The Bhattacharyya distance is recommended by Landgrebe (2003) as having a close relationship with the probability of correct classification. Wang et al. (2004c) use the Bhattacharyya distance to compare the class separability at the pixel level with the separability at the object level after segmentation with different scale parameters (using the mean spectral values of the resulting object in the separability calculation).

Comparing several separability measures, Gong et al. (1992) found that Jeffries-Matusita and average transformed divergence performed similarly in the feature selection; and Treitz and

Howarth (2000b) found that in their case study, the Jeffries-Matusita distance and transformed divergence were better indicators for classification success than Bhattacharyya distance and simple divergence.

Benediktsson et al. (1990) do not apply the above mentioned separability measures for a case of multisource data classification including topographic data, because the estimation of separability with a Gaussian assumption requires the computation of covariance matrices, and the fact that class-specific topographic data sometimes have very little variation can prevent the computation of a covariance matrix. It is difficult to compute separability measures without the Gaussian assumption.

Maximum likelihood classification

Maximum likelihood classification (MLC) is the most widespread supervised classification technique in remote sensing. It has been widely used for the digital classification of satellite imagery since the 1970s (Strahler 1980). The term 'maximum likelihood classifier' is used here in the sense of the quadratic (Gaussian) classifier only. This is a statistical classifier which calculates the probability that an observation (pixel vector) belongs to a certain class according to a multivariate normal (Gaussian) density function. This involves a calculation of the distance between the observation and the mean vector of the class in feature space, corrected for the covariance of the class (modified Mahalanobis distance) (Liu et al. 2002b, Strahler 1980). The training samples are used to estimate the mean vector and covariance matrix for each class. The probability functions are calculated for all classes and the pixel is assigned to the class for which it has the maximum likelihood of membership. The class space in feature space can be limited by a so called 'Gaussian threshold', which is the radius (in standard deviation units) of a hyperellipsoid around the mean of the class in feature space (PCI 2001). In this case, observations which do not lie within the hyperellipsoid of any class are assigned to a 'null class'.

MLC assumes that the training data statistics are Gaussian in nature. If it is true that the class probability density functions are Gaussian, MLC is the optimal classifier which minimises the overall probability of error (Liu et al. 2002b). But experience shows that the maximum likelihood classifier is rather robust (Gong et al. 1992). It can tolerate moderate violations of its underlying assumptions and still yield classification results which may be superior to those of classifiers which do not employ the Gaussian model. Benediktsson et al. (1990) found that even for data which were not all normally distributed, the MLC yielded a better classification result than a minimum Euclidian distance classifier.

For a statistical classifier using the multivariate Gaussian model, the computing cost grows as the square of the number of features (channels used) (Benediktsson et al. 1990). The required number of training samples to estimate the class statistics for a Gaussian (quadratic) classifier is also related to the square of the number of features (Fukunaga 1990). This gives rise to the 'Hughes effect': For

a finite number of training samples, the classification accuracy rises at first with the number of features (or measurement complexity), but then it reaches a maximum and starts to decrease when more features are added. While the class separability is always higher for higher dimensionality data (more measurements), the accuracy of the statistics estimation with a given number of training samples decreases when the dimensionality becomes too high, and at some point this leads to a lower classification accuracy in spite of better theoretical class separability (Landgrebe 2003).

Hay et al. (1996) used a maximum of seven channels for the MLC because they feared a reduction of classification accuracy for higher dimension data sets. Peddle (1993) found that MCL was not a good classification technique for multi-source data sets (consisting of spectral, textural and DEM extracted data). The accuracies of classifications including the texture and / or the DEM derived data were lower than of those involving only the three spectral channels, except for the case when only the elevation was added as a fourth channel. The usability of MLC is limited for data sets with many channels, with data which are not normally distributed or with multi-source data with differing scales of measurement (Arora & Mathur 2001, Peddle 1993).

The high spatial resolution satellite data which are available today tend to exhibit increased within-class variability compared to the medium resolution satellite data which are traditionally classified with MLC. This means that the volume of feature space occupied by each class is expanded, leading to increased possibilities of class overlap in feature space. (Qiu & Jensen 2004). Statistical approaches which work satisfactorily for relatively low spatial resolution imagery with a limited number of channels may not be suitable for the high resolution and / or high dimensionality data sets which are increasingly used in digital land cover classifications. Moreover, ancillary data included in a classification are in most cases unlikely to conform to the assumptions of MLC.

Alternative (non-parametric) classification methods

Non-parametric classifiers are distribution-free, i.e. they do not make any assumptions about the mathematical form of the density functions (Fukunaga 1990).

The k-nearest-neighbour classifier (k-NN) is a simple and robust non-parametric classification method (Debeir et al. 2002). It works by extending a local region around the vector of an unclassified image primitive until its kth nearest neighbour among the training sample vectors is found (according to the Euclidian distance in feature space). The class labels of these k nearest neighbours are determined and the unclassified vector is assigned to the majority class of its k nearest neighbours (Landgrebe 2003). The k-NN classifier is suitable for high dimensionality data. However, the number of samples which are needed becomes very large for a large number of channels. Fukunaga (1990) shows that for normal distributions and k=5, 150 samples are needed for 8 channels, but for 16 channels the number of samples needed is already 34,000. Larger values of k are recommended for data with high variance (PCI 2001). Debeir et al. (2002) use a 5-NN classifier

for the classification of a large data set containing spectral, textural and ancillary data. Tuominen & Pekkarinen (2005) use a k-NN classifier with k=5 for the classification of a large data set derived from orthophotos (three spectral channels, channel ratios, texture features), aiming for an estimation of forest attributes. They find that for a combination of more than 10 features, the accuracy is not significantly increased any more. Collins et al. (2004) successfully classify a stacked vector data set consisting of Landsat multispectral channels, topographic data (elevation, slope and aspect) and modelled environmental gradients using a k-NN classifier, also with k=5.

Another non-parametric classifier is the Artificial Neural Networks (ANN) classifier. Artificial neural networks are computational systems which imitate biological systems of information processing (artificial intelligence). They have been increasingly employed in remote sensing research since the 1990s (Franklin 1995, Sugumaran 2001). Neural networks are networks of interconnected artificial neurons (processing elements, also called nodes). The nodes are organised in layers (one input layer, usually one or several hidden layers, one output layer). Each node in one layer is connected to the nodes in the adjoining layers. The nodes in the input layer receive data from outside the network (e.g. one input node receiving the information from one remote sensing data channel) and pass on an output to the nodes in the next layer. The nodes in the other layers receive inputs from the nodes in the preceding layer and produce one output which they pass on. The output is produced by adding the weighted input from the nodes in the preceding layer and putting the sum through an activation function. In many cases, this is the sigmoid function, which reaches one when the input sum goes to infinity and zero when the input sum goes to minus infinity. The output of the nodes in the output layer indicates the classification result (Paola & Schowengerdt 1995, PCI 2001).

All the connections between the nodes carry weights which are set to random values before the network is trained. Training consists of finding the appropriate weights through an adaptive training procedure so that the output error is minimised. There are several learning algorithms for neural networks. In remote sensing and image classification, the most widely used learning algorithm is a supervised algorithm called back-propagation (Arora & Mathur 2001), employing the 'generalised delta rule'. During the first phase of training a back-propagation network, the training sample vectors (with known classes / target outputs) are used as input for the network and propagated forward to compute the output values for each output node. The error between the actual and desired output is calculated. (In the case where each output node represents one class, the desired output is a high value, e.g. 0.9, for the node of the correct class, and a low value, e.g. 0.1, for the other nodes.) The second training phase is a backward pass from the output nodes through the network, during which the weights are changed according to the learning rate and the error signal passed backwards to each node (Benediktsson et al. 1990). This process (entering the training data, calculating the output error, adjusting the weights of the connections) is repeated many times (Foody 2004) until some condition is fulfilled, preferably until the network has stabilised so that the

error and the weight changes per cycle have become very small (iterative training). Once the network is trained, i.e. appropriate weights are found and fixed, all pixel vectors are fed into the network and classified.

ANN classification has the advantage that it makes no assumptions about the data set, so that different kinds of data can be used as input. Typically, all input channels are scaled to a common range (usually values between 0 and 1 like the node output values) before training and classification. Benediktsson et al. (1990) conclude that neural networks need to be trained with carefully selected representative samples. But according to Paola & Schowengerdt (1995) and Qiu & Jensen (2004), ANN classifiers are robust to noise in the training data and able to generalise.

It is often seen as a disadvantage of neural networks that they operate as a 'black box' (Franklin 1995, Qiu & Jensen 2004) without the capability to explain the relationship between input and output. Due to their heuristic nature and the element of random variations in the results (because the weights of the connections are randomised before training), performance prediction and the analysis of results are difficult. Another disadvantage is that iterative training requires much more computation than parametric discriminant functions (Landgrebe 2003, Paola & Schowengerdt 1995). Once the network is trained, however, the classification process as such is fast (Pal & Pal 1993).

Kimes et al. (1999) successfully employed neural networks to differentiate between primary and secondary tropical forest and less successfully for mapping secondary forest age using SPOT HRV spectral and textural data. Linderman et al. (2004) use ANN to map understorey bamboo from Landsat data. Comparing ANN and MLC, Paola & Schowengerdt (1995) found that maps produced from Landsat TM data were similar for both methods, but ANN was better at classifying mixed pixels and for one image produced a higher overall accuracy. Sugumaran (2001), classifying tropical forest and plantation types using IRS-LISS-III channels 1-3 (23.5 m resolution), achieved somewhat better results with ANN than MLC. Arora & Mathur (2001) find ANN superior for the multi-source classification of five broad land cover classes in a Himalayan region (using medium resolution spectral data and slope and aspect maps). Liu et al. (2002b) also achieve better results with ANN than with MLC for a land cover classification with medium resolution multispectral and ancillary GIS data layers. Most studies find ANN classifications result in higher accuracy than MLC, but that it takes a long time to train the neural networks (Sunar Erbek et al. 2004).

To my knowledge, neural networks have not yet been used for tropical forest classification with high spatial resolution satellite data, but it does seem to be a promising approach especially for data sets which combine satellite and ancillary data.

Classification of segmented images (object-based classification)

In a segmented image (see chapter 2.4), each segment (image object primitive) is characterised by an integrated measurement vector, consisting, in the most basic case, of the mean values (in *n* spectral channels) of the pixels forming the segment. Using the mean spectral values of the image object primitives increases the signal-to-noise ratio (Baatz et al. 2002) and reduces the spectral overlap between classes, especially in the case of high resolution data. It is possible to use image segmentation without per-object classification. Image segmentation and the calculation of per-segment mean values can be simply used as a means of reducing the within-class variability while still subsequently using pixel-based training and classification methods, e.g. MLC (Hill 1999).

In most cases, however, it is advantageous to classify a segmented image using image object primitives as the basic processing units (object-based classification). One of the advantages is that object-based image processing is compatible with vector-based GIS. In principle, image object primitives with their measurement vectors can be classified with the same methods as single pixels. The main difference is that there are fewer units to be classified if not every single pixel needs to be handled, which helps to increase the classification speed. On the other hand, the possible number of training samples is also reduced if objects instead of pixels are used as training samples. This can mean that it is not possible to find enough training fields to produce a good estimate of the class covariance matrices, especially for land cover classes which cover only a small percentage of a study are (Lobo 1997). This can preclude the successful application of statistical classifiers like MLC.

In order to avoid the calculation of covariance matrices, non-parametric classification methods are often used in object-oriented image processing. Ma et al. (2001) use a nearest neighbour algorithm to assign classes to regions. The software eCognition also supports nearest neighbour classification for the classification of image object primitives in a multidimensional feature space. Here, each object is assigned to the class of its nearest neighbour (closest sample object) in feature space. This technique works with a small number of samples as long as the number of features used is also small (Baatz et al. 2002). De Kok et al. (2000) use eCognition for an object-oriented forest classification. Object-oriented image processing makes it possible to use features beyond the layer values as such, like object shape or the relationship to other objects or within-object texture (i.e. texture features which do not depend on a fixed window size). The hierarchical network of image objects of different scales, which can be constructed after multiresolution segmentation with eCognition, can be used to classify objects at one level based on the classification of their sub-objects or super-objects (Mitri & Gitas 2004).

'Soft' or fuzzy classification versus 'hard' classification

Conventional 'hard' supervised classification techniques assume that the classes are exhaustively defined and mutually exclusive (Foody 2004), so that each pixel belongs to one and only one of the pre-defined training classes. However, in the reality of land cover classification, and in particular in the classification of natural vegetation with remote sensing, there are several sources of uncertainty (ambiguity and boundary vagueness).

Firstly, there are ambiguities on the ground. Natural vegetation often does not occur in discrete spatial and thematic units. Instead, it may vary continuously according to environmental gradients, leading to gradual transitions between the defined classes (vegetation types) with broad areas of high ambiguity in the transition zones. Another source of uncertainty is the fragmentation of land cover types or environmental heterogeneity, i.e. the inclusion of small areas of one land cover type in another type (Brown 1998). Even where there is a discrete boundary between vegetation types, due to abrupt spatial changes in environmental factors or due to the disturbance or land use history, individual interpreters might still draw the boundary lines slightly differently (depending on the level of generalisation, among other things). In addition, there are temporal continua, e.g. a secondary succession starting with a mainly herbaceous land cover, which develops first into a shrub-dominated land cover, then into a secondary forest and finally a mature forest (Brondizio et al. 1996). This entails that there are stages in the succession when the land cover is in a transitional stage between the defined land cover types of a classification scheme. Different classes may contain common elements (two forest types could for example share a tree species or the same kind of understorey vegetation). If such similar classes occur adjacent to each other, the boundary between them will be more vague than for classes with larger differences in their definitions. Numerical thresholds in the definition of land cover classes (like percent crown cover, or trees being defined as woody plants greater than 5 m in height) are idealisations of the natural world (Baatz et al. 2002). If we define open forest as forest with a crown cover below 60 % and then encounter a forest area with around 60 % crown cover, it will be impossible to determine a definite boundary line between open and closed forest which all interpreters would exactly agree on.

Secondly, there are inherent uncertainties in the remotely sensed data which impede a direct, unambiguous link between the data and the type of the land cover. The same land cover type can be connected to different observations in different images (or even in different parts of the same image) depending on factors like illumination (sun-sensor-target geometry), season or weather. The sensor measurements have a limited radiometric, spectral and spatial resolution. The limited spatial resolution leads to the possibility of class mixtures within one pixel. Limits in the spatial, spectral and radiometric resolution (signal to noise ratio) of the sensor, together with spectral similarities between different land cover types, can cause it to be impossible to differentiate some land cover types with the measurements provided by the sensor (Baatz et al. 2002).

Due to all these factors, it is often not possible to assign every image primitive to exactly one correct class, even if the data processing methods, the training data and the classifier used are all optimal. Moreover, sometimes it would indeed be more appropriate to assign an image primitive partially to several classes, for example if it is a mixed pixel, or if the land cover (represented by the measurement) is in a transitional zone or a transitional stage between the pre-defined classes.

In the object-oriented (GIS) context, two types of uncertainty are distinguished: attribute ambiguity (uncertainty about the thematic class to which objects or image primitives belong) and spatial vagueness, i.e. uncertainty about the location of object boundaries (Cheng et al. 2001). In a raster-based classification, both types are closely interlinked (Zhang & Stuart 2001). Attribute ambiguity – as far as it is due to the similarity of adjacent land cover types, gradual transitions between land cover types or uncertainty in labelling mixed pixels at class borders – leads to uncertainty about the location of boundaries between classes. Ambiguity tends to decrease with distance from boundaries (Brown 1998).

Soft classifiers, in contrast to hard (or 'crisp') classifiers, are not limited to labelling one class as true and all others as false. Fuzzy classification, based on fuzzy set theory (originally introduced in 1965 by Zadeh, cited in Cheng 2002 and Ricotta 2004), takes uncertainty into account by permitting partial membership to a class (set). Every image primitive is assigned a membership value in the range of 0 and 1 to every class, with 0 denoting no membership and 1 denoting certain membership. These values denote possibilities, not probabilities, so the values for all classes of one location need not sum to 1. Another approach to handle uncertainty is rough classification, where image primitives can be assigned three possible values for each class: not a member, maybe a member or certainly a member (Ahlqvist et al. 2000). Both approaches allow for overlaps between classes, i.e. image primitives belonging to more than one class simultaneously.

The eCognition software produces a fuzzy output with its object-oriented classification. If the nearest neighbour classification is used, values in the range of 0 to 1 are assigned to every image object for every class, according to the distance in feature space to the nearest sample objects of each class. It is also possible to use fuzzy conditions for class membership (fuzzy logic) in eCognition (Baatz et al. 2002). Soft classifications can also be produced by 'softening' the output of 'hard' classifiers (Woodcock & Gopal 2000). In MLC, instead of only assigning a pixel to the class of maximum likelihood in a binary decision, the next most likely classes (and possibly their probability functions) can also be retained in additional output channels, or the *a posteriori* class probability can be calculated and used as a measure of the relative strength of class membership (Paola & Schowengerdt 1995, Palubinskas et al. 1995, Ricotta 2004). In ANN classifications, the output values (between 0 and 1) of all output nodes (representing the classes) can also be used to produce a fuzzy classification output (Paola & Schowengerdt 1995).

Nevertheless, for the production of a vegetation map, it is usually seen as a practical necessity to classify the vegetation into a number of discrete vegetation types and to depict the class areas on the map with discrete boundaries. (Although there are some cartographic approaches like 'epsilon bands' where uncertain boundaries or transition zones are represented by more or less broad boundary lines or other symbols.) Even the results of soft classifiers are usually 'defuzzified' to produce standard land cover maps showing just the most likely class for every point (instead of a separate map sheet for every class, showing its probability or membership distribution over the whole area). The primary map output for display will usually be such a 'hard' classification, but geographical information systems could store fuzzy information as additional attribute information.

2.7 Considerations for the Assessment of Classification Accuracy

Thematic maps resulting from the classification of remotely sensed data should be accompanied by information about their accuracy, so that the user can estimate their reliability and applicability for the purpose at hand. Quantitative accuracy measures are also necessary to compare the relative accuracies resulting from different data processing methods.

Classification accuracy is assessed by measuring the agreement between the classified image and reference data which is assumed to be correct (Campbell 1996). Site specific reference data ('truth') may consist of another map, if there is already a high accuracy map with a compatible classification of the area, but usually the reference data consist of a number of sample points (or areas). The class of these testing points is identified on the ground, or through manual interpretation of high or very high resolution remotely sensed data. Neither method guaranties that the reference data are 100 % correct – even if the classes of the sample points are determined in the field, there may still be errors due to a time lag between the field work and the acquisition of the classified image, or due to a lack of positional accuracy. This means that the reference data usually represents only a 'relative truth' and errors in the reference data, or in the registration between reference and classified image, will negatively influence the accuracy values which are calculated for satellite data classifications (Langford & Bell 1997).

The degree of agreement between a classified image and reference data can be measured using several methods. In remote sensing studies, the classification accuracy is usually determined using measures based on an error matrix (also called confusion matrix or contingency table). For n classes, this is an $n \times n$ array where the rows represent the classified data while the columns represent the reference data, or vice versa. A number of techniques can be used to derive statistical measures of accuracy from the error matrix. The most simple of these accuracy measures is the overall classification accuracy (percentage correct), which is computed by dividing the sum of the elements in the main diagonal of the matrix (representing the number of samples with complete agreement) by the total number of samples (Congalton 1991). Accuracies for individual classes can

also be computed from the error matrix. For each class, two accuracy values (producer's accuracy and user's accuracy) have to be distinguished. The producer's accuracy indicates the percentage of reference points of a certain class which have been assigned to the same class in the classified image. In other words, it measures the errors of omission. The user's accuracy indicates the percentage of pixels assigned to a certain class in the classification which agree with the reference data. This is equivalent to errors of commission.

The overall accuracy value (as described above) contains a proportion that is attributable to chance agreement between the two data sets. Cohen (1960) developed the Kappa coefficient as a measure of agreement which is adjusted for chance agreement. The expected chance agreement is calculated by adding the products of the row and column totals for each cell of the main diagonal of the error matrix, thus indirectly incorporating off-diagonal elements in the calculation (Congalton 1991). The Kappa index of agreement (KIA) is not as widespread as the overall accuracy (percentage correct) as a measure of classification accuracy in remote sensing studies, but it is also used by many authors (e.g. Dikshit & Roy 1996, Cingolani et al. 2004). Næsset (1996) describes the use of a weighted Kappa coefficient to evaluate the classification accuracy if all errors are not equally serious, i.e. if there are informational classes which are more closely related to each other than others.

The measured accuracy of a classification depends on many factors besides the classification method. As a classification becomes more detailed (containing more informational classes which are defined more precisely), the potential information content of the resulting map increases, but at the same time the opportunity for classification errors also increases (Campbell 1996). It is usually possible to increase the overall classification accuracy by decreasing the detail or precision of the classification, e.g. by mapping just one general forest class instead of differentiating between several forest types (Laba et al. 2002). However, this may result in highly accurate maps which do not provide the information necessary for a certain purpose (e.g. monitoring the distribution of a specific ecosystem type like cloud forest).

Mixed pixels and other edge effects can be a major source of classification errors, especially in a heterogeneous landscape. Many authors exclude areas near class boundaries from the accuracy assessment, with the argument that errors in these areas could be due to misregistration between the classified image and reference data. Some select testing pixels only in areas that clearly belong to the typical 'core' of classes, avoiding mixed pixels in border areas or areas of transition between defined classes (Hill 1999, Schlerf et al. 2003, Langford & Bell 1997). In some cases (where there are no independent testing points because of economic or temporal constraints) the same pixels that were already used to train the classifier are used for testing the accuracy (Strahler 1980). Such samples are obviously biased. All of these tactics lead to exaggerated accuracy values which do not represent the real classification accuracy for the whole image.

Both the sample size (number of samples) and the sampling method have to be considered for the creation of an appropriate testing set. The sample size determines the confidence intervals of the accuracy estimates (Brogaard & Ólafsdóttir 1997, Næsset 1996). If confident estimates of the classification accuracies for individual classes are required, the sample size needs to be larger than for an equally confident estimate of the overall accuracy. Larger samples than for a simple calculation of the overall accuracy are also needed in order to adequately represent the confusion between all pairs of classes in the error matrix (Congalton 1991). The sample size is restricted by the expense of determining the truth values for a large number of testing points (Congalton 1991, Langford & Bell 1997).

Sampling should be random in order to meet the statistical requirements of the Kappa analysis, among other statistical techniques that are based on the error matrix (Congalton 1991). However, pure random sampling may mean that classes of small extent fail to be represented in the sample, so stratified random sampling is frequently used in order to ensure that samples from all classes are included in the accuracy assessment (e.g. Helmer et al. 2002, Qiu & Jensen 2004). Stratified random sampling is also recommended by Congalton (1991). The prerequisite for a stratification of the sample is an existing map depicting the distribution of the class areas, so this is usually done after classification. Random sampling may lead to problems if the resulting samples are located in inaccessible areas where the true class cannot be determined. Because of this, some authors use cluster sampling, involving the selection of samples in previously known areas. Sampling of this type also helps to reduce the field access cost per sample. However, this will lead to a biased testing sample and an overestimation of the classification accuracy (Arora & Mathur 2001). Cluster sampling, and also systematic sampling, can produce spatially autocorrelated data. These sampling methods do not ensure that every individual in the population has an equal chance of being included in the sample, thus violating the requirements for inferential statistics (Næsset 1996, Brogaard & Ólafsdóttir 1997, Arora & Mathur 2001).

Even if the same testing sample is used, the measured accuracy still depends on whether the interpreters assigning the 'truth' values to the sampling locations do this independently (blindly) or whether they know the classification result to be assessed and can be influenced by it, giving the benefit of the doubt in ambiguous cases. The latter method can lead to a strong increase in the overall accuracy value (Langford & Bell 1997).

A per-pixel accuracy assessment with an error matrix is also possible for object-based classification results, and is used by some authors (e.g. Wang et al. 2004c). However, this way a single large misclassified object can have a disproportionate impact on the overall accuracy (de Kok et al. 2000). This is why in some cases reference objects are used instead of reference pixels, but this may again lead to the problem that not enough samples can be found (Lobo 1997). Per-segment accuracy assessment also does not address the question whether object borders match class borders – an

object primitive covering two land cover classes could be assigned to the majority class in both classification and reference, so no error for the misclassified part of the segment would be noted. There is not yet any generally accepted standard for automatic accuracy assessment of object-oriented classifications, and the accuracy is sometimes evaluated only visually (de Kok et al. 2000). The accuracy assessment of object-based classifications in the eCognition environment can be conducted on a pixel basis or on a segment basis (Baatz et al. 2002).

The accuracy assessment methods discussed above, which are based on the error matrix, assume a hard classification with mutually exclusive classes, where every classification decision is either completely correct or completely incorrect. As discussed at the end of chapter 2.6, this rigorous definition of accuracy is often not appropriate when land cover (natural vegetation) types are classified with remotely sensed data. Several approaches have been suggested to 'soften' accuracy assessments. When interpretations of aerial photographs are used to produce the reference data for a Landsat-based classification, some authors take account of the mixed pixel effect, and of uncertainties in locating each Landsat pixel on the aerial photographs, by recording several classes to be counted as 'correct' for each testing sample (Strahler 1980, Helmer et al. 2002). Gopal & Woodcock (1994, quoted in Woodcock & Gopal 2000) published a fuzzy accuracy assessment method for a hard classification with fuzzy ground truth. They use five linguistic grades to gradually differentiate between 'absolutely right' and 'absolutely wrong'. So for one testing point, the ground truth could for example pronounce one class 'absolutely right', and several other classes 'reasonable or acceptable'. This makes it possible to generate a number of accuracy measures beyond the 'hard' accuracy. For instance, in addition to the proportion of 'best choice' assignments, the proportion of at least 'acceptable' class assignments (the sum of 'absolutely right', 'good' and 'reasonable or acceptable' answers) can be calculated (Woodcock & Gopal 2000). This technique was adopted by Laba et al. (2002) and Ma et al. (2001). Ricotta (2004) proposes a method to evaluate the accuracy of fuzzy maps, where a fuzzy classification output is compared to the true fuzzy land cover. The weighted Kappa described by Næsset (1996) is also a way to 'soften' the accuracy assessment by taking account of the fact that not every classification error is equally serious.

On the whole, there are many variations in the methods which are used to measure classification accuracy. Some methods are more rigid, while others can lead to an overestimation of accuracy. So even if widely used accuracy measures, like overall accuracy or Kappa, are reported, they are not directly comparable without information about how they were derived.

3 Forest Resources and Land Cover in the Dominican Republic, with Special Regard to the Upper Catchment Area of the Río Yaque del Norte

3.1 The Environment

The Dominican Republic is a Caribbean country located between 17°30' N and 20° N, and 72° W and 68°20' W, sharing the island of Hispaniola with the Republic of Haiti. Hispaniola, one of the Greater Antilles, covers an area of 77480 km², the eastern two thirds of which – 49730 km² – belong to the Dominican Republic (figure 4).
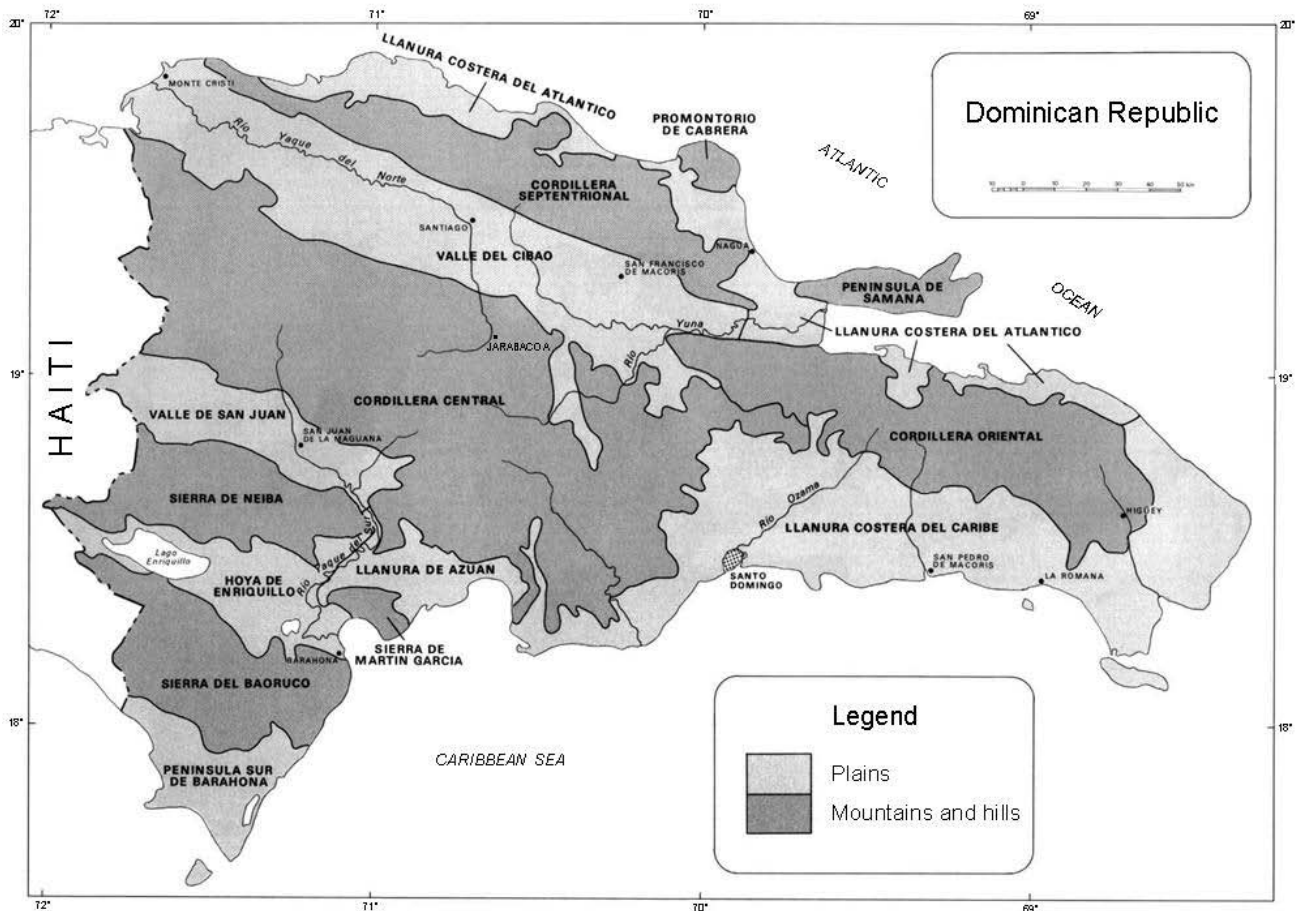
Figure 4: The Dominican Republic. Source: OAS (1984), modified.

The study area "Upper Catchment Area of the Río Yaque del Norte" (UCRYN) is located in the central Dominican Republic at 18°55' to 19°18' N and 70°30' to 70°58' W. The UCRYN covers approximately 785 km² upstream of the reservoir "Embalse Tavera" in the north-eastern Cordillera Central and belongs to the province of La Vega. The most detailed studies were done in a core test area of 20 km² located on the eastern border of the UCRYN, covering part of the Scientific Reserve Ebano Verde and the Río Jimenoa valley to its west (figure 5).
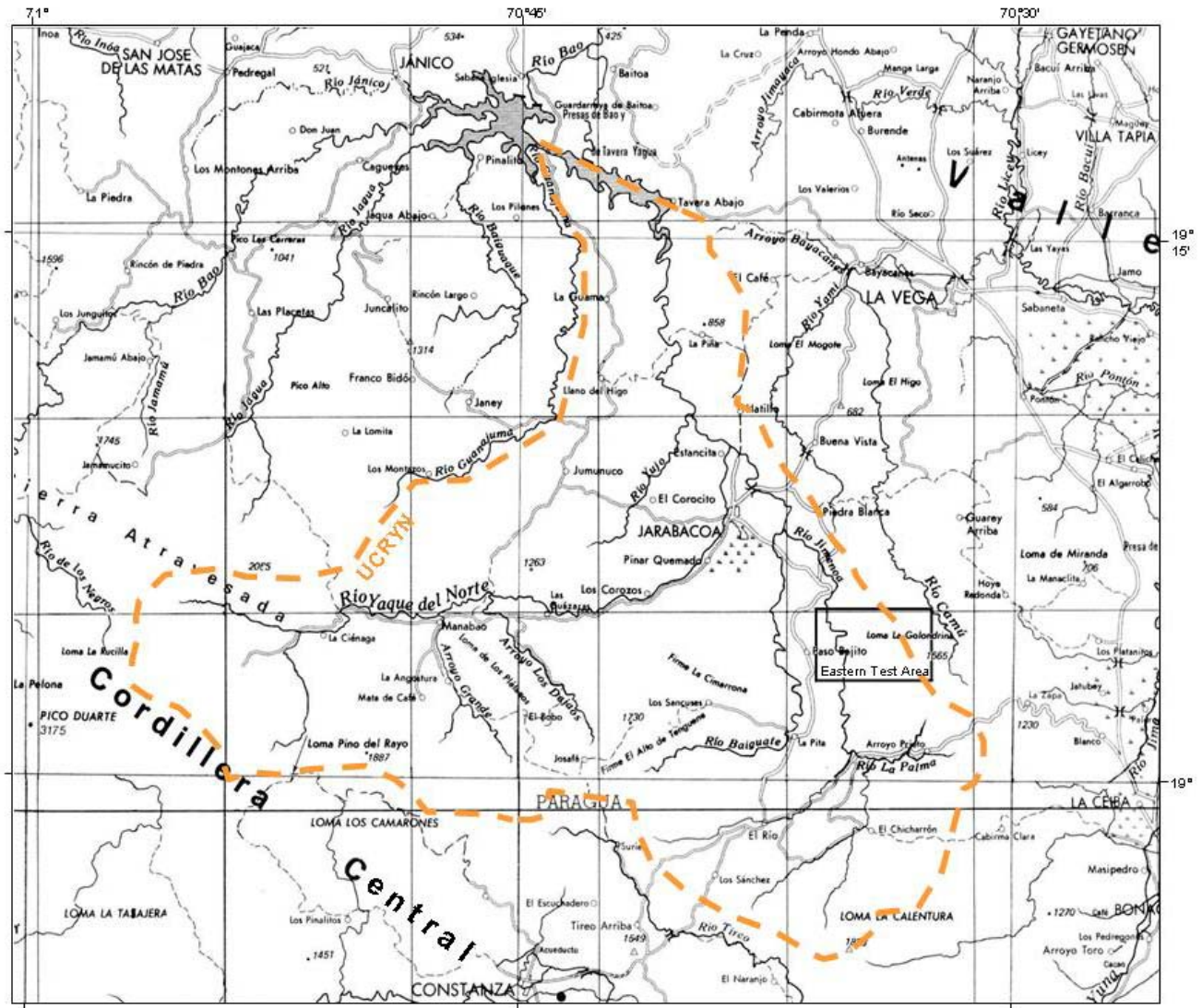
Figure 5: The study area "Upper Catchment Area of the Río Yaque del Norte" (UCRYN). Source: Mapa Geológico de la República Dominicana; Mapa de Localización de Muestras Paleontologicas 1:500,000, BGR 1991, modified.

3.1.1 Geology and Relief

Relief

There are four major mountain ranges in the Dominican Republic which run west-northwest to east-southeast and parallel to each other. From north to south these are the Cordillera Septentrional, the Cordillera Central, the Sierra de Neiba and the Sierra de Bahoruco. They are separated by basins, the Cibao Valley, the San Juan Valley, and the Enriquillo Basin. The less mountainous eastern part of the country consists of the Eastern Plains (Llanura Costera) and the Cordillera Oriental, a minor mountain range, to their north (figure 4).

The Cordillera Central is the highest of the Dominican Republic's mountain ranges. Its highest peak, the Pico Duarte (3175 m a.s.l.), is at the same time the highest mountain of the Caribbean. The Sierra de Bahoruco and the Sierra de Neiba, with the sub-sea-level depression of the Enriquillo Basin between them, both reach elevations of over 2000 m, while the Cordillera Septentrional has just one peak above 1000 m.

The upper catchment area of the Río Yaque del Norte has elevations between 320 m (Tavera reservoir) and 3038 m (Loma La Rucilla). The area is characterized by large and small valleys with steep slopes. Slopes of more than 40 % make up the majority of the UCRYN. The only extended area with low gradients is the valley around Jarabacoa.

The mountainous nature of the Dominican Republic and the whole island of Hispaniola is due to its position at a plate boundary zone and the resulting tectonic activities.

Geologic and tectonic development

Hispaniola is situated in the northern Caribbean plate boundary zone where the Caribbean plate meets the North America plate (Erikson et al. 1998). Since Jurassic time, convergent and transcurrent tectonics in this zone have led to the development of the Greater Antilles islands (Lewis & Draper 1990).

The core of the island of Hispaniola consists of Early Cretaceous to Eocene island arc terranes formed at a convergent plate boundary. During these times, phases of subduction and the associated island-arc plutonism, volcanism, and metamorphism (mainly in a submarine environment) alternated with phases of uplift, deformation and erosion (Mann et al. 1991a). The resulting metamorphic rocks can be found today in central and northern Hispaniola. In addition, there are several terranes of volcanic, volcaniclastic and associated sedimentary rocks of mainly Upper Cretaceous to Eocene age, and a fragment of a back-arc basin with marine sandstone, siltstone and limestone. Intrusive rocks were emplaced mainly in Central Hispaniola during episodes of magmatism until the Early Eocene (Kesler et al. 1991). To the south of the island, an oceanic plateau grew during Late Cretaceous time, with basalts, pelagic limestone and chert. Paleocene to early Miocene subsidence was accompanied by continued deep-sea carbonate sedimentation in this area (Lewis & Draper 1990).

In the Eocene, the island arc collided with the southern edge of the North America plate (Bahama carbonate platform), leading to uplift of the submerged arc and putting an end to island-arc volcanism and plutonism. The relative movement of the plates in the boundary region changed from convergent to mainly east-west strike-slip faulting, with the Caribbean plate moving east relative to the North America plate. In northern Hispaniola, Oligocene sedimentary basins developed within a strike-slip fault system at the edges of today's Cibao valley, resulting in the Tavera belt in the

northern foothills of the Cordillera Central and the El Mamey Belt of the Cordillera Septentrional (Dolan et al. 1991).

The oblique collision of the southern oceanic plateau with island-arc Hispaniola during Miocene time resulted in the suturing of the involved terranes and initiated the Miocene to recent transpressional phase of Hispaniola's tectonic history (Mann et al. 1991a). Uplift and erosion occured across Hispaniola. The southern oceanic plateau terrane was folded and emerged in the form of the southern limestone mountain ranges (Sierra de Bahoruco in the Dominican Republic). Under the conditions of oblique convergence in the northern Caribbean plate boundary zone, many terrane boundaries were reactivated as oblique-slip faults. Today's fault-bounded west-northwest striking mountain ranges with interjacent basins were formed. Three deep sedimentary basins developed and were filled with neogene clastic sediments: the Cibao, the San Juan-Azua, and the Enriquillo-Cul-de-Sac Basin. Left-lateral strike-slip faults, in accordance with the relative plate motion, bound the northern edge of the Cibao basin and transect the Enriquillo-Cul-de-Sac basin, while the margins of the San Juan and Enriquillo basins are bounded by thrust and reverse faults due to transpression (Mann et al. 1991b).

Earthquakes occurring in the Dominican Republic make it clear that the region is still tectonically active (Cross 1992), and rapid uplift and erosion of the mountain ranges in central and western Hispaniola are continuing (Mann et al. 1991b).

Regional geology of the upper catchment area of the Río Yaque del Norte

The UCRYN is situated in the north-eastern Cordillera Central, which is dominated by Cretaceous volcanic rocks with upper Cretaceous to Eocene granitoid intrusions (figure 6). To the south of the Guacara fault, the El Rio batholith has intruded into volcanic and volcaniclastic rocks of the Tireo formation. This large intrusion consists of unfoliated tonalite, a silicic coarse-grained intrusive rock (Kesler et al. 1991). The rocks of the Tireo Group which surround the batholith are of upper Cretaceous age. They comprise mainly vitric tuffs with intercalated sediments (mudstones, limestones), besides basaltic flows (for instance around the Pico Duarte) and more acidic rocks like quartz keratophyres (Lewis et al. 1991).

To the north of the Guacara fault, the Duarte Complex forms an extensive metamorphic belt, which is intruded by several tonalite plutons (Draper & Lewis 1991). In addition, there are smaller areas of hornblendite and diorite intrusive rocks. The Duarte Complex, which is probably of lower Cretaceous age, comprises greenschist, weakly metamorphosed subgreenschist and amphibolite metamorphic facies. Mafic metabasalts of the Duarte Complex dominate the area along the Río Yaque del Norte to the north of Jarabacoa, with some subgreenschist facies rocks further north. Amphibolites are developed in the proximity of the plutons. Only small parts of the UCRYN are taken up by the serpentinized peridotite which forms a belt at the north-eastern border of the Duarte

Complex. These rocks are very conspicuous for example in Landsat images, especially in the main part of the belt just outside the study area, because their ultramafic nature results in infertile soils and a different vegetation (pine forest) compared to the surrounding areas.

The northern boundary of the Duarte Complex is formed by the Hispaniola Fault Zone. This broad fault zone contains, in the area of the Tavera reservoir, Oligocene sedimentary rocks of the Tavera belt, namely conglomerate, mudstone, sandstone, and limestone (Dolan et al 1991).

Quarternary fluvial deposits cover the valley floors, especially where the valleys widen around Jarabacoa and in the area of Manabao.
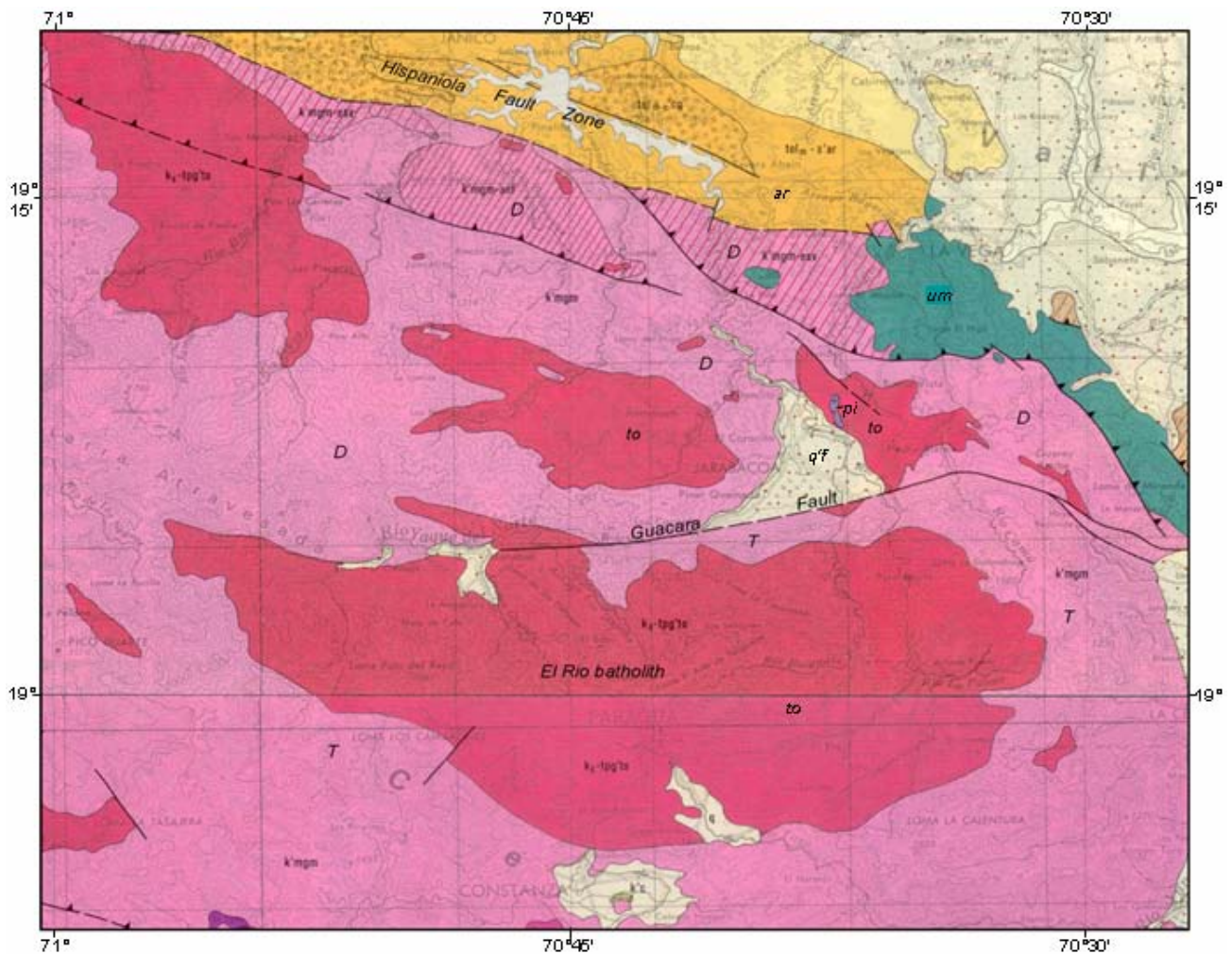
Figure 6: Geological map of the study area. D: Duarte Complex, T: Tireo Group, to: tonalites, um: ultramafic, pi: hornblendite, ar: sandstone, conglomerate et al. of Tavera belt, q'f: alluvium. Source: Mapa Geológico de la República Dominicana 1:250,000, BGR 1991, modified.

3.1.2 Climate

The climate of the Dominican Republic is defined by the country's location in the trade wind zone of the outer tropics. The island of Hispaniola is surrounded by warm seas with surface water temperatures around 27°C. Warm ocean surface currents – the Caribbean Current to the south of the island and the Antilles Current to the north, coming from the ESE as extensions of the North Equatorial and South Equatorial Currents – pass the island's shores (Tomczak & Godfrey 2003). Air temperatures are tropical and generally exhibit a low temporal variability. Seasonal differences (less than 5°C between warmer summer months and cooler winter months) are smaller than daily fluctuations, which amount to 8°C on average. The mean annual temperature is 25°C in the lowlands and as high as 28°C in the Enriquillo basin. Lowland temperatures usually don't fall below 10°C. Temperature gradients in the mountains are relatively high, especially in the mid-elevations of the north slopes, where increasing cloudiness with elevation contributes to very high temperature gradients. Schubert & Medina (1982) calculated an average temperature gradient for the Cordillera Central of 0.7°C per 100 m. Temperatures below freezing occur above 2100 m elevation in the Cordillera Central and near the crest of the Sierra de Bahoruco and also in some valleys below 2100 m where cold air pools (Orvis et al. 1997, SEA/DVS 1994). Increased solar irradiation and larger daily temperature amplitudes characterise the climate of the highest mountain areas of the UCRYN. The temperature range from the lowlands to the highest mountains is equivalent to *tierra caliente*, *tierra templada* and *tierra fria* in the South and Central American nomenclature.

Typically for the tropics, rainfall is the most highly variable climate element, both temporally and spatially. There are large regional differences in rainfall, with a general gradient from a humid northeast to a drier southwest. North-easterly trade winds, which take up moisture over the Atlantic Ocean, bring about rainfall especially on the windward slopes and sides of the mountain ranges, while lesser amounts of rainfall occur on the leeward slopes (Gray 1993). The northeast trades come from a north-north-easterly to easterly sector. The mountain ranges of the Dominican Republic run almost perpendicular to this prevailing direction of circulation, amplifying the precipitation gradient in Hispaniola from the wet northeast to the dry southwest. Especially the Cordillera Central, which rises above the trade wind layer with its highest ridges, produces a strong rain-shadow effect (Weischet 1996). In addition to orographic uplift, mesoscale disturbances linked to convergence zones of tropical waves ('easterly waves') are another important mechanism causing rainfall (Gray 1993).

Although there is a lack of climatic measurements in the mountains of Hispaniola, it is understood that precipitation, like elsewhere in the tropics, increases with elevation up to an altitude of maximum precipitation. This zone of maximum precipitation is probably to be found between 1000 and 1500 m a.s.l. and is situated below the altitude of maximum cloud formation (Lauer et al. 2003). The trade wind inversion base has a height of around 2150 m over Hispaniola (Schubert et

al. 1995). Above the trade wind inversion, rainfall amounts can be expected to be lower because of persistent descending dry air at this altitude.

Over the year, precipitation is bimodal in most areas. The main dry season lasts from December to March and is caused by the strong influence of the subtropical high in this season. Trade winds are stable. Descending air in the Caribbean troposphere (subsidence), and decreased water moisture uptake in the atmosphere with accordingly low amounts of transported water vapour (Weischet 1996) result in reduced amounts of rainfall during this time. There are local differences, however, caused by local convergence and orographic uplift. The dry winter season cannot be observed along the northern coast of the Dominican Republic.

The summer precipitation is generally higher than the winter precipitation because of weaker atmospheric stability (weak or absent trade wind inversion) and more precipitation through convection. Disturbances, such as easterly waves, are also more frequent in the summer season. An early precipitation maximum is reached in May in most parts of the Dominican Republic (Weischet 1996).

A secondary dry season, the so called *veranillo*, occurs during the following summer months. The tropical upper tropospheric trough moves from the Caribbean to the Gulf of Mexico during this time, reducing the cyclonic rainfall in the Dominican Republic.

The second summer precipitation maximum in August-October coincides with the hurricane season, further increasing the rainfall averages for these months. Hurricanes are tropical cyclones with a wind force of 12 Beaufort, corresponding to a peak wind velocity of at least 35 m/sec. Tropical cyclones with peak wind velocities between 18 and 34 m/sec are referred to as tropical storms (Weischet 1996). Both bring large amounts of rainfall to the affected regions. For the development of a tropical cyclone, the surface of the sea has to have a temperature of over 26°C, and a disturbance has to occur at least 4° away from the equator. Hurricanes can occur in the Caribbean between June and November, and they are most frequent in the Dominican Republic between early August and mid-October (Horst 1992). Since 1871, 36 hurricanes have struck the Dominican Republic, on average once every 3.6 years. With wind speeds of 120 to over 200 km/h and extremely heavy rainfall, hurricanes are a natural hazard with serious effects on vegetation, soils, animals, humans and the economy (Walker et al. 1991). The last hurricane which passed directly over the Dominican Republic was Hurricane George, in September 1998. It caused extensive damage in the UCRYN, including a large number of landslides. In September 2004, Hurricane Jeanne approached Hispaniola from the east, but was reduced to tropical storm strength when passing over the northern Dominican Republic.

Climate of the upper catchment area of the Río Yaque del Norte

In the study area (UCRYN) with its exposure towards the north-east, the trade winds have a strong influence on the precipitation regime. The northern part of the UCRYN is the least humid. Tavera, at 300 m a.s.l. and at the northern border of the study area, has a mean annual precipitation (1968-1988) of 1234 mm and a mean temperature of 24.5°C (Vicioso 2002, INDRHI data). This low lying area is affected by the rain shadow of the Cordillera Septentrional.

Jarabacoa, at 500 m a.s.l., has a mean annual temperature of 22.1°C and a mean annual precipitation of 1537 mm (Vicioso 2002). Average monthly conditions are humid throughout the year. January, February and March are relatively dry. May is the month with maximum average precipitation, while June and July have the lowest precipitation with just over 80 mm per month. A second precipitation maximum is reached in November (figure 7).
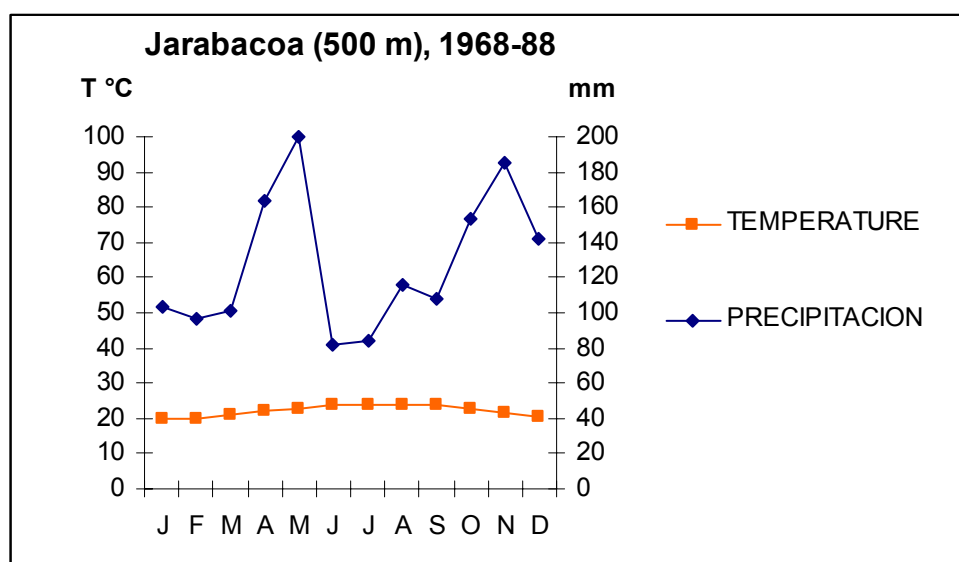
Fig. 7: Climate chart for Jarabacoa. Source: Vicioso 2002, quoting data of the INDHRI (National Institute for Water Resources).

The mountains to the west and to the south of Jarabacoa are certain to have higher precipitation, at least as far as they are exposed toward the east and northeast, but there is a lack of climatic data for the mountain areas.

The eastern border area of the UCRYN (Loma La Sal, Loma La Golondrina, Casabito) is a mountain ridge reaching elevations of 1300 to 1565 m. It is exposed to the easterly and north-easterly winds and thus very humid and often cloudy. In the cloud zone, which starts at elevations between 800 and 900 m at this north-eastern edge of the Cordillera Central and reaches the local summits, annual precipitation can exceed 3000 mm. Cloud stripping (the direct canopy interception of cloud water) contributes more than rainfall to that sum (Kappas 1999). The eastern edge is the most humid area of the Cordillera Central, because the trade winds reach this area directly from the

Atlantic Ocean without having passed over any other major mountains. The town of Bonao at an elevation of 180 m at the eastern foot of the Cordillera already has an annual precipitation of 2230 mm. At about 1400 m a.s.l. on the Loma Casabito, the mean annual precipitation of the years 1995-1999 was 3853 mm; the mean temperature here is 16.3°C (Mejía et al. 2000). The high precipitation quickly decreases at the western (leeward) side of these easternmost summits. El Río at 1100 m a.s.l. in the valley of the Río Jimenoa for example has an annual precipitation of only 1318 mm (acqweather.com).

In the western UCRYN the precipitation at the same elevations is somewhat lower compared to the Loma La Golondrina area, and the lower limit of the cloud zone is higher. The cloud zone is characterised by reduced diurnal variations of temperature and humidity. The western study area also includes areas above the cloud zone, where increased solar irradiation leads to large differences between day and night temperatures and thus very different climatic conditions.

Throughout the study area, climatic variations can be large even across small distances, depending on elevation, exposition and inclination of the slopes, as well as rain shadow effects. The local climate is also influenced by the vegetation (Kappas 1999).

3.1.3 Hydrology

Most of the major river systems of the Dominican Republic have their headwaters in the Cordillera Central: those of the Río Yaque del Norte, the Río Yaque del Sur, the Río Yuna, and the Río Nizao. The Haitian Artibonite river system also has some tributaries here. The Eastern Plain and Coastal Atlantic Plain (including the northern slopes of the Cordillera Septentrional) contain several rivers flowing into the sea. The small and mostly seasonal rivers of the northern Sierra de Bahoruco and the southern Sierra de Neiba flow into the Lago Enriquillo basin, which has no drainage. The small rivers of the rest of the Sierra de Bahoruco flow into the Caribbean.

The Río Yaque del Norte is the major river of the Dominican Republic, both in terms of its catchment area and of its importance as a water source (Vicioso 2002). It originates in the area of the Loma La Rucilla at elevations of almost 3000 m a.s.l. Its headwaters flow east towards the valley of Jarabacoa, where the Río Yaque del Norte is met by its tributary, the Río Jimenoa, coming from the south. The river then flows north down into the Cibao Valley. At 300 m a.s.l. it is dammed by the *Presa de Tavera*, built in 1973. In the Cibao Valley, the Río Yaque del Norte flows west-northwest, draining the western half of this valley and, through its tributaries, the northern slopes of the Cordillera Central and the southern slopes of the Cordillera Septentrional. It meets the Atlantic Ocean after 253 km in the bay of Monte Cristi.

The mountain rivers of the Dominican Republic are characterised by a seasonal discharge following the seasonality of precipitation and periodic high-magnitude floods at times of tropical storms and hurricanes (Ahmad et al. 1993). The Río Yaque del Norte at Pinar Quemado (to the west of Jarabacoa) has a maximum mean monthly discharge (1956-2001) of 14.6 m³/sec in May and a minimum mean monthly discharge of 7.1 m³/sec in February. The discharge of the Río Jimenoa, measured at Hato Viejo close to the confluence with the Río Yaque del Norte (1956-1995), is less variable with its minimum monthly mean in July of 5.6 m³/sec only a third below the May monthly mean of 8.5 m³/sec (Vicioso 2002).

3.1.4 Morphology

The typical Dominican montane landscape at elevations below 2000 m a.s.l. shares its major morphological characteristics with that of other islands of the Greater Antilles (Ahmad et al. 1993). It is defined by narrow valleys and steep slopes, from where rainstorm-related mass-movements (even on undisturbed forested slopes) periodically supply large amounts of sediment to the rivers. Landslides and the resulting denudation, especially of the midslopes, are part of a geomorphic system controlled by neotectonics (transpression, uplift, steep faults) and periodic high-magnitude rainfall and floods. The sediment supplied to the rivers has a wide textural range including a significant coarse fraction. Boulders accumulate in the rivers and are moved only during floods with very high velocities. The stream network is often structure-guided: part of the valley of the Río Yaque del Norte (upstream of Jarabacoa), for example, coincides with the Guacara-Bonao fault zone. The channels have steep side slopes as well as high stream gradients in the long profile with local waterfalls and rapids. In some flatter sections of the streams, for example in the La Ciénaga – Manabao section of the Río Yaque del Norte, the valley bottom is an accumulative surface (GWB / GFA-Agrar 1998).

In the highlands of the Cordillera Central, above 2000 m, the valleys are less steeply incised (Orvis et al. 1997). Schubert & Medina (1982) interpreted some geomorphic features (such as cirques and bog-filled depressions) in the highest parts of the Cordillera Central as glacial relicts and postulated the existence of a glacial snowline at elevations as low as 2200-2300 m. Orvis et al. (1997) also found indications of cryogenic processes, such as block fields and deposits of unsorted mixtures of clasts near the high central ridge of the Cordillera. The authors conclude that they were formed under climatic regimes quite different from today's, although the mixed deposits could also be hurricane- or earthquake-induced debris flows instead of morainic till.

3.1.5 Soils

Many different soil types occur in the Dominican Republic depending on relief, bedrock, and climatic conditions. The main soil units which can be found according to the FAO-Unesco Soil Map of the World (1975) are described below using the nomenclature of the FAO-Unesco classification (1988/1990).

In areas of siliceous rocks (such as siliceous tuffs and quartz diorites), lithic Dystric Cambisols and Lithic Leptosols can be found. Dystric Nitisols have developed on basic intrusive rocks and tuffs. These soils are generally deep soils but prone to erosion so that lithic phases also occur. Lithic Eutric and Chromic Cambisols as well as Rendzic and Lithic Leptosols can be found in areas of calcareous sediments and limestones. Lithic Calcic Cambisols occur in the arid and semi-arid areas. Acrisols are developed in humid areas on rocks high in quartz. Ferralsols derived from serpentinized ultrabasic rocks are infertile soils occurring in limited areas.

The soils of the UCRYN have not been mapped in detail (GWB / GFA-Agrar 1998). As can be inferred from the geology, they are mostly Dystric and Eutric Cambisols and Dystric Nitisols. The soils are moderately deep in areas of moderate relief and shallower in the mountains. The most productive soils can be found on the fluvial terraces of the valley of Jarabacoa (GWB / GFA-Agrar 1998).

3.1.6 Natural Vegetation

Owing to the island's varied relief, climatic and edaphic conditions, the flora of Hispaniola is one of the most diverse of the Caribbean islands (surpassed only by Cuba's). There are an estimated 5000 species of vascular plants (flowering plants and conifers) to be found in Hispaniola. About a third of these are endemic to this island. There are also numerous ferns, mosses and other plants, many of which have not been inventoried yet (Zanoni 1989). The flora is mostly neotropical, but there are also some holarctic species of North American origin.

Myers et al. (2000) identified the Caribbean islands as one of the world's leading biodiversity hotspots with a very high number of endemics (2.3 % of the world's vascular plant species grow only here) in spite of retaining only 11.3 % of its primary vegetation.

In the Dominican Republic, the floristically most diverse regions with the highest number of endemics are located in the mountains (May 2001). This is because of the varied terrain and microhabitats and the generally higher rainfall in the mountains. Besides, very little is left of the original vegetation in the lowlands (Zanoni 1989).

The natural vegetation of the Dominican Republic consists almost entirely of forests, with the exception of coastal and aquatic vegetation types, small areas of natural grassland (*sabanas*) and, in the most arid parts of the country, dry woodland and thorn thickets (Hager & Zanoni 1993).

Table 1: Comparison of three classifications of forest and woodland types of the Dominican Republic (mostly formation level, sometimes groups or alliances).

Vegetation units in the inventory of Tolentino & Peña (1998)	Formations according to the ICEC (Areces-Mallea et al. 1999)	Natural vegetation types as classified by Hager & Zanoni (1993)
Bosque Conífera Denso (Dense Coniferous Forest)	Montane Pine Forest; Mixed Pine-Broadleaved Forest	*Pinares de la zona alta de la Cordillera Central; Pinares de elevación intermedia*
Bosque Conífera Abierto (Open Coniferous Forest) (40-60 % crown cover)	Pine Woodland (25-60 % crown cover)	*Pinares de la zona alta de la Cordillera Central; Pinares de elevación intermedia*
Bosque Latifoliado Nublado (Broadleaved Cloud Forest)	Cloud Forest; Montane Rain Forest (in part)	*Bosques Latifoliados Nublados*
Bosque Latifoliado Húmedo (Humid Broadleaved Forest)	Submontane Rain Forest; Lowland and Submontane Seasonal Evergreen Forest	*Bosques Ombrofilos (*including *Bosques latifoliados siempre verde de lluias estacionales)*
Included in Humid Broadl. For. / not mapped for reasons of scale	Riparian Forest	*Bosques Ribereños*
Bosque Latifoliado Semihúmedo (Semi-Humid Broadleaved Forest)	Lowland Semi-Deciduous Forest	*Bosques Semideciduos (Bosques de la Llanura Costera & B. de Swietenia-Coccoloba)*
Bosque Seco (Dry forest)	Lowland or Submontane Drought-Deciduous Forest	*Bosque Seco (natural)*
Bosque Humedales Salobres Permanentemente/Temporalmente Inundados (Permanently/ Temporally Flooded Halophytic Wetland Forest)	Mangrove	*Manglares*
Bosque Humedales de Agua Dulce (Freshwater Wetland Forest)	Seasonally Flooded/Saturated Semi-Deciduous Forest	*Bosque Ribereño de Pterocarpus officinalis*
Matorral Latifoliado (Broadleaved Shrubland)	Several formations of evergreen woodland and shrubland	Not included in natural vegetation classes
Matorral Seco (Dry Shrubland)	Lowland or submontane broad-leaved drought-deciduous woodland; Cactus woodland	*Bosque seco perturbado; Bosque seco con abundancia de Cactaceae*

Ciferri (1936) wrote an early comprehensive geobotanical description of the country's vegetation types. In the following decades, the life zone system of Holdridge was used several times to classify the vegetation types of Hispaniola (Holdridge et al. 1971, map of Tasaico 1967 referred to in Hager & Zanoni 1993). However, this is a system of potential vegetation based solely on climatic factors,

and it cannot always do justice to the diverse vegetation of this island, which is also influenced by other factors like relief and soil (Hager & Zanoni 1993).

The first synopsis of the natural vegetation of the entire country after 1967 was devised by Hager & Zanoni (1993). In their classification, they group the Dominican Republic's natural vegetation into six major units, based on vegetation structure and composition: halophytic vegetation, dry forests, semi-deciduous forests, broadleaved evergreen forests, pine forests, and aquatic and wetland vegetation. Each unit contains several types of vegetation, mostly forest types. Harcourt & Ottenwalder (1996) used Hager and Zanoni's forest description in their chapter on Hispaniola in the "Conservation Atlas of Tropical Forests". May (1997), in his description of the mountain forests of the Dominican Republic, also uses some of their observations.

Tolentino & Peña (1998) classified the Dominican Republic's present vegetation and land use for an inventory using Landsat data, applying a slightly different classification scheme. This scheme was also adopted in the Dominican Republic's 'Inventory of Forest Cover' published by SEMARENA (2001a).

Areces-Mallea et al. (1999) used the International Classification of Ecological Communities (ICEC) as a standardized classification system for all Caribbean islands. The ICEC is based on the UNESCO system which uses physiognomic characteristics (vegetation structure) to classify vegetation worldwide at the formations level. The ICEC also adds finer levels of classification (alliances and associations) incorporating floristic characteristics.

Table 1 compares the major recent classification systems for the forest and woodland types of the Dominican Republic.

The major types of natural and semi-natural forest vegetation of the Dominican Republic are described below, with emphasis on the mountain forests occurring in the study area.

Pine forests (plates 1-4)

Dense and open montane and submontane pine forests can be found in the Cordillera Central, the Sierra de Bahoruco (Chardón 1941) and the Sierra de Neiba (Darrow & Zanoni 1991). In the Cordillera Central, natural pine forests cover the highest areas (above 2200 m up to the summit of the Pico Duarte) to the exclusion of all other forest types, but they can also be found below 2000 m, especially in leeward positions, growing on dry slopes and on infertile, shallow soils (May 1997). *Pinus occidentalis* Sw., the only native pine of Hispaniola, is ecologically very diverse. It grows on soils developed on limestone as well as on acid bedrock, and under very diverse climatic regimes with annual rainfall over 2300 mm and as low as 800 mm (Darrow & Zanoni 1991). It is the only

Hispaniolan tree growing above 2200 m, where night time temperatures can fall below 0 °C, but it can also be found at elevations as low as 400 m (Hager & Zanoni 1993).

Pinus occidentalis is very dominant in most pine forests, it is usually even the only tree species present. The understorey of the pine forests is dominated by shrubs and ferns in the more humid locations, while at drier or more exposed locations, the ground is covered by grasses like *Danthonia domingensis* and other herbaceous plants (Areces-Mallea et al. 1999). At altitudes above the zone of maximum precipitation, where rainfall is relatively low but mist or clouds contribute additional moisture (around 1600-1800 m), the pines are often draped with *Tillandsia usneoides* ('Spanish moss') and lichens (*Usnea* spp.) (Darrow & Zanoni 1991). By contrast, pine forests in the highest elevations and in dry locations are often rather open with a substantial ground cover of grasses.

Fire is an important element in the ecology of pine forests of the Dominican Republic and has played a role since pre-human times (Horn et al. 2000). The fire frequency has increased with the human influence. Mature trees of the species *Pinus occidentalis* are able to survive forest fires, so that repeated fires promote the development of open pine forests even in mid and low altitudes of the Cordillera Central. The fern *Pteridium aquilinum* (bracken) spreads in the early post fire succession stage (May 2000), and it often forms the main component of the herbaceous cover in areas of semi-natural open pine forests in these lower areas. Pine forests with broadleaved under-growth and mixed pine and broadleaved forests can be found in humid locations below 2000 m. A lack of natural regeneration of pines indicates that at least some of these forests represent a successional stage. They occupy sites where the natural broadleaved forest was disturbed for example through fire or grazing, allowing pines to colonise the disturbed areas as a pioneer species (May 1997, Hager & Zanoni 1993).

Broadleaved cloud forest (plates 5-8)

Cloud forests are montane forests which can occur within a very wide range of rainfall regimes (500-10,000 mm/year). There is a gradual transition of montane rain forest into cloud forest in many places, which makes it difficult to clearly define tropical mountain cloud forest (TMCF). During the Puerto Rico Tropical Cloud Forest Symposium held in 1993, the following working definition was developed: "The tropical montane cloud forest is composed of forest ecosystems of distinctive floristic and structural form. It typically occurs as a relatively narrow altitudinal zone where the atmospheric environment is characterized by persistent, frequent or seasonal cloud cover at the vegetation level. Enveloping clouds influence the atmospheric interaction through reduced solar radiation and vapour deficit, canopy wetting, and general suppression of evapotranspiration. The net precipitation (throughfall) in such forests is significantly enhanced (beyond rainfall contribution) through direct canopy interception of cloud water (horizontal precipitation or cloud stripping) and low water use by the vegetation. In comparison with lower altitude tropical moist

forest, the stand characteristics generally include reduced tree stature and increased stem density. Canopy trees usually exhibit gnarled trunks and branches; dense, compact crowns; and small, thick, and hard (sclerophyll) leaves. TMCF is also characterized by having a high proportion of biomass as epiphytes ..." (Hamilton et al. 1995:3). Cloud forests are naturally fragmented with a small extent on any particular mountain site; at the same time, these are areas of very high endemism. They belong to the world's most threatened ecosystems, as farming and cattle raising advances into these zones in many places, and warming in the course of climate change could lead to shifts of the cloud zone, with a consequent drying-out of the cloud forest (Bubb et al. 2002, Aldrich 2000). In the Dominican Republic, remaining areas of cloud forest can be found in the Cordillera Central as well as in the Sierra de Bahoruco and Sierra de Neiba.

Several types of cloud forest can be differentiated in the Dominican Republic. Dwarf or elfin cloud forest, with small tress of 5 to 7 m in height and a layer of mosses, is known from just one site in the western Cordillera Central (Loma Nalga de Maco). There, it grows on the mountain top above 1900 m under conditions of high winds and persistent cloud cover (Hager & Zanoni 1993).

Another type, the *Didymopanax tremulus - Podocarpus aristulatus* cloud forest, can be found at elevations between 1600 and 2200 m with frequent cloud cover in the Cordillera Central, Sierra de Bahoruco and Sierra de Neiba. The dominant emergent tree species, which reach heights of 15 m to 20 m and do not form a closed canopy, are *Didymopanax tremulus, Podocarpus aristulatus* and *Ocotea wrightii*. The second tree layer, forming a closed canopy 8 to 13 m high, contains the tree species *Weinmannia pinnata* and *Brunellia comocladifolia*. Tree ferns are also characteristic, as are epiphytes. Mature cloud forests on the summits of the Sierra de Neiba and above 1800 m in the Cordillera Central are taller and denser, and *Podocarpus aristulatus* is more dominant here (Areces-Mallea et al. 1999, Hager & Zanoni 1993).

The *Magnolia* (Spanish: *Ebano*) type of cloud forest is characterised by trees of the species *Magnolia pallescens* in the Cordillera Central and *Magnolia harmorii* in the Sierra de Bahoruco. It grows in the eastern Cordillera Central at elevations between 1100 and 2100 m and in the eastern Sierra de Bahoruco at elevations between 950 and 1500 m, often on mountain tops and ridges exposed to the wind. The crown cover is irregular, with single trees more than 15 m high, and a second tree layer at 10 to 12 m. Epiphytes are abundant. While *Magnolia* spp. is the characteristic tree for this forest type, *Didymopanax tremulus* is also a dominant species among the tall trees. *Prestoea montana* (also known as *Prestoea acuminata*) is frequent in the second tree layer in some areas. The herbaceous layer is mainly comprised of ferns, and there are also tree ferns, shrubs, lianas and many epiphytes (Hager & Zanoni 1993). In the Valle Nuevo area of the south-eastern Cordillera Central at elevations between 1700 and 2100 m, *Tabebuia vinosa* is a dominant tree of the second layer, and *Prestoea montana* is usually absent. Areces-Mallea et al. (1999) list only this latter association as *Magnolia pallescens* cloud forest, while they classify the other *Magnolia*

pallescens and *Magnolia harmorii* forest alliances as montane rain forest. May (1997), Hager & Zanoni (1993) and Tolentino & Peña (1998), however, address them all as cloud forest. Some authors subdivide the *Magnolia pallescens* cloud forest of the eastern Cordillera Central into firstly *Didymopanax tremulus* cloud forest, where tall trees of this species dominate the appearance of the forest and *Magnolia pallescens* is the main associated tree, and secondly *Magnolia pallescens* cloud forest growing on steep slopes exposed to the wind, where *Magnolia pallescens* is dominant and *Didymopanax tremulus* is just one of several associated trees (Mejía et al. 2000).

In the *Didymopanax tremulus - Magnolia pallescens* cloud forest of the eastern test area (Scientific Reserve Ebano Verde), the upper canopy is dominated by *Didymopanax tremulus*. Associated tree species on the mountain ridges (which reach elevations of up to 1565 m) are *Clusia clusioides*, *Magnolia pallescens* and *Haenianthus salicifolius* var. *ovatus*, among others. In a part of the forest which has survived intact below 1200 m, the trees are taller and *Cyrilla racemiflora* emerges above the canopy, reaching about 30 m in height (García et al. 1994).

As already noted by Ciferri (1936), disturbed sites in the humid mountain forest (mainly in the cloud forest zone) are often occupied by a dense cover of ferns of the *Gleicheniaceae* family (García et al. 1994, May 2000). The native species *Dicranopteris pectinata* and, to a lesser degree, *Gleichenia bifida* form stable communities called *'calimetales'* (plate 9), inhibiting the regrowth of woody species (Slocum et al. 2000). These *calimetales* naturally occupy clearings, caused e.g. by hurricanes, and the cloud forest recovers only slowly in such areas. The first pioneer tree species to invade disturbed areas above 900 m is often *Brunellia comocladifolia* (García et al. 1994).

Prestoea montana palm forest (plate 10)

Classified as another type of cloud forest by Hager & Zanoni (1993) and as a montane rain forest alliance by Areces-Mallea et al. (1999), the *Prestoea montana* forest has a very distinct canopy dominated by palm trees. The palm *Prestoea montana* is called *manacla* in Spanish, and the forest type dominated by this species is called *Manaclar*. It is an edaphic vegetation type, occurring on wet (frequently saturated) and stony soils, mostly on steep northern slopes and in mountain valleys, under similar climatic conditions as the cloud forest (García et al. 1994), in the altitudinal zone between 800 and 1500 m (May 1997). This palm forest is rich in ferns, including tree ferns (*Cyathea* spp.) (Harcourt & Ottenwalder 1996). There is sometimes a gradual transition between montane broadleaved riparian forest containing *Prestoea montana* as a subdominant species (plate 10) and palm tree dominated forest in some parts of the Cordillera Central. But *Manaclares* occur not only as riparian forests but also in patches removed from the streams. There is also a gradual transition between cloud forest and palm forest which can be observed in the Scientific Reserve Ebano Verde, consisting of a mixture of the dominant trees *Didymopanax tremulus* and *Prestoea montana* (Gracía et al. 1994).

Humid evergreen broadleaved forest (plates 12-13)

Humid evergreen broadleaved forests can be found in all mountain ranges of the Dominican Republic at elevations of up to 1500 m (in some cases 1800 m), and in some parts of the lowlands (Tolentino & Peña 1998). They can be subdivided into the seasonal forests, where some leaves are lost during relatively dry seasons, and the rain forests growing in humid climates without water shortages at any time. The annual precipitation is around 2000 mm.

Little is left of the lowland humid forests of the Dominican Republic. Some remnants can be found in the limestone valleys of Los Haitises in the north-eastern part of the country (*Oxandra laurifolia - Tetragrastis balsamifera* forest alliance according to Areces-Mallea et al. 1999).

Another rain forest alliance, the *Mora abottii* forest, is distributed in areas of very high precipitation (around 2400 mm/a) on the north-eastern side of the Cordillera Septentrional and in the eastern Cordillera Central at elevations between 150 and 800 m (below the cloud zone). This evergreen forest is 25 m tall, with emergent trees reaching 35 m. *Mora abottii* is usually the prevalent species; co-dominant tree species are *Cyrilla racemiflora* and *Ocotea leucoxylon*. Some areas are also dominated by *Sloanea berteriana* (Hager & Zanoni 1993, Areces-Mallea et al. 1999, May 1997).

Remains of the submontane humid evergreen broadleaved forests of the *Sloanea berteriana – Ormosia krugii* alliance occur in the Cordillera Oriental and Cordillera Central (Areces-Mallea et al. 1999, Hager & Zanoni 1993). These up to 25 m tall forests have two canopy layers and seem to have been widespread in these mountains in the past.

In the western Cordillera Central, where the winter months are relatively dry, the otherwise humid broadleaved forest at elevations between 650 and 1500 m is dominated by the drought-deciduous *Sloanea ilicifolia*, which can become up to 40 m tall (Hager & Zanoni 1993, May 1997). At higher, more humid locations, *Sloanea* becomes less dominant, and species like *Brunellia comocladifolia* and *Didymopanax tremulus* are to be found.

Broadleaved riparian forest (plates 11, 14-16)

The species composition of a riparian forest, growing by the sides of a stream, differs from that of the surrounding forest. This is due to the high ground water level and humid soil, different microclimatic conditions with higher air moisture, and disturbances e.g. through floods. The riparian forests of the Dominican Republic can be classified into four types: two types growing along rivers in humid lowland areas, one along permanent rivers in arid areas and one occurring in the mountains (Schubert 1993, Hager & Zanoni 1993).

The submontane to montane riparian forests of the Cordillera Central grow at elevations between 600 and 1600 m. They form narrow bands (of often less than 10 m width) on both sides of the

streams and rivers. The broadleaved riparian forest can grade into the surrounding broadleaved forest. Where it borders on pine forests, the transition is usually more abrupt. The trees of the riparian forests of the Cordillera Central reach 15 to 20 m of height. The typical species of this forest type are broadleaved, with large leaves. Ferns (including tree ferns), mosses and epiphytes are abundant due to the elevated humidity (Hager & Zanoni 1993). These forests are generally species-rich, with many different kinds of trees and shrubs and without a single dominant species. Trees frequently to be found in the riparian forests of the UCRYN are for example *Ocotea* sp., *Prestoea montana* and *Turpinia occidentalis* (Slocum et al. 2000, Garía et al. 1994).

Today, riparian forests are often the only forest remains in agriculturally used areas (plates 15, 16). Forming narrow forest corridors bordered by pastures and fields, they contain a reduced number of primary species and some secondary species (Kalácska et al. 2004).

Broadleaved semi-deciduous forest (plate 17)

There is a transition between humid evergreen broadleaved forest and dry forest, with a gradual increase of deciduous species which loose theirs leaves during the dry seasons. The semi-deciduous forests (called mesophytic forests by Ciferri 1936) grow in areas below 900 m a.s.l. with distinct dry seasons and an annual precipitation between 1000 and 1800 mm (Hager & Zanoni 1993, Tolentino & Peña 1998). They have a diverse floristic composition including species from both the dry and the humid evergreen broadleaved forests. Degraded semi-deciduous forests, or secondary forests growing on land originally occupied by semi-deciduous forests, are floristically less diverse and contain a larger proportion of deciduous and thorn-bearing plants (Roth 1999). They are usually dominated by the same few species of woody legumes as degraded dry forests (see below).

Semi-deciduous forest is the natural vegetation of the Llanura Costera in the Eastern Dominican Republic, where some remnants of it are left along the coast. The forest at the base of the Cordilleras, especially in rain shadow areas around the Sierra de Neiba, but also in some places at the northern and southern side of the Cordillera Central, used to be a semi-deciduous *Swietenia-Coccoloba* forest. This was characterized by the frequent occurrence of *Swietenia mahagoni* and *Coccoloba diversifolia*, together with some species of the adjoining dry forest like *Phyllostylon rhamnoindes* and *Bursera simaruba* (Ciferri 1936, Hager & Zanoni 1993).

This is probably the natural vegetation of some parts of the northern UCRYN, but there is no undisturbed *Swietenia-Coccoloba* forest left in the northern foothills of the Cordillera Central (May 1997). Ciferri (1936) mapped pine forests as the vegetation of most of the northern UCRYN, but he still found some semi-deciduous forest in the area surrounding today's Tavera Reservoir, at elevations of around 450 m.

Dry forest

Dry forests are the natural vegetation of the lowlands of the south-western Dominican Republic and of the north-western Cibao Valley, where the dry seasons are long and pronounced and the annual precipitation is below 1000 mm. There are several types of dry forest in the Dominican Republic. In most places, the trees do not grow taller than 14 m, some of them are deciduous, and the understorey is poorly developed. In the driest locations, on sandy and rocky ground, the dry forest is reduced to a thorn woodland with an open canopy of small trees and a large portion of cacti (*Cactaceae*) (Hager & Zanoni 1993). Dry forests constitute a large part of the forests of the tropics and subtropics (Murphy et al. 1995), but most of them are heavily disturbed. This is also the case in the Dominican Republic (Erhart 1995), where the forests are used for pasture and fuel extraction resulting in dry degraded or secondary forests and dry shrubland (*matorral seco*) marked by the frequent occurrence of *Prosopis juliflora* and/or *Acacia macracantha*. Dry forest does not occur in the UCRYN.

Mangroves and wetland forest

There are four native halophytic mangrove species. These trees grow in permanently and temporally flooded areas along the coast, in zones which are not too exposed to the waves, for example in the Bahía de Samaná. The temporally flooded *Conocarpus erectus* mangrove type also grows in the salty lagoons of the Enriquillo basin. The *Pterocarpus officinalis* wetland forest can be found in the freshwater areas of some river estuaries (Hager & Zanoni 1993).

3.2 Human Influence on Forest and Land Cover in the Dominican Republic

The Caribbean islands have been populated for about 7000 years (Lundberg 1997). The earliest settlers in Hispaniola were hunters, fishers and gatherers with little impact on the natural vegetation. Since those times, the human impact has increased progessively.

When Columbus first reached Hispaniola in 1492, the population of this island consisted of an estimated 300,000 to 500,000 people (Cassá 1984 quoted in Bolay 1997) who lived of agriculture, fishery and hunting.

In 2001, the Dominican Republic had a population of 8.507 million, or 176 per square kilometer (Statistisches Bundesamt 2002), with an annual population growth rate of 1.9 %. 60 % of the population are classified as urban (Harcourt & Ottenwalder 1996), while 33 % of the working population are occupied in the agricultural sector (Statistisches Bundesamt 1996). According to a 1993 census, the upper catchment area of the Río Yaque del Norte had a rural population of 33.750 persons in 7.080 households (GWB/GFA-Agrar 1998). Additionally, the town of Jarabacoa in the

UCRYN has approximately 40.000 inhabitants. Today's Dominican Republic is a densely populated developing country with an accordingly high pressure on its natural resources.

3.2.1 History of Deforestation and Forest Degradation

Before European settlement most of the primary forest of Hispaniola was untouched, although agriculture had been practised on this island since about 250 AD. In the three centuries preceding the Spanish arrival, the Taino (Island Arawak) occupied most of Hispaniola. They lived in agricultural villages, cultivating manioc (*Manihot esculenta*) and other plants. Their *conuco* (shifting cultivation) agriculture created pockets of cultivated land and secondary vegetation which were surrounded by forest (Watts 1987).

After the arrival of the Spanish, the number of natives on Hispaniola diminished quickly, mainly due to forced labour and diseases. After only 50 years, they were practically extinguished. With them ended their traditional, ecologically well adapted land use practices. Much of the former *conuco* land was abandoned and given over to secondary vegetation as the number of people working in agriculture diminished. The Taino did not have any herbivore domestic animals except guinea-pigs, but the Spanish settlers introduced cattle, pigs, horses, sheep and goat, most of which were left to run wild on the island and of which especially the pigs and cattle quickly multiplied in the absence of predators. Being the first large, hoofed herbivores on Hispaniola, they had some impact on the natural vegetation and helped spread pioneer vegetation (herbs and grasses). Localized soil loss and gullying (*arroyo* landforms in the mountains) occurred due to animal trampling.

In the early 16th century, cane plantations were established in southern Hispaniola. The labour was supplied by slaves who were brought in from Africa. The colonists and African slaves also continued to grow manioc, which had been the most important plant in the Taino *conuco* system, and they introduced vegetables and other food crops from Europe and Africa (Watts 1987). As the Spanish interest in Hispaniola decreased during the 16th century and Santo Domingo ceased to be the central city of Spanish America, the population and sugar production in this colony were also reduced. With few Spanish settlers remaining on the island, cattle hides became the most important export product of Hispaniola until 1665. Semi-wild cattle were hunted in the wooded lowlands. The mountains continued to be uninhabited (Blume 1968).

Ciferri (1936:261) reports that, when he was visiting the country, cattle and wild pigs were still being hunted in the forests of the Dominican Republic. The hunters used to burn the undergrowth of the forest, leaving the pine forest able to recover but often completely destroying the neighbouring broadleaved forest, so that the fraction of pine forest outside its core area in the high mountains was increased.

Starting in 1665, the French began to encourage agricultural settlers to move to western Hispaniola, which they regarded as extremely fertile, and to develop estates in this region. With the treaty of Rijswijk in 1697, western Hispaniola, now called St Domingue, became an acknowledged French colony based on an intensive plantation economy. In St Domingue most lowland forests had been cleared for sugar estates and other agriculture by 1791. Even in Spanish Santo Domingo (today's Dominican Republic) the forest cover was somewhat reduced during the 18th century, when lowland areas (rain forest and seasonal forest) were cleared for sugar cane production. However, due to the restricted economic development (small population, shortage of labour) in this Spanish colony, much of its lowland forest cover was still retained (Watts 1987:435). Despite some population growth during the 18th century, only about 110,000 whites and 15,000 slaves lived in Spanish Santo Domingo in 1789, and small-scale agriculture was more prevalent than large sugar estates.

The situation on Hispaniola was changed when slave uprisings in St Domingue started in 1791, leading ultimately to the independence of Haiti in 1804. Slavery was abolished and most of the plantation owners had to leave Haiti. Sugar estates were abandoned, leading to severe soil loss on the unattended slopes. Spanish Santo Domingo was occupied several times between 1795 and 1844, when the independence of the Dominican Republic was declared and the last slaves were freed even here. The end of slavery in Hispaniola in the 19th century lead to an increase in small farmers (peasants), joining the numbers of escaped slaves who had lived in the mountains of Hispaniola for generations. The peasants cultivated the remoter parts of the land, which were not yet occupied by plantations, using slash and burn methods (still called *conuco*). The number of smaller grazing animals (mainly goats) also increased in the course of this development.

During the time of the French and Haitian occupation of Spanish Santo Domingo, in the first half of the 19th century, the exploitation of the forests for valuable woods to be exported got under way. The most sought-after tree was Caoba (*Swietenia mahagoni* Jacq.), a native tree of the broadleaved semi-deciduous forest. The logging of Caoba and other exotic woods continued during the first decades of the Dominican independence. Because of the low population density in the Dominican Republic, only some of the logged areas, e.g. in the central Cibao valley, were subsequently cultivated, while most became degraded or secondary forest (Moya Pons 1994).

In spite of political disturbances, the population of the Dominican Republic grew rapidly from 200,000 in 1850 to 700,000 in 1900. During the 20th century, the massive population growth continued. In 1960, there were already three million Dominicans, 5.6 million in 1981, and 7.6 million in 1993 (UNO estimate). The urban population (especially in Santo Domingo) grew even faster than the rural population. Many Dominicans emigrated to the U.S.A., but at the same time there was (illegal) immigration from Haitians in search of work.

In the 1880s and 1890s, cane production in the Dominican Republic was extended again (with major plantations along the southern coast, and some smaller properties). At the same time, the forests of the eastern plains were much reduced, because of the increased demand for firewood to feed the recently introduced steam engines which were used in sugar production. Large cacao and coffee estates were established in the Vega Real (Valle de Cibao) during the 1890s. In the 20th century, sugar production was increased even further and the overall area under cultivation was greatly expanded (Watts 1987). This meant that most remaining forests were removed in the lowlands, and the mountain forest cover was also reduced. Soil erosion on hill-sides became more of a problem.

According to Durland (1922), Hispaniola still had a forest cover of at least 75 % in the early 20th century, although Erickson (1940) considers this number to be exaggerated, especially with regard to the slash and burn agriculture that was already ongoing in the mountains.

When Ciferri (1936) conducted his geobotanical studies in the Dominican Republic, he also found that most of its area was still covered by natural and semi-natural vegetation. However, most of the Cibao valley and the Llanura Costera and some other coastal plains were under cultivation, so that there were only small remains of semi-deciduous and lowland rain forest. The mountains were still largely forested, with the exception of some isolated cultivated valleys, for example the areas around Jarabacoa and Constanza in the Cordillera Central.

With the lowland broadleaved forests already very much reduced, the mountain pine forests were now increasingly exploited. The dictator Trujillo, who ruled the Dominican Republic between 1930 and 1961, recognized the economic value of the country's large pine forests and used them as a source of capital without bothering to replant the cleared areas. Starting in the late 1930s, an increasing number of sawmills and an improving road network accelerated the deforestation (Dotzauer 1993). Scarff (1940) gives a figure of 60 % for forested land, while he notes that some valuable tree species were already being close to being exhausted and that the pine forest in the accessible parts of the Cordillera Central was being exploited, cut and burnt at a rate which reduced the forest cover very quickly. In the UCRYN, deforestation took place especially in the areas around Jarabacao and El Río. When the forest was cleared in an area, the former sawmill workers became landless farmers. They were employed by the cattle-breeding landowners to clear the land again more thoroughly, and in return they were allowed to grow beans or potatoes on it for the first two or three years. After that, the soil fertility was reduced and the land was turned into pasture (Moya Pons 1994). By 1960 the forest cover had shrunk to about 30 % (Martínez 1990 quoted in May 1997). Pine production peaked in 1964, when 92,000 m³ of timber were harvested (Russo 1987 quoted in Dotzauer 1993). After 1967, when the closure of all sawmills was ordered, slash and burn agriculture became the main cause of further deforestation in the mountains. Demographic pressure, together with limited employment and low incomes in rural areas of the Dominican Republic,

contributed to an increasing number of landless farmers, who invaded the remaining forest areas in the mountains in order to produce subsistence crops. The productivity of the marginal mountainous land which is still available is very low. The productivity also decreases quickly when the land is used agriculturally, resulting in the clearing of still more forest to create new plots to shift to, short fallow periods, and finally erosion and possibly permanent land degradation (Dotzauer 1993). Fires are also used to reduce the forest cover of the mountains and turn forest land into pasture.

There is a small class of land owners with large estates, mostly used through extensive farming. Furthermore, large parts of agriculturally usable land are state-owned. By contrast, the majority of small land users lack land titles, especially in mountain regions like the UCRYN. This situation discourages long-term investments in more sustainable kinds of land use, and also tends to make it impossible for farmers to finance such measures (GWB/GFA-Agrar 1998).

During the 1990s, the rate of deforestation seems to have been reduced because of the remoteness of much of the remaining forest, the protected state of large parts of the remaining forest, the widespread substitution of charcoal and firewood by liquefied petroleum gas and the out-migration from rural areas (SEMARENA 2002). Today extensive animal husbandry is the dominant land use in mountainous areas, while slash and burn agriculture is practised only by the poorest and most marginalised parts of the rural population (SEMARENA 2002). Still, the population pressure remains high, and deforestation and degradation are still happening as a result (Sambrook et al. 1999). By contrast, some areas formerly under agricultural use have been left unmanaged because they have become unprofitable or because they are located in protected areas, giving rise to the development of *matorral* (shrubland) and secondary forests, so that it is not clear whether there has been a net gain or loss in forest area since the late 1980s.

Only about a quarter of the Dominican Republic is currently forested (the most recent forest cover estimates range from 10 % to 29 %, see chapter 3.3) and undisturbed primary forest makes up just a fraction of these areas. According to Schubert (1993), almost 90 % of the natural forests have been lost due to human activities. The largest contiguous areas of natural forest ecosystems remaining in the Dominican Republic today are located in the Cordillera Central and in the Sierra de Bahoruco. Outside these core areas, the remaining forest is mostly very fragmented and/or degraded (see the vegetation map of Tolentino & Peña 1998).

The ecological conditions in the Dominican Republic are still favourable compared to those in seriously degraded Haiti, where just about 3 % of the land are still covered by forests (FAO 2001).

3.2.2 Consequences of Deforestation

Tropical deforestation is a leading cause of worldwide loss of biodiversity (Sanchez-Azofeifa et al. 2002). This holds true especially for the diverse mountainous regions of the Dominican Republic, which constitute a biodiversity hotspot with many endemic species (Myers et al. 2000, May 2001). Only a small percentage of the Dominican Republic's humid evergreen broadleaved forests and cloud forests remains intact today. Apart from threatening plant biodiversity, deforestation also results in a loss of habitat for birds and other native animals. Several species of native mammals, birds and reptiles have become extinct in the Dominican Republic during the course of the 20th century; other native and endemic species of plants and animals are endangered (SEMARENA 2002, Schubert 1993). Not only the total loss of forested areas, but also the fragmentation of remaining areas of mature forest poses a threat to biodiversity. As the contiguous area of a particular habitat becomes smaller, it becomes increasingly vulnerable to disturbances including extreme climatic events or climatic change.

It is, however, not only the biological riches which are under threat, but also the long-term livelihoods of the Dominican population, which are based on the natural resources of this country. The degradation of the forest resources affects other natural resources like soils and water, with consequences not only for the population of the areas where the deforestation is taking place, but also for those living downstream, in the lowlands. Water from the mountain regions is needed in the lowlands as drinking water, for irrigation, for industrial use and for the generation of electricity.

Steep slopes and/or shallow soils limit the long-term land use potential of more than half of the area of the Dominican Republic. Such areas should ideally be covered by protection forest and managed forests (May 1997). The "*Departamento de Inventario de los Recursos Naturales*" recommends that 60 % of the UCRYN should be forested, 31 % should be used for agroforestry and silvopastoral systems and only 9 % for other agriculture. In reality, more than 60 % of the area is used agriculturally (GWB/GFA-Agrar 1998). Deforestation and maladjusted forms of land use on slopes lead to erosion and loss of soil fertility, and thus to decreasing productivity and general land degradation (Kappas & Schöggl 2005). The economic effects of land degradation as a result of unsustainable forms of land use are especially tangible in mountainous areas. The agricultural use (even as pasture) of many areas is no longer profitable. Besides, the Dominican Republic needs to import wood products for about US$ 200 million every year (FAOSTAT data, 2004). These could be produced within the country if areas more suited for forest use than for agricultural use were reforested and used for commercial forestry.

Undisturbed tropical mountain forest systems, with their water retention, can work as buffers in times of intensive rainfall and reduce the runoff compared to agriculturally used areas (Kleinhans 2003). Disturbed areas, including those of degraded forest and secondary vegetation, are more

vulnerable to landslides than areas of undisturbed vegetation (Erler 2004). Increased rates of erosion and the more frequent occurrence of mass-movements mean increased amounts of soil ending up in the watercourses, leading to siltation, eutrophication and sedimentation. The latter is a problem especially for the reservoirs. The *Presa de Tavera* (plate 18) at the northern end of the UCRYN, built in 1973, is important for the water supply and irrigation in the Cibao valley, the generation of hydroelectric power, and flood control. By 1993, 36 million m³ of sediments had been accumulated in the reservoir, reducing its storing capacity by 21 %. This corresponds to an average of 23 m³ of solid material per hectare of the catchment area which was transported from the UCRYN into the reservoir *per year* during the first 20 years of its existence. The rate of sedimentation has increased over the years; during the first five years (1973-1978) it was only 13 m³/(ha·a) (GWB/GFA-Agrar 1998). The sedimentation leads to a large increase in maintenance costs for the dam, so that the operator (Corporación Dominicana de Electricidad) would be ready to provide funds for measures which are shown to reduce the soil erosion in the catchment area (Heindrichs 2004).

Discharge rates, especially peak discharge rates, are also affected by deforestation. The gauging station in Manabao measured a mean monthly maximum flow rate of 8.78 m³/s during the period of 1964-1978 compared to 16.69 m³/s during the period of 1980-1997. This increase is ascribed to the deforestation and erosion in the area of La Ciénaga and other areas upstream of Manabao during those decades, leading to accelerated discharge. In gauging stations further downstream no such increase was observed, though (Vicioso 2002). Accelerated discharge at times of heavy rainfall leads to an increased risk of inundations downstream. Inundations are a regular problem for example in the Cibao Valley (Consorcio Ingeniería CAURA - ESRI - DESAGRO 2002).

The presence or absence of mountain forests is also a factor for the local climate. The plants of the cloud forest are not only on the receiving end of the humidity of the mist which envelopes them, but also generate part of that humidity themselves. When the forest is removed, the frequency of fog and the humidity of the soil decrease (Kappas 1999). On a larger scale, the tropical forests, through their part in carbon sequestration, also influence the global climate.

The balancing and attenuating effects of forests on hydrological and climatic conditions are a stabilising factor for the whole ecosystem, protecting the natural resources of the mountains.

Tourism is another economic area where intact natural forests can be an asset, increasing the attractiveness of the Dominican Republic as a travel destination for ecologically minded tourists, and increasing the attractiveness of the interior mountain regions for domestic and foreign tourists alike.

3.2.3 Forest Laws and Forest Policy

A number of laws, decrees and regulations concerning the protection of the Dominican Republic's biological resources have been issued since the early years of the country's independence. A decree issued in 1884 banned clearing the forest near river beds and springs and demanded that every farm should keep 5 % of its area under forest cover (Dotzauer 1993). The law "concerning the conservation of forests and waters" from 1934 also banned the deforestation of river banks, edges of gullies and springs, among other things (Scarff 1940). The effects of these rules can still be observed in agricultural landscape in the Dominican Republic, where indeed the riparian forest alongside river banks and *arroyos* is left standing in many instances. In general, however, the protective laws of this time were seldom enforced, both due to a lack of trained foresters and to a lack of political will. In the 1930s and 1940s, under the dictator Trujillo, the emphasis was placed on the revenue that could be gained for the government from exploiting the country's forest resources. In contrast to the forest protection laws, the law about the tax on sawed wood from 1937, for example, was enforced quite rigidly (Scarff 1940).

Beginning in the 1950s, a number of national parks were established to protect some selected areas of natural forests (see chapter 3.2.5 below). The laws and decrees concerning the biological resources which were issued in the second half of the 20th century were mostly of a prohibitive nature. The most radical measure was introduced under president Balaguer in 1967 when, in the face of the alarming rate of deforestation which had been reached in the 1960s, all sawmills were closed and all tree harvesting was prohibited (Dotzauer 1993). However, this law did not address the causes of deforestation and, indeed, made it very undesirable to have forest on one's land as forested areas didn't have any economic value. Thus the legal situation did not encourage afforestation and entailed illegal actions to further reduce the country's forest cover. During the presidency of Balaguer (1966-1978 and 1986-1996), the emphasis of environmental policy was on the protection of natural areas, often by force, without making allowance for the interests of the local population (Ulbert 1999). The rural population regarded the forestry administation and the forest as such as enemies of the farmer, because if on fallow-land the woody vegetation reached heights above 1-2 m, the farmer lost the right to use this land. Consequently, the emergence of secondary forests was prevented through fires and grazing, and existing forests were also burnt and destroyed (plate 19). In the 1990s the forestry office in Jarabacoa estimated that 1 % of the forest in its area was burnt each year (GWB/GFA-Agrar 1998). At the same time, Balaguer's government created new institutions in the environmental sector, resulting in more than 12 public institutions, with overlapping responsibilities, which were involved in the management and conservation of natural resources (Schubert 1993). Responsibility for the country's forests was shared by the national forest authority FORESTA, the technical forest commission CONATEF, several departments of the ministry of agriculture, and the national park authority (DNP) (Ulbert 1999).

The lack of coordination between these institutions prevented the development of a coherent forestry policy.

A national campaign for reforestation was launched in 1983, and a 1985 law established incentives for forestry investment (Rodríguez 2004), but landowners were still uncertain whether it would be possible to harvest planted trees. In the late 1990s, forest management was increasingly encouraged (Peter 2003), and the forest law 118-99 explicitly allowed forest cutting in 1999.

However, when the government of president Hipólito Mejía (Partido Revolucionario Dominicano) came to power in 2000, this permission was temporarily revoked. Older laws regarding the environment were superseded by the new 'General Law of the Environment and Natural Resources' (Law 64-00) from August 2000. Law 64-00 provides a legal framework for the whole field of environmental policy. Among other things, the law stipulates that the forest has to be managed and used sustainably, it forbids the destruction of primary forests but allows the use of forest plantations, provided that a national forest inventory is conducted separating native and artificial forests and forests in protected areas, forests with the purpose of protection and forests with the purpose of production. The law also creates the Ministry for Environment (SEMARENA). All institutions responsible for aspects regarding the country's natural resources are now subordinate to this new ministry (República Dominicana 2000). In 2001, the new Ministry for Environment published the required '*Inventario Forestal*' (see chapter 3.3), and issued forestry regulations (Reglamento Forestal, SEMARENA 2001e) and technical standards (SEMARENA 2001c, 2001d, 2001e) supplementing law 64-00 with more detailed regulations regarding the management of forests and determining the conditions under which commercial forestry is allowed. Forests around springs and along rivers and streams continue to be protected, and forests on steep slopes (> 60 %) are also classified as protection forests with management restrictions.

Public statements of the government are very much in favour of encouraging reforestation and forest management. A national program for reforestation and a national program for land use change (from extensive pasture to forestry) are presented on the web site of the ministry for environment (http://www.ceiba.gov.do/2004/index_esp.html). Under the current conditions however, it is too costly for many smaller farmers to obtain the official permission for commercial use of their forests. They would need a management plan elaborated by a forestry professional, then wait for up to 6 months for approval of the plan and submit to control by government officials. Not being able to afford this, many smallholders continue to illegally transform their forests into agriculture. Besides, government forest policy is regarded as unstable, so many landowners harvest what they can today without being willing to make any long-term investments. There is only a small group of forest owners who have both the interest and the possibility to manage their forest on a sustainable basis and to develop a private forestry sector (Peter 2003).

Leonel Fernández of the Partido de la Liberación Dominicana, who had already been president from 1996 to 2000, won a majority in the county's presidential elections on 16 May 2004 and has replaced president Hipólito Mejía on 16 August of the same year. It remains to be seen what this will mean for the country's forest policy and to what extent the policies can be implemented during the currently critical economic situation of the country.

3.2.4 Reforestation Efforts and Commercial Forestry

Some public reforestation projects got under way in 1973. Among them were plantations in the area of Manabao and the Loma la Sal in the UCRYN (Rodríguez 2004). According to the archives of the 'Certificates of Plantations with the Right to Felling' (which were introduced in 1988), 360 km² of forest plantations for production, both private and public, had been registered in the Dominican Republic by 2001. In addition, 123 km² of forest had been planted for the protection of steep slopes and riparian zones (SEMARENA 2001a). Together, this corresponds to less than 1 % of the Dominican Republic's land area. Armenteros Ruis (1989) called for the reforestation of approximately 3500 km² of protective forests in the vital watersheds of the country; only a small proportion of this has been realised. Despite attempts during the last decades to create incentives for forestry investment, no significant private forestry sector has emerged and commercial forest plantations are still very rare in the Dominican Republic as a whole.

However, plantations of pine trees (usually *Pinus caribaea*) are relatively widespread in the UCRYN and adjacent mountain areas (plates 20 & 21). Plantations of native pines (*Pinus occidentalis*) are rare because this is not an established species in commercial forestry (Darrow & Zanoni 1991). In the UCRYN, young pines planted recently can be found as well as pine plantations from the 1970s and 1980s. There are also plantations of broadleaved trees, consisting mostly of fast-growing species like *Acacia mangium* (plate 22). In the eastern test area, an effort was made between 1972 and 1975 to reforest the deforested and degraded (only sparsely wooded) slopes below the areas of remaining cloud forest with *Pinus caribaea*, *Pinus taeda* and also *Pinus occidentalis*. Not all of these plantations were looked after in the following years. This resulted in some dense pine forests and some areas of closed and open forests where the pine trees are mixed with broadleaved pioneer species like *Brunellia comocladifolia* and in some places with regenerating cloud forest.

In addition to plantations, SEMARENA (2001a) classified 44.5 % of the country's forests (5521 km²) as potential productive natural forests which can now be utilised according to the forestry regulations for sustainable forest managment (SEMARENA 2001b). By December 2002, 167 management plans had been approved, legalising the utilization of 295 km² of natural forest, and 24,336 m³ of timber (*Pinus occidentalis*) had been extracted (Rodríguez 2004).

3.2.5 National Parks and Protected Areas

There have been efforts to protect the mountain forests of the Dominican Republic since the 1920s. The catchment area of the upper course of the Río Yaque del Norte was declared a protected area in 1928. The first national park was established in the Cordillera Central in 1956, but the legislation determining the aims and functions of national parks followed only in 1974, when the National Park Administration (DNP) was established. Since 1956 over 30 protected areas (national parks, scientific reserves, natural monuments) have been set up in the Dominican Republic; seven national parks and ten scientific reserves of these had been placed in areas of remaining mountain forests by 1997 (Schubert 1993, May 1997). The largest protected areas are the national parks. These are areas where the exploitation of natural resources or large-scale modifications of the ecosystem are prohibited but recreational and scientific activities are allowed. The scientific reserves of the Dominican Republic have the legal status of strict nature reserves where human access is more restricted with the exceptions of scientific investigations, environmental monitoring and education (SEMARENA web page URL: http://www.ceiba.gov.do/2004/areas_naturales/esp/areas_proteccion /areas_prot_esp.html). According to SEMARENA (2002), 4770 km² of forest are located in protected areas, including 65 % of the remaining cloud forest and 58 % of the coniferous forest, 30 % of the humid broadleaved forest and 19 % of the dry forest. All types of natural forests are now represented in protected areas in accordance with the aim to conserve the country's biodiversity. However, the delimitation of protected areas is often based on incomplete or deficient biological and cartographic information, so that some small and well preserved mountain forests are still not protected while some protected areas include secondary forests and agriculturally used areas and settlements, giving rise to conflicts with the local population (May 1997). Buffer zones have only been added to a minority of the protected areas and often violations of the prohibitions of utilisation cannot be stopped. In July 2004, a controversial law for protected areas was introduced. It somewhat reduced the total area under protection and modified the categories of protected areas, allowing more economical activities like mining and the building of tourism infrastructure. This law was heavily criticised by the new minister of environment, Max Puig, for being "deficient and contradictory" and inapplicable, because it prohibits access to areas containing settlements while leaving important sensitive areas without protection. Puig announced that his ministry was preparing a new law for protected areas (Listín Diario 12.2.05).

The national parks (NP) and scientific reserves in the region of the UCRYN are described in more detail below.

NP Armando Bermúdez and **NP José del Carmen Ramírez**, established in 1956 and 1958 respectively, are the oldest national parks of the Dominican Republic. Together, these two adjoining national parks cover 1504 km² on the northern and southern side of the central Cordillera Central including the highest peaks of the country and the headwaters of the Río Yaque del Norte and the

Río Yaque del Sur (Schubert 1993). The parks protect large areas of humid mountain forest (mainly pine forest, but also cloud forest, humid evergreen broadleaved forest, riparian forest and patches of palm forest) in the Cordillera Central. However, there is no buffer zone established around these parks, and the current boundary of the NP José del Carmen Ramírez is ill defined. There are encroachments of coffee plantations and slash-and-burn agriculture, and illegal logging has denuded part of the parks (Bolay 1997). Forest fires, both natural and man-made, are a regular occurrence in the pine forests of this area. In March 2005, the drought, probably in combination slash and burn practices, led to a large number of forest fires in the Cordillera Central, also affecting the NP Armando Bermúdez, and burning a larger area of forests in the Dominican Republic than at any time since the fire season of 1997 (Listín Diario 19.03., 20.03., 22.03, 24.03. & 30.03.2005). The eastern NP Armando Bermúdez is part of the upper catchment area of the Río Yaque del Norte.

The **Scientific Reserve Ebano Verde** is located in the eastern UCRYN and extends into the adjacent catchment area of the Río Camú. It was established in 1989 with the primary aim of protecting the threatened endemic tree *Magnolia pallescens* (Spanish: ébano verde) in its cloud forest habitat. The reserve is managed by the foundation PROGRESSIO (*Fundación para el Mejoramiento Humano*), based on a treaty with the *Dirección Nationál de Parques* (DNP), which is a singular form of management in the Dominican Republic (Bolay 1997). The reserve is small (originally 23 km², today 29 km²) but relatively well protected, although large parts of it were deforested or degraded in the past when, among other things, the valuable timber of *Magnolia pallescens* was extracted from the cloud forest. The area around the reserve is assigned as a buffer zone. Elevations range form 800 to 1565 m a.s.l. 686 species of vascular plants have been recorded in this reserve, 158 of which are endemic to Hispaniola. There are 89 different tree species. Most of the reserve is covered by *Didymopanax tremulus - Magnolia pallescens* cloud forest. This cloud forest grades into *Prestoea montana* palm forest in some wet valleys in the eastern part of the reserve. Broadleaved riparian forest grows along most of the streams outside the palm forest area. Previously deforested areas mainly in the western and south-western reserve have been reforested with *Pinus occidentalis*, *Pinus caribaea* and *Pinus taeda* since 1972, resulting in some dense pine plantations in addition to a small area of natural pine forest on a dry slope in the westernmost reserve. Most pine plantations, having been left untended after the sowing, have been invaded by broadleaved species. A secondary forest has developed in these areas where *Brunellia comocladifolia* (*sangre de gallo*) and other broadleaved pioneer species are mixed with some remaining pine trees and the development is toward the regeneration of a cloud forest or, below the cloud zone, a humid evergreen broadleaved forest. Areas where the tree layer has been disturbed either by man or by hurricanes are covered by fern (*calimetales*) (García et al. 1994).

The **NP Valle Nuevo** is located in the south-eastern Cordillera Central to the south and to the east of the valley of Constanza. Its northernmost part extends into the southernmost UCRYN. The NP was established as a scientific reserve in 1983 and used to cover 409 km² (Schubert 1993) but has

been enlarged to 910 km². Valle Nuevo contains both natural and historic sights, but due to easy access into the park, not all of them are intact. The centre of the park is a plateau at 2200 m elevation. The park's vegetation consists mostly of pine forest and cloud forest.

Las Neblinas is a new reserve established in 1996. It covers 36 km² in the eastern Cordillera Central, bordering on the UCRYN and extending the area of protected cloud forest of the Scientific Reserve Ebano Verde towards the south-east (SEMARENA web page URL: http://www.ceiba. gov.do/2004/areas_naturales/esp/areas_proteccion/areas_prot_esp.html).

3.2.6 Environmental Projects

National and international non-governmental organisations (NGOs) have implemented several land management projects in the Dominican Republic, sometimes in co-operation with the Dominican government (e.g. Plan Sierra in the northern Cordillera Central). Some of these projects focus on the UCRYN or parts of it.

PROCARYN

The "Project for the management and conservation of the upper catchment area of the Río Yaque del Norte" (PROCARYN) became operational in 2001 after some preliminary studies and preparations done since 1998 (GWB / GFA-Agrar 1998, Vicioso 2002). It is a project of cooperation between the Dominican ministry of the environment (Secretaría de Estado de Medio Ambiente y Recursos Naturales – SEMARENA) and German development agencies (GTZ, KfW, DED).

The project area of 840 km² includes the upper catchment area of the Río Yaque del Norte together with a small area to its northwest down to the Río Guanajuma. Its aim is to achieve forest and soil protection through incentives for farmers to manage their land more sustainably. The project has an agroforestry-agriculture component and a forestry component. The latter supports smallholder farmers with reforestation and sustainable management of forests on their lands, including co-financing, help with the bureaucratic requirements and technical support. Farmers are also educated and involved in the decision-making process to motivate them to participate, as forest protection, reforestation and soil protection measures can be counterproductive in the long run if they do not contribute to the livelihoods of the rural population (Peter 2004, Heindrichs 2004).

PROCARYN was a factor in choosing the UCRYN as study area for this work. The project provided important infrastructure during fieldwork, shared data and was interested in the resulting land cover maps; it received the earlier results of this work for use in the project's land cover and land use monitoring. The PROCARYN project completed its first phase in 2004 and is currently not active, although it was originally planned for five years (GWB/GFA-Agrar 1998).

PROGRESSIO

PROGRESSIO (*Fundación para el Mejoramiento Humano* / Foundation for Human Improvement) is a Dominican environmental NGO established in 1983. It is a member of the World Conservation Union (IUCN). PROGRESSIO's primary concerns are the conservation of biodiversity and sustainable development for the benefit of the quality of life of the human population. Its main project is the management and development of the Scientific Reserve Ebano Verde. It is also active in supporting the sustainable development in the buffer zone around the reserve. In other areas of the Dominican Republic, PROGRESSIO is involved in the introduction of new crops for agriculture and agroforestry and in environmental education (URL: http://www.cad.org.do/progressio.html).

3.2.7 Agricultural Land Use in the Study Area (Plates 23-31)

While only about a third of the UCRYN is still covered by forests within and outside of protected areas, most of the catchment area is used agriculturally. Agriculture is the main economic activity in the rural zones of the UCRYN. Most people cultivate their own land or leased fields or work for other farmers (GWB/GFA-Agrar 1998).

Extensive livestock farming for the production of milk and meat is the dominant form of land use in the mountainous areas of the Dominican Republic. The number of cattle in the country has increased by 41 % between 1979 and 1998 (SEMARENA 2002). About a quarter of the UCRYN, mostly the land of medium and large land owners, is used as pasture. This type of land use is especially dominant in the relatively dry northern part of the catchment area, on the hill slopes between Jarabacoa and the Tavera reservoir. There is some intensive grassland in the vicinity of settlements, but most of the grassland of the study area is used as extensive pasture. The herbaceous layer of these areas is mostly composed of grasses like the introduced *Melinis minutiflora*, but ferns like *Pteridium aquilinum* (bracken) are also present in many places and can become dominant. On steep slopes, grazing animals cause the development of tracks parallel to the contour lines ("Viehgangeln"). In overgrazed and dry areas, the vegetation cover can be incomplete so that at the end of the dry season, large areas of bare soil are exposed to the first strong rainfall (GWB/GFA-Agrar 1998). The pasture-land often contains dispersed trees or groups of trees which can be either relicts of a former forest or pioneer trees and shrubs (May & Peguero 2000). Older remnant trees are mostly pine trees, but broadleaved trees and palm trees, the latter mostly in the lower areas of the UCRYN, can also be found on pasture-land.

The most wide-spread crop of those which are grown in the UCRYN is coffee (*Coffea* spp.). Coffee is grown in large and small plantations, partly with shadow trees, at elevations up to about 1500 m. In some coffee plantations pesticides are used to kill herbs resulting in an incomplete overall vegetation cover, especially where the coffee plants are still small. Beans (*Phaseolus vulgaris;*

Spanish: habichuelas) are the second most wide-spread crop. Traditional bean cultivation on slopes can lead to large rates of erosion as long as appropriate soil conservation practises are not applied (GWB/GFA-Agrar 1998, Kappas & Schöggl 2005). In the area of Paso Bajito (eastern test area), deforested steep slopes are used for the widespread cultivation of beans without soil conservation practices. This subsistence agriculture has increased in the area since the 1980s when this area was mostly used only as pasture (Vicioso 2002). Other crops traditionally grown in the UCRYN include maize, manioc, tobacco and sweet potato/yam (*Ipomoea batatas*).

More recently the cultivation of cabbage and other vegetables and of flowers has spread in some parts of the UCRYN (GWB/GFA-Agrar 1998). Some of these are grown in greenhouses. Especially conspicuous is the spread of chayote cultivation on plains and moderate slopes, with a centre in the area upstream of Manabao (La Ciénaga). Chayote (*Sechium edule; Spanish: tayota*) is a vegetable from the family of *Cucurbitaceae*, which grows on a perennial vine and needs the construction of a framework on which it forms a dense cover of leafs. Chayote fields are often irrigated. During the last decade, they have replaced many former coffee plantations in the UCRYN (Vicioso 2002, GWB/GFA-Agrar 1998). The establishment of chayote fields is also connected to deforestation because of the wooden stakes needed for the framework.

3.2.8 Agroforestry (Plates 32-34)

Agroforestry can be defined as the incorporation of trees in agricultural systems. This is a type of land use that can contribute to sustainable mountain development (Atta-Krah & Tang Ya 2000). Potential benefits include the preservation of soil fertility and reduction of soil erosion, water conservation and a higher biodiversity and ecosystem connectivity compared to tree-less agriculture (Beer et al. 2003). The trees used in agroforestry are often legumes, which contribute to soil fertility replentishment through nitrogen fixing. Agroforestry systems provide additional products and services to the farmer and to the wider environment, but they are often labour intensive, so that they may not be the most profitable option for the individual farmer.

Common traditional agroforestry systems in the Dominican Republic include firstly coffee (*Coffea* spp.) under shade trees (typically *Inga vera* or *Cordia alliodora*) and banana plants (*Musa* spp.), secondly cocoa (*Thobrama cacao*) under shade trees, citrics and banana plants and thirdly silvopastoral systems (Hernández 1995).

In the UCRYN, agroforestry typically consists of medium-sized to large coffee plantations (mostly *Coffea arabica*) with shade trees on the one hand and, on the other hand, agroforestry on small plots in the form of mixed homegardens where bananas, coffee and other crops are grown on a subsistence basis.

Although most agroforestry systems of the UCRYN include coffee, there is a large variety of species and species mixtures which can be part of these systems. *Inga vera* Willd. (Spanish: *guaba*, locally known as *guama*) is a legume used frequently as a shade tree in this area, which also provides wood (mainly for fuel) and nectar for bees. Mixtures of different broadleaved trees which sometimes seem to be the remnants of the original forest can also be found in the tree layer, as well as palm trees, which are used both as shade and fruit trees. There are also plantations of coffee under pine trees in the study area.

Due to the prohibition to cut trees that was in place between 1967 and the late 1990s, some coffee plantations with shade trees became unproductive through lack of light. Especially smaller plantations sometimes ended up with a complete crown cover of *Inga vera* or other shade trees.

Investments in the creation and maintenance of traditional coffee and cacao agroforestry plantations in the Dominican Republic have declined in recent years because of adverse conditions on the world market (SEMARENA 2002). Low coffee prices since 1997 have resulted in unprofitable plantations which are sometimes left unused, sometimes also cleared for use as pasture or to cultivate other crops (Vicioso 2002). In spite of this, some new coffee plantations with a low density of shade trees have been established in the hills to the south of the Río Yaque del Norte (to the south-west of Jarabacoa), replacing formerly forested areas.

Apart from the agroforestry systems with coffee, silvopastoral systems are also common in the UCRYN, where many pasture areas include single trees, groups of trees and transitions from pasture to open forest. The trees in those pasture areas are mostly pine trees, which, unlike the trees in silvopastoral systems in the dry forest areas of the Dominican Republic (Erhart 1995), do not provide fodder for livestock.

3.2.9 Degraded and Secondary (Semi-Natural) Vegetation in the Study Area

While grazing and fires have degraded areas of natural vegetation, there area also substantial areas which were formerly used agriculturally and have been left fallow or unmanaged for several years. These are areas formerly used for migratory agriculture, which was most intensive in the UCRYN in the 1980s (Vicioso 2002), areas where land degeneration has made pasture use unprofitable and areas of abandoned agroforestry plantations. Unmanaged regeneration has lead to the development of areas of *matorral* (shrubland) and secondary forest (plates 37-41).

Matorral areas, covered with shrubs, ferns and grasses, have developed for example on abandoned pasture-land and agricultural fields, often on steep slopes. The *matorral* vegetation may be a successional stage on the way to a secondary forest, or it may be the case that the woody vegetation does not reach the stage of a forest because the site is too degraded and/or the vegetation continues

to be disturbed by grazing or occasional fires. The herbaceous layer of *matorral* areas is often fern dominated, and woody species like *Myrsine coriacea, Baccharis myrsinites* or *Piper aduncum* form an open or closed layer of shrubs (May & Peguero 2000, May 1994). Dispersed trees can also be found in some of these areas. In the eastern test area, in the buffer zone of the scientific reserve, many slopes are covered by this kind of vegetation.

The humid secondary forests which develop through natural regeneration in the study area are quite diverse, depending on their age, the kind and duration of former land use and environmental factors. Generally, secondary forests contain an increased amount of pioneer species and if they remain undisturbed, the succession leads back to the climax vegetation of the respective environment. The secondary forest in the eastern test area has already been mentioned in chapter 3.2.5. May (1994) studied an area of secondary forest in the eastern test area at 1250 m a.s.l. 12 years after the *conucos* of this area had been abandoned in 1980-1981. By this time, a secondary forest had developed with 16 woody species (shrubs and trees) in the 170 m² botanical study area. Most frequent among the plants which had already reached tree height (> 5 m) were *Brunellia comocladifolia, Myrsine coriacea, Turpina occidentalis* and *Ocotea leucoxylon*. The herbaceous layer was dominated by the grass *Homolepis glutinosa*, with ferns also present. Among the young regeneration in the understorey, pioneer species like *Brunellia* and *Turpina* were absent while species typical for a mature cloud forest like *Prestoea montana* and *Podocarpus aristulatus* were present, indicating that a succession towards a more mature forest was under way.

On the Mogote Mountain in the south-central UCRYN, former coffee plantations at about 1000 m a.s.l. have developed into broadleaved secondary forests with a dominance of *Inga vera* in the tree canopy. In other places, an open canopy of *Pinus occidentalis* dominates the secondary vegetation. Further tree species abundant in the secondary forest of the mid-elevations of the Mogote are *Cupania americana* and *Alchornea latifolia*, among others. Lianas like *Mikania venosa* are also abundant, especially in places where Hurrican George felled many trees. In areas of open secondary forest on the Mogote, the herbaceous layer is dominated by the grass *Melinis minutiflora* (May & Peguero 2000).

In the UCRYN there are many places with degraded remnants of the lower montane pine forest which covered much of the area in the early 20th century. These open pine forests, where ferns or grasses dominate the herbaceous layer, are sometimes used as pasture areas. In the southern UCRYN there are large areas of open pine forests with low crown cover resulting in a spectral signature in the satellite images which is defined mainly by the fern (bracken) of the herbaceous layer (plate 35).

3.3 Information for Forest and Land Use Management in the Dominican Republic

3.3.1   Forest Mapping and Inventories since 1950

In the past decades, expert estimates, interpretation of aerial photographs and classification of medium resolution satellite data have been used to gain information about the forests of the Dominican Republic. The earliest attempts to use remote sensing for investigating the country's vegetation occurred in the 1950s. A set of 1:60,000 black-and-white aerial photographs taken in 1958-1959 were used in the 1960s by the Organization of American States (OEA) for an evaluation of the natural resources of the Dominican Republic. Black-and-white aerial photographs at the scale of 1:20,000, taken between 1966 and 1968 during an aerial survey conducted by the OEA, were used for a 1973 FAO inventory of natural resources (Tolentino & Peña 1998). In the late 1970s, satellite images were used for the first time in the Dominican Republic for a land cover / land use classification through visual interpretation of Landsat MSS imagery conducted by CRIES and USAID. The CRIES study defined forests as areas with at least 70 % tree crown cover, thus excluding, among other things, most of the pine forests of Dominican Republic and classifying only 14 % of the country as forested (CRIES 1980 quoted in Russell & Fournier 1992). 1:40,000 black-and-white aerial photographs of the whole country were taken in 1983-1984 and used for the preparation of a land use map by DIRENA, the Department for the Inventory of Natural Resources of the Ministry of Agriculture (Tolentino & Peña 1998). This was the last nation-wide inventory to date which was based on high-resolution remote sensing data, and DIRENA concluded from the photographs that in 1983/1984, 28.8 % of the country was covered by forests (6.1 % pine forest, 6 % broadleaved forest and 16.7 % dry forest) (Consorcio Ingeniería CAURA - ESRI - DESAGRO 2002).

No country-wide aerial survey was conducted in the 1990s, so that for this decade, information about the national land cover can only be based on expert estimates and one Landsat TM classification. The results are not very conclusive. The forest cover estimates for the Dominican Republic for the 1990s range from 10 % to 29 %. Bolay (1997:336) thinks it is less than 11 %, May (1997) estimates the forest cover at 10-15 %, and the Statistisches Bundesamt (1996) gives the figure as 12.5 %. SEMARENA (2002) gives the forest cover at the beginning of the 1990s as 14 %. In contrast, Ulbert (1999) quotes the *Informe National* of the Dominican Government (1991) which states a forest cover of 29 1 % (mostly dry forest) and Tolentino & Peña (1998) state a forest cover of 27.5 % based on the classification of Landsat TM images from the years 1988-1996, which is also the result accepted by SEMARENA (2001a) in its national forest inventory and the source of the statistics of FRA 2000 (FAO 2001 / FAO 31.12.2000). The numbers for forest cover quoted above show a considerable variation in forest cover estimates for the 1990s. This disparity is partly due to inconsistent or loose forest definitions (e.g. what degree of crown cover constitutes a forest

and where to draw the line between shrubland and forest) but it is also due to different error sources depending on how the numbers were derived. Without either a recent forest inventory involving country-wide field sampling or country-wide up-to-date detailed mapping based on high resolution remotely sensed data it is hard to say which numbers are the most accurate ones. In general, if the Landsat classification is supposed to give a fairly correct overview over the distribution of the main land cover types, it seems that the experts overestimated the amount of deforestation which happened since the mid-1980s, or some did not include the dry forest in their forest definition. A similar situation of incompatible forest cover assessments, carried out by different organizations with different objectives, class definitions, information sources and methods, resulting in an overestimation of deforestation for the 1990s, is reported for Jamaica by Evelyn & Camirand (2003).

There have also been forest mapping efforts which covered only parts of the Dominican Republic. Russell & Fournier (1992) studied the land cover changes in the western half of the Dominican Republic on the basis of Landsat images of the years 1972/1973, 1979 and 1985/1986, using consistent methods. They found that the area of coniferous and broadleaved forests (without dry forests) decreased from 28 % to 19 % of their study area from the early 1970s to the mid-1980s. Hudson (1991) interpreted aerial photographs of montane forests in the Sierra de Bahoruco. Another example of local forest and land cover mapping in the Dominican Republic is the study of Laba et al. (1997) who used Landsat TM data to classify the land cover, including the mangroves, of the lower Yuna River watershed.

The country-wide forest and land cover information which is currently most widely used is the Landsat-based one (Tolentino & Peña 1998). In 1993, the Department for the Inventory of Natural Resources (DIRENA) started the project 'inventory and evaluation of the natural resources of the Dominican Republic'. Its aim was to collect up-to-date information about the country's vegetation with the help of remote sensing and to create a basis of georeferenced data for management planning. The methods that were used and the results of the vegetation mapping are described by Tolentino & Peña (1998). The classification was mainly based on digital Landsat data of the years 1988, 1992 and 1996 covering the whole country. The satellite data were classified using a supervised classification based on about 250 field sampling plots and complemented by a visual interpretation of the Landsat data as well as information derived from the 1983-1984 aerial photographs. The resulting land use and land cover map at the scale of 1:500,000 shows a forest cover of 27.5 % (6.3 % coniferous forest, 13.1 % broadleaved forest, 7.6 % dry forest and 0.5 % wetland forest). Additionally, 14.1 % of the country is covered by shrubland (*matorrales*), according to these results. Tolentino & Peña (1998) do not report that any accuracy assessment was conducted for this Landsat-based vegetation map.

The *'Inventario Forestal'* published by the Dominican Ministry of Environment (SEMARENA 2001a) uses the results of this study and further subdivides the mapped forest into forest within protected areas (36.7 %) and outside of protected areas (63.3 %). The latter is further subdivided into production forest (67 %) and protection forest (33 %). (Protection forests are forests outside of protected areas but with management restrictions; this includes riparian forests, forests on steep slopes, cloud forests and wetland forests.) The *'Inventario Forestal'* also quantifies the total timber volume of the national forests using estimated average volumes (m³/ha) for dense coniferous, open coniferous, broadleaved and dry forests and plantations. SEMARENA (2001a) announced a plan to update the Landsat-based map using more recent Landsat data and aerial photographs of a new aerial survey which started in 2001. This survey is conducted by the National Institute for Water Resources (INDRHI), producing 1:20.000 colour photographs. It had covered 95 % of the country by August 2003 (with exceptions mostly in mountain areas with frequent cloud cover), but the photographs were not yet completely pre-processed nor available (http://www.indrhi.gov.do/). The Ministry of Environment announced in July 2004 on its website (http://www.ceiba.gov.do/ 2004/noticias/esp/jul-04/0727_esp.html) that an update of the map of Tolentino & Peña (1998) had been done using Landsat data of the years 1996 and 2003, with the result that the forested areas had increased to 32.9 % of the country.

3.3.2   Information Needs

As in many tropical developing countries, there is a lack of high quality forest and land cover information in the Dominican Republic. Reliable and regularly updated information about the extent and location of land cover types and their changes over time would be an important basis for the development of policies and measures leading to reasonable and increasingly sustainable forest and land use management practices. Vegetation maps or 'inventories' based principally on the classification of medium resolution satellite data are not sufficiently detailed to be used as a basis for forest management plans. In the field of commercial forestry, the administration could also use regularly updated high resolution maps to supplement their knowledge (in the spatial domain) about whether the measures to encourage afforestation are effective, and to control whether the establishment of plantations and the management of natural forests are conducted according to the propositions.

SEMARENA (2002:35) bemoans the lack of information, order and continuity in the study and monitoring of the state of the environment and the natural resources. This makes it difficult to put into action the principle of the polluters' financial responsibility for contamination established in the law 64-00. Proposed payment schemes for environmental services in watersheds (Heindrichs 2004) need regularly updated information about the natural resources in order to become operational.

The insufficient quality of the available biological and cartographic information (May 1997) still entails ill defined or arbitrary borders of protected areas. As a basis for improving the legislation and management regarding protected areas, high-quality spatial information is needed in order to answer for example the following questions:

- Which areas are covered by which type of primary forests?

- Do the primary forests change over time regarding their area or their qualities?

- Which forest types are threatened / in need of additional protection?

- Are there non-natural types of land cover included within the current boundaries of protected areas? Where? What types of land cover or land use?

- Are the protective measures effective or are there unwanted land cover changes in protected areas?

The development of largely automated processing methods for high resolution remotely sensed data is required in order to make the repeated production of up-to-date high quality forest and land cover maps feasible for tropical mountain regions. One of the aims of this study is to contribute to the knowledge about the utility of several methods to derive the required information from high resolution satellite data.

4 Data and Tools

Two kinds of satellite data (medium resolution Landsat and high resolution IKONOS) were used in this study. Additionally, a Digital Elevation Model (DEM), aerial photographs and topographic as well as thematic maps were available as sources of spatial information.

4.1 Satellite data

4.1.1 Landsat-7 ETM+

Landsat-7 is the most recent in the series of Landsat satellites, which have been used to acquire medium resolution imagery of the Earth since 1972 (USGS 01.03.2005). Landsat-7, carrying the Enhanced Thematic Mapper Plus (ETM+) instrument, was launched in April 1999. Four years later, on 31 May 2003, the scan line corrector failed, introducing data gaps in the ETM+ images and thus reducing the coverage of full quality Landsat ETM+ data.

The satellite has a sun-synchronous orbit with a 98-degree inclination and an altitude of 705 km. It has a swath width of 185 km and a repeat coverage interval of 16 days. The ETM+ is the latest version of the Thematic Mapper (TM) instrument carried by Landsat-4 and -5. The ETM+ instrument records essentially the same spectral bands as its predecessor, but it has an additional panchromatic band with 15 m ground resolution and a better ground resolution in band 6 (thermal infra-red) (table 2).

Table 2: ETM+ characteristics.

Band Number	Spectral Range (µm)	Ground Resolution (m)
1	0.45 to 0.515	30
2	0.525 to 0.605	30
3	0.63 to 0.69	30
4	0.75 to 0.90	30
5	1.55 to 1.75	30
6	10.4 to 12.5	60
7	2.09 to 2.35	30
Pan (8)	0.52 to 0.90	15

The Landsat-7 ETM+ scene used here has the path/row numbers 08/47 and covers the central and western Dominican Republic. It was acquired on 15 September 2000 at 14:59 GMT (Greenwich mean time). The illumination is characterized by a sun azimuth angle of 120° and a sun elevation

angle of 60.5°, and the image was processed to Level 0R (see metadata in appendix 3). The Level 0R Landsat product is reformatted raw data delivered with a radiometric resolution of 8 bit. Values are Digital Numbers (DN). The scene is very clear over the study area with no visible atmospheric effects except for a few small clouds (see figure 8).
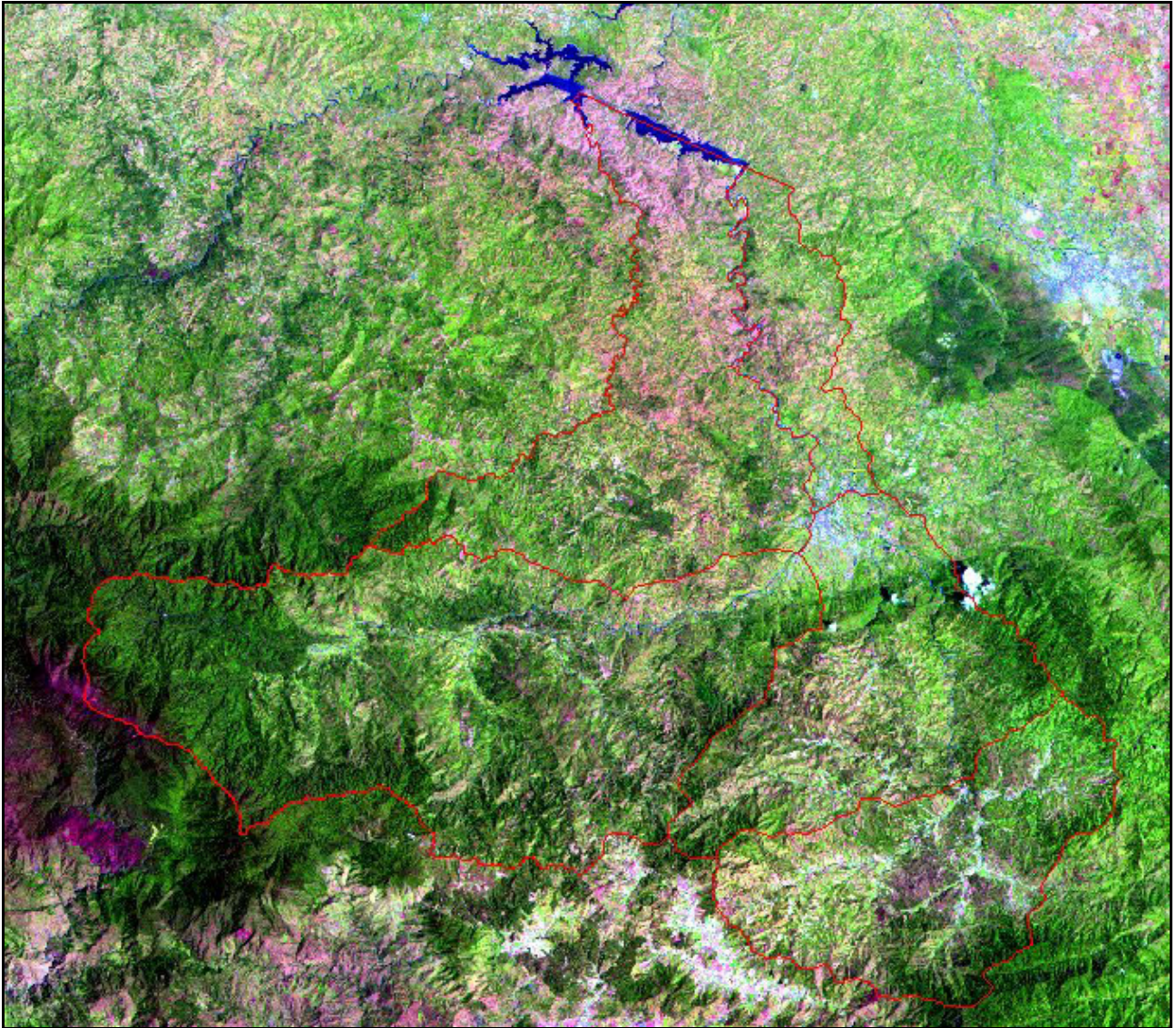
Figure 8: Landsat-7 ETM+ image subset of the upper catchment area of the Río Yaque del Norte, RGB 583.

4.1.2 IKONOS

The IKONOS-2 satellite was launched in September 1999 and has been delivering commercial data since early 2000. IKONOS is the first of a new generation of high spatial resolution satellites which by now also include QuickBird-2, OrbView-3 and Eros A1. The IKONOS sensor uses a large telescope and pushbroom detector technology to simultaneously record four channels of multispectral data at 4 metre resolution and one panchromatic channel with 1 metre resolution

(nominal resolutions at < 26° off nadir). The spectral range of the multispectral channels is almost identical to that of the first four Landsat channels (see table 3). The IKONOS satellite is in a sun-synchronous orbit with a 14 days repeat cycle but is has a 1 to 3 day revisit time due to its pointing capability of 30° in any direction (Van der Meer et al. 2002). Further orbital information is listed in table 4. IKONOS data is collected as 11 bits per pixel (2048 grey tones).

Table 3: IKONOS-2 instrument characteristics.

Band Number	Spectral Range (µm)	Ground Resolution (m)
1	0.45 to 0.52	4
2	0.52 to 0.60	4
3	0.63 to 0.69	4
4	0.76 to 0.90	4
Pan	0.45 to 0.90	1

Table 4: IKONOS-2 orbital information (Dial et al. 2003).

Altitude	681 kilometers
Inclination	98.1 degrees
Orbit time	98 minutes
Orbit type	sun-synchronous
Descending nodal crossing time	~10:30 a.m. local solar time
Nominal swath width	13 km at nadir
Revisit frequency	3 days at 1 meter resolution (60° collection elevation / 26° off nadir) These values are for targets at 40 degrees latitude. The revisit times will be less frequent for latitudes closer to the equator.
Viewing angle	Agile spacecraft - in-track and cross-track pointing

IKONOS is thus the first satellite delivering commercially available high resolution multispectral data with global coverage and constant acquisition parameters (apart from the variable viewing geometry). This makes it possible for the user to acquire near photographic quality satellite imagery of anywhere in the world (except for polar regions).

IKONOS data are marketed by Space Imaging. The data are collected on request only and can be ordered as a new collection (scheduling and tasking of the satellite), or from Space Imaging's imagery archive if data of that location has already been collected. The pricing varies considerably depending on the area of interest (km²) and its location, the product (processing level) and the type of licence, among other factors. In Europe, the non-orthorectified 'Geo product' including all five bands cost 27.50 US $ per km² for a new collection and 21 US $ per km² for archived data in 2004.

The prices are higher for orthorectified products, stereo pairs and in case of 'priority tasking' (fixed acquisition time frame). The imagery which is delivered can contain up to 20 % cloud cover.

The IKONOS data which were available for this study belong to the 'Geo product' category. Image distortions which are due to the collection geometry are removed in this product, and the imagery is resampled to a uniform pixel spacing and a specified map projection. There is no correction of terrain effects, though (Space Imaging 2004).

12 IKONOS images of diverse quality (in terms of haziness and geometric distortions) cover the UCRYN. They are partly cloudy, so that they contain information about somewhat less than 100 % of the surface of the catchment area. They were acquired between September 2000 and June 2002. Two of these images, which are of relatively high quality, were used for further processing (beyond visual enhancements). Their acquisition parameters are presented in table 5 (see also appendix 4).

Table 5: Acquisition parameters of IKONOS images used in this study.

	Eastern image (the eastern test area is a subset of this image)	Western image (Manabao).
Acquisition date/time	19 April 2001 15:19 GMT	22 May 2002 15:37 GMT
Sun angle azimuth	109.9°	According to metadata file 81.6°, but looking at time of acquisition, sun angle elevation and shadows in the image, this must be an error; the real value is ~120°.
Sun angle elevation	68.3°	75.1°
Nominal collection azimuth	220.2°	322.0°
Nominal collection elevation	81.3°	66.9°
Acquired nominal GSD (ground sample distance) cross scan	0.83 m	0.91 m
Acquired nominal GSD (ground sample distance) along scan	0.83 m	0.93 m

Both images have relatively high sun elevations (68° and 75°), leading to only slight topographic illumination effects. The eastern image (figures 9 and 10) also has a high collection elevation (81°), while the Manabao image has a collection elevation of only 67°, leading to stronger geometric distortions through terrain displacement.

Figure 9: IKONOS multispectral sub-image of the eastern test area (red dotted line: western border of the Scientific Reserve Ebano Verde), RGB 321.
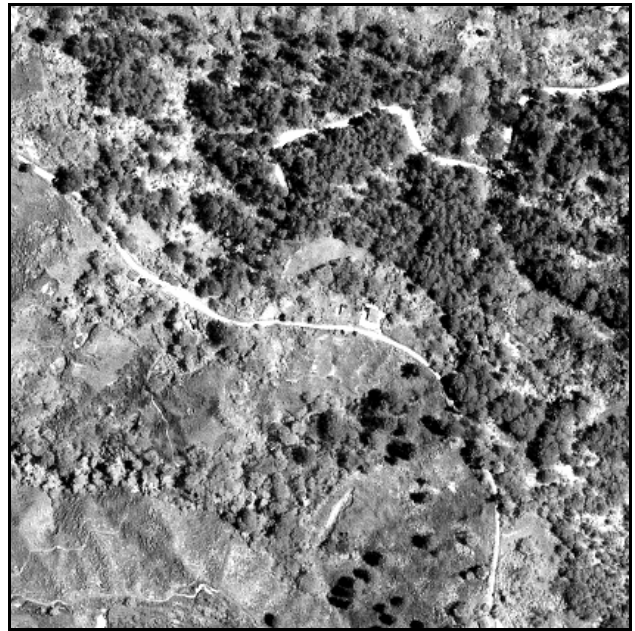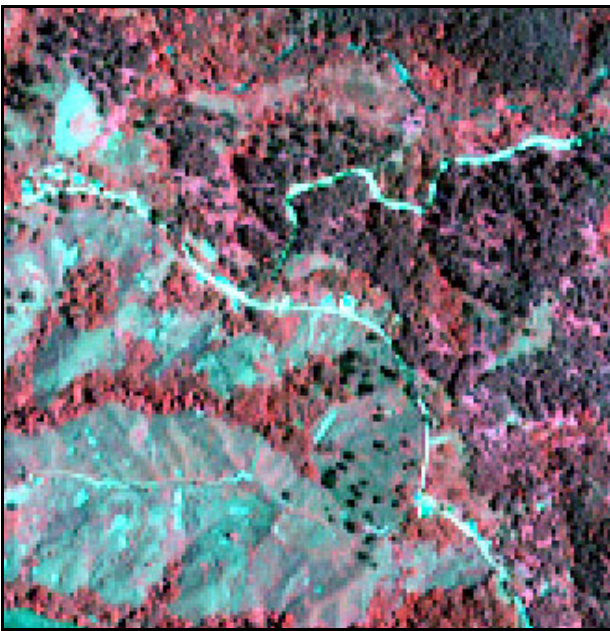
Figure 10: IKONOS multispectral data, 4 m resolution, RGB 432 (left) and panchromatic data, 1m resolution (right).

4.2 Aerial photographs

Black-and-white vertical aerial photographs from April 1966 (scale 1:20,000) and March 1984 (1:40,000) for use as reference were available for the south-eastern part of the study area (the area

between the valley of the Río Jimenoa and the eastern declivity of the Cordillera Central, including the Scientific Reserve Ebano Verde).

In the course of my fieldwork, an aerial survey was conducted over the UCRYN on 23 March 2003, taking 300 oblique aerial photographs out of the windows of a Cessna 172 airplane using handheld cameras (a Nikon Coolpix 995 digital camera, a Canon G series digital camera and a Canon F1 analogue camera with slide film). The flight passed over the UCRYN from east to west, circling over the Río Jimenoa/La Sal/Ebano Verde area, over the Arroyo Grande valley south of Manabao and around La Ciénaga and finally passing the Pico del Yaque at the western edge of the catchment area, before leaving the UCRYN in a north-easterly direction.

4.3 Digital Elevation Model

A 50 m resolution digital elevation model (DEM) in raster format was available, providing information about the approximate elevation of every point of the study area. The DEM is based on contour lines digitised from 1:50,000 topographic maps in conjunction with the DIRENA project 'Inventory and Evaluation of the Natural Resources of the Dominican Republic'. Only the 100 m interval contour lines were digitised in the mountainous areas, so that the elevation values in the 50 m grid are a product of interpolation with large featureless triangles in areas of low relief like the valley of Jarabacoa. The actual resolution of this DEM is lower than 50 m. There are also artefacts which have probably been introduced through errors during the digitisation. Li (1994:2) found that "the accuracy of DTMs derived from (photogrammetrically measured) contour data, in terms of RMSE (root mean square error) or σ (standard deviation), is about 1/3 to 1/5 of the contour interval, depending on the characteristics of the terrain topography." For the terrain data at hand, this would correspond to an RMSE between 33 m and 50 m.

4.4 Maps

Topographic maps of the scale 1:50,000 covering the whole UCRYN were used in this study. These maps were originally compiled in the 1960s and most of the map sheets have been updated by the *Instituto Cartográphico Militar* (ICM) with the help of the 1984 aerial photographs. A 1:250,000 geological map of the Dominican Republic and two land cover and vegetation maps of the Scientific Reserve Ebano Verde (Progressio 1995, García et al. 1994: fig. 5) were also available.

4.5 Tools

The PCI Geomatica software (versions 8 to 9.1.4) was used for the vast majority of image processing and classification in this study. If not specified otherwise, the applications of this

software were used for the data processing described in the following chapters. PCI Geomatica's GIS-functionality was also utilised for some tasks. The software used for image segmentation and object-oriented classification was eCognition 3.0. ArcInfo/ArcView was used for the handling and transfer (importing/exporting) of some of the data in vector format.

Excursus: Software Problems ('Bugs') Encountered during Image Processing

Corruption of bitmaps (masks) in PCI Geomatica

The software (Focus Version 8) used to add areas along the right edge of the image to bitmaps (without user input). This led to some considerable extra work, repairing the affected bitmaps and checking whether such masks (without me noticing the change in time) had been used to define training samples, thus possibly influencing class signatures and classification results.

Corruption of PCI Geomatica files of the western test area

Project files of the western test area (which is four times as large as the eastern test area) were corrupted after they had been orthorectified and texture channels had been calculated and added. This happened in the form of a sudden misalignment between data layers. The necessary data restoration delayed the data processing for the western test area. In the end, the testing of classification methods was limited to the eastern test area because of time constraints.

---

5 Field Work

In 2002 and 2003, two field work campaigns were conducted in the study area. I spent my time in the Dominican Republic (20 February to 27 March 2002 and 4 March to 6 April 2003) mainly in the UCRYN (based in Jarabacoa), apart from a round trip through the country accompanying a geographical field course during the first two weeks and two short geobotanical field trips in the Sierra de Baoruco. The time in the UCRYN was used to establish contacts with people working in the area, to collect ground data and other locally available information, and to gain firsthand experience of the physiogeographical nature of the Cordillera Central and the conditions under which its rural population lives and farms. The main purpose of the field work was the collection of spatially determined land cover information. These field data were acquired primarily as a basis for the establishment of training areas for the intended supervised image classifications and secondarily to enable a subsequent verification of results.

In 2002, 49 field plots, including all the desired classes for the Landsat classification (chapter 7.1), were established. This was done with the help of two geography students from the University of Göttingen and two students of the Instituto Superior de Agricultura (ISA) in Santiago who were interns at PROCARYN. The field plots were required to be located in an area of at least 1 ha of the class under consideration to make sure that at least a couple of pure Landsat pixels representing the particular class could be identified. The position of the plot was described and recorded using a handheld GPS (Global Positioning System). Each plot was assigned to a class and the dominant species of trees, shrubs and herbs (or a more general description where the exact species could not be determined) were recorded together with the estimated tree crown cover, overall vegetation cover and, in mountainous terrain, slope and aspect. Distinctive features of the plots, like observations of soil characteristics or evident land use or additional information about the land use history, were also noted down and photographs of the plots were taken with a digital camera. As one and a half years had passed since the acquisition of the Landsat imagery in September 2000, local farmers were asked for information about land use changes during the last years in some cases where it was possible that such changes had happened. There was for example a hillside covered by fern and small bushes which we were told had been an unprofitable coffee plantation in 2000 and which still looked like the neighbouring coffee plantations with low vegetation cover in the Landsat image. In other cases, there were young pine plantations which had not yet been there in 2000, or recently established chayote fields.

In addition to these standardised field plots for the Landsat classification, several hundred land cover observations were recorded in 2002 and 2003 with different levels of detail. For these potential training and testing areas, at least the position and the vegetation type (land cover class) are known, partly with additional information including distinctive species, estimated crown cover and tree height or age. The land cover was documented with ground photographs (see examples in

appendix 1) and the location was measured with the GPS and/or marked directly onto the paper copies of the IKONOS images carried in the field. These observations, recorded mainly as a basis for a more detailed image analysis involving the IKONOS imagery, include a larger number of different forest types, and the minimum area of 1 ha does not apply here, so that for example narrow riparian forests, small agroforestry plots or small groups of pine trees are also recorded.

The field plots were distributed over the whole UCRYN study area, as far as the access and the time frame permitted, i.e. mainly in the vicinity of roads and of tracks that were negotiable with all-terrain vehicles. For field work further away from the roads, access on foot was gained during several hikes in the Scientific Reserve Ebano Verde and its surroundings and in the mountains of the westernmost UCRYN. In order to gain a third perspective of the study area, intermediary between the satellite imagery and the view from the ground, and also to have a look at some more remote areas with difficult access, a flight in a Cessna 172 was conducted over the study area in March 2003. Oblique aerial photographs were taken from the low flying aircraft (chapter 4.2). These aerial photographs also served to document the land cover situation in the UCRYN in 2003 and to identify some cases of short-term land cover change in comparison to the IKONOS images, most of which were acquired in 2001 and 2002.

The area of the Scientific Reserve Ebano Verde and its western surroundings in the south-eastern UCRYN is a main focus of this study with a high data density including good quality IKONOS data and black-and-white aerial photography. Accordingly, the field work was also concentrated here resulting in a high density of training areas. This eastern test area is about two thirds forested. Another focus area with a high overall density of field plots and observations is the region of Manabao in the western UCRYN.

In addition to establishing training areas, ground control points identifiable in the IKONOS images, like road junctions, footpaths, corners of buildings or individual trees, were measured on the ground with a GPS in order to improve the possibility to geometrically correct the imagery of the special interest areas. Measurements were taken with a handheld GPS (Garmin GPS 12) and averaged over a period of time before saving them, aiming at accuracies of ±8 m or better depending on the reception (terrain and vegetation dependent visibility of satellites).

Apart from the field work as such, the stays in the Dominican Republic were used to get into contact with local scientists like Ramón Elias Castillo of the PROGRESSIO foundation, who accompanied me into the Scientific Reserve Ebano Verde, botanist Dr. Thomas May, who is a resident of Jarabacoa, and staff members and freelance technical advisers of the PROCARYN project. Information in the form of maps and literature about the study area was collected in Jarabacoa and Santo Domingo, through visits at the Botanical Garden of Santo Domingo, the

Geographical Institute of the Universidad Autónoma de Santo Domingo, the Instituto Cartográfico Militar (Military Geographic Institute) and the Head Office of National Parks in Santo Domingo.

Figure 11: Field work. Above: Entrance to the core area of the 'Reserva Scientífica Ebano Verde', eastern test area. Below left: Crossing the Río Yaque del Norte on the way into the westernmost UCRYN. Below right: On foot in the 'Reserva Scientífica Ebano Verde', measuring the location of a *calimetal* area in the eastern test area.

6   Data Pre-Processing

6.1 Landsat ETM+ Pre-Processing

The Landsat multispectral and panchromatic images were imported into PCI file format and a preliminary subset of the whole UCRYN and its neighbourhood was prepared.

Channel 6 (thermal infrared) and the panchromatic channel of the Landsat-7 Level 0 R data contained cyclical striping effects caused by uneven detector signal response in the ETM+ detector array. These channels were destriped using a histogram modification. This involves setting a cycle according to the number of detectors, calculating a histogram each for all the lines sensed by the same detector and then matching the 'cycle' number of histograms. No further radiometric distortions were visible in the data and no further radiometric correction was conducted.

In order to be able to combine all Landsat channels in one file with a common spatial resolution and to enable a more accurate geometric correction, channels 1 to 7 were resampled to half the pixel size so that all channels had the same spatial resolution as the panchromatic channel. This was done using nearest-neighbour resampling so that the digital numbers of the pixels were not changed. All channels were then transferred to a single file with the panchromatic channel as channel number 8.

The scan-misalignment (figure 12) in the raw data was corrected using a procedure written for PCI's EASI software (see appendix 3), which shifts the image every 32 lines to compensate for the offset.
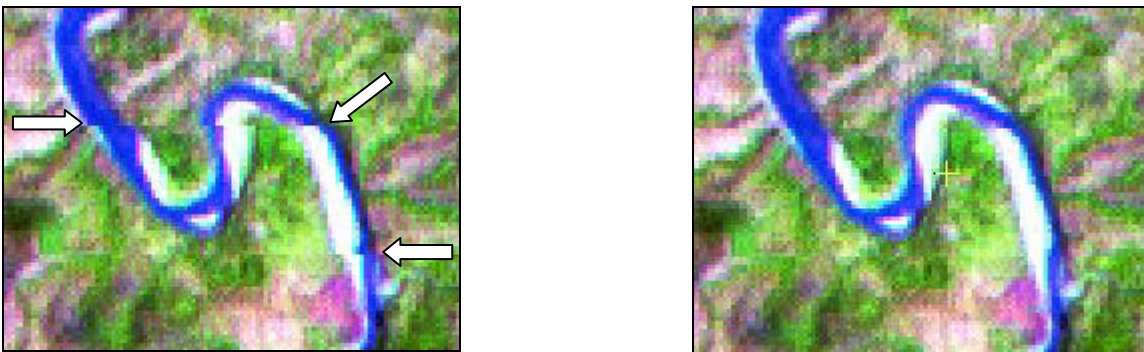
Figure 12: Scan-misalignment in the Landsat-7 ETM+ Level 0R data (left) and the area after correction (right) (RGB=583).

The 8-channel Landsat ETM+ subset was then georeferenced to the UTM projection using 37 ground control points (GCPs) derived from the 1:50,000 topographical maps. A second-order polynomial transformation was used for the geometric correction. The image was resampled to 15 m resolution using the nearest neighbour method. The root mean square error (RMSE) achieved was 1.8 in the x-direction and 1.2 in the y-direction, referring to 15-m-pixels. This corresponds to

sub-pixel accuracy (0.9 and 0.6) with respect to the original multispectral Landsat pixels. Topographic effects on the image geometry were relatively small because of the near-nadir viewing angle of Landsat, and were not corrected for beyond the correction through the second-order polynomial transformation. After the geometric correction, the final rectangular subset of the study area (UCRYN) was cut out.

The ETM+ image used appears very clear on the whole, without any conspicuous unevenness of atmospheric contamination across the scene (apart from the small clouds). No atmospheric correction was conducted. To accurately convert the sensor measurements to surface reflectance using radiative transfer codes would require accurate knowledge about the state of the atmosphere at the time of image acquisition, which is not available in this case. That said, for the spectral bands of the Landsat ETM+ sensor (and also of the IKONOS sensor), the main atmospheric effect is scattering. This effect is additive to the detected signal and could be corrected by subtracting a band-specific constant from all pixel values in the image. But such a linear transformation does not change the relationship between the classes in the feature space (does not change the variance-covariance matrix for the classes) and thus has no influence on the result of a maximum likelihood classification (Song et al. 2001). A correction of topographic illumination effects was not conducted either, as these effects were not very strong in the image because of the high sun elevation angle at the time of the image acquisition. Besides, for an image of this heterogeneous landscape, topographic normalisation would have been complicated by the fact that topographic effects differ between land cover types with different canopy structures (Allen 2000). The low quality and resolution of the available DEM would also have decreased the effectiveness of a topographic normalisation attempt.

6.2 IKONOS Pre-Processing

The twelve IKONOS images covering the study area were imported into the PCI Geomatica environment. The multispectral and panchromatic images were visually examined. For some areas of special interest, panchromatic and multispectral channels were fused using the IHS (intensity, hue, saturation) transformation in order to produce colour images at 1 m resolution. This pan-sharpening had the purpose to enhance the possibilities of visual interpretation for training areas and accuracy assessment and to help to recognise the position in the real world (in the field) on the images.

Paper prints of images at reduced and full resolution were produced and used during the field work (chapter 5.2). The IKONOS images of the whole UCRYN were also used as reference for the Landsat classification and accuracy assessment.

For reasons of time and disk space, the IKONOS data were not further processed for the whole catchment area. Only subsets of two of the twelve images were used to test high resolution image processing methods. These two test areas were selected because they were of special ecological and economical interest. The subsets of one image of the eastern and one of the western UCRYN show a large variety of forest types, including plantations, natural and semi-natural forests, and other land cover types of the UCRYN. The IKONOS data covering these areas were of good quality (low cloud cover and atmospheric contamination), and the information density through field work and ancillary data was particularly high for these areas, especially for the eastern test area, which was used as the main IKONOS test area. This area includes the land cover types of the Scientific Reserve Ebano Verde and its buffer zone, from the agriculturally used slopes on both sides of the Río Jimenoa in the west to the centre of the reserve with the cloud forest of the 'Loma La Sal' and 'Loma La Golondrina' in the east of this test area. The western test area is located to the west of the town of Manabao and includes areas of coffee and pine plantations and the natural forest at the edges of the Armando Bermúdez National Park.

No radiometric distortions or striping were noticeable in the images. No atmospheric correction was conducted for the reasons mentioned in chapter 6.1 (a possible atmospheric correction would not change the relationship between the classes in the feature space). The high sun elevation angles (68.3° in the eastern image and 75.1° in the western image) lead to relatively consistent illumination conditions in the images so that, also in view of the fact that the resolution of the available DEM was very much coarser than that of the IKONOS images, no topographic normalisation was attempted.

The IKONOS data were converted from 11 bit to 8 bit radiometric resolution. The distribution of the grey levels in the visible multispectral IKONOS bands (bands one to three) did not make use of the 11 bit radiometric resolution. Excluding extreme values that belonged only to cloud areas, the data spanned only between 250 and 500 grey levels, i.e. about 8 to 9 bit. The range of values in the NIR and panchromatic bands was somewhat larger, with up to about 1000 grey levels representing the objects of interest (again excluding clouds). All bands were scaled down to 8 bit before further processing in order to make the data more manageable and reduce processing times. In the case of the eastern test area, automatic normalised quantisation was used to reduce the radiometric resolution to 8 bit. This algorithm maps the median value of the input image to the middle of the output range and renders the central portion of the data range with little distortion while gradually compressing the high and low portions of the input range (PCI 2001).

Geometric correction of IKONOS data

The IKONOS images, being 'Geo products', were already resampled to the UTM projection. They do, however, contain some residual positional errors and they are not corrected for terrain effects.

Geometric errors of some tens of metres could still be found even in those images acquired with relatively high collection angles (low off nadir angles), rising to hundreds of metres in images with less favourable collection parameters. This requires additional geometric corrections, especially if the data are intended to be combined with other georeferenced data.

The eastern IKONOS image has a high nominal collection angle of 81.3°, resulting in only moderate relief displacement (15 m per 100 m elevation, corresponding to 10 m to the west and 12 m to the south at the nominal collection azimuth of 220.2°). In view of the fact that no high quality DEM was available, this image was not orthocorrected (Toutin 2004) but geometrically corrected using a polynomial transformation. To do this, both the panchromatic and the multispectral image were subset to an area of high ground truth density (eastern test area). 26 ground control points were identified on the panchromatic image using reference points measured with the GPS in the field as well as points identified on the topographic map. Choosing a first order polynomial transformation resulted in an RMSE of 6.73 m in the x-direction and 9.21 m in the y-direction. Since the RMSE was not reduced by applying higher order models, the registration was performed using a first order polynomial transformation and the nearest neighbour resampling technique. The GCPs were saved and the same set of GCPs was used to geometrically correct the multispectral image using the same parameters. In order to be able to integrate Landsat and IKONOS data, a Landsat subset of this area was tied down to the corrected panchromatic IKONOS image. 73 GCPs were identified both in the 15 m resolution panchromatic Landsat channel and in the IKONOS image, achieving RMS errors of 0.30 (4.5 m) in the x-direction and 0.32 (4.8 m) in the y-direction using a fourth order polynomial transformation. All three images were then trimmed to a common rectangular area, which will be referred to as 'eastern test area' in the following.

Most of the other IKONOS images of the UCRYN have lower nominal collection angles than this eastern image. The western IKONOS image (Manabao) for example has a nominal collection angle of 66.9°, resulting in a relief displacement of 43 m per 100 m elevation difference (corresponding to 26 m displacement to the west and 34 m to the north at a collection azimuth of 332°). This made the use of orthocorrection necessary if an acceptable geometric accuracy was to be achieved in this high relief area. A test was conducted to orthorectify this image with the available DEM.

Orthocorrection was performed on a subset of the western IKONOS image using the Rational Functions Model (PCI Geomatics 2001). This model uses ratios of two polynomial functions respectively to compute image row and column. The model was computed from 25 GCPs identified on the pan-sharpened 1 m resolution image (figure 13). The DEM used was a DEM with 10 m grid spacing which had been generated from the 50 m resolution DEM using the kriging method for the interpolation (PCI 2001). The number of coefficients used in the fitted polynomial was 4. This resulted in an overall RMS error of 19.86 m (13.41 m in the x-direction and 14.65 m in the y-direction). This is accurate to within one Landsat ETM pixel, but not close to sub-pixel-accuracy

regarding the IKONOS data. However, sub-pixel accuracy is not a realistic objective for IKONOS data even in flat terrain (Toutin & Cheng 2001) and even when using high quality DEMs (Davis & Wang 2003). In high-resolution imagery like this, GCPs cannot always be placed on the image with sub-pixel accuracy. The limited accuracy of the GPS which measured GCP locations in the field and of the 1:50000 topographic map used as a basis for part of the GCP coordinates contribute to errors, and the DEM used introduces additional error. Considering the limitations of the underlying data, the above mentioned accuracy seems reasonable and is certainly much better than the accuracy of the non-orthocorrected Geo product.
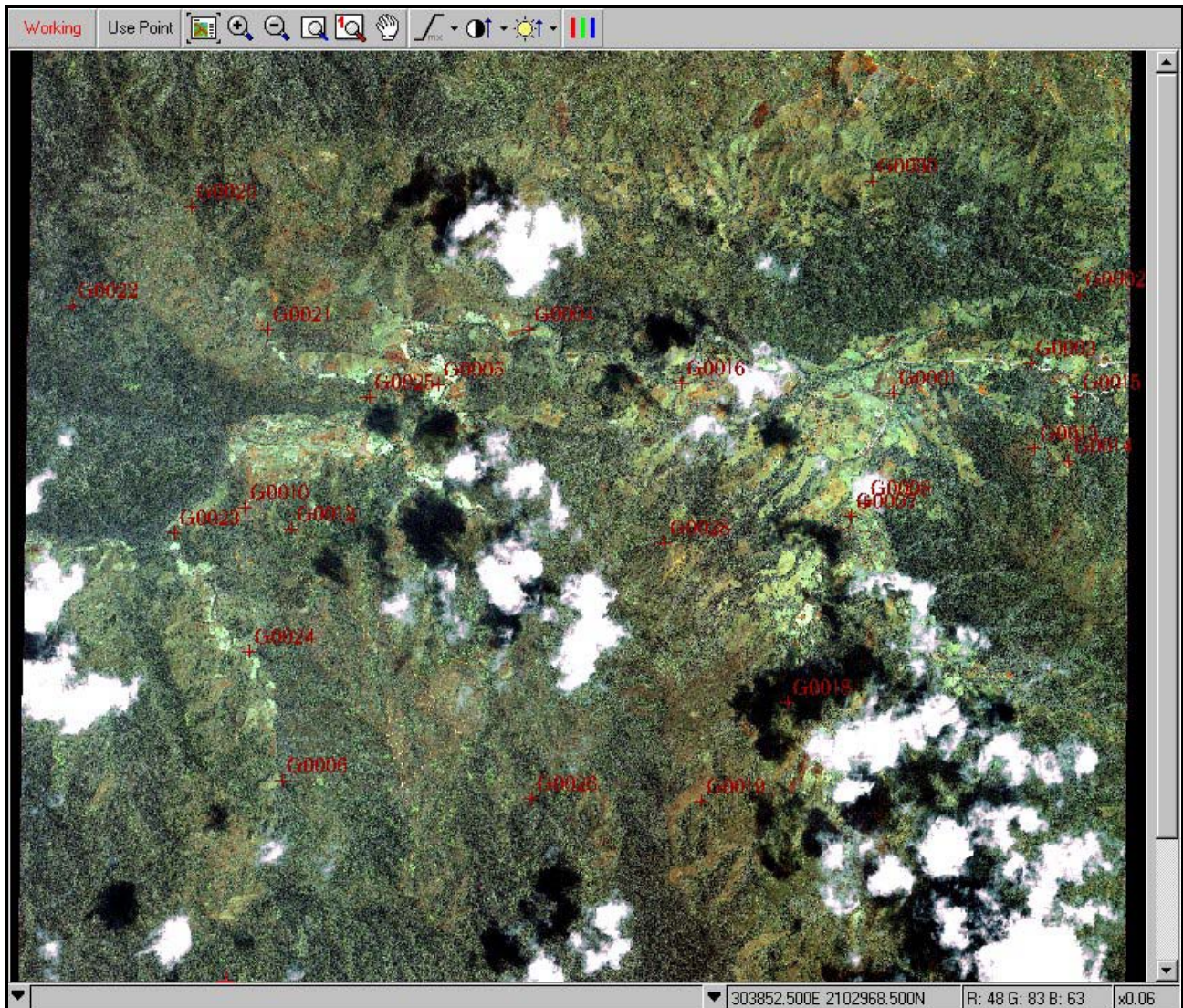
Figure 13: Distribution of GCPs in the western sub-image during orthocorrection (OrthoEngine environment).

6.3 Digital Elevation Model

The DEM was imported into the PCI Geomatica file format, resulting in a 16 bit data channel with 50 m spatial resolution and digital numbers corresponding to the elevation in metres. As the DEM

had been derived from digitised contours of the same topographical maps which were used as reference for the geometric correction of the satellite images, its UTM coordinates were already correct. The DEM was subset to an area corresponding to the rectangular Landsat subset of the UCRYN. The elevation values were checked for overall agreement with the topographical maps. Some obvious artefacts in the area of Jarabacoa (where the valley was rendered as a convex form) were manually corrected.

Kriging is a useful interpolation method when the surface is not adequately sampled (Robinson 1994). It was used for the generation of a DEM with 10 m grid spacing needed for orthorectification of the western image (chapter 6.2). A DEM with 8 m grid spacing for processing together with the IKONOS data of the eastern test area was also generated through kriging.

When gridded DEMs are created from contours without identification of drainage lines and ridge lines, flat areas along curved contours can be created by triangulation or during interpolation (Robinson 1994). There is evidence of this effect in the histogram of the DEM used here for the area of the UCRYN which shows sharp peaks at the digitised contour values, especially at 300, 500, 600 and 800 m. This effect is going to introduce errors in slope and aspect calculations, but there is no evidence of it in the more mountainous areas above 800 m, including the eastern test area, because of the reduced horizontal distance between the 100 m contour lines.

In the future, the SRTM 90-m DEM of the world might be a better quality alternative for correcting medium resolution satellite data, but its resolution is not sufficient to combine it with IKONOS data. High resolution DEMs for high quality IKONOS corrections would have to be derived from optical high resolution stereo data (e.g. IKONOS stereo product), but that would make them rather expensive. (The IKONOS Stereo product is 4 to 5 times as expensive as the Geo product.)

7   Landsat ETM+ Classification

The Landsat ETM+ data were used to create a base-map of the whole study area (UCRYN). The aim was to explore the possibilities and limitations of a standard (maximum likelihood) Landsat classification in this kind of landscape, in order to have a basis to which to compare the results achieved with higher resolution data and more extended methods. The results were also passed on as a base-map of land cover and land use in the year 2000 to the people working for improved land use management in the study area (PROCARYN project).

7.1 Initial Scheme of Informational Classes

Chapter 3 describes the many different natural, semi-natural and anthropogenic land cover types of the UCRYN. It is not to be expected, however, that for example all the different natural forest types (formations) and their secondary and degraded variations can be extracted as spectrally distinct classes from Landsat data. Furthermore, the sampling density over the whole UCRYN was not sufficient to have separate training areas for all the smaller land cover classes like specific crops. The informational classes that members of the PROCARYN project expressed their interest in were broadleaved forest, closed coniferous forest, open coniferous forest, young coniferous plantations, mixed (broadleaved and coniferous) forest, *matorral* (shrubland), agroforestry (coffee with shade trees), coffee without shade, other cultivated land, grassland (pasture), and areas of bare soil. This list was used as the basis for the Landsat classification. Additional informational classes (land cover types not included in the PROCARYN list but obviously present in the image) were 'water' and 'built-up areas'.

7.2 Classification of Landsat 7 ETM+ data

The Landsat ETM+ data of the UCRYN were explored using unsupervised classifications (K-means clustering) and test runs of supervised maximum likelihood classifications with different groups of training samples to arrive at an improved set of spectral classes to be used in the final classification.

Training areas for the land cover classes described above were created based on the field plots established in 2002. Additional information about field plots for the classes 'young coniferous plantations', '*matorral*' and 'coffee without shade' was provided by PROCARYN because there had been a lack of training areas for these classes. The positions of the field plots were located in the Landsat image and, avoiding border pixels (possible mixed pixels), the pixels in the centre of each field plot were used as training pixels. In order not to neglect the montane areas of the forest classes, training areas based on observations and GPS-measurements during a hike in the national park 'Armando Bermúdez' in the western UCRYN were also used. Training areas for the classes 'water' and 'built-up areas' were established without the help of field plots in image areas

obviously belonging to these classes (broad river sections, Tavera reservoir, urban area of Jarabacoa).

The resulting training samples for all classes were checked for normal distribution of their digital numbers in the Landsat multispectral bands. Where the training samples differed strongly from normal distributions (e.g. bimodal distributions), the samples were split into two more homogeneous spectral classes if the sample had a sufficient size to allow this. Based on these training samples, class signatures were generated using Landsat ETM+ bands 1-5 and 7, i.e. all multispectral bands except the thermal infrared (figure 14).
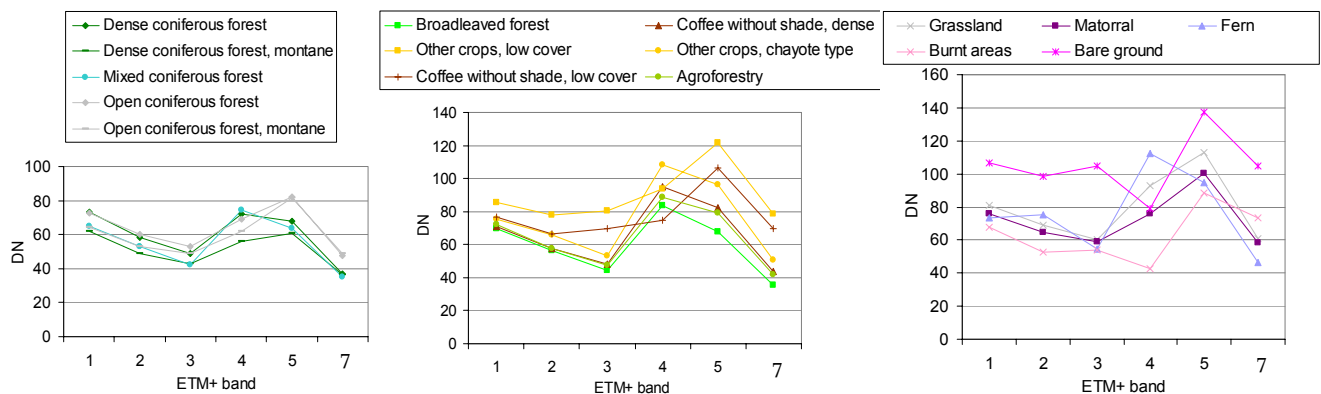
Figure 14: Spectral class signatures (channel means) from Landsat data.

After having tested different combinations of class signatures, changing the number of spectral classes where it was necessary, the Landsat data were finally classified into 19 spectral-informational classes (including clouds). This was done using the maximum likelihood classification method without a null class.

7.3 Post-Classification Processing

Cloud areas were masked after the classification, excluding them from further processing and accuracy assessment. Spectrally split classes belonging to the same informational class were recombined.

The classified image was then post-processed with the help of the DEM. The 50 m resolution DEM was transferred to the Landsat file as an additional channel using nearest neighbour resampling. Pixels with an elevation of more than 1600 m which had been classified as agroforestry (coffee with shade trees) were allocated to the class 'broadleaved forest'. Pixels classified as 'coffee without shade' were allocated to the class 'open coniferous forest' if their elevation was higher than 1700 m

(table 6). This was based on the knowledge that coffee plantations above 1500 m are rare in the study area, and plantations close to the upper cultivation limit usually do not include shade trees.

Table 6: Decision rules applied during post-classification sorting.

MLC result (class)	Decision rule	Final class
Agroforestry	If elevation is > 1600 m.………. otherwise………………………	Broadleaved forest Agroforestry
Coffee without shade	If elevation is > 1700 m.……….. otherwise………………………	Open coniferous forest Coffee without shade

Finally, the classified image was mode filtered using a 3 by 3 filter window, eliminating single pixels, the classification of which was not in agreement with that of their spatial neighbours.

7.4 Accuracy Assessment

512 points were distributed over the classified study area using stratified random sampling so that sampling points were distributed over all classes and the whole classified area. For 304 of these points, the land cover class could be identified, mostly with the help of pan-sharpened IKONOS images, recorded ground observations and aerial photographs. In some cases, the DEM was also used, e.g. to judge the probability of a coffee plantation occurring at a particular site, as opposed to brushland (*matorral*), which may look similar in high resolution remotely sensed imagery. An accuracy assessment was conducted for these 304 reference points, producing a confusion matrix and calculating the overall accuracy and producer's and user's accuracies for the individual classes (table 8). The overall accuracy was also calculated for a coarser classification level with just five classes (table 9), for which the classes were aggregated after the classification.

7.5 Results and Discussion

In the course of the classification test runs, it turned out that the original classification scheme had to be modified. There were some land cover types (fern and burnt areas) which had not been defined beforehand but turned out to be spectrally distinct and were added to the informational classes. By contrast, the informational class 'young coniferous plantations' was not at all spectrally separable in the Landsat image on the basis of the available training data, so the class had to be dropped. Mixed forests with a high percentage of broadleaved species were not spectrally separable from other broadleaved forest, so only the mixed coniferous forest in the mountain areas (pine forest with less than 50 % of broadleaved trees) was retained as a separate class. Some of the informational classes were spectrally heterogeneous and were split for the purpose of classification. The mountainous coniferous forests (both dense and open) had a spectral signature which was distinct from that of the coniferous forests of the lower elevations and had to be classified

separately. The informational class 'other cultivated land' was split into two spectral classes, the one including fields with a very dense green vegetation cover (training areas were chayote fields) and the other including fields with a larger proportion of visible soil (fields of beans and other crops). The informational class 'coffee without shadow' was similarly split into dense plantations on the one hand and plantations with visible bare soil between the rows on the other hand. These classes were recombined for the final map and for the accuracy assessment. The final classes are specified in table 7.

Table 7: Land cover classes in the UCRYN Landsat classification.

Class name	Definition
Dense coniferous forest (PFd)	Pine forest with over 60 % crown cover
Open coniferous forest (PFo)	Pine forest with 25-60 % crown cover, herbaceous layer usually consisting of grasses and/or ferns
Broadleaved forest (BF)	Forest with a majority of broadleaved tree species, may contain pine trees
Mixed coniferous forest (MF)	Mixed coniferous-broadleaved forest with a majority of pine trees
Burnt areas (brn)	Areas of recent forest fires or other burning (spectral signature controlled by ash, charcoal and reduced vegetation in the months following a fire)
Matorral (Mat)	Areas with over 25 % shrub cover, besides ferns and grasses
Fern (Cal)	Areas dominated by the fern *Dicranopteris pectinata*, sometimes with a proportion of other fern species
Agroforestry (AF)	Coffee and other crops with shade trees
Coffee without shade (Cof)	Coffee plantations without shade trees, or with single trees amounting to less than 25 % crown cover
Grassland (GL)	Herbaceous vegetation cover, mostly grasses, combined coverage of shrubs and trees below 30 %, used mostly for low-intensity pasture, partly intensive pasture/managed grassland
Other crops (Cr)	Cultivated agricultural areas (except coffee) without shade trees
Bare ground (BG)	No or very sparse vegetation cover
Built-up areas (bu)	Urban areas and smaller settlements where most of the ground is covered by buildings and paved streets
Water (W)	Rivers and lakes
No information	Land cover not classifiable because of clouds in the image

These classes could be separated sufficiently well to create a land cover map which provides information about the overall spatial distribution of the main land cover classes of the UCRYN (plate 43). However, the overall classification accuracy as calculated from the confusion matrix (table 8) is only 40 %, and the estimated Kappa coefficient is 0.343, representing poor agreement.

Table 8: Confusion matrix for the Landsat classification. For class abbreviations see table 7. RD: Reference Data, CD: Classified Data, UA: User's Accuracy, PA: Producer's Accuracy, OA: Overall Accuracy.

RD \ CD	PFd	PFo	BF	MF	brn	Mat	Cal	AF	Cof	GL	Cr	BG	bu	W	Sum	UA (%)
PFd	**14**	4	11	2						1				1	33	42.4
PFo	6	**3**	3			8	2			1				1	24	12.5
BF	2		**13**	10		2	1	1						2	31	41.9
MF	5		4	**2**				1							12	16.7
brn	1	12			**6**										19	31.6
Mat		2	2			**8**		1	1	1					15	53.3
Cal		1	1			3	**7**					1			13	53.8
AF	1	1	18			1		**3**							24	12.5
Cof		1	3		1	4			**0**				1		10	0.0
GL		5	5			3	1			**23**	2	1			40	57.5
Cr	1	1	9			3		2		4	**10**		2		32	31.3
BG			1			1			1	2	4	**4**	4	1	18	22.2
bu											1	1	**11**		13	84.6
W												2	1	**17**	20	85.0
Sum	30	30	70	14	7	33	11	8	2	32	17	9	19	22	304	
PA (%)	46.7	10.0	18.6	14.3	85.7	24.2	63.6	37.5	0.0	71.9	58.8	44.4	57.9	77.3		**OA: 39.8**

The classes with the best class-specific user's and producer's accuracies were 'grassland', 'water' and 'built up area'. The forest classes had low class-specific accuracies. The most accurately classified forest class was 'dense pine forest' with a producer's accuracy of 47 % and a user's accuracy of 42 %. 'Broadleaved forest' was often misclassified as 'agroforestry' and also as 'dense pine forest'. Many errors can be attributed to mixed pixel effects and some class signature similarities (figure 12). Using only Landsat multispectral data and post-classification sorting with elevation information, it was not possible to distinguish coffee without shade from *matorral*, agroforestry from broadleaved forest and open coniferous forest from *matorral* with any confidence. In some cases, part of the error might also originate from the reference data, which is based mostly on the visual interpretation of high resolution remotely sensed data where it can also be difficult to see the difference between agroforestry and broadleaved forest or between coffee without shade and matorral. An additional potential error source is the fact that the ground data and high resolution data used as source for the reference data set were, apart from three of the IKONOS images, not acquired simultaneously with the Landsat data but with a time lag of up to two and a half years. Some types of misclassification can be partly attributed to gradual transitions (spatial

and temporal) between classes. Examples are the classification of 'open pine forest' as 'burnt area', of '*matorral*' as 'open pine forest' or of 'mixed coniferous forest' as 'broadleaved forest'. These would not all be counted as completely wrong in a fuzzy classification or fuzzy accuracy assessment.

An inherent classification problem is the fact that there is no one-to-one relationship between informational classes and spectral classes. On the one hand, there is quite a large spectral variation within large classes like broadleaved forest: the spectral signature of broadleaved cloud forest is quite different from other types of broadleaved forest (montane/submontane rain forest and riparian forest) and more similar to pine forest. On the other hand, for example the classes 'broadleaved forest' and 'agroforestry' are spectrally very similar with a large overlap in feature space, but from a land management standpoint it would be very desirable to have separate information about these two classes with their different types of land use. The class 'broadleaved forest' could not be partitioned into a number of more spectrally homogeneous different broadleaved forest types because the Landsat training data was not sufficiently comprehensive to split it into training areas which would have included samples adequately representing each of the spectral-informational broadleaved forest types of the UCRYN.

Table 9: Reduction of classification detail through class aggregation.

14 class scheme	5 class (land use) scheme
Dense coniferous forest (PFd)	Forest (including burnt areas, which are mostly burnt forest, but not agroforestry)
Open coniferous forest (PFo)	
Broadleaved forest (BF)	
Mixed coniferous forest (MF)	
Burnt areas (brn)	
Matorral (Mat)	Shrub and herb dominated semi-natural vegetation
Fern (Cal)	
Agroforestry (AF)	Agricultural land use
Coffee without shade (Cof)	
Grassland (GL)	
Other crops (Cr)	
Bare ground (BG)	Land with no or sparse vegetation
Built up areas (bu)	
Water (W)	Water

The large diversity of forest formations and other types of land cover in the heterogeneous, mountainous study area is not conductive to high classification accuracies when using medium

resolution remotely sensed data. The overall accuracy of 40 % achieved here is similar to the results of Langford & Bell (1997) who mapped the land cover of a similarly heterogeneous tropical hillside (10 classes) with Landsat TM data. Reducing the detail (precision) of the map by aggregating the 14 classes into five groups after classification (table 9) leads to the more acceptable overall accuracy value of 61 %, but there are still many problems of confusion between classes which could not be joined in one meaningful informational class.

According to this Landsat ETM+ classification, the total forest cover of the study area was 48 % in the year 2000. This is significantly more than the estimate of 33 % given in the GWB/GFA-Agrar (1998) study. Also, the confusion matrix for the aggregated classes indicates that the total forest area in my map was somewhat underestimated rather than overestimated. (According to the reference sample, 65 % of the 'true' forest was classified as forest, while 82 % of the forest in the map really is forest.) 36 % of the forest in the classification consists of open pine forest. The gradual transitions between open pine forest and some non-forest-classes and the fact that forest definitions may differ with respect to the lower crown cover threshold may, together with temporal change and misclassifications or -estimations, explain some of the above mentioned discrepancy.

The results point out the limitations of standard classifications of Landsat data for land cover classifications in landscapes of the type found in the UCRYN. There is certainly room for improvement regarding the accuracy and the precision of the classification with the help of higher resolution data and more advanced data processing methods, especially if looking at limited areas (e.g. special interest subsets of the catchment area).

8 Methods for an Optimised Information Extraction from IKONOS Data for Forest and Land Cover Mapping

A sub-area of the UCRYN was used to intensively test and compare a number of image processing and classification methods involving the high resolution IKONOS data (see flowchart figure 15). These operations were limited to a smaller test area in order to reduce calculation costs and to concentrate on an area of high data and ground truth density. This main test area is the eastern test area depicted in figure 9.
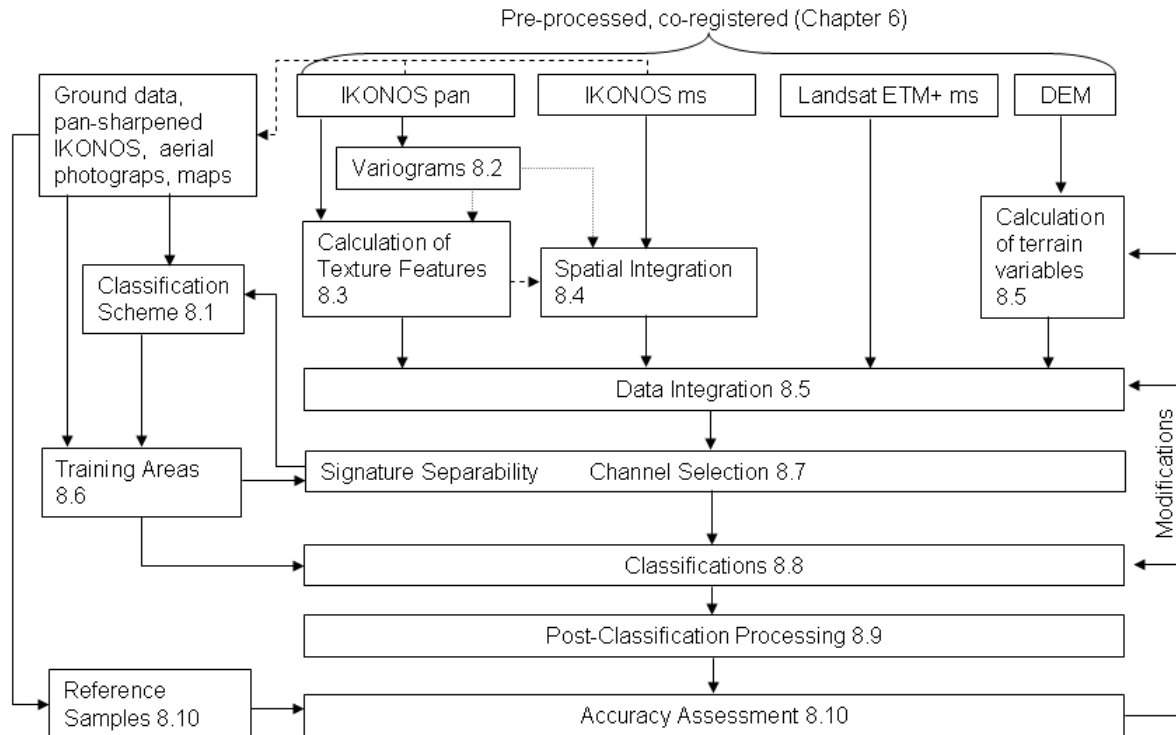
Figure 15: Sequence of processing operations for the classification of data sets involving IKONOS data.

8.1 Classification Scheme for the Eastern Test Area

There is a large diversity of land cover classes even in the 18.4 km² of the eastern test area, including natural and semi-natural vegetation in the Scientific Reserve Ebano Verde (chapter 3.2.5) and semi-natural vegetation and agriculturally used areas in the buffer zone. The natural and semi-natural vegetation patterns, being the result of natural environmental gradients combined with the influence of past and present disturbances (e.g. human land use, animal grazing, fires and hurricane damage), are rather complex and heterogeneous. Nevertheless, a number of discrete informational land cover units can be defined for the eastern test area (table 10). Most of the classes used in the Landsat classification of the whole UCRYN can be found here, with the exception of built-up areas, coffee without shade, burnt forest and mixed coniferous forest (there is some mixed forest among the secondary forest in the eastern test area, but it has a majority of broadleaved trees).

Table 10: Land cover classes in the eastern test area.

Class	Description
Dense pine forest (PFd)	Pine dominated (often pure pine) forest with over 60 % crown cover (these are mostly plantations in the eastern test area) (plate 21)
Open pine forest (PFo)	Pines with 25-60 % crown cover, herbaceous layer usually consisting of ferns and/or grasses (this includes groups of remnant mature pine trees in agriculturally used areas)
Cloud forest (CF)	Montane broadleaved cloud forest of the *Didymopanax-Magnolia* type, partly disturbed by past logging activities (plate 5)
Dense secondary forest (SFd)	Natural regeneration of a broadleaved forest, pioneer broadleaved species sometimes mixed with pine trees, over 60 % crown cover (plate 38)
Open secondary forest (SFo)	Natural regeneration of broadleaved forest, pioneer broadleaved species sometimes mixed with pine trees, 25-60 % crown cover, undergrowth usually fern dominated (plate 39)
Palm dominated forest (PmF)	Edaphic forest type dominated by the palm tree *Prestoea Montana*
Broadleaved riparian forest (BRF)	Evergreen broadleaved riparian forest (plates 11, 16) (some small remains of non-riparian humid broadleaved forest are also assigned to this class)
Matorral (Mat)	Areas with over 25 % shrub cover, besides ferns and grasses (plate 41), tree crown cover below 25 % (in most cases no trees at all)
Calimetal (Cal)	Areas dominated by the fern *Dicranopteris pectinata*, sometimes with a proportion of other fern species, with no or very few emerging shrubs and trees (plate 9)
Agroforestry (AF)	Crops (mostly coffee and bananas) with shade trees (plate 33)
Grassland (GL)	Herbaceous vegetation cover, mostly grasses, also ferns (but not dominated by *Dicranopteris pectinata*), combined coverage of shrubs and trees below 25 %, mostly used for low-intensity pasture in the buffer zone of the reserve (plate 23)
Crops (Cr)	Cultivated agricultural areas, mostly beans, no shade trees
Bare ground (BG)	No or very sparse vegetation cover (roads, landslide scars, river bars, agricultural areas with seasonal lack of vegetation cover)
Water (W)	Open water (river)

The classification scheme used for the classification of the eastern test area is more detailed than the Landsat classification scheme with regard to the forest classes. Broadleaved forest is not treated as a single class but split into a number of forest formations. These are cloud forest, dense and open secondary forest, broadleaved riparian forest and palm forest. (The latter is not classified as a separate formation by most authors, but has a spectrally and structurally distinct upper layer resulting in a distinct appearance in the high resolution imagery.) Mapping a larger number of forest classes should result in additional information about the spatial distribution of ecologically important forest types in the Scientific Reserve Ebano Verde and its buffer zone. The differentiation is also methodically useful because, as has been seen in the case of the Landsat classification, there

is a very large spectral variation within the broadleaved forest classes of the study area and particularly also of the eastern test area – the spectral signature of cloud forest, for example, is more similar to that of pine forest than to that of other kinds of broadleaved forest. Also, to make an attempt to discern the agroforestry class, which is spectrally very similar to broadleaved forest, a partition of the broadleaved forest class into spectrally more homogeneous classes is going to be necessary.

The classification scheme for the natural and semi-natural vegetation is compatible as far as possible with the existing classifications of the regional vegetation described in table 1 and chapter 3.1.6. The ICEC's 'pine woodland' is called 'open pine forest' here but has the same definition (25-60 % crown cover), while it differs somewhat from the definition of open coniferous forest (40-60 % crown cover) given by Tolentino & Peña (1998). The cloud forest type of the Reserva Scientífica Ebano Verde is addressed as a type of montane rain forest (alliance: *Magnolia pallescens* montane rain forest, association: *Magnolia pallescens - Didymopanax tremulus - Prestoea montana* forest) by Areces-Mallea et al. (1999), but is included in the cloud forest definitions of Tolentino & Peña (1998) and Hager & Zanoni (1993) and will also be addressed as 'cloud forest' in this classification. A minimum area criterion for the definition of forest cannot be applied during the classification process itself, so even small groups of trees can be classified as 'forest'. This leaves the option to label small 'forest' class areas as 'trees outside forest' in a post-classification step based on GIS functionality, if the class area is below a certain threshold and separated from other forest areas.

8.2 Spatial Exploration of IKONOS Data Using Variograms

To explore the spatial variations of the land cover classes, particularly of the forest classes, as they are captured in the high resolution imagery, experimental variograms were derived from the linearly scaled 8 bit IKONOS panchromatic data. Subsets of 100 × 100 pixels (figure 16) each showing one type of land cover (cloud forest, dense pine forest, open secondary forest, broadleaved riparian forest and grassland) were sampled using 100 pixels long transects in two directions. The DNs (Digital Numbers) of these transects were exported into a spreadsheet program (Excel), where they were used to calculate the average semivariance values.
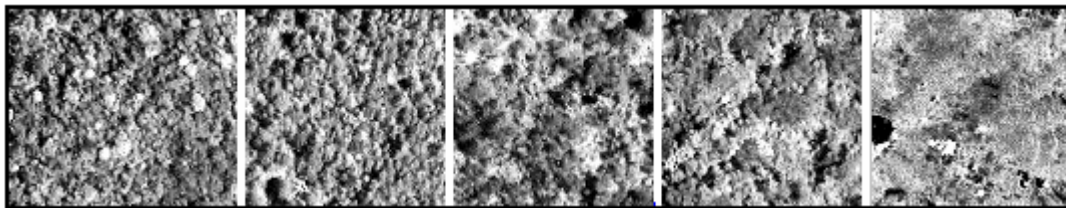
Figure 16: 1 m resolution panchromatic image subsets used for the calculation of experimental semivariograms (from left to right: cloud forest, dense pine forest, open secondary forest, broadleaved riparian forest, grassland).

For lags between 1 and 20 pixels (=m) within these transects, the average semivariance was calculated as

$$\gamma(h) = \frac{1}{2N(h)} \sum_{i=1}^{N(h)} [z(x_i) - z(x_i + h)]^2 \qquad (1)$$

where h is the lag (distance in pixels, which in this case equals distance in metres) over which the semivariance γ is measured, $N(h)$ is the number of pairs of observations separated by the lag h, and $z(x_i)$ is the value (DN) of the pixel with the position x_i. The mean of nine experimental variograms for each direction (N-S, being approximately perpendicular to the sun azimuth and E-W, being approximately parallel to the illumination) was calculated and plotted, together with a variogram for a single central transect in each direction (figure 17).
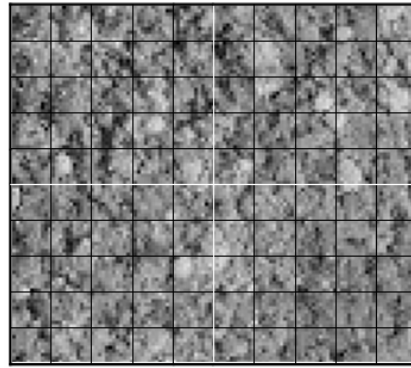
Figure 17: 100×100 pixels subset of a cloud forest area in the panchromatic IKONOS image with nine vertical and nine horizontal transects.

8.3 Extraction of Texture Parameters from High Resolution Data

8.3.1 GLCM texture

Considering the fact that GLCM texture calculations need large window sizes to produce stable texture measures (Franklin 2001b), while still endeavouring to avoid the calculation of between-class texture for large proportions of the pixels (Ferro & Warner 2002), GLCM texture was calculated making use of the highest resolution IKONOS imagery available – the panchromatic channel with 1 m spatial resolution. GLCM texture features were calculated from the symmetric normalised co-occurrence matrix using the PCI Geomatica 'TEX' module. The input data were scaled down to 32 levels (5 bit) for the GLCM texture calculation. The window sizes used were 9×9, 15×15, and 25×25 pixels, the inter-pixel sampling distance (δ) was 1 and the four main orientations were averaged (direction invariant spatial relationship).

After first calculating texture measures for all three window sizes, the texture images resulting from the different window sizes were compared visually. The images calculated using 9×9 and 25×25

window sizes were discarded as containing less class-specific information than those calculated using the 15×15 window size. The individual forest classes appeared very inhomogeneous in the texture images resulting from the use of the 9×9 filter windows, while the texture images calculated using the 25×25 filter windows appeared rather blurred. Only the 15×15 window size was finally used for all the GLCM texture calculations. This should result in texture measures which are representative of their respective land cover classes (see also variogram results in chapter 9.1) while avoiding unnecessarily strong edge effects.

The following GLCM texture features were generated:

Contrast

$$CONT = \sum_{i,j=0}^{N-1} P(i,j) \cdot (i-j)^2 \tag{2}$$

where N is the number of grey levels after rescaling (equivalent to the columns or rows in the co-occurrence matrix) and $P(i,j)$ is the probability of co-occurrence of the grey levels i and j (the normalised value in the cell i,j of the co-occurrence matrix)

Angular Second Moment

$$ASM = \sum_{i,j=0}^{N-1} P(i,j)^2 \tag{3}$$

Entropy

$$ENT = \sum_{i,j=0}^{N-1} - P(i,j) \cdot \ln(P(i,j)) \quad \text{assuming that } 0 \cdot \ln(0)=0 \tag{4}$$

Homogeneity

$$HOM = \sum_{i,j=0}^{N-1} \frac{P(i,j)}{1+(i-j)^2} \tag{5}$$

Dissimilarity

$$DISS = \sum_{i,j=0}^{N-1} P(i,j) \cdot |i-j| \tag{6}$$

Mean

$$MEAN_i = \sum_{i,j=0}^{N-1} i \cdot P(i,j) \tag{7}$$

Standard Deviation

$$SD = \sqrt{\sum_{i,j=0}^{N-1} P(i,j) \cdot (i - MEAN_i)^2}$$ (8)

and Correlation

$$CORR = \sum_{i,j=0}^{N-1} P_{ij} \left[\frac{(i - MEAN_i)(j - MEAN_j)}{\sqrt{(VAR_i \cdot VAR_j)}} \right]$$ (9)

where $VAR_i = \sum_{i,j=0}^{N-1} P(i,j) \cdot (i - MEAN_i)^2$ and $VAR_j = \sum_{i,j=0}^{N-1} P(i,j) \cdot (j - MEAN_j)^2$.

Apart from these eight GLCM features, two texture features were calculated using Grey-Level-Co-occurrence Vectors (GLDV). The GLDV counts the occurrence of absolute grey level differences of reference and neighbour pixel, thus containing the sum of the diagonals of the GLCM. GLDV *ASM* and GLDV *ENT* were calculated, but were found to be highly correlated with GLCM *ASM* and GLCM *ENT* (with correlation coefficients of 0.97 between GLCM *ASM* and GLDV *ASM* and of 0.96 between GLCM *ENT* and GLDV *ENT* for the eastern test area). The GLDV features were thus not considered to contain significant amounts of additional information and not used any further.

The resulting 32 bit texture images were scaled to 8 bit with a linear function, except for the *ASM* image which was rescaled with a square root function because the original distribution of its values was considerably skewed. Figure 18 shows a colour composite of three GLCM texture features.

8.3.2 Local Variance

Subsequently, local variance was calculated as a first order texture measure for comparison and possible combination with the GLCM second order texture measures. An EASI script (appendix 3) was written for the calculation of the local variance image layers in PCI Geomatica making use of the EASI image modelling function. Equation (11) was applied in 9×9 and 15×15 filter windows over the panchromatic image channel.

$$\sigma^2 = \frac{\sum (x_i - \mu)^2}{N}$$ (10)

where x_i are the single DNs in the filter window, μ is their mean, and N is the number of pixels in the window.

The resulting 32 bit variance images were scaled to 8 bit with a linear function.
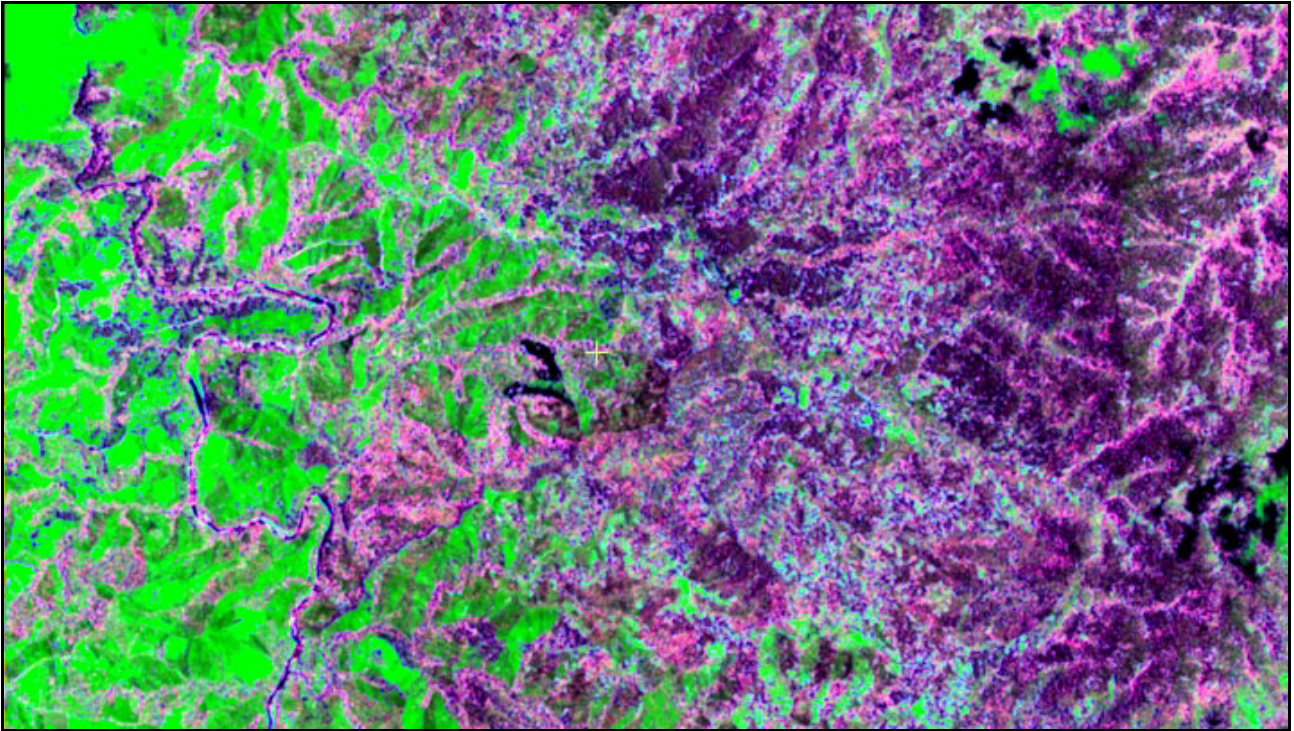
Figure 18: Texture colour composite (RGB: GLCM Contrast, GLCM Mean, GLCM Standard Deviation).

8.4 Spatial Integration of IKONOS Data

The 4 m resolution (16 m²) IKONOS pixels are often not large enough to integrate all the different components of a forest class, resulting in high within-class spectral variability. Three separate methods are tested to create image primitives which are more representative of their whole class, and to reduce the within-class variability of the data.

8.4.1 Spatial Aggregation in Square Windows

The first method to aggregate groups of pixels is non-overlapping averaging in square windows (block averaging): The image is divided into non-overlapping square windows of 2 by 2, 3 by 3 and 4 by 4 pixels forming the new image primitives. The mean of the DNs (Digital Numbers) of the pixels within each window is calculated and assigned to this primitive, which is subsequently treated as a coarser resolution pixel (using the PCI Geomatica IIIAVG algorithm). This leads to upscaled versions of the multispectral image with 8 m, 12 m and 16 m spatial resolution (figure 19). This corresponds to pixel (image primitive) areas of 64 m², 144 m² and 256 m² respectively. Hay et al. (1997) showed that this is a simple method for approximating the spectral response of a coarser resolution image, although the aggregated data is not exactly equivalent to data acquired at a coarser resolution, because the square window averaging does not take into account the effects of the

modulation transfer function (MTF) of the sensor and the atmospheric effects, both of which cause an inclusion of some information from neighbouring surfaces.
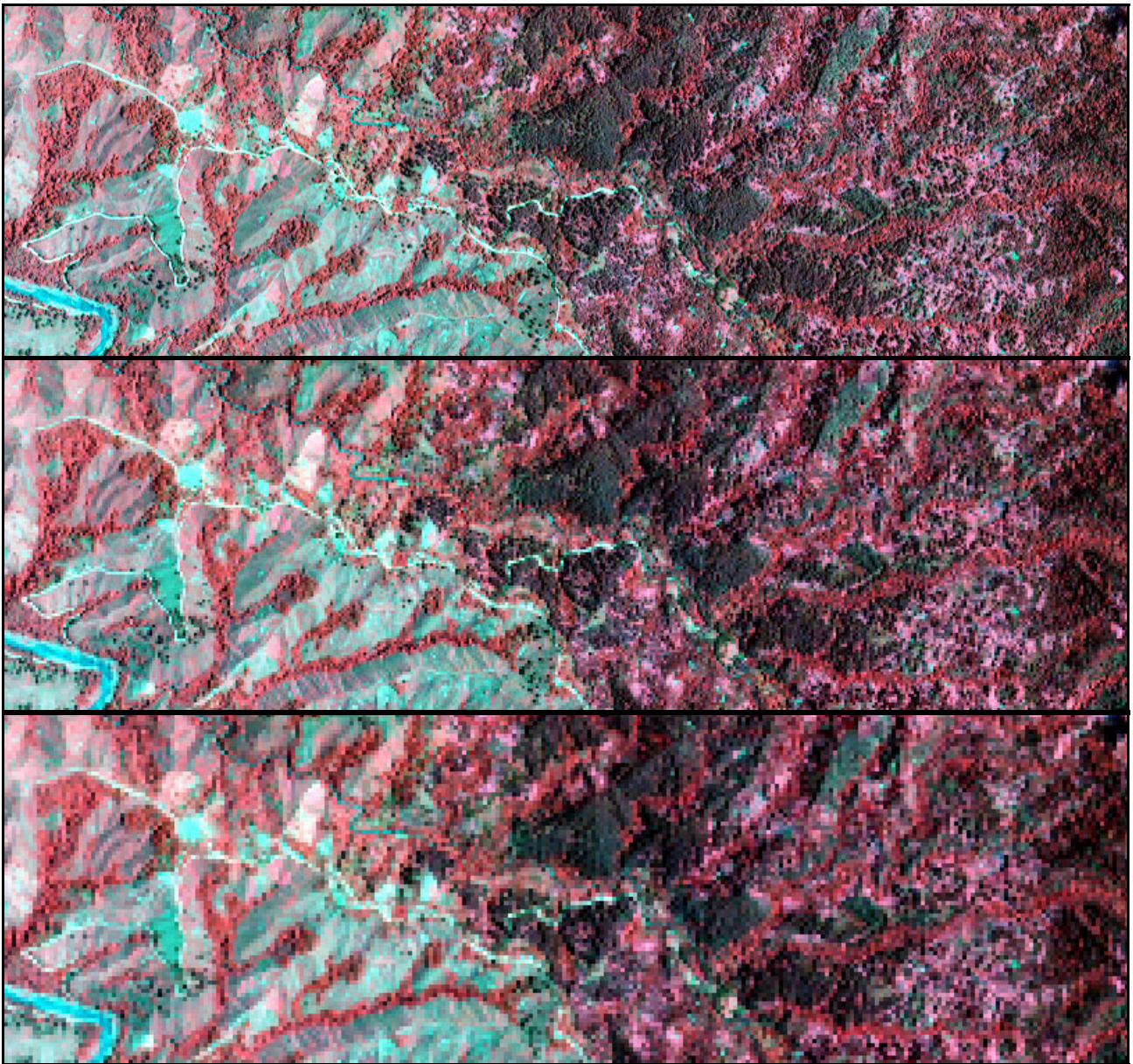
Figure 19: A detail of the 4 m resolution multispectral IKONOS image (RGB 432, above) and the same area after averaging in square windows to 8 m resolution (centre) and 12 m resolution (below).

8.4.2 Low Pass Filtering

Low pass filtering is used to reduce the within-class variability while keeping the spatial resolution at 4 m. An average (mean) filter is employed to smooth the four multispectral IKONOS image channels using 3 × 3 and 5 × 5 filter windows (figure 20). By calculating the mean value for areas of 12 × 12 m or 20 × 20 m and assigning it to the central 4 × 4 m pixel, this pixel now carries

information about that whole area. This was only done for the multispectral channels and not for the texture channels because the latter, having been calculated in 15 × 15 m windows, do already contain information about the surrounding pixels. Alternatively, median filtering of the four multispectral channels in windows of 3 × 3 and 5 × 5 is performed to smooth the image while preserving the edges.
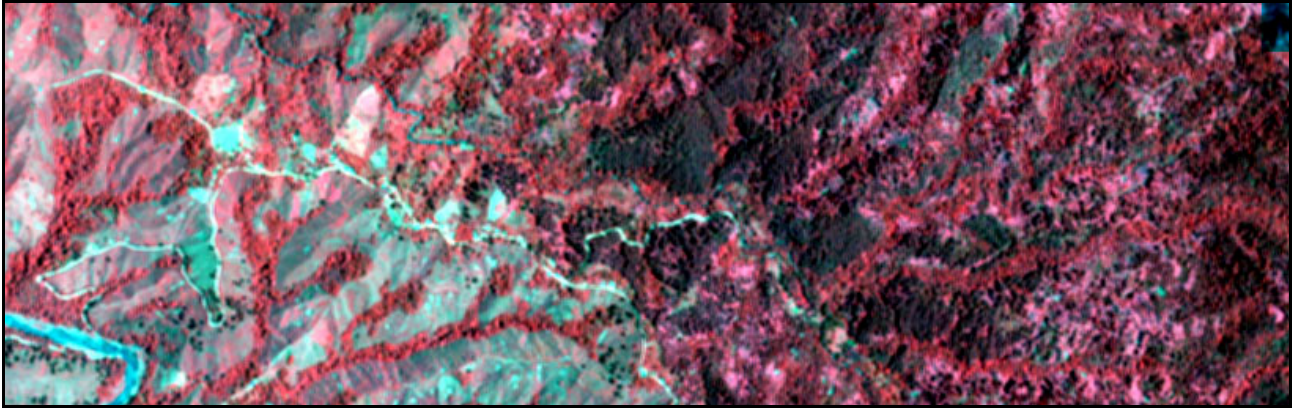
Figure 20: The IKONOS sub-image after low pass filtering (3x3 average filter).

8.4.3   Image Segmentation

Another method for pixel aggregation is image segmentation. This method takes into account the similarity between the pixels that are grouped together and aims at producing meaningful image object primitives which can represent image objects or parts of image objects. The software eCognition was used for the image segmentation, with its region merging technique based on local spectral homogeneity and a shape criterion favouring compact forms (Baatz et al. 2002, see also chapter 2.3).

The four multispectral IKONOS channels (4 m resolution) were used as input for the segmentation, and in some variations also the GLCM entropy texture parameter calculated from the panchromatic band and resampled to 4 m resolution.

User defined parameters like input channels, weights and the scale parameter were adapted through interactive experiments until the resulting segmentations were satisfactory according to a visual inspection. The aim was to arrive at segmentations with homogeneous object primitives, i.e. without 'mixed objects' incorporating areas belonging to different classes (undersegmentation). At the same time the object primitives should be large and compact enough to integrate the elements of any one forest class, avoiding oversegmentation in the sense of the creation of object primitives which contain only a subset of class elements, for example only pixels representing the shaded parts of tree crowns.

Both spectral heterogeneity (h_{spec}) and shape heterogeneity (h_{shape}) were used to define the degree of fitting f (overall heterogeneity criterion) for a proposed merge between two object primitives.

$$f = w \cdot h_{spec} + (1 - w) \cdot h_{shape} \tag{11}$$

The weight w for h_{spec} ('color criterion') was finally set to 0.75, leaving a weight of 0.25 for the shape criterion. (Increasing the weight for the spectral heterogeneity criterion resulted in smaller segments on average.)

The shape criterion h_{shape} is a combination of 'smoothness' h_{smooth} and 'compactness' h_{cmpct} in the form

$$h_{shape} = w_{smooth} \cdot h_{smooth} + (1 - w_{smooth}) \cdot h_{cmpct} \ . \tag{12}$$

The smoothness value is calculated as

$$h_{smooth} = n_{Merge} \cdot \frac{l_{Merge}}{b_{Merge}} - \left(n_{OP1} \cdot \frac{l_{OP1}}{b_{OP1}} + n_{OP2} \cdot \frac{l_{OP2}}{b_{OP2}} \right) \tag{13}$$

where n is the size of the object primitives *OP1* and *OP2* and the proposed *Merge* of the two, l is the length of the object perimeter and b the perimeter of the bounding box (drawn around the object parallel to the raster). The weight for smoothness w_{smooth} within the shape criterion was set to 0.9, leaving a weight of 0.1 for the compactness value which is calculated as

$$h_{cmpct} = n_{Merge} \cdot \frac{l_{Merge}}{\sqrt{n_{Merge}}} - \left(n_{OP1} \cdot \frac{l_{OP1}}{\sqrt{n_{OP1}}} + n_{OP2} \cdot \frac{l_{OP2}}{\sqrt{n_{OP2}}} \right). \tag{14}$$

The heterogeneity in the feature space h_{spec} is calculated as the sum of the standard deviations σ of the DNs in the channels used as input for the classification:

$$h_{spec} = \sum_c w_c \left[(n_{OP1} + n_{OP2}) \cdot \sigma_c^{Merge} - \left(n_{OP1} \cdot \sigma_c^{OP1} + n_{OP2} \cdot \sigma_c^{OP2} \right) \right] \tag{15}$$

The weights for the channels w_c were set to 0.5 for the blue channel, 1 for the green, red and GLCM entropy channels and 1.5 for the NIR channel.

Different scale parameters were set to influence the threshold of the degree of fitting f requested for a merge, resulting in different sizes of the image object primitives (figure 21, table 11). A multi-resolution segmentation was conducted producing four segmentation levels using the scale parameters 12, 16, 20 and 30.

Table 11: Scale parameters and sizes of resulting image object primitives in the segmentation of the eastern test area.

Scale parameter	Area of the resulting image object primitives		
	Average area	Minimum area	Maximum area
12 (level 1)	833 m²	16 m²	7 980 m²
16 (level 2)	1 478 m²	32 m²	9 810 m²
20 (level 3)	2 635 m²	80 m²	31 500 m²
30 (level 4)	6 171 m²	160 m²	35 800 m²
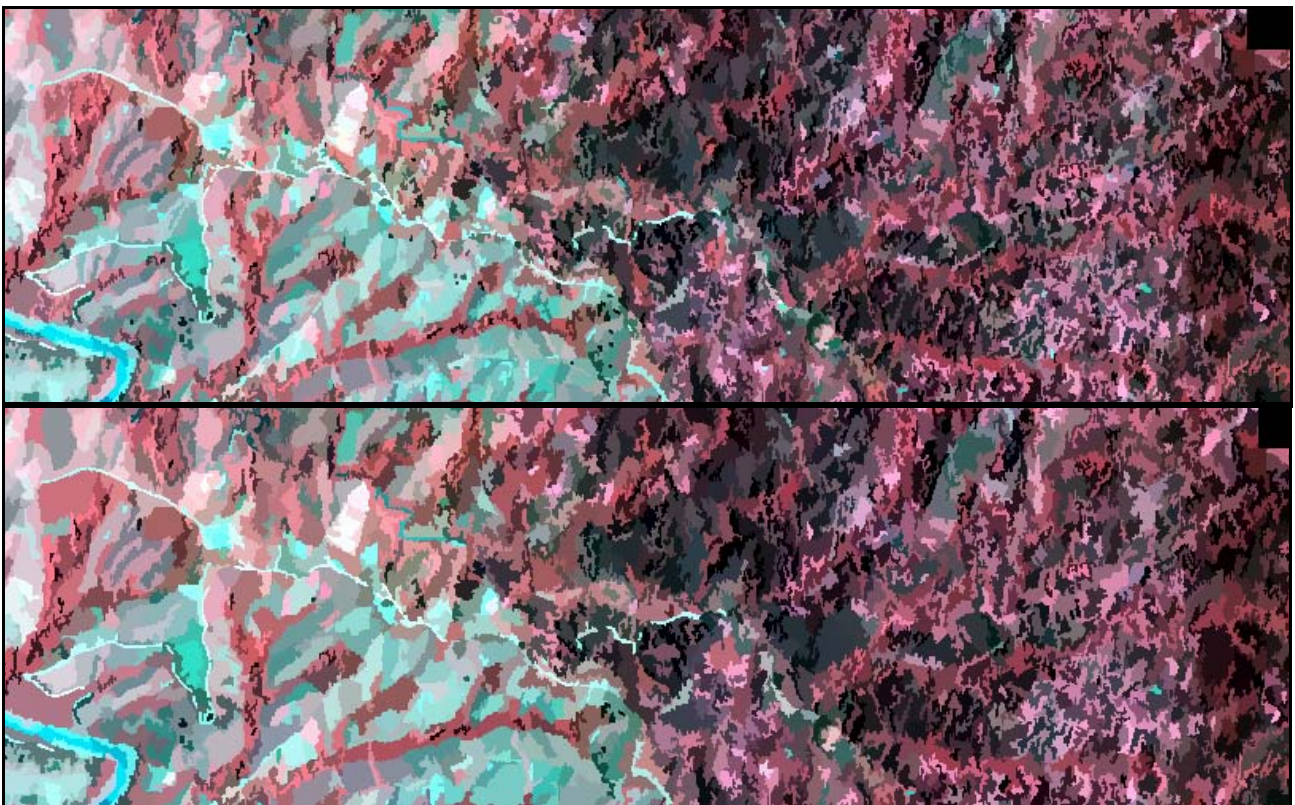
Figure 21: Multiresolution image segmentation with scale parameter 16 (above) and 20 (below).

After the segmentation, eCognition's vectorisation functionality was used to produce polygons representing the shapes of the object primitives. The object primitives were used for classification within the eCognition environment and additionally, the objects including their shapes and their mean values in four multispectral and three textural channels were exported as .shp files and used to create raster layers within the PCI Geomatica environment, where the pixel values were averaged for the object primitives created in eCognition.

8.5 Data Integration

8.5.1 IKONOS Spectral-Textural Data Integration

The channels containing the texture features generated at 1 m spatial resolution from the panchromatic channel were integrated with the multispectral channels by reducing the spatial resolution of the texture channels to the resolutions of the files containing the multispectral data (4 m, 8 m, 12 m and 16 m) and adding them as additional channels. The texture channels were resampled to the resolution of the multispectral data using nearest neighbour resampling, or block averaging for addition to the low pass filtered multispectral data. Figure 22 shows a spectral-textural colour composite at 4 m resolution. In the case of the segmented images, the texture channels had been integrated with the multispectral channels at 4 m resolution before segmentation and afterwards the within-segment mean values were calculated for multispectral and texture channels alike.
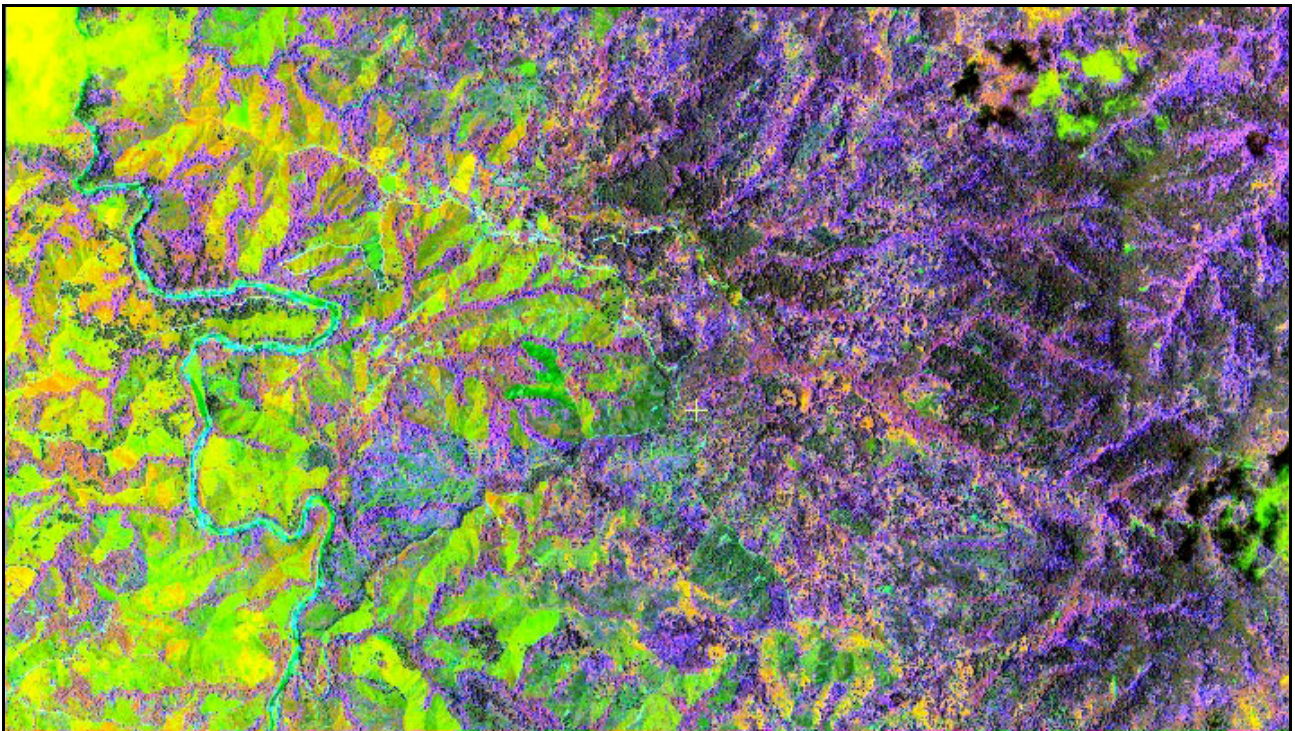
Figure 22: Spectral-textural colour composite (RGB: NIR, red, GLCM Contrast) at 4 m resolution.

8.5.2 Multi-Source Data Integration

To test whether the integration of available multi-source data could improve the mapping beyond the possibilities of the IKONOS data alone, IKONOS data and IKONOS derived data channels were integrated with Landsat ETM+ data on the one hand and DEM-derived data on the other hand.

Landsat ETM+ and IKONOS

There is a time lag of seven months between the acquisition dates of the Landsat and the IKONOS data of the eastern test area (see chapter 4). To make the two data sets more compatible, those areas which were affected by clouds and cloud shadow in the IKONOS image, and an area which had been burned between the acquisition dates, were manually masked out (DNs set to zero) and thus excluded from the classification runs for both data sets.

The multispectral channels 5 to 7 of the co-registered Landsat data subset of the eastern test area were used as additional spectral channels with the IKONOS multispectral channels 1 to 4. The two types of multispectral data were integrated at 8 m spatial resolution (block averaged IKONOS data and cubic convolution resampled Landsat data). The objective was to test whether the integration of additional spectral information could be useful for the land cover classification in spite of the lower resolution of the Landsat data.

As a second example of data integration, the texture channels derived from the IKONOS panchromatic data were added to the co-registered Landsat data file at 15 m spatial resolution (in effect combining texture information calculated in 15 m x 15 m windows with multispectral pixels covering the same area). The objective was to test whether Landsat multispectral information can be enhanced by texture information derived from higher resolution data but resampled to medium resolution.

Ancillary data and IKONOS

The amount of ancillary information available about environmental factors which could influence the spatial distribution of the vegetation types of the study area is limited. The soils of the study area have not been mapped with any detail. The geology, mapped at a scale of 1:250.000 (figure 6), could explain some of the vegetation distribution in the UCRYN as a whole, but for the eastern test area, the available map differentiates only between the tonalite of the El Rio batholith underlying most of the area and the broad class of volcanic and volcaniclastic rocks of the Tireo formation in the north-eastern corner of the test area. The density of climatic measurements is very low in the Cordillera Central and does not suffice for the creation of GIS-layers of climatic variables like temperature and precipitation through interpolation of the known point values. Feiden (2004) regionalised the annual precipitation of the Dominican Republic making use of the fact that topographical parameters, among them the exposure to the prevalent wind direction, play a large roll for the spatial distribution of the annual precipitation. Using regression functions, she assigned an annual precipitation value to every raster point of a DEM with 400 m grid spacing. However, in areas of low data densities, like the higher mountains, the resulting values can only be interpreted as relative approximations. The complexity of the precipitation processes e.g. in the cloud forest zone cannot be reliably mapped through regionalisation of the existing measurements of annual

precipitation sums (Feiden 2004). On the whole, the ancillary information available is not sufficient to allow the modelling of directly influencing factors like nutrient availability or moisture regime at a scale appropriate for the use with high resolution satellite data.

There is, however, the DEM, and the models of terrain variables which can be derived from it, with their potential (indirect) influence on the land cover, and particularly on the vegetation. Topographic variables like elevation, slope and aspect can be presumed to influence, among other things, the local moisture regime and temperature regime and thus the vegetation.

The DEM with 8 m grid spacing, generated from the 50 m DEM through kriging (chapter 6.3), was used to provide elevation data. The slope, calculated from this DEM, was used as the second topographic channel. To calculate the local slope, the four immediate neighbours of each pixel are used to calculate two vectors (in x-direction and y-direction) across the central pixel employing the horizontal distances and elevation differences of the left and right neighbour pixels on the one hand and the top and bottom neighbour pixel on the other hand. These two vectors form a plane the normal vector of which can be calculated as the cross product of the two original vectors. The normal vector is then used to calculate the slope of the plane, which is assigned to the central pixel as the slope value (in degrees between 0 and 90) (PCI 2001).

A third basic topographic parameter is the aspect (orientation of the slope). Directional aspect values in degrees (e.g. clockwise from north) have the disadvantage for classification that some directions can end up with very different values even if the orientation in reality is very similar (2° is much closer to 358° than to 30°, for example). This circularity makes it impossible to perform conventional statistical classification in a meaningful way on such aspect data, so that they are not suitable as input for a statistical classifier. A non-circular measure which contains aspect information is the 'angle of incidence'. The incidence angle of solar radiation can be computed as a function of aspect and slope and of the solar azimuth and elevation angles. Instead of calculating the incidence angle for radiation from a light source, an azimuth of 60° and an elevation of 20° were chosen to give a rough approximation of the exposure to the east-northeasterly winds which bring most of the moisture into the study area. The resulting image has high values at slopes exposed to the east and north and very low values (0° in some areas) at leeward slopes. Aspect was thus substituted by an 'angle of incidence' as a non-circular measure containing information about the (windward and leeward) orientation of slopes ('incidence60').

These three topographic channels with 8 m grid spacing (figure 23) were added as additional channels to the 8 m resolution IKONOS data. The 16 bit elevation channel was linearly scaled down to 8 bit before being used as input for classification. The elevation data with 8 m grid spacing was also resampled to 4 m pixel size using cubic convolution to integrate it with the 4 m resolution IKONOS data.
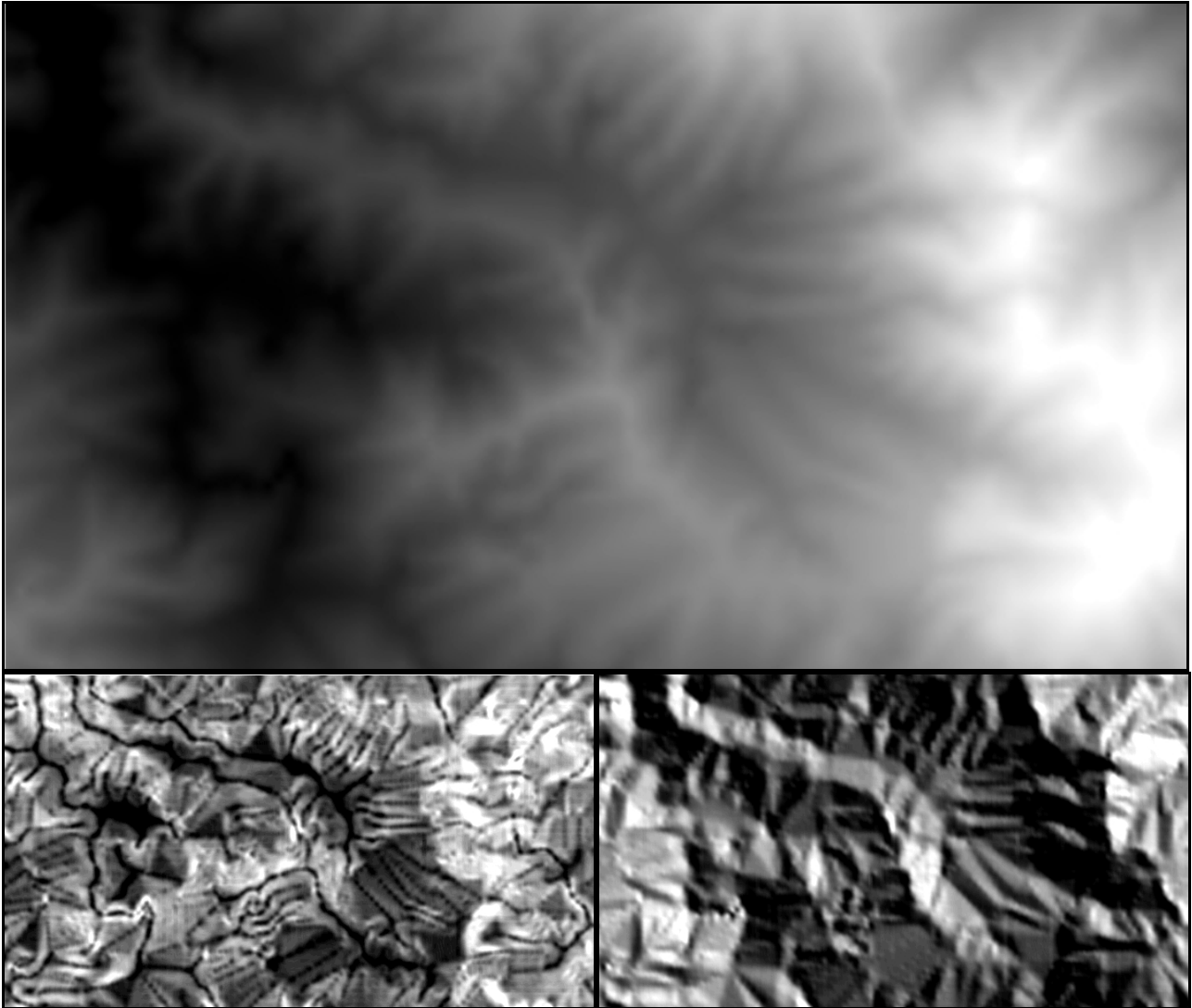
Figure 23: Elevation (above), slope (left) and 'incidence60'(right) images generated from the DEM.

The ancillary data was thus incorporated as additional channels to be used during the classifications instead of using it for a stratification of the study area before the classification. A stratification of the eastern test area was not done because this test area is already quite small. Its vegetation patterns are determined not only by environmental gradients, which could be partly substituted by the DEM-derived data, but also by the disturbance history and current human land use. To define abrupt DEM-based boundaries, excluding some of the land cover classes from sub-areas of the eastern test area, would be inappropriate, given the inaccuracy of the DEM data and the lack of information about definite environmental boundaries for most of the classes in the test area. (For the use of ancillary data in post-classification sorting see chapter 8.9.)

8.6 Creation of Training Areas and Calculation of Class Statistics

Training areas were created for the 14 land cover classes listed in table 10. Training samples were selected manually for each class, based mostly on the ground data gained through field work and aided by the aerial photographs, the panchromatic IKONOS image and maps. The training samples form contiguous groups (block sampling), but for every class, between six and 23 spatially separate training areas were created (figure 24). The aim was to create representative training samples for each class, avoiding mixed pixels but containing examples of the whole spectrum of class-subtypes in the test area (e.g. for the class 'dense pine forest', training samples were placed in areas of mature pine forest as well as pine plantations from the 1970s). Although random training samples are theoretically preferable for the creation of representative class statistics, it is usually not possible in practice to assemble a sufficient number of field work dependent training samples without the use of block sampling (Debeir et al. 2002). The training areas were saved as masks (bitmaps) and transferred to all image files of the eastern test area so that the same training areas could be used for the creation of class signatures from all data sets, including the co-registered Landsat data. This entails that the number of training pixels becomes smaller for the data sets with reduced spatial resolution. The number of training samples per class for the case of 4 and 8 m resolution pixels is listed in table 12.

Table 12: Training pixels per class at 4 m resolution.

Class	Number of training samples at 4 m resolution	Number of training samples at 8 m resolution
Dense pine forest (PFd)	2760	702
Open pine forest (PFo)	1660	415
Cloud forest (CF)	4048	1012
Dense secondary forest (SFd)	2658	669
Open secondary forest (SFo)	2868	717
Palm dominated forest (PmF)	1762	446
Broadleaved riparian forest (BRF)	3702	921
Matorral (Mat)	3092	777
Calimetal (Cal)	1508	379
Agroforestry (AF)	1324	332
Grassland (GL)	2892	723
Crops (Cr)	2120	533
Bare ground (BG)	616	154
Water (W)	1444	360

The training samples for all classes were checked for normal distribution in the spectral and textural channels and the channels containing DEM-derived data. For this purpose, histograms of the DNs under the training area mask were created for each channel. The histograms were visually evaluated to see whether they were unimodal and approximately symmetric and bell-shaped and the central tendencies (mean, median and mode) were compared. The same training samples were used for all classifications and all data sets, except for the classifications in eCognition which required object primitives as training samples. For the statistical classifications (MLC), class signatures (containing among other things the mean vector for n selected channels and the $n \cdot n$ class covariance matrix) are computed from the training pixels. It is recommended for reasons of statistical confidence that for n channels to be used in the classification, training sites should be at least $5 \cdot (n \cdot n + n)$ pixels (samples) large (PCI 2001). This corresponds to 100 pixels for four input channels and 280 pixels for seven input channels. The recommended value for seven channels is reached for all classes at 4 m resolution and for all classes except 'bare ground' at 8 m resolution. For four channels, the recommended value is reached for most classes even at 16 m resolution.
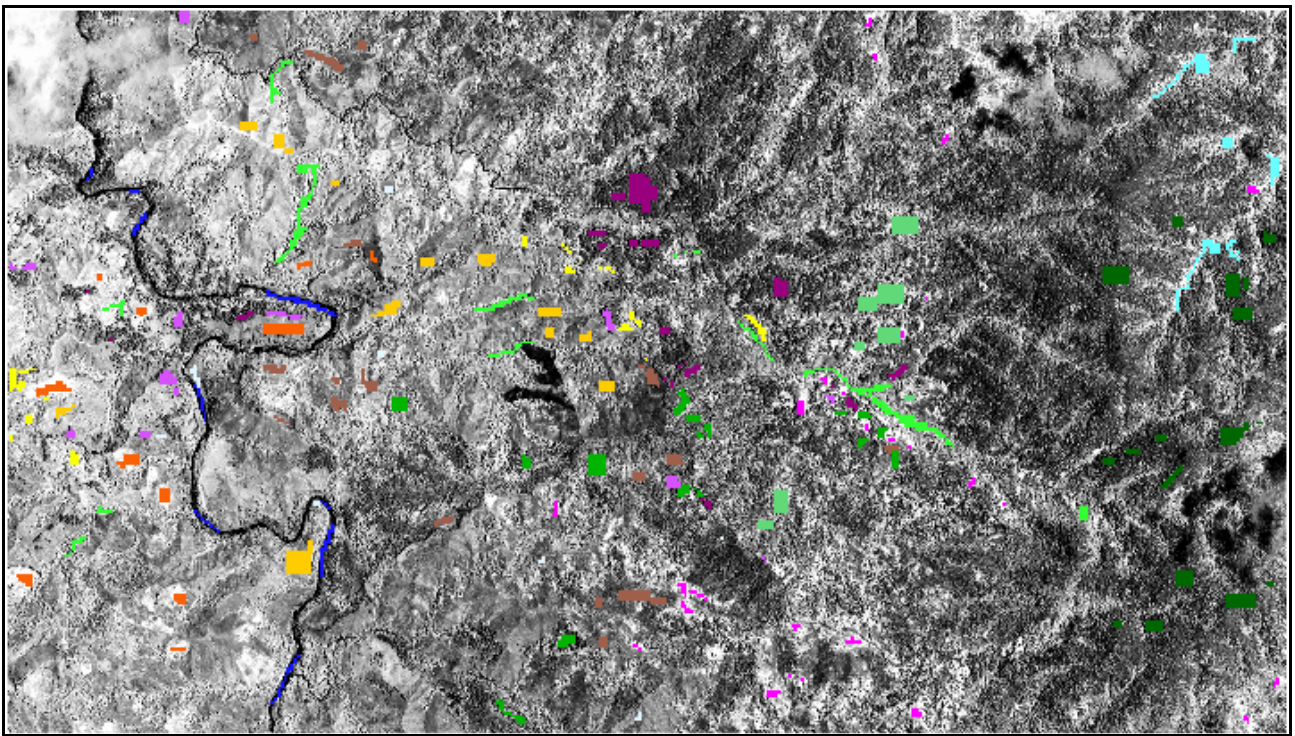
Figure 24: The training areas in the eastern test area. For the colour scheme see legend plate 44, appendix 2.

8.7 Feature Selection and Signature Separability

Quadratic classifiers like the MLC have limitations in handling data sets of high dimensionality (see chapter 2.6). The data set now available for the eastern test area comprises four IKONOS multi-spectral channels and ten texture features, with the possible inclusion of Landsat multispectral

channels and ancillary topographic data channels. This necessitates the selection of a channel subset before using them as input in a classification.

8.7.1 Reduction of Texture Channels after Correlation Analysis

A correlation analysis was conducted as a first step to reduce the large number of generated texture features (before adding the remaining channels to the multispectral channels). The correlation coefficients between the ten texture images were calculated for the eastern test area (table 13). Out of groups of highly correlated texture channels (with absolute values of correlation coefficients larger than 0.85 for the eastern test area), in each case the one which appeared visually most meaningful for forest discrimination was selected while the others were discarded, resulting in five (out of ten) retained texture channels. These were GLCM *Entropy*, *Standard Deviation*, *Contrast*, *Mean*, and *Correlation*. The maximum correlation coefficient between these remaining texture channels is 0.82.

Variance, when calculated in the same 15 m × 15 m size windows as the GLCM texture features (VAR 15), is highly correlated (r = 0.96) with GLCM standard deviation. The 9 × 9 window local variance (VAR 9) is also quite strongly correlated with both the GLCM standard deviation and the local variance calculated in the 15 × 15 window.

Table 13: Correlation coefficients for texture channels (scaled to 8 bit), eastern test area.

	ASM	*ENT*	*HOM*	*CONT*	*DISS*	*SD*	*MEAN*	*CORR*	VAR 9	VAR 15
ASM	1									
ENT	**-0.96**	1								
HOM	**0.93**	**-0.96**	1							
CONT	-0.66	0.79	-0.80	1						
DISS	-0.81	**0.91**	**-0.93**	**0.96**	1					
SD	-0.71	0.83	-0.72	0.82	0.81	1				
MEAN	0.45	-0.43	0.42	-0.20	-0.31	-0.27	1			
CORR	-0.18	0.23	0.01	0.02	0.00	0.52	-0.10	1		
VAR 9	-0.50	0.63	-0.53	0.73	0.68	**0.87**	-0.17	0.44	1	
VAR 15	-0.52	0.67	-0.53	0.74	0.68	**0.96**	-0.17	0.56	**0.89**	1

The channels of the first three multispectral IKONOS bands (visible) are also highly correlated to each other (with r ≥ 0.95). But as there are only four multispectral IKONOS bands, they were, at least initially, all retained for the combination with the texture channels. Their correlation was only taken into account as a basis for channel reduction when the multispectral data were combined with texture as well as ancillary topographic data channels.

8.7.2 Feature Selection

These five texture channels combined with the four IKONOS multispectral channels were still more than the assumed optimum number of channels for a maximum likelihood classification (Peddle 1993, Hay et al. 1996). To select the best reduced channel combination for discriminating between different forest types and adjacent land cover types, class signatures were calculated based on training sites for all the forest classes, *matorral*, *calimetal* and grassland.

The seven optimal channels out of the four multispectral and five texture channels were selected using the criterion of maximised average transformed divergence between these class signatures. The same criterion was used to select the best combination of seven channels from the combination of the eight Landsat channels and five texture channels, and to select the best seven out of eight Landsat channels.

The divergence (Gaussian form) between the classes *i* and *j*, *D(i,j)* is calculated from the class sample means and covariance matrices:

$$D(i,j) = \frac{1}{2}(M_i - M_j)^T \cdot \left[(\Sigma_i)^{-1} + (\Sigma_j)^{-1}\right] \cdot (M_i - M_j) + \frac{1}{2} Trace\left[(\Sigma_i)^{-1} \cdot \Sigma_j + (\Sigma_j)^{-1} \cdot \Sigma_i - 2 \cdot I\right] \quad (16)$$

where

M_i = sample mean vector of class *i*, this vector has *n* elements, where *n* is the number of channels in the current set

Σ_i = covariance matrix for class *i*, which has *n* by *n* elements

$(\ )^T$ = transpose of matrix

$(\ )^{-1}$ = inverse of matrix

Trace[ ] = trace of matrix (sum of diagonal elements)

I = identity matrix

The transformed divergence between the classes *i* and *j*, *TD(i,j)*, is calcualted as:

$$TD(i,j) = 2 \cdot \left[1 - \exp(-D(i,j)/8)\right] \quad (17)$$

This restricts the transformed divergence to values between 0 and 2.

Finally, the average transformed divergence (*TDV*) for all the *NCLASS·(NCLASS-1)* class pairs is calculated as:

$$TDV = \frac{1}{NCLASS \cdot (NCLASS - 1)} \cdot \sum TD(i,j) \quad (18)$$

where $\sum$ is the sum over all values of *i* and *j, i < j.*

124

The PCI 'CHNSEL' algorithm was used to find the best subset of seven out of nine (or more) channels using the criterion of maximised average transformed divergence. A branch and bound algorithm (optimisation over subproblems) is employed to perform this optimisation task (PCI Geomatics 2003).

For data sets including topographic data, separability measures were not employed in the overall channel selection because the terrain data cannot be assumed to have a Gaussian distribution for the classes under examination (Benediktsson et al. 1990). In this case, the non-topographic channels as selected before were combined with one or several topographic channels, and their contribution was evaluated through the results of test classifications.

8.7.3 Signature Separability

Signature separability matrices with the pairwise Bhattacharyya distance as the separability measure were calculated in order to evaluate to what extent the 14 classes of the original classification scheme are separable with the help of the IKONOS data and to assess the contribution of the texture features to the separability of the classes. Using the class signatures of the 14 classes, generated from the four multispectral IKONOS channels at 8 m resolution, the signature separability between all pairs of classes was calculated employing the PCI 'SIGSEP' algorithm. This was compared to the separability of the class signatures generated from the four multispectral channels and the three texture channels GLCM *entropy*, GLCM *standard deviation* and GLCM *contrast*, which had been selected as the optimal seven channel combination of IKONOS data.

The Bhattacharyya distance between two classes (class *i* and class *j*) is calculated from class means and class covariance matrices using equation 20:

$$BD(i,j) = 2 \cdot \left[1 - \exp\left(- a(i,j) \right) \right] \tag{19}$$

where

$$a(i,j) = \frac{1}{8} \left(M_i - M_j \right)^T \cdot \left[\frac{\Sigma_i + \Sigma_j}{2} \right]^{-1} \cdot \left(M_i - M_j \right) + \frac{1}{2} \ln \left(\frac{\left| \frac{1}{2} \cdot \left(\Sigma_i + \Sigma_j \right) \right|}{\sqrt{\left| \Sigma_i \right| \cdot \left| \Sigma_j \right|}} \right)$$

where

M_i = mean vector of class *i*, where the vector has *n* elements (*n* is the number of channels used)

Σ_i = covariance matrix for class *i*, which has *n* by *n* elements

$\left| \Sigma_i \right|$ = determinant of the covariance matrix for class *i*

$(\ )^T$ = transpose of matrix

$[\ ]^{-1}$ = inverse of matrix

(PCI Geomatics 2003).

The resulting signature separability matrices were examined and compared. For informational classes which still had very poor separability even after the inclusion of the texture features, the merging or discarding of classes was considered. The signatures of the class pair with the minimum separability value (dense and open secondary forest) were merged. Most of the later classifications were conducted with secondary forest as one class, resulting in a total of 13 instead of 14 classes.

8.8 Classifications of the Eastern Test Area

The calculation of texture features, the implementation of several types of spatial integration of the multispectral data and, in some cases, the additional integration of Landsat data or terrain variables allowed the creation of a large number of different data sets. These data sets (characterised by different channel combinations and/or different types and degrees of spatial integration) were classified to create a basis for the comparison of their respective factual usefulness for the creation of forest and land cover maps of the test area. Table 14 provides a list of the classified datasets and the classification methods applied to them.

Table 14: Classifications conducted for the eastern test area.

Data set		Classification techniques	No. of classes
No.	Channel combination	Spatial resolution / integration		
1	IKONOS ms channels 1-4	4 m	MLC	13, 14
2	IKONOS ms channels 1-4	8 m (block averaged)	MLC	13, 14
3	IKONOS ms channels 1-4	12 m (block averaged)	MLC	13, 14
4	IKONOS ms channels 1-4	16 m (block averaged)	MLC	14
5	IKONOS ms channels 1-4	4 m, 3×3 mean low pass filtered	MLC	13, 14
6	IKONOS ms channels 1-4	4 m, 5×5 mean low pass filtered	MLC	13, 14
7	IKONOS ms channels 1-4	4 m, 7×7 mean low pass filtered	MLC	14
8	IKONOS ms channels 1-4	4 m, 3×3 median low pass filtered	MLC	14
9	IKONOS ms channels 1-4	Segmentation with scale parameter 12	StNN	14
10	IKONOS ms channels 1-4	Segmentation with scale parameter 16	StNN	13, 14
11	IKONOS ms channels 1-4	Segmentation with scale parameter 20	StNN, MLC	13, 14
12	IKONOS ms channels 1-4	Segmentation with scale parameter 30	StNN	14
13	IKONOS ms channels 1-4, GLCM *ENT, SD, CONT*	4 m	MLC	13, 14
14	IKONOS ms channels 1-4, GLCM *ENT, SD, CONT*	8 m (block averaged)	MLC, k-NN, ANN	13, 14

Table 14: Classifications conducted for the eastern test area (continued).

Data set		Classification techniques	No. of classes
No.	Channel combination	Spatial resolution / integration		
15	IKONOS ms channels 1-4, GLCM *ENT, SD, CONT*	12 m (block averaged)	MLC	13
16	IKONOS ms channels 1-4, GLCM *ENT, SD, CONT*	16 m (block averaged)	MLC	13
17	IKONOS ms channels 1-4, GLCM *ENT, SD, CONT*	4 m, ms channels 3×3 median low pass filtered	MLC	13
18	IKONOS ms channels 1-4, GLCM *ENT, SD, CONT*	4 m, ms channels 3×3 mean low pass filtered	MLC	13, 14
19	IKONOS ms channels 1-4, GLCM *ENT, SD, CONT*	4 m, ms channels 5×5 mean low pass filtered	MLC	13
20	IKONOS ms channels 1-4, GLCM *ENT, SD, CONT*	Segmentation with scale parameter 16	StNN, MLC	13
21	IKONOS ms channels 1-4, GLCM *ENT, SD, CONT*	Segmentation with scale parameter 20	StNN, MLC	13
22	GLCM *ENT, SD, CONT, MEAN, CORR*	8 m	MLC	13, 14
23	Landsat ETM+ channels 1-5, 7, 8	15 m (Landsat channels 1-5 & 7 resampled from 30 m)	MLC	13, 14
24	IKONOS ms channels 1-4, Landsat ms channels 5 & 7	8 m (block averaged for IKONOS, resampled for Landsat)	MLC	13
25	IKONOS ms channels 1-4, Landsat ms channels 5-7	8 m (block averaged IKONOS data, resampled Landsat data)	MLC	13
26	Landsat ETM+ channels 2, 4, 6, 7, GLCM *ENT, SD, CONT*	15 m (Landsat channels 1-5 & 7 resampled from 30 m)	MLC	13, 14
27	IKONOS ms channels 1-4, elevation, slope and incidence60	8 m (IKONOS ms data block averaged, elevation data interpolated through kriging)	MLC, k-NN, ANN	13
28	IKONOS ms channels 1,2,4, GLCM texture *ENT*, *SD*, *CONT*, elevation	8 m (IKONOS ms data block averaged, elevation data interpolated through kriging)	MLC	13
29	IKONOS ms channels 1,2,4, GLCM texture *ENT*, *SD*, *CONT*, slope	8 m (IKONOS ms data block averaged, elevation data interpolated through kriging)	MLC	13
30	IKONOS ms channels 1,2,4, GLCM texture *ENT*, *SD*, *CONT*, incidence60	8 m (IKONOS ms data block averaged, elevation data interpolated through kriging)	MLC	13

Table 14: Classifications conducted for the eastern test area (continued).

	Data set		Classification techniques	No. of classes
No.	Channel combination	Spatial resolution / integration		
31	IKONOS ms channels 1,2,4, GLCM texture *ENT*, *SD*, *CONT*, elevation	4 m (elevation data interpolated to 8 m through kriging and resampled to 4 m)	MLC	13
32	IKONOS ms channels 1-4, GLCM texture *ENT*, *SD*, *CONT*, elevation	8 m (IKONOS ms data block averaged, elevation data interpolated through kriging)	k-NN, ANN	13
33	IKONOS ms channels 1-4, GLCM texture *ENT*, *SD*, *CONT*, slope	8 m (IKONOS ms data block averaged, elevation data interpolated through kriging)	k-NN, ANN	13
34	IKONOS ms channels 1-4, GLCM texture *ENT*, *SD*, *CONT*, incidence60	8 m (IKONOS ms data block averaged, elevation data interpolated through kriging)	k-NN, ANN	13
35	IKONOS ms channels 1-4, GLCM *ENT*, *SD*, *CONT*, elevation, slope, incidence60	8 m (IKONOS ms data block averaged, elevation data interpolated through kriging)	k-NN, ANN	13

The Maximum Likelihood Classification technique was used for the classification of most of the datasets. The DNs in the training areas were normally distributed in the multispectral bands and GLCM texture channels for most of the classes (table 15). There are only some exceptions, mainly for land cover types which occupy only small proportions of the study area, like water and bare ground. Consequently, MLC could be expected to be the optimal classifier for the data sets containing multispectral and textural data. Besides MLC, object-oriented nearest neighbour methods were used for the classification of the segmented data. Those data sets which include DEM-derived data channels (and for comparison also some data sets without ancillary data) were classified with non-parametric classification methods in addition to MLC, because of the mix of different types of data in these data sets and the lack of normal distribution in some of the terrain data.

Table 15: Normal distribution of channel DNs in the class training areas. ∨: normally distributed, ○: moderate deviation from normal distribution (e.g. histogram somewhat skewed but unimodal, or similar central tendencies but not bell-shaped), –: strong deviation from normal distribution. (Estimated using the histograms of the 4 m resolution data for the multi-spectral and texture channels, and the histograms of the 8 m resolution DEM derived data, which is based on the 8 m DEM generated through kriging.)

Training Class	IKONOS ms 1 (blue)	IKONOS ms 2 (green)	IKONOS ms 3 (red)	IKONOS ms 4 (NIR)	GLCM *ENT*	GLCM *SD*	GLCM *CONT*	DEM elevation	Slope	Incidence 60
Dense pine forest (PFd)	∨	∨	∨	∨	∨	∨	∨	○	∨	∨
Open pine forest (PFo)	∨	∨	∨	∨	∨	∨	∨	–	○	–
Cloud forest (CF)	∨	∨	∨	∨	∨	∨	∨	○	∨	○
Dense secondary forest (SFd)	∨	∨	∨	∨	∨	∨	∨	○	○	–
Open secondary forest (SFo)	∨	∨	∨	∨	∨	∨	∨	∨	∨	○
Palm dominated forest (PmF)	∨	∨	∨	○	∨	∨	∨	○	∨	∨
Broadl. riparian forest (BRF)	∨	∨	∨	∨	∨	∨	∨	○	∨	○
Matorral (Mat)	∨	∨	∨	∨	○	○	○	–	∨	○
Calimetal (Cal)	∨	○	∨	○	∨	∨	∨	○	∨	○
Agroforestry (AF)	∨	∨	∨	∨	∨	∨	∨	○	∨	○
Grassland (GL)	∨	∨	∨	∨	∨	∨	∨	○	∨	–
Crops (Cr)	∨	∨	∨	–	○	∨	∨	–	–	○
Bare ground (BG)	○	○	○	∨	○	○	–	–	○	○
Water (W)	∨	∨	∨	–	○	○	○	∨	∨	∨

8.8.1   Maximum Likelihood Classification

The training areas described in chapter 8.6 were used to calculate class signatures from the data sets listed in table 14. This provides the variables necessary for a maximum likelihood classification. The MLC algorithm provided by PCI (2001) was used to conduct these classifications (equation 21). This algorithm calculates a discriminant function $G_i(X)$ (as an expression of the relative likelihood that the pixel or observation X belongs to class i) for each class. $G_i(X)$ is based on the log of the multivariate Gaussian probability density function $P(X|i)$, modified by a term accounting for the prior probability of the class.

$$G_i(X) = \log_e\left(P(X|i)\right) + \log_e(P_i)$$

$$= \frac{1}{2}(X - M_i)^T \cdot [\Sigma_i]^{-1}(X - M_i) - \frac{n}{2}\log_e(2\pi) - \frac{1}{2}\log_e|\Sigma_i| + \log_e(P_i) \qquad (20)$$

where

$P(X|i)$ = the probability that the observation X will occur, given that it belongs to class i (under the Gaussian assumption)

n = number of channels used in the classification

X = n-dimensional measurement vector

M_i = n-dimensional mean vector of class i

Σ_i = covariance matrix for class i, which has n by n elements

$(\ )^T$ = transpose of matrix

$[\ ]^{-1}$ = inverse of matrix

$|\Sigma_i|$ = determinant of the covariance matrix for class i

P_i = *a priori* probability for class i

The *a priori* probability is calculated from the class-specific bias B_i (which is chosen by the user) as

$$P_i = \frac{B_i}{\sum\limits_{i=1}^{m} B_i} \quad \text{where } \sum\limits_{i=1}^{m} B_i \text{ is the sum of biases for all } m \text{ classes used in the classification.}$$

M_i, Σ_i and $|\Sigma_i|$ are estimated from the training sample of class i which is used to calculate the class signature. Together, they define the position, shape and orientation of the class' hyperellipsoid in feature space. The class bias B_i, as determined by the user, is also stored in the class signature segment.

For each pixel X, $G_i(X)$ is calculated for all classes, and the pixel is assigned to the class for which the value of G_i (likelihood of membership) is highest. No threshold was specified for class membership and no null class created, so all pixels without exception were assigned to the most probable class according to equation 21. In one case, two additional output channels were generated receiving the classes for which the G_i value was second and third highest.

Preliminary classifications of several data sets, with a uniform class bias for all classes, showed that the classes 'water', 'crops', 'agroforestry' and 'bare ground', which in reality cover only small proportions of the test area, were substantially overrepresented in the resulting maps. Consequently, the class bias was progressively reduced to 0.1 for these classes, while it was left at its default value of 1 for the other classes. The MLC algorithm uses the bias values to calculate the *a priori* probability P_i for each class (PCI 2001). This weighs the other classes in favour of the classes with reduced prior probabilities in the classification. If all other factors are equal, the G_i value is reduced by 1 for the classes with the bias 0.1 compared to the classes with a bias of 1.

The *a posteriori* probability for the most likely class (the class to which a pixel measurement was assigned) was also calculated for some classifications. In one case, *a posteriori* probabilities were calculated for the three most likely classes. The *a posteriori* probability $P(i|X)$ is the probability of class i, given the measurement vector X. It is calculated from the a priori probability P_i and the probability density function $P(X|i)$, using Bayes' theorem.

$$P(i|X) = \frac{P(X|i)P_i}{P(X)}$$
(21)

where *P(X)* is the 'mixture density function' for all *m* classes: $P(X) = \sum_{i=1}^{m} P(X|i)P_i$.

The *a posteriori* probability denotes the relative probability of a class assignment on the assumption that the pixel area does belong to one of the training classes. If these probabilities were calculated for all classes, they would sum to 1 (Paola & Schowengerdt 1995, PCI 2001).

8.8.2 K-Nearest-Neighbours Classification

The seven channel spectral-textural data set at 8 m resolution (data set 14) and several data sets including DEM-derived data channels were classified using the k-nearest neighbour classifier. The same samples which were used to calculate the class signatures for MLC were also used as samples for the k-NN classification. The PCI Geomatics 'KNN' algorithm reduces the number of samples per class to 200 by default (PCI 2001), but better results were achieved with larger numbers of samples, so the value for the maximum number of samples per class was increased to 1400. Thus all the training samples at 8 m resolution (table 12) were used in the calculations. The number of nearest neighbours (*k*) was chosen to be 8. This relatively large *k*-value – compared to the number 5 used by many authors, e.g. Collins et al. (2004) and Debeir et al. (2002) – was chosen because of the high resolution (high within-class variance) of the data and because of the large number of samples (see also Fukunaga 1990:276).

The k-NN algorithm used here calculates the Euclidian distance in feature space between the measurement vector *X* and each training sample vector. It finds the 8 nearest training samples in feature space, determines the majority class among them and assigns *X* to that class. This is repeated for all unclassified pixels (measurement vectors).

8.8.3 Artificial Neural Network Classification

The PCI Geomatica neural network programs 'NNCREAT', 'NNTRAIN' and 'NNCLASS' (PCI 2001) were used to create and train neural networks and to conduct neural network classifications of several data sets for the eastern test area. As neural network classifiers do not have the same

limitations with regard to the number of channels as MLC, data sets with up to ten channels (consisting of multispectral, textural and DEM-derived data channels) were classified with this method. See chapter 2.6 for background information about artificial neural networks and their training. In this case, a neural network was created which had an input layer with one node for each input channel (between 7 and 10), one hidden layer with 13 nodes and an output layer with 13 nodes (one for each class).

The created back-propagation neural network uses the 'generalised delta rule' during the learning phase. The network was trained using the same class training samples which were also used in MLC and k-NN. The learning rate was set to 0.1 and the momentum rate to 0.9. The training cycle (adjustment of weights after forward and backward propagation of values through the network) was repeated for a maximum of 1000 iterations or until the maximum normalised total error was less than 0.01 or the maximum individual error was less than 0.001. The latter two cases did not actually occur, so that the training was always conducted for 1000 iterations. (The individual error is the sum of errors in the output values for one sample, meaning the difference between target value and output value of each output node. The normalised total error is calculated as half the sum of the squares of the individual errors, divided by the number of samples.) The error plot was then looked at to see whether the value for the normalised total error had stabilised before the 1000th iteration. This was the case for all classifications conducted here, even if the total error was still between 0.45 and 0.52. In a second step, the learning and momentum rates were lowered to 0.04 and 0.1 respectively, for a slower, more stable training with smaller step increments for a fine-tuning of the network weights (PCI 2001). 1000 further iterations were conducted with these parameters, resulting in final maximum total errors between 0.42 and 0.49.

8.8.4 Object-Oriented Nearest-Neighbour Classification of Segmented Data

A 'standard nearest neighbour classification' (StNN) was used to assign the image object primitives of the segmented images to the sampled classes within the eCognition environment. (The term 'standard nearest neighbour' means that the same set of features is used for all classes in the calculations of the distance to the nearest neighbours.) For this object-oriented nearest neighbour classification, sample objects are required instead of sample pixels. The segments which were used as sample objects for the classification were chosen to match the training areas in the per-pixel training sample as closely as possible. The eCognition nearest neighbour algorithm computes the distance d in feature space between an image object and a sample object as the Euclidian distance standardised by the standard deviation of all feature values:

$$d = \sqrt{\sum_f \left(\frac{v_f^s - v_f^o}{\sigma_f} \right)^2} \tag{22}$$

where

d = distance between sample object s and image object o

v_f^s = feature value of sample object s for feature f

v_f^o = feature value of image object o for feature f

σ_f = standard deviation of the feature values for feature f

For each image object, a fuzzy class membership value in the range of 0 to 1 is calculated for every class. This is done by finding the image object's closest sample object of each class in feature space and calculating an exponential membership function $z(d)$ based on the distance d.

$$z(d) = e^{-k \cdot d^2} \tag{23}$$

where k was defined as $k = \ln(5)$.

The image object is then assigned to the class for which it has the highest degree of membership (Baatz et al. 2002). The membership values for the agroforestry class were multiplied by 0.96 before the class assignment to reduce the assignments to this class. This fulfils the same purpose as the reduction of the class bias in the maximum likelihood classification.

The eCognition software offers many possibilities to fine-tune a classification using the intrinsic features of the image object primitives, like layer values, texture and object shapes, and additional class-specific conditions, including relationships to other objects. However, it would have been very time-consuming to test the many options, using iterative loops of classifications at different hierarchical levels etc. So, keeping in mind that the classification of the segmented data should be comparable to the classifications of the data sets created with other types of spatial integration, only one-step (data-driven) classifications were conducted in eCognition, using only the same features (channel values) which were also used in the classifications of the other data sets.

8.9 Post-Classification Processing

The classification results (except for those of the segmented data) were mode filtered with filter sizes of 3 × 3, 5 × 5 and 7 × 7. The mode filter computes the mode, i.e. the value that occurs most frequently in the filter kernel and assigns it to the central pixel. Isolated pixel values are thus replaced by whatever value constitutes the majority in their neighbourhood. This reduces the noise in a classification and could be regarded as a kind of post-classification spatial integration.

As an alternative to the post-classification processing with a mode filter, a sieve filter (removing class polygons containing less than a specified number of pixels by merging them with their largest neighbour) was also employed in some cases. Sieve filtering did, however, not lead to the same

amount of accuracy improvement as mode filtering, so that it was abandoned in favour of the easy and straightforward mode filtering.

A post-classification sorting with the help of the DEM data, like for the Landsat classification of the whole UCRYN (chapter 7.3), was also taken into consideration. There is, however, only a relatively small range of elevations in the eastern test area (800 m to 1565 m), offering fewer possibilities to define decision rules involving absolute thresholds.

8.10 Accuracy Assessment

The classification results were displayed in the form of thematic maps and visually evaluated and compared to each other and to the ground knowledge. A sample-based accuracy assessment based on error matrices was conducted to calculate quantitative accuracy measures.

900 points were distributed over the classified eastern test area using stratified random sampling. The stratification made sure that the "number of samples chosen randomly from each class are proportional to the percentage of the image occupied by each class" (PCI Geomatics 2003). (The stratification was based partly on the 14-class MLC result of data set 14 and partly on the MLC result of data set 26, see table 14.) This was done after the classification and also after the last field work campaign, so that the determination of the land cover classes had to rely on the previously collected data. Not all the sample sites had been visited on the ground. (And some parts of the eastern test area, particularly in the Scientific Reserve Ebano Verde, were not accessible on the ground anyway.)

The land cover classes of 583 of these 900 sample points could be determined using a combination of the knowledge and data collected on the ground during field work (e.g. annotations on the paper copies of the IKONOS image, ground photographs and notes relating to GPS waypoints) and visual interpretation of the IKONOS image itself (using several channel combinations, including pan-sharpened, for the display) and of the oblique and the historical aerial photographs. In some cases, the DEM, the Progressio (1995) land use map and a vegetation map of the Scientific Reserve Ebano Verde (García et al. 1994: fig. 5) also helped to determine the true land cover class. Not all of the sample sites had been visited during field work, but in many cases the land cover class could still be identified using the other available data. If a class could be clearly identified in the IKONOS image itself, this had the advantage that there could not be any geometric registration error or temporal difference between reference data and classified data. The historical aerial photographs helped to differentiate between mature cloud forest (forest in all the images) and secondary forest (treeless areas in 1966). The 1984 aerial photographs, showing the young pine plantations of that time, helped to distinguish pine plantations from other kinds of forest. The reference class was assigned if a majority land cover type could be identified in the 4 m × 4 m as well as the 8 m × 8 m area which

the sample point referred to. However, for a third of the points, the land cover class could not be determined with confidence, so they were dropped from the sample. This affected mostly sample points in areas without ground truth where the manual interpretation of the remote sensing data did not deliver unambiguous results. By contrast, sample points in transitional land cover areas or stages, e.g. between grassland and *matorral* or between *matorral* and secondary forest, were not dropped, but a decision was made to assign one of the classes to them. In all cases, the reference class was assigned blindly, i.e. without knowing the result of any of the classifications for the point in question.

The reference data were originally produced for the 14 class classification scheme. Both open and closed secondary forest reference points were later allocated to the merged class of secondary forest to test the accuracy of the 13 class classifications.
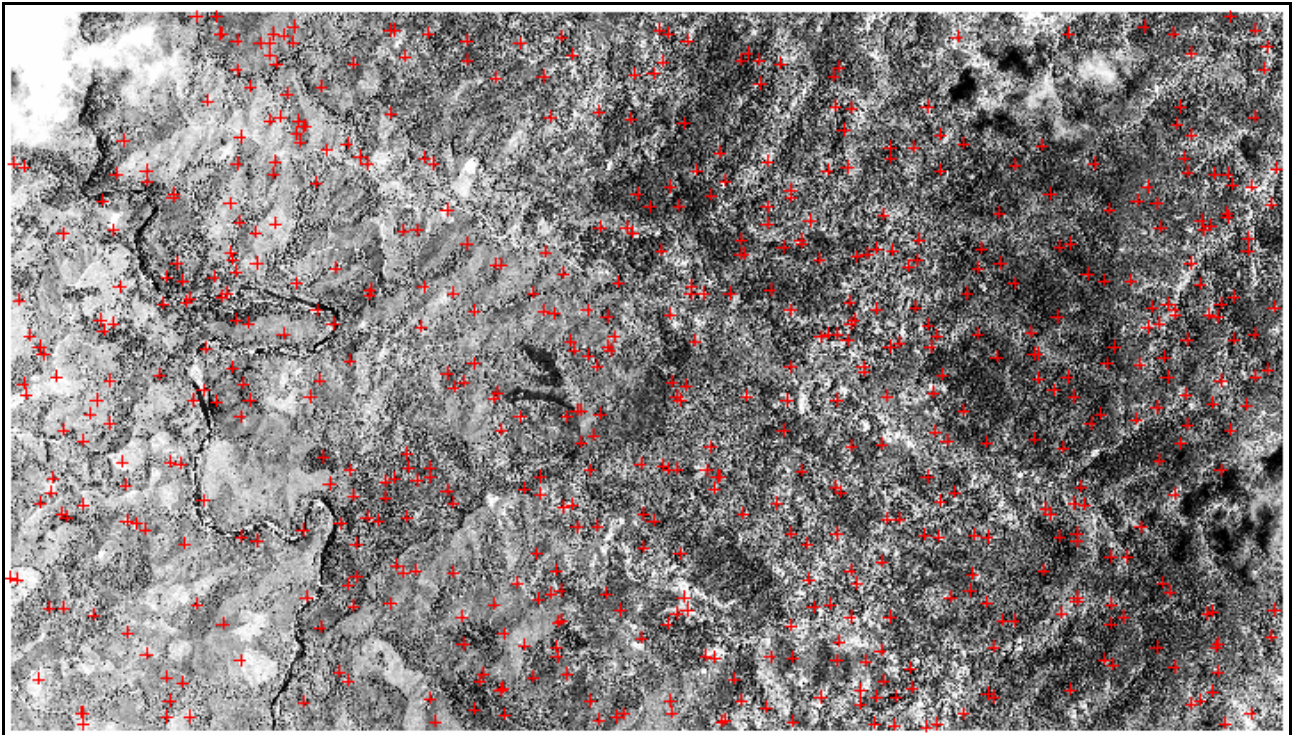
Figure 25: The reference points used for the accuracy assessment in the eastern test area.

The resulting 583 reference points were distributed over all classes and over the whole classified area (figure 25), including points close to class boundaries. For some kinds of spatially integrated data, up to six of the reference points ended up in non-classified areas and were then not used in the accuracy calculations. The testing data are independent of the training data. Using this set of reference points, accuracy assessments were conducted for all classifications of the eastern test area, comparing the reference classes and the classes predicted by the classifier (and possibly modified during post-classification processing). The results of the comparisons were reported in the form of error matrices.

The overall classification accuracy (percentage correct) was calculated for all classifications, as well as the class-specific user's and producer's accuracies. To make the class-specific accuracies comparable to each other without having to differentiate between user's and producer's accuracies, these two values were multiplied for each class. The 95 % confidence interval was calculated for the overall classification accuracy and the per-class user's and producer's accuracies as a function of the number of samples and the proportion of correctly classified samples.

Additionally, the Kappa index of agreement (Cohen 1960) was calculated as the actually observed agreement $A_{correct}$ adjusted by the expected chance agreement A_{chance}.

$$\text{KIA} = \frac{A_{Correct} - A_{Chance}}{1 - A_{Chance}} \tag{24}$$

where $A_{Correct}$ is the overall accuracy, i.e. the sum of observations x_{ii} in row i and column i (in the agreement diagonal) of an error matrix for r classes divided by the total number of observations N:

$$A_{Correct} = \frac{\sum_{i=1}^{r} x_{ii}}{N} \tag{25}$$

and A_{Chance} is determined by multiplying the marginal totals of row i (x_{i+}) and of column i (x_{+i}) and dividing the sum of the resulting chance values in the agreement diagonal by N^2:

$$A_{Chance} = \frac{\sum_{i=1}^{r} (x_{i+} \cdot x_{+i})}{N^2} \tag{26}$$

To test the amount of error introduced by mixed pixels and by edge effects in the texture data, all reference points closer than 12 m to a land cover boundary (as interpreted in the pan-sharpened IKONOS image) were deleted from the test sample, reducing it to 333 points. This should eliminate those testing pixels for which the texture values calculated in a 15 m × 15 m window are likely to be influenced by between-class texture. Accuracy assessments for the spectral-textural classifications at 4, 8, 12 and 16 m resolution were conducted with this set of reference points and the overall accuracies were compared to those produced with the complete set of 583 points.

The reference sample for the accuracy assessment of one classification was 'fuzzified' by reassessing the misclassified pixels according to the linguistic scale of Woodcock & Gopal (2000). For each reference point in the subset, all classes were assigned discrete levels of class membership between 1 and 5, according to the following description:

"(5) *Absolutely right*: No doubt about the match. Perfect.
 (4) *Good answer*: Would be happy to find this answer given on the map.
 (3) *Reasonable or acceptable answer*: Maybe no the best possible answer but it is acceptable; this
     answer does not pose a problem to the user if it is seen on the map.

(2) *Understandable but wrong* [...]

(1) *Absolutely wrong*" (Woodcock & Gopal 2000:156).

Classes with scores of at least 3 (at least acceptable answers) were then counted as 'right' for the reference point. This made it possible to calculate a fuzzy overall accuracy, i.e. the percentage of pixels for which the classified value matches at least one reference class with a score between 3 and 5.

Finally, some classes were aggregated in the error matrix to calculate the overall accuracy for less detailed classifications.

9 Results and Discussion of Processing Methods and Classifications Involving IKONOS Data

9.1 Interpretation of Experimental Variograms

The experimental variograms calculated for the transects as described in chapter 8.2 are shown in figures 26 and 27. The resulting variograms and derived parameters have to be interpreted cautiously, keeping in mind that the results depend on the chosen transects and on the resolution (1 m) and waveband (450-900 nm) of the sampled imagery (see chapter 2.2). The experimental variograms for the selected single transects are typically periodic in the case of the forest areas. This reflects the alternation of illuminated crown parts and shaded crowns and background. The single experimental variograms of the riparian forest area are not as clearly periodic as those of the other forest types, probably because of the dense cover of large and smaller crowns which creates a less repetitive pattern than the pine plantation for example. In the case of grassland, the single horizontal transect produces an aspatial experimental variogram, indicating that the theoretic range for this vegetation type is smaller than the 1 m support of the image (Curran 1988). Most of the mean experimental variograms approach the classic form of variograms (figure 1). Some degree of periodicity is preserved in part of the mean forest variograms, but it has to be kept in mind that they are only averages of nine variograms representing parallel transects in the same sample area.

Semivariance values calculated from the scaled panchromatic data are not meaningful as absolute values but only in relation to the other semivariance values calculated from the same image. Among the mean experimental variograms of the sampled land cover classes, the one of the open secondary forest has the highest sill (maximum level of semivariance), followed by broadleaved riparian forest. The sills of mean variograms of cloud forest and dense pine forest are similar to each other, while the grassland sill is the lowest by far, with only about 10 % of the maximum semivariance compared to open secondary forest. This reflects the relative homogeneity of the grassland area compared to the forest areas, and particularly to the very heterogeneous area of open secondary forest, which includes a large number of spectrally different elements (broadleaved trees, pine trees, shade, shrubs, patches of *Dicranopteris pectinata* and other undergrowth).
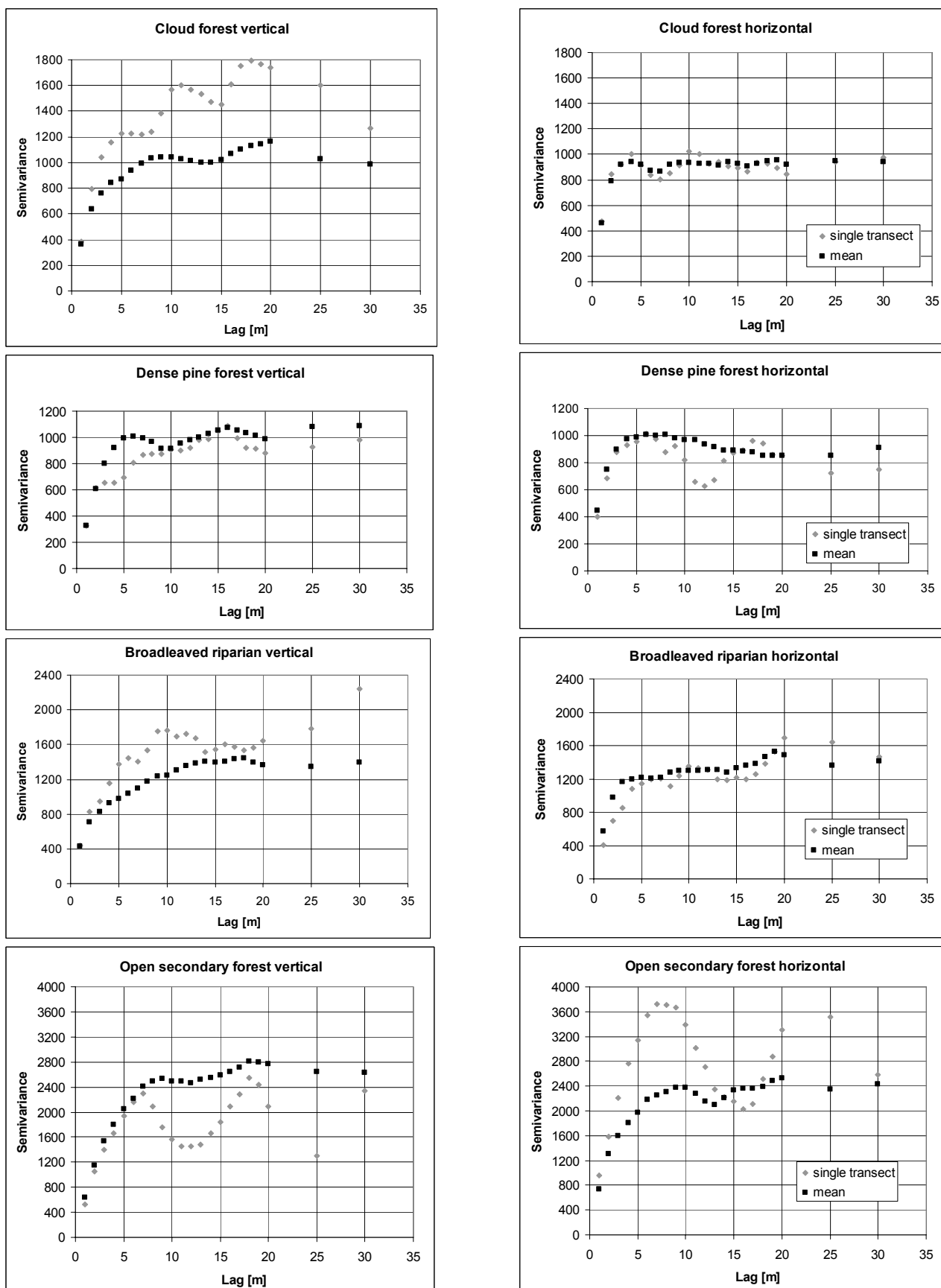
Figure 26: Experimental variograms of forest transects, from 1 m resolution panchromatic (450-900 nm) data.
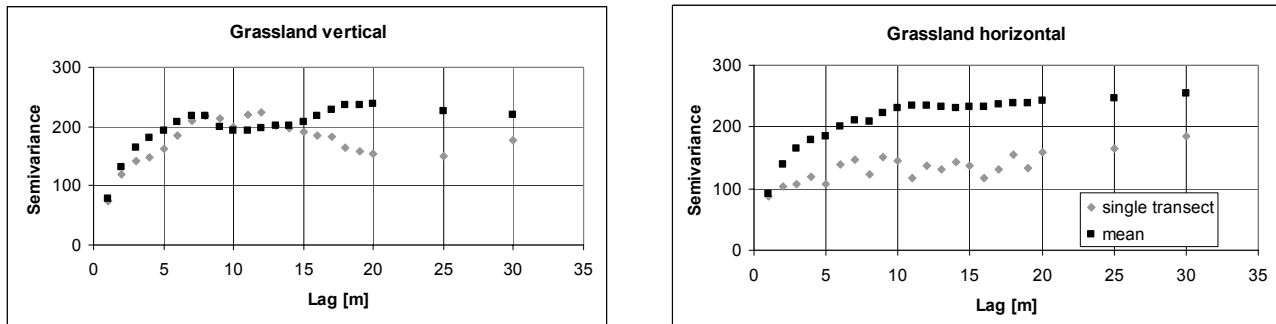
Figure 27: Experimental variograms of grassland transects, from 1 m resolution panchromatic (450-900 nm) data.

The ranges (lags where the semivariance reaches a maximum) of the mean experimental variograms vary between just 4 m for the mean horizontal variogram of the cloud forest to 14 m for the mean vertical variogram for the broadleaved riparian forest. The range of 6 m for the dense pine forest area approximately corresponds to the average distance between trees in this plantation. The average range for all sampled forest areas is 8 m. These values give an indication how far the spatial dependency between 1 m resolution panchromatic pixel values extends. The range values found here correspond roughly to the mean ranges which Treitz (2001) and Sampson et al. (2001) found for forest stands in Canada. Grassland has a mean range of 7 m, probably reflecting the varying terrain illumination and the distribution of some shrubs in the sample area.

The mean range of the experimental variogram is regarded as indicative of the optimal spatial resolution for a per-pixel classification, as it provides a measure of the size of the elements in the sampled image area (Treitz & Howarth 2000a). Pixels should be larger than the range in order to average the within-class spectral variability and be representative of their class (Curran 1988). According to the range values derived from the panchromatic data, the resolution for a classification of the eastern test area should be coarser than 8 m in order to fulfil this condition for most of the land cover classes in the area. On the whole, the mean experimental variogram ranges indicate that some kind of spatial integration of the pixel values should be useful for a land cover classification with the IKONOS multispectral data.

By contrast, pixels smaller than the range carry information about within-class variations, so for calculations of within-class texture the pixels must be smaller than the range of the variogram (Curran 1988). In the case of the forest classes tested here, this means that texture could be calculated both from the 1 m resolution panchromatic and the 4 m resolution multispectral IKONOS pixels. The windows used for the texture calculation, on the other hand, should again cover areas larger than the range (in both directions) in order to produce texture measures which are representative of the land cover classes.

9.2 Results of Spatial Integration

9.2.1   Effects of Spatial Integration on Within-Class Variability

The standard deviation of the digital numbers within the training samples for the individual land cover classes (the standard deviation of the class signature) was used as an indicator of within-class spectral variability.

The assumption that spatial aggregation in square windows (block averaging) and low pass filtering will reduce the within-class spectral variability can be confirmed. The classes with the highest initial standard deviations (open secondary forest, open pine forest, broadleaved riparian forest and dense secondary forest) also have the steepest decline of standard deviation when the data are spatially integrated. Generally, the spectral variability for the vegetation classes is larger in channel 4 (NIR) than in the first three channels. Low pass (mean) filtering consistently reduces the within-class variability in all multispectral channels. The strongest reduction in within-class variability can be seen between no filter and the 3×3 mean filter (figure 28). When the filter size is increased from 3×3 to 5×5 and from 5×5 to 7×7, the variability continues to decrease, but not as steeply.

The reduction of the spatial resolution to 8, 12 and 16 m reduces the within-class spatial variability in a way similar to low pass filtering. However, the decrease is not as consistent as with low pass filtering. For example, the standard deviation of the visible channels in the *matorral* areas increases when the resolution is changed from 12 to 16 m, as does the standard deviation in the NIR channel in the crops areas. In the non-forest classes, calculating the mean of several 4 m resolution pixels is not necessarily tantamount to the integration of several class elements. As a consequence, the connection between spatial resolution (aggregation level) and standard deviation is not as strong as for the forest classes. In the case of broadleaved riparian forest, the fact that the standard deviation of the visible channels fails to decrease between 12 and 16 m is probably due to the fact that some of the 16 m pixels cover not only the riparian forest but in part already areas beyond the narrow band of this forest. The deviations in the case of the *calimetal* could be due to the fact that this class only occurs in small patches (of pure *calimetal*). The training areas are accordingly small and the fact that the training masks at different resolutions can not always fit exactly onto each other (e.g. a 16 m × 16 m training area at 8 or 16 m resolution has to be rendered as a 12 m × 12 m or 12 m × 24 m training area at 12 m resolution) has more of an effect on the training area statistics than for the other classes which have larger training areas on average.

The mean values of the training samples are not much affected by either block averaging or mean filtering.
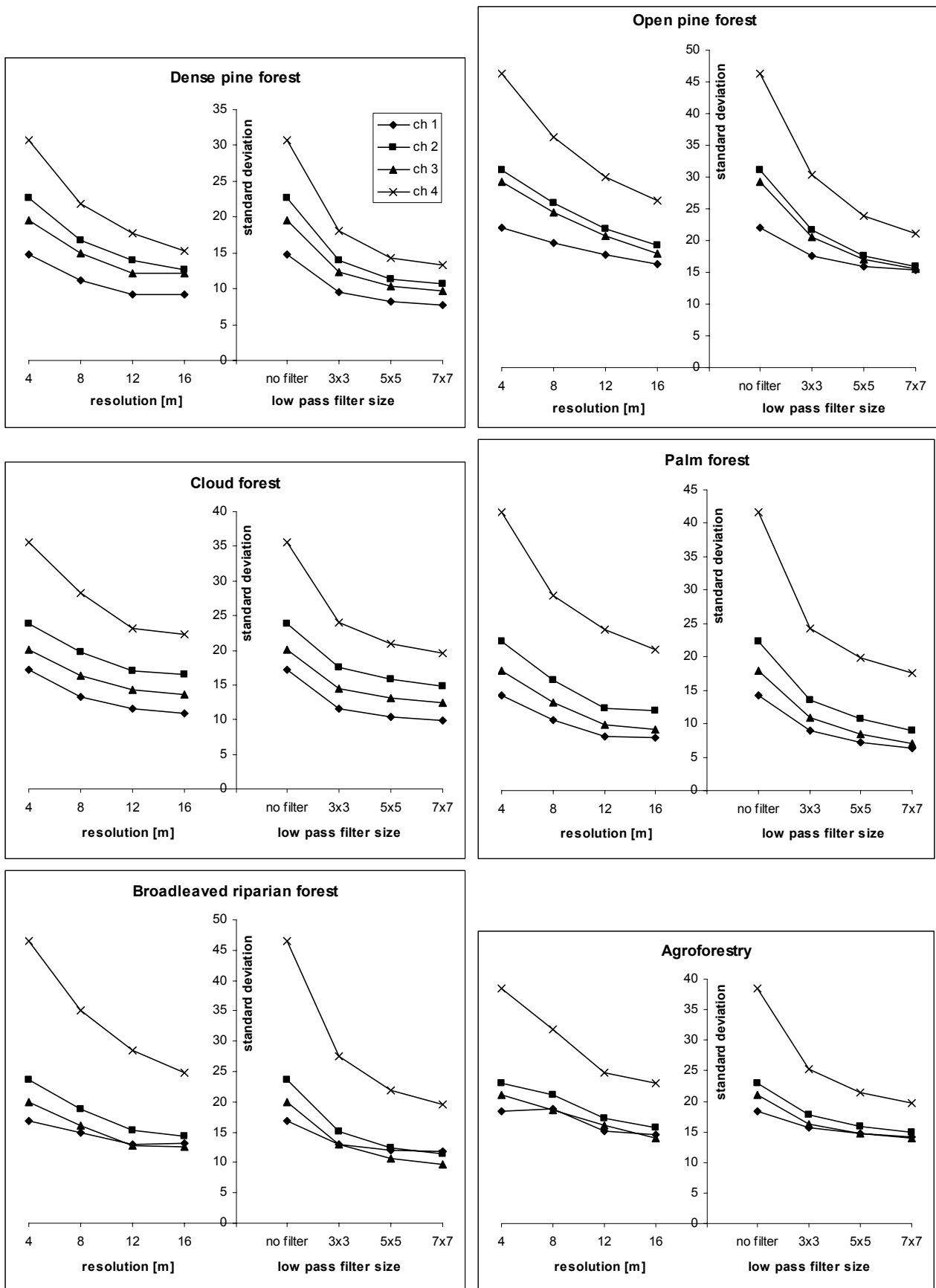
Figure 28a: Within-class standard deviation at different spatial resolutions after block averaging and at 4 m resolution after mean filtering.
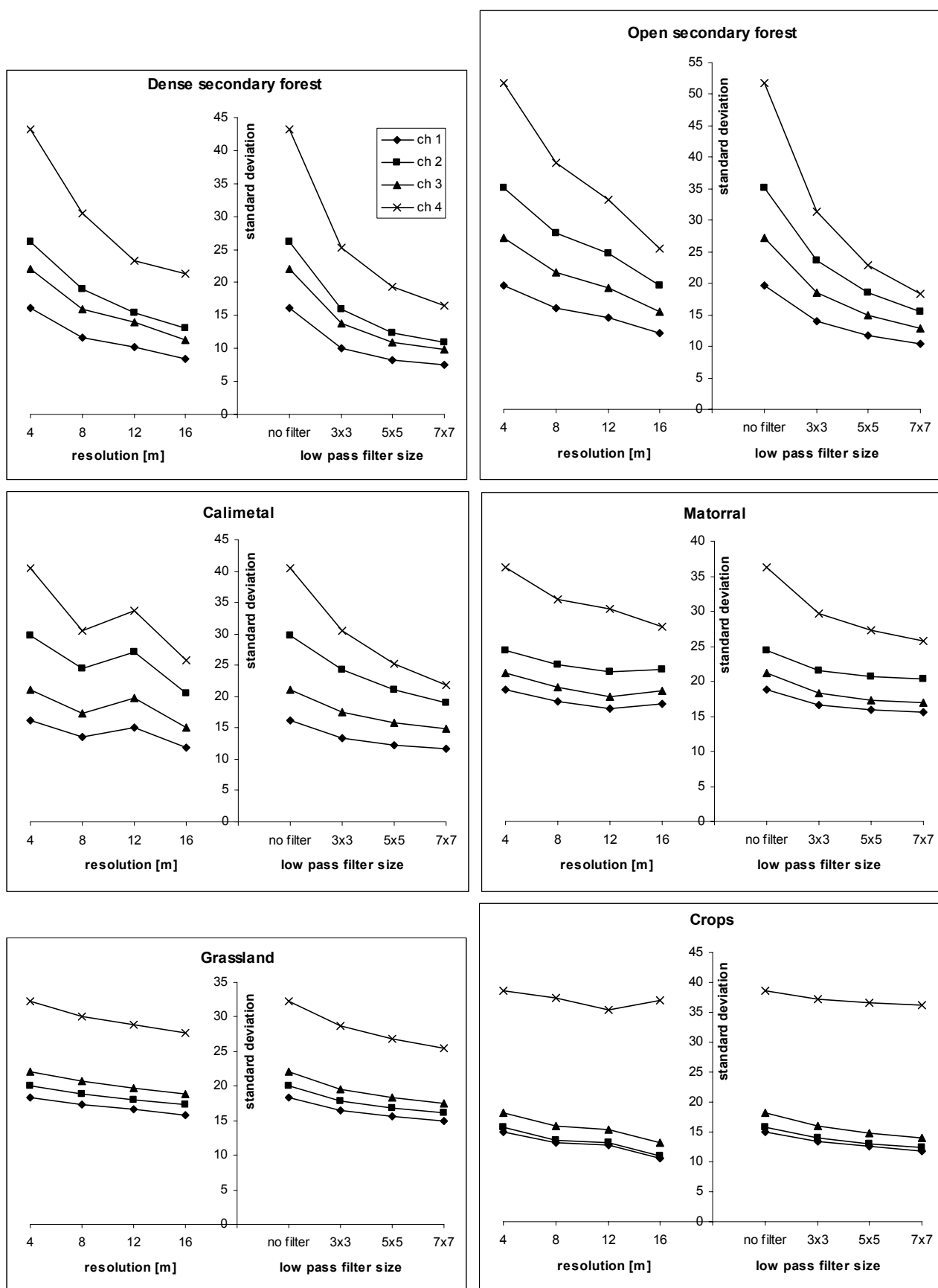
Figure 28b: Within-class standard deviation at different spatial resolutions after block averaging and at 4 m resolution after mean filtering.

9.2.2 Effects of Spatial Integration on Classification Accuracy

In the following, the effects of several spatial integration techniques on the classification accuracy are compared for 14-class maximum likelihood classifications. The overall agreement between classified data and the reference sample is just 40.5 % when the four multispectral IKONOS channels are used as input for the classification without any kind of spatial integration. The resulting map is very noisy (figure 29), manifesting the need for some kind of spatial integration.
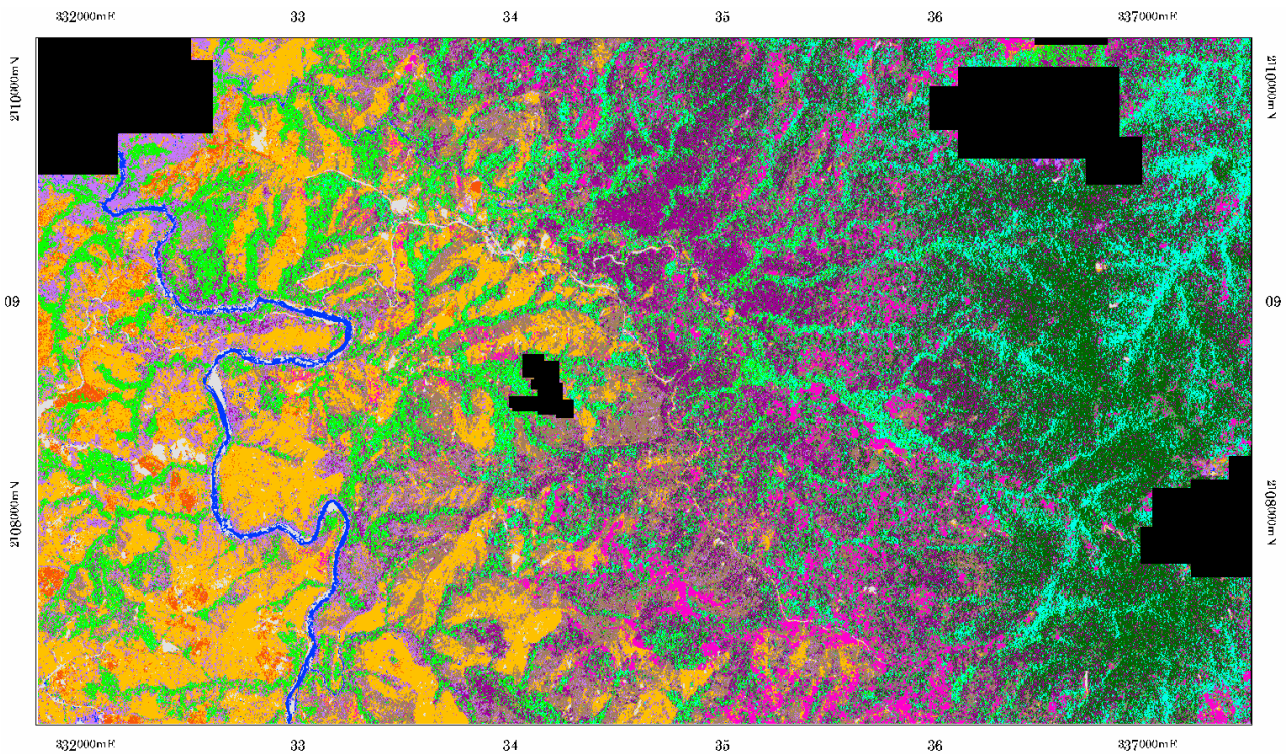
Figure 29: Classification of the 4 m multispectral data without any spatial integration. For the legend see plate 44, appendix 2.

Spatial aggregation in square windows (block averaging) and post-classification mode filtering

When the spatial resolution of the four multispectral IKONOS channels is reduced from 4 m to 8 m, 12 m and 16 m through block averaging, the classification accuracy is enhanced compared to the results for the 4 m resolution image (table 16). However, the accuracy values for the unfiltered classification results of the block averaged images do not differ significantly at the 95 % confidence interval, which is around ± 4.1 % for the overall accuracy values in tables 16 and 17.

When the results are mode filtered, classification accuracies are significantly increased. The effects of mode filtering exceed the effects of block averaging. 5×5 or 7×7 pixels are indicated as the optimal sizes for post classification mode filters. Even when the resolution is already reduced to 16 m, mode filtering still enhances classification accuracies significantly. The single highest overall accuracy value of 58.2 % is achieved when using the 8 m resolution data in combination with 5×5

post-classification mode filtering, but the accuracies achieved with a 7×7 mode filter or 4 m resolution data and the same mode filters are very similar (no significant differences).

Table 16: IKONOS ms channels 1-4, eastern test area, 14 class classification, overall accuracy [%], (overall Kappa index of agreement in brackets).

Resolution	Post-classification mode filter			
	No filter	3×3	5×5	7×7
4 m	40.5 (0.342)	50.4 (0.447)	56.3 (0.512)	56.9 (0.520)
8 m	44.1 (0.379)	54.9 (0.495)	**58.2 (0.531)**	57.0 (0.516)
12 m	45.7 (0.397)	52.8 (0.471)	54.3 (0.488)	53.5 (0.479)
16 m	44.9 (0.386)	50.3 (0.442)	53.5 (0.478)	53.6 (0.479)

When the initial spatial resolution is already lowered to 8 m or less, 7×7 mode filtering suppresses a lot of spatial detail, producing maps which are not visually appealing. So even if the overall accuracy calculated from the reference sample is still high after 7×7 mode filtering the classification results of the block averaged data sets, the mode filter size in this case should be restricted to 3×3 or 5×5, which is enough to eliminate small misclassified areas. 7×7 mode filtering should only be applied to 4 m resolution data.

Although many of the single accuracy values in table 14 do not differ significantly from their neighbouring values (at the 95 % confidence level), the diagram in figure 27 points out the consistency in the accuracy values resulting from block averaging and mode filtering. There is a clear low point where the data are not spatially integrated at all and a clear peak at or close to 8 m resolution and a mode filter size between 5×5 and 7×7 (see also figure 31).

Optimal spatial resolution

The classification results show that, for the per-pixel multispectral classification of forest in this type of heterogeneous environment, the spatial resolution of 4 m is unnecessarily high. Assuming that no other kind of data integration takes place, the optimal resolution would be at least between 8 m and 12 m. This would be the spatial resolution to look for in data acquired for such a per-pixel multispectral classification. However, when one is already working with 4 m resolution data like IKONOS, one could argue that, as the classification accuracy using 8 m pixels is not significantly higher than for the 4 m pixels (especially if the results are mode filtered), the effort of pixel aggregation is not worthwhile and the original 4 m pixel size might be used as well, as long as the reduction of the file size through the reduction of the spatial resolution is not a desired effect.

As it was already indicated by the variograms and by the different rates of reduction of within-class variability with decreasing spatial resolution, the individual classes have different spatial characteristics, so that there are different 'optimal resolutions' for different classes. Figure 30 shows the products of class-specific user's and producer's accuracies for selected individual classes after classification and 5×5 mode filtering at different spatial resolutions. Among the examples, the class 'dense pine forest' seems to profit most from block averaging up to 16 m pixels, while 4 m seems to be the optimal resolution for *matorral* and broadleaved riparian forest. These class-specific accuracy values have to be interpreted with restraint, because the number of testing samples per class is only between 28 and 105 for these classes, leading to large and often overlapping confidence intervals. Even if different class-specific optimal resolutions were to be clearly established, it would not be practicable to conduct classifications with a separate resolution for each class, especially as the individual class areas are not known beforehand. For a general forest and land cover classification, a compromise spatial resolution has to be found, resulting in the best overall classification accuracy as described above.
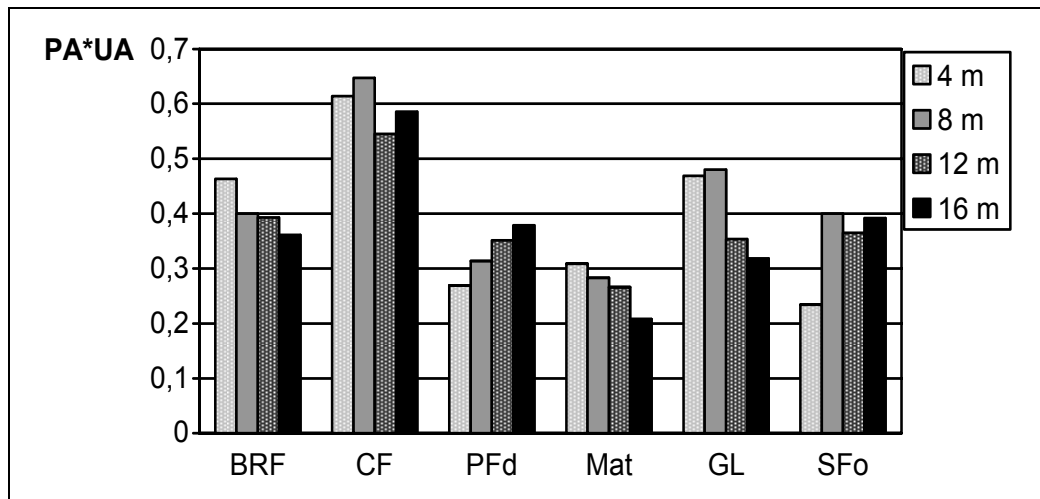
Figure 30: Product of user's accuracy (UA) and producer's accuracy (PA) for selected classes for IKONOS 4 channel 14 class classification (5×5 mode filtered).

Low pass filtering and post-classification mode filtering

Mean filtering enhances the classification results significantly and also significantly more than block averaging, where the best result without additional mode filtering was 45.8 % overall accuracy for 8 m resolution, compared to 57.3 % for the 5×5 mean filter (table 15). Post-classification mode filtering leads to additional significant accuracy improvements in combination with the 3×3 mean filter. When the results of mean and median filtering are compared, the median filtered images look better (less blurred), but the classification results are not as good. The overall accuracy is 45.8 % for the 3×3 median filter and 52.7 % after additional 3×3 post-classification

mode filtering, compared to values of 51.6 % and 56.6 % when a mean filter is used. Accordingly, only the mean filtered channels were used as a basis for further classifications.

Table 17: Overall accuracies [%] for 14 class classifications of low pass filtered Ikonos ms channels 1-4, eastern test area (Kappa index of agreement in brackets).

Pre-classification mean filter	Post-classification mode filter			
	No filter	3 × 3	5 × 5	7 × 7
No filter (4 m orig.)	40.5 (0.342)	50.4 (0.447)	56.3 (0.512)	56.9 (0.520)
3 × 3	51.6 (0.461)	56.6 (0.515)	59.0 (0.542)	**61.1 (0.563)**
5 × 5	57.3 (0.523)	57.8 (0.529)	59.0 (0.542)	59.2 (0.544)
7 × 7	55.7 (0.507)	57.1 (0.522)	56.4 (0.514)	56.1 (0.511)
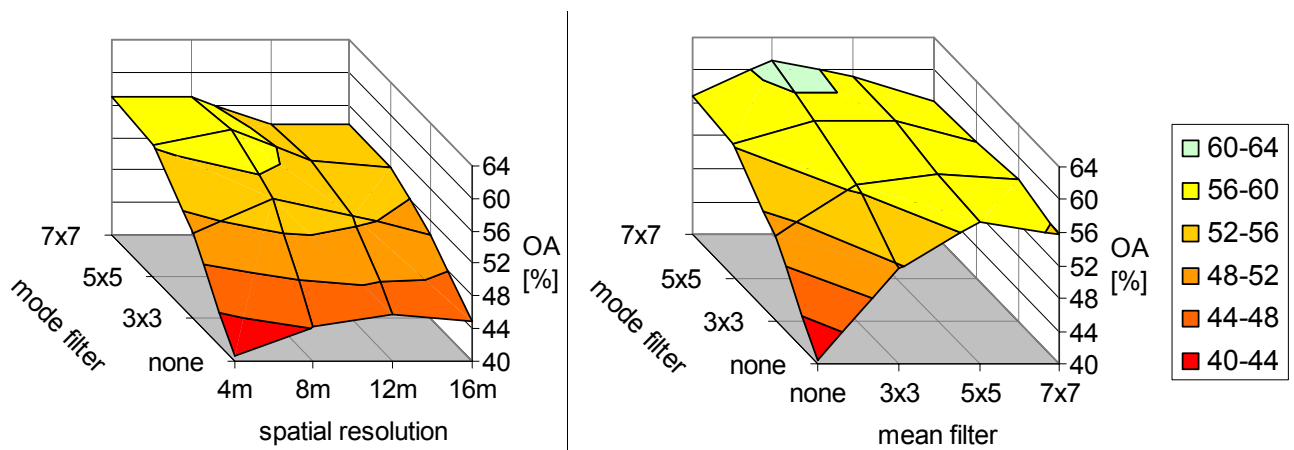
Figure 31: Diagrams of overall accuracies for 4 channel multispectral classification (14 classes) with different spatial resolutions, pre-classification mean filters and post-classification mode filters used.

The 7×7 mean filter integrates the spectral response of an area of 28 m × 28 m, about the size of a Landsat multispectral pixel, creating an increased number of pixels with 'mixed class signatures'. This leads to locally low classification accuracies, especially along class borders, and the erroneous appearance of 'intermediate classes' in these areas (e.g. '*matorral*' erroneously appearing in the map between riparian forest and pasture, or areas along the border between pine forest and riparian forest being classified as dense secondary forest). This effect is also visible, but less pronounced, in the classification of the 5×5 mean filtered image. Although the 7×7 mean filtering also leads to improved overall accuracies compared to the unfiltered image, there is an unnecessary amount of blurring and loss of information through averaging associated with this filter size. In contrast, particularly the 3×3 mean filtering in conjunction with post-classification mode filtering is a very

effective method to increase classification accuracies through the spatial integration of high resolution data. The maximum overall accuracy for 14 classes achieved with this method and the four multispectral IKONOS channels is 61.1 % (table 17, figure 31).

Segmentation

The results of the nearest neighbour classification of the segmented images are listed in table 18 for four different scale parameters. The classified segmented images were not mode filtered, because there are no isolated pixel values in an object-based classification. Segmentation followed by an object-based nearest neighbour classification does not lead to significantly higher overall accuracy values than simple block averaging without mode filter followed by MLC. This is probably due to the inferiority of the nearest neighbour classification technique.

The lower classification accuracy for the level 4 segmentation (scale parameter 30) indicates that too many of the large object primitives from this segmentation cover several target classes (mixed objects / undersegmentation). By contrast, the use of the scale parameter 12 results in an overseg-mented image with small homogeneous object primitives which do not integrate the elements of the heterogeneous forest classes. This is confirmed by the fact that after the classification of the level 1 (scale parameter 12) object primitives, the classification accuracy does increase when the result is mode filtered after all, indicating that the original spatial integration was not sufficient. Scale parameters 16 and 20 seem to be most appropriate for the creation of image object primitives for object-based classifications or simply for the production of meaningful boundaries within which the data can be spatially integrated (averaged).

Table 18: Overall accuracies [%] for four segmentation levels achieved with object-based nearest neighbour classifications, and in one case MLC.

Hierarchical segmentation level	OA for Object-based StNN	Per-pixel MLC
1 (scale parameter 12)	45.8	
2 (scale parameter 16)	45.4	
3 (scale parameter 20)	46.8	54.4
4 (scale parameter 30)	42.5	

The object primitives resulting from the level 3 segmentation (scale parameter 20) were exported into the PCI Geomatica environment with their mean values. This resulted in a 4 m resolution multispectral data set where the pixels belonging to one object primitive had identical values. In spite of the reduced number of training pixels with different values and the connected problems for the estimation of class statistics for a parametric classifier, class signatures were calculated from

this data (based on the training areas also used for the other per-pixel classifications), and a per-pixel maximum likelihood classification was conducted. The result was a map where every pixel of the same image object primitive had to be assigned to the same class. The overall classification accuracy of this map was 54.4 %, which is significantly higher than for the object-based nearest neighbour classification. This overall accuracy is also significantly higher than the accuracies achieved with block averaging without mode filtering, but not higher than the accuracies achieved with mean filtering or block averaging in combination with mode filtering.

Recapitulating, when using only the four multispectral IKONOS channels in the classification of the eastern test area, the best results were achieved with a combination of 3×3 low pass (mean) filtering of the multispectral channels before classification and a 7×7 post-classification mode filtering. The classification accuracy achieved with this method was 61.1 % for 14 classes (64.2 % for 13 classes, figure 32). The reduction of the spatial resolution through block averaging to 8 m (or even up to 12 or 16 m) leads to increased classification accuracies, but filtering operations were more successful in significantly increasing classification accuracies. Segmentation (figure 33) does not seem to be a competitive method for spatial integration in this context. An attempt could be made to improve the results of the object-based classification by fine-tuning the object-based classification algorithm, but this would need a lot of additional effort.

Trying to differentiate between 14 classes using just the four IKONOS multispectral channels does not result in very high accuracy values in any case, but spatial integration methods do lead to significantly increased overall accuracies compared to the initial value of 40.5 % for the case without spatial integration.

Obviously, there can also be too much spatial integration (e.g. a combination of 7×7 mean filtering and 7×7 post-classification mode filtering), leading to mixed pixel effects and a loss of spatial detail. The loss of spatial detail through mode filtering becomes apparent upon a visual inspection of the classification results (maps) before is leads to reduced accuracy measures as calculated from the reference points.

9.3 Effects of Integrating Texture Features

Through the GLCM texture calculations based on the 1 m panchromatic IKONOS image, some of the spatial information contained in the channel with the highest available resolution was integrated with the 4 m resolution multispectral IKONOS data sets, with the and 8 m and 12 m block averaged data sets and with the 15 m resolution Landsat data.
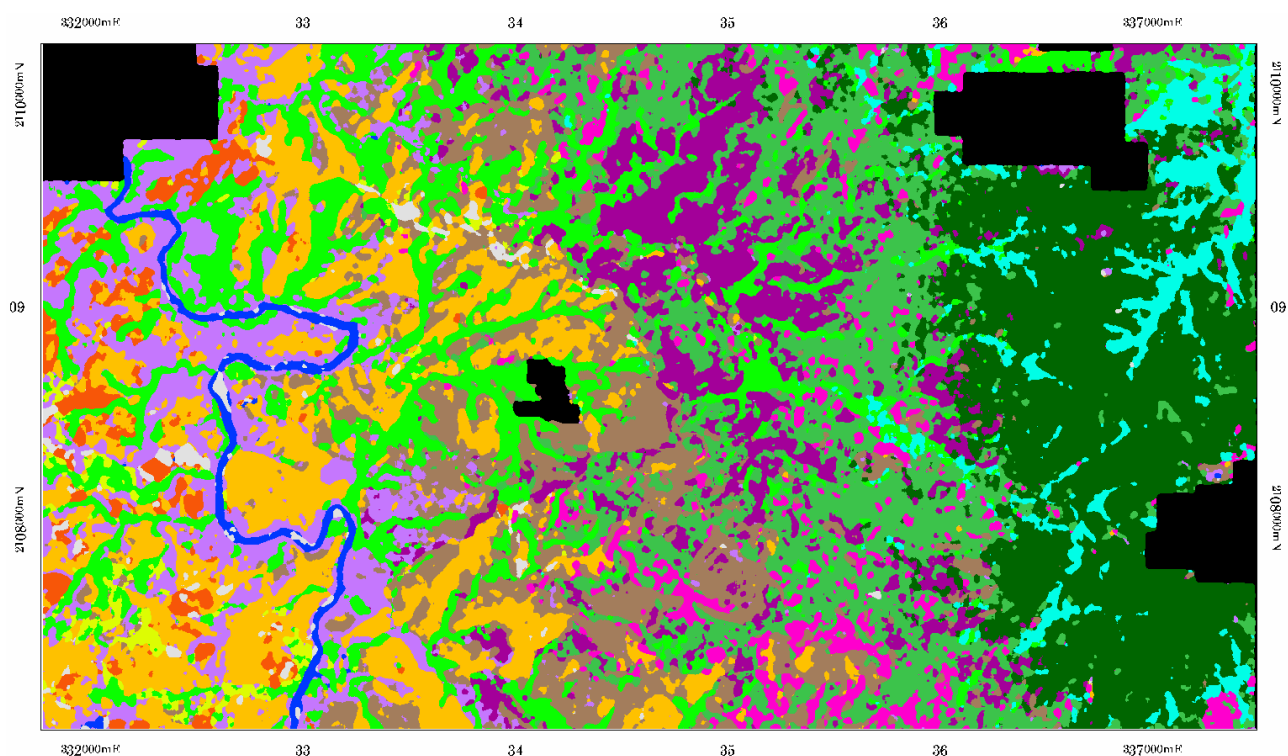
Figure 32: Classification of the 3×3 mean filtered multispectral data set, results are 7×7 mode filtered. For the legend see plate 44, appendix 2.
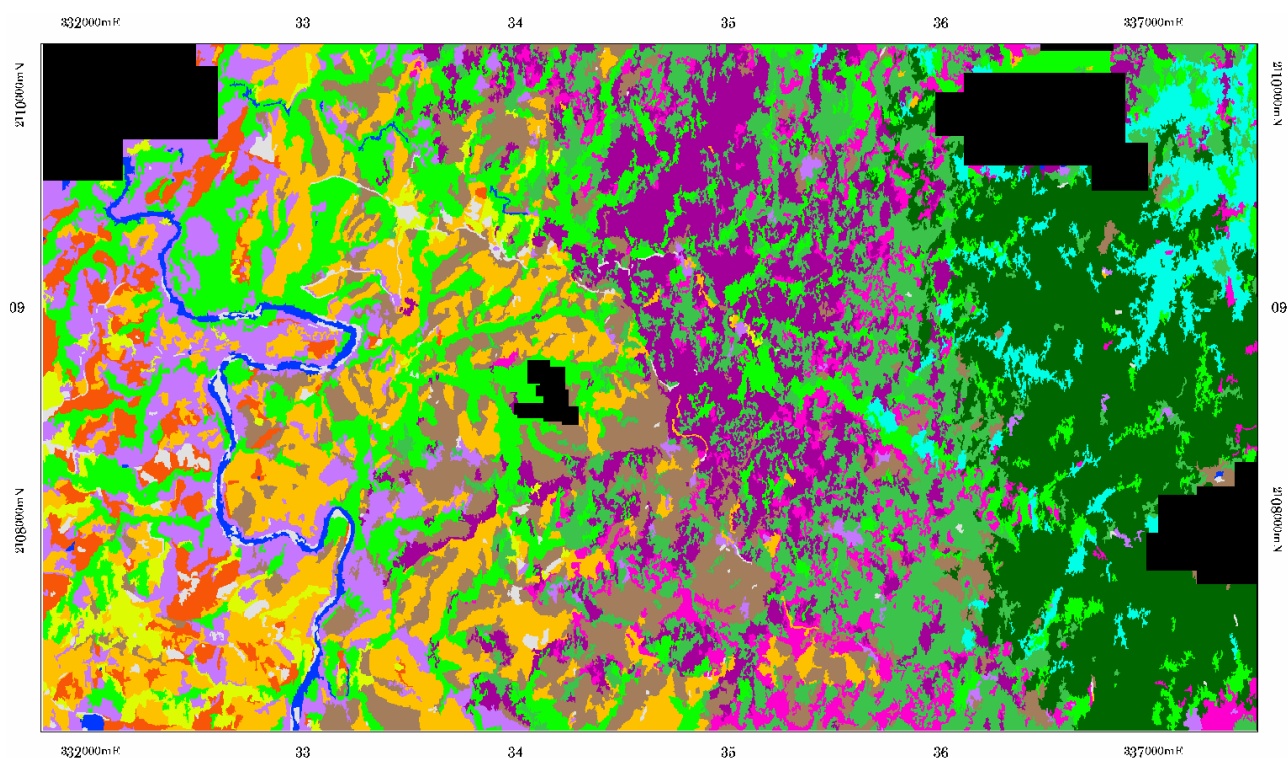
Figure 33: Maximum likelihood classification of segmented multispectral data (scale parameter 20). For the legend see plate 44, appendix 2.

9.3.1   Class Separability with and without Texture Channels

Signature separability according to the Bhattacharyya distance (BD) as calculated from equation 20 can take values between 0 and 2, with 0 representing no separability and 2 representing perfect separability. As indications for class separability, BD values below 1 are regarded as representing very poor separability, values between 1 and 1.5 represent poor separability, values between 1.5 and 1.9 moderate separability and values over 1.9 good separability.

The different class signature separabilites between all pairs of classes, based on the multispectral data with and without the inclusion of three texture channels, are described and discussed in the following with the 8 m resolution data sets as an example.

As can be seen in table 19, class separabilities according to the Bhattacharyya distance between the class signatures generated from the four multispectral channels at 8 m resolution were very poor in many cases. Only 26 of 91 class pairs are well separable (BD above 1.9) and 11 had BD values below 1 (very poor separability). Most of the separability values between the forest classes were below 1.5 (poor separability). With separability values below 0.5, the separation of open pine forest and *matorral*, of dense and open secondary forest, and of broadleaved riparian forest and agroforestry appears especially unpromising. This corresponds to the overall accuracy values below 60 % as presented in chapter 9.2.2 (44.1 % for the unfiltered 8 m data).

The inclusion of three GLCM texture channels in the generation of the class signatures increases all the separability values by an average of 0.2 and reduces the number of class pairs with Bhattacharyya distances below 1 (very poor separability) from 11 to 3 (table 20). There are no more values below 0.5. The largest increases in signature separability are registered for the class pairs *matorral* and open pine forest, grassland and open pine forest, as well as grassland and *matorral*. This demonstrates how spectrally similar classes (e.g. open pine forest where the spectral signature is dominated by the undergrowth and thus very similar to that of *matorral* or grassland) can become much better separable when texture parameters are included. Among the forest types, the texture parameters particularly increased the separability between dense pine forest and dense as well as open secondary forest, between broadleaved riparian and palm forest, between dense pine and broadleaved riparian forest and between dense and open pine forest.

The BD values between forest types are now mostly above 1.5, and they are all above 1 except for two cases: dense and open secondary forest, and broadleaved riparian and dense secondary forest.

Table 19: Signature separability (Bhattacharyya distance), using the four IKONOS multispectral bands at 8 m resolution. CF: cloud forest, PFd: dense pine forest, PFo: open pine forest, SFd: dense secondary forest, SFo: open secondary forest, PmF: palm dominated forest, BRF: broadleaved riparian forest, AF: agroforestry, Mat: *matorral*, Cal: *calimetal*, GL: grassland, Cr: Crops, BG: bare ground. Very poor separabilities are indicated in *italics*.

	CF	PFd	PFo	SFd	SFo	PmF	BRF	AF	Mat	Cal	GL	Cr	BG
PFd	1.441												
PFo	1.745	1.193											
SFd	1.400	*0.594*	1.115										
SFo	1.410	1.027	1.397	*0.493*									
PmF	1.602	1.907	1.913	1.494	1.638								
BRF	1.426	1.219	1.331	*0.569*	1.163	1.001							
AF	1.535	1.491	*0.985*	0.880	1.417	1.270	*0.462*						
Mat	1.610	1.333	*0.494*	0.962	1.162	1.812	1.377	1.033					
Cal	1.887	1.894	1.778	1.502	*0.884*	1.798	1.721	1.757	1.601				
GL	1.943	1.839	*0.866*	1.602	1.619	1.955	1.750	1.511	*0.604*	1.732			
Cr	1.998	1.993	1.422	1.962	1.974	1.993	1.882	1.574	1.529	1.980	1.012		
BG	1.996	1.997	1.810	1.992	1.996	1.998	1.994	1.956	1.885	1.998	1.572	1.619	
W	1.998	1.986	1.777	1.981	1.991	1.998	1.973	1.914	1.882	1.997	1.823	1.810	1.506

Table 20: Signature separability (Bhattacharyya distance), using the four IKONOS multispectral bands at 8 m resolution and GLCM *standard deviation*, *contrast* and *entropy*. Very poor separabilities are indicated in *italics*, Bhattacharrya distances increased by more than 0.4 compared to the distances without texture features are printed **bold**.

	CF	PFd	PFo	SFd	SFo	PmF	BRF	AF	Mat	Cal	GL	Cr	BG
PFd	1.488												
PFo	1.856	1.561											
SFd	1.632	**1.227**	1.451										
SFo	1.706	**1.593**	1.521	*0.640*									
PmF	1.920	1.986	1.976	1.721	1.808								
BRF	1.677	1.607	1.581	*0.805*	1.327	**1.473**							
AF	1.728	1.696	1.340	1.099	1.522	**1.693**	*0.710*						
Mat	1.818	1.708	**1.365**	**1.409**	**1.624**	1.935	1.611	1.329					
Cal	1.950	1.953	1.829	1.761	**1.427**	1.952	1.849	1.842	1.785				
GL	1.987	1.951	**1.723**	1.962	1.972	1.999	1.943	1.878	**1.276**	1.901			
Cr	2.000	2.000	**1.953**	2.000	2.000	2.000	1.998	**1.988**	1.882	1.996	1.322		
BG	1.999	1.999	1.899	1.997	1.998	2.000	1.997	1.975	1.951	1.999	1.822	1.894	
W	2.000	1.998	1.894	1.996	1.998	1.998	1.990	1.969	1.973	1.999	1.972	1.986	1.817

The class signatures of open and dense secondary forest, which represent closely related informational classes and which exhibit the lowest separability (0.64) of all class pairs in the spectral-textural separability matrix, were merged. The separability matrix for the revised classification scheme of 13 classes is shown in table 21.

Agroforestry and broadleaved riparian forest still have very poor separability, too, but to merge them would result in a mixed informational class. The separability between broadleaved riparian and secondary forest is also critical, but it was decided not to merge these signatures in order not to prematurely preclude the precision of the classification. There is still the option to merge these classes after classification – if the primary aim is to improve the overall accuracy (reliability) of the map. The signature separability of 65 of the 78 class pairs in the 13 class classification scheme is moderate or good (above 1.5). Among the forest classes, the forest types that are most separable from the other types are palm dominated forest and cloud forest. The only class with a BD below 1.5 to palm dominated forest is broadleaved riparian forest and the only class with a BD below 1.5 to cloud forest is dense pine forest.

Table 21: Signature separability (Bhattacharyya distance), using the four IKONOS multispectral bands at 8 m resolution and GLCM *standard deviation*, *contrast* and *entropy* for 13 classes (after merging the class signatures of Sfo and SFd). Very poor separabilities are indicated in *italics*.

	CF	PFd	PFo	SF	PmF	BRF	AF	Mat	Cal	GL	Cr	BG
PFd	1.488											
PFo	1.856	1.561										
SF	1.660	1.403	1.433									
PmF	1.920	1.986	1.976	1.753								
BRF	1.677	1.607	1.581	*0.996*	1.473							
AF	1.728	1.696	1.340	1.233	1.693	*0.710*						
Mat	1.818	1.708	1.365	1.457	1.935	1.611	1.329					
Cal	1.950	1.953	1.829	1.542	1.952	1.849	1.842	1.785				
GL	1.987	1.951	1.723	1.959	1.999	1.943	1.878	1.276	1.901			
Cr	2.000	2.000	1.953	1.999	2.000	1.998	1.988	1.882	1.996	1.322		
BG	1.999	1.999	1.899	1.997	2.000	1.997	1.975	1.951	1.999	1.822	1.894	
W	2.000	1.998	1.894	1.996	1.998	1.990	1.969	1.973	1.999	1.972	1.986	1.817

The increased signature separabilities after the inclusion of texture indicate that texture features can be expected to help improve classification results. However, it has to be kept in mind that the signature separabilites are only calculated for the training samples, which represent typical areas of their respective classes and mostly not areas close to class boundaries in the image. Additional edge effects introduced through the texture features which were calculated in 15 m × 15 m windows will

thus not affect the signature separability but might adversely affect the overall classification accuracy.

9.3.2 Classification Accuracy with Spectral and Textural Features

Classification with texture features only

Using the five GLCM texture features *Entropy*, *Standard Deviation*, *Contrast, Mean* and *Correlation* as the only input channels for a maximum likelihood classification at 8 m spatial resolution resulted in classification accuracies between 35 % without mode filtering and 43 % with 5×5 or 7×7 mode filtering. The texture classification fails to separate cloud forest from dense pine forest, assigning pixels of both classes to the dense pine forest class (figure 34). It also fails to identify broadleaved riparian forest, which is classified as either palm dominated or secondary forest. Agroforestry does not appear in the map either. Shade dominated pixels in the forest areas are classified as water. By contrast, the classification accuracies for grassland and open pine forest are good, as is the producer's accuracy for dense pine forest.
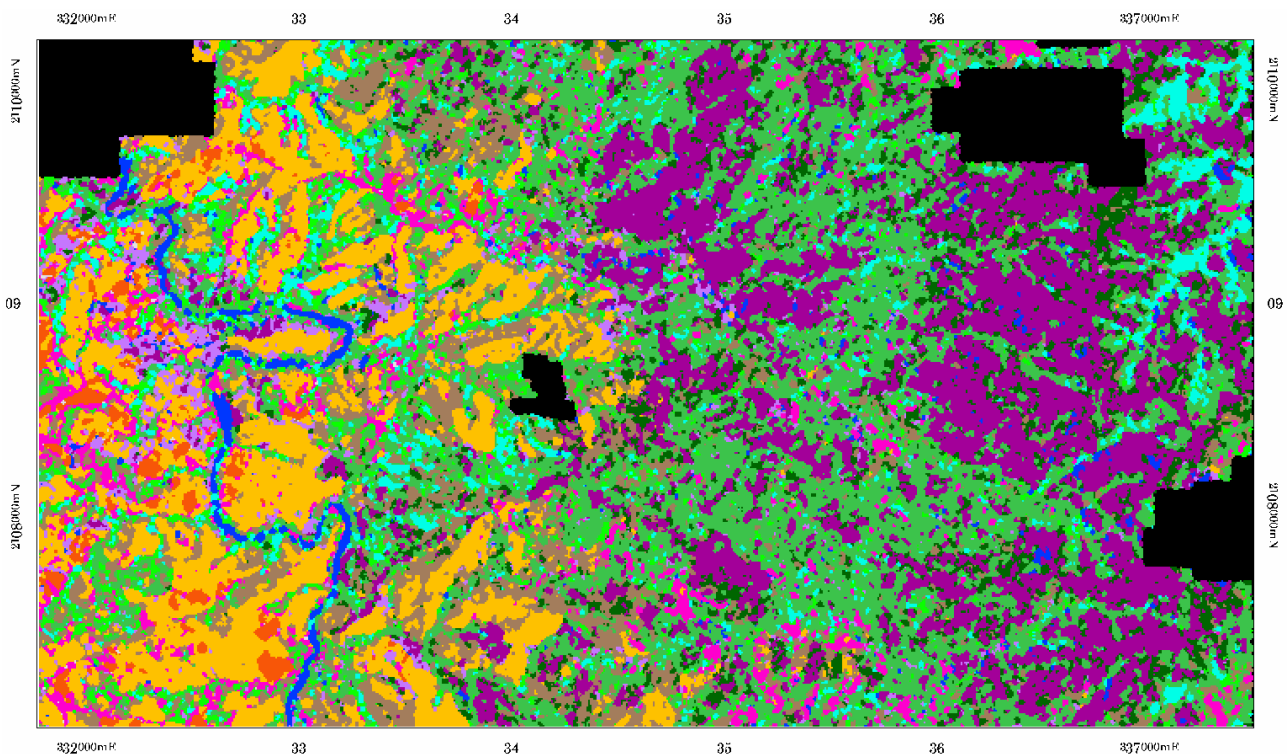
Figure 34: Classification based on texture data only (data set 22), results are 3×3 mode filtered. For the legend see plate 44, appendix 2.

There is obviously some information lacking in the texture data (which is all derived from the IKONOS panchromatic channel), preventing the identification of all 13 land cover classes. Better results can be achieved using only the multispectral IKONOS data. However, both data sets have

their strengths and weaknesses; many classes are better identified with the multispectral data, but for some other classes, the texture data provides important discriminant information.

Comparison of classification results achieved with the spectral and the spectral-textural data sets

In the following, the classification results are compared for two feature combinations: the first consists of the four multispectral IKONOS channels, the second is a combination of the same four spectral channels plus the three GLCM texture features *Entropy*, *Standard Deviation* and *Contrast.* This spectral-textural feature combination is the optimal seven channel subset of the four multispectral and five texture channels according to the average transformed divergence (see chapter 8.7). Both feature combinations exist with several versions of spatial integration of the multispectral data (see table 14 and chapters 8.4 and 9.2). All data sets (including the segmented data) were classified using MLC.

Table 22 shows the classification accuracies (overall accuracy and Kappa) for the case without any post-classification processing (mode filtering). The addition of three texture channels to the different spatially integrated data sets and to the unchanged 4 m data set leads to improved classification accuracies in all cases. The largest improvement can be seen for the unchanged 4 m multispectral data set. The addition of texture features which were calculated in 15 m × 15 m windows contributes some spatial information from the neighbourhood of the 4 m by 4 m pixels to this data set. The margin of improvement becomes smaller when the texture channels are added to the spatially integrated data. The overall accuracy for the 5×5 mean filtered data, which is already 62.8 % without texture data, is increased by only 2.2 % through the inclusion of texture channels, which is not a significant margin at the 95 % confidence level. But the overall accuracy achieved with the combination of mean filtered multispectral data with texture channels is significantly higher than the OA achieved when texture is combined with the unchanged 4 m multispectral data. Comparing the classification results for the spectral-textural data sets without post-classification processing, the best results are achieved with the 5×5 mean filtered data set (OA = 65 %), followed by the 3×3 mean filtered data and the segmented data (scale parameter 16 or 20).

Table 22: Comparison of overall accuracy [%] and Kappa index of agreement (in brackets) for the IKONOS multispectral data with and without the inclusion of texture features in the classification (13 classes).

Feature Combination	Pre-Classification Spatial Integration of Multispectral Data						
	4 m unchanged	8 m block averaged	12 m block averaged	3×3 mean filtered	5×5 mean filtered	Segm. scale p. 16	Segm. scale p. 20
IKONOS ms channels 1-4	41.0 (0.342)	45.6 (0.387)	48.0 (0.410)	55.6 (0.496)	62.8 (0.574)	54.7 (0.487)	56.6 (0.509)
IKONOS ms ch. 1-4, GLCM texture *ENT, SD, CONT*	52.3 (0.456)	53.7 (0.471)	52.6 (0.449)	61.2 (0.555)	65.0 (0.598)	59.3 (0.533)	58.7 (0.526)

This advantage of the data sets with pre-classification spatial integration is cancelled if the classification results are additionally mode filtered (table 23). (The segmented data sets could not be included in this comparison because it does not make sense to apply per-pixel mode filtering to per-segment classification results.) Post-classification mode filtering improves the results for all spectral-textural data sets, but does so least for the data sets with most pre-classification spatial integration. The results for the 4 m spectral-textural data set with unchanged multispectral channels are improved most. After 5×5 or 7×7 mode filtering, none of the results of the spatially integrated spectral-textural data sets are significantly better than the results of the 4 m spectral-textural data set with unchanged multispectral channels. The textural channels contribute spatial information about an area larger than the pixels to all data sets, as the texture was calculated in 15 m × 15 m windows. For the unchanged 4 m multispectral data, the integration of the texture channels in the data set, in combination with post-classification mode filtering, provides a certain degree of spatial integration. This makes this data set competitive with the data sets including multispectral data with pre-classification spatial integration. Figure 35 shows the 7×7 mode filtered classification result for the spectral-textural data set 18, for which an overall accuracy of 70.4 % was estimated.
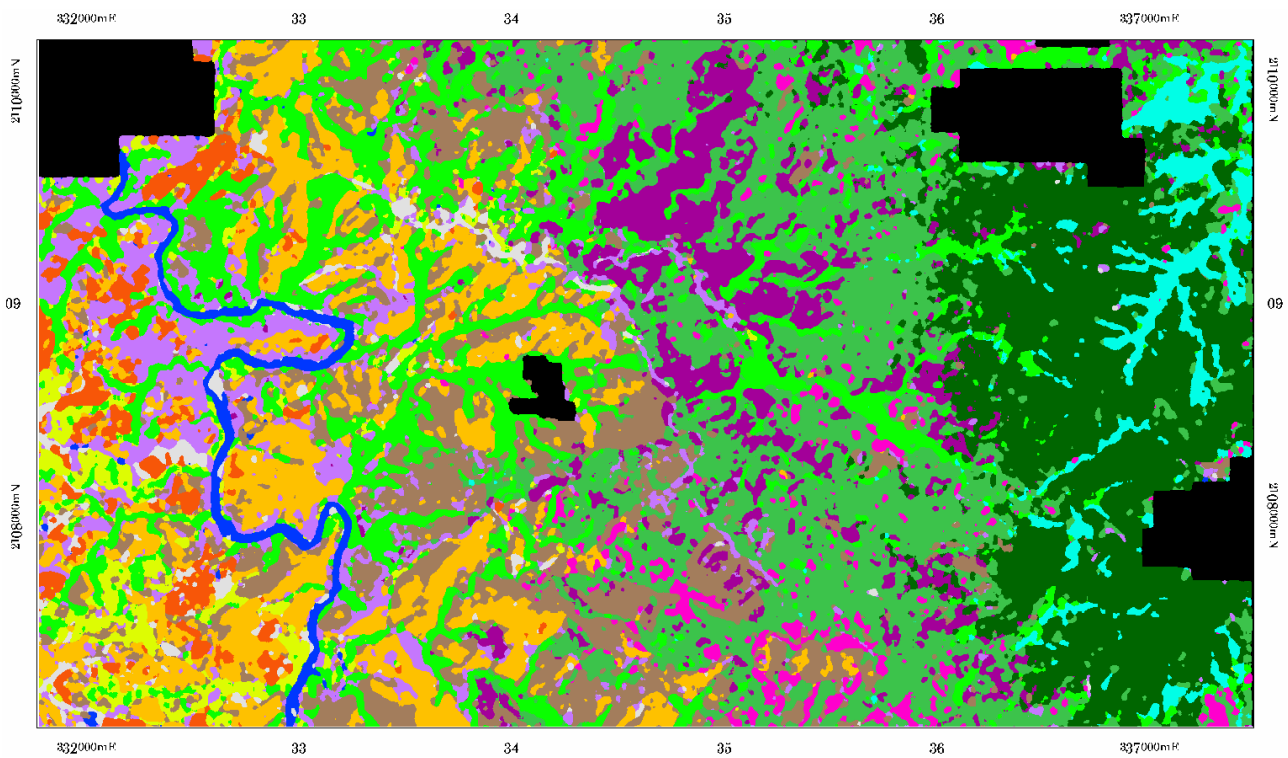
Figure 35: Classification of the spectral-textural data set 18 (3x3 mean filtered multispectral data and three texture channels), results are 7×7 mode filtered. For the legend see plate 44, appendix 2.

The accuracies after 5×5 mode filtering of the classification results are not significantly lower than after 7×7 mode filtering (table 23). If one is aiming to maintain a high degree of spatial detail in the map, the smaller (5×5) mode filter should be used rather than the 7×7 mode filter, especially in the case of block averaged data with pixel sizes of 8 m × 8 m or larger.

Table 23: Comparison of overall accuracy [%] and Kappa index of agreement (in brackets) for the IKONOS multispectral data with and without the inclusion of texture features in the classification and with post-classification mode-filtering (13 classes).

Channel Combination	Post-class. mode filter	Pre-classification Spatial Integration of Multispectral Data				
		4 m unchanged	8 m block averaged	12 m block averaged	3×3 mean filtered	5×5 mean filtered
IKONOS ms channels 1-4	5×5	55.6 (0.502)	61.7 (0.561)	58.6 (0.527)	63.1 (0.579)	64.2 (0.589)
	7×7	56.1 (0.510)	61.0 (0.554)	58.5 (0.524)	64.2 (0.590)	64.0 (0.588)
IKONOS ms ch. 1-4, GLCM texture *ENT*, *SD*, *CONT*	5×5	67.8 (0.628)	66.0 (0.607)	64.0 (0.582)	69.3 (0.646)	67.9 (0.631)
	7×7	70.0 (0.653)	67.4 (0.622)	65.3 (0.597)	70.4 (0.659)	68.3 (0.634)

The maximum overall classification accuracy which was achieved with the segmented data, using the spectral-textural feature combination and MLC, was 59.3 %. This accuracy is significantly exceeded by the classification accuracies achieved with the spectral-textural data sets with different types of spatial integration, including mode filtering (tables 20 and 21) (see also Gleitsmann & Kappas 2005). Because of this, segmentation was not further pursued as a method for the spatial integration of the high resolution multispectral data, although it might be possible to achieve better results with segmented data if the object-oriented classification method could be improved (see chapter 8.8.4).

Class-specific results

Figure 36 gives an overview over class-specific classification accuracies for spectral and spectral-textural data sets. Only classes with at least 20 reference points per class were included in this presentation. Among them, only the classes secondary forest, broadleaved riparian forest, cloud forest, *matorral* and grassland have more than the 50 samples per class recommended by Congalton (1991) for class-specific interpretations of the error matrix. So the class-specific results described here can only give indications of general trends in the results, and small differences between accuracy measures should not be over-interpreted.

In the case of the forest classes, the classification accuracy is always higher for the data sets with texture than for the purely multispectral data sets. The increase in accuracy through texture is most pronounced for the classes palm forest and secondary forest and (although on a lower overall level) open pine forest. Among the non-forest classes, *matorral* profits most from the inclusion of texture. *Calimetal* is the only class in figure 36 for which the accuracy is consistently lower with texture than without.
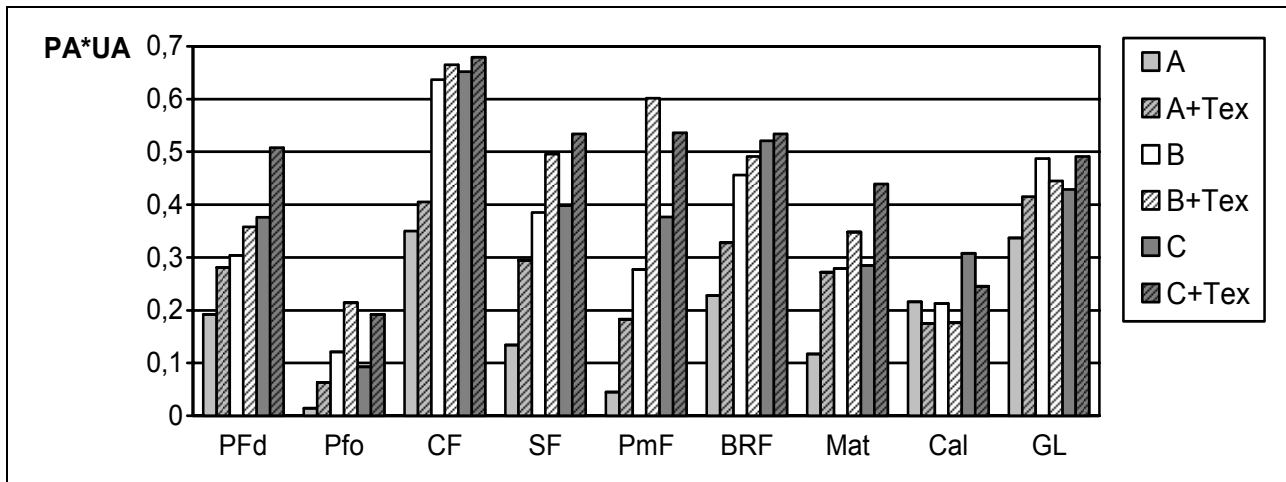
Figure 36: Class-specific accuracy measure (product of user's accuracy and producer's accuracy) for three spatial resolution/integration cases (A: 4 m without spatial integration, B: 8 m block averaged and post-classification 5×5 mode filtered, C. 4 m 3×3 mean filtered and post-classification 5×5 mode filtered) with and without the inclusion of texture features in the classification.

These class specific results concur with what could be expected after a visual analysis of the imagery. The inclusion of texture features in the classification improves the accuracy for classes which are similar to others in colour (spectral signature) while differing in their textural characteristics. An example is the palm dominated forest, where the mean digital numbers in the four multispectral bands are similar to those of broadleaved riparian forest, but which has a different canopy structure, dominated by just one tree species with small, finely structured crowns, while the canopy of the broadleaved riparian consists of crowns of variable sizes and tree species. This is visible at the resolution of the panchromatic IKONOS image. *Matorral* and open pine forest are other obvious examples where the increased class separability through texture features was already predicted by the Bhattacharyya distance (chapter 9.2.1). The class *calimetal*, by contrast, has a very distinct colour (spectral signature). This makes it spectrally clearly distinguishable from other land cover types except for (open) secondary forest and *matorral*. These two classes can contain a proportion of the fern *Dicranopteris pectinata*, with the possibility of gradual transitions to pure *calimetal* areas. In this case, apparently the inclusion of texture features does not help to reduce the ambiguity or boundary vagueness either.

The class-specific accuracy for cloud forest is not increased much through the inclusion of texture features, but it is increased a lot through spatial integration (figure 34). Cloud forest has the highest class-specific accuracy values among all the forest classes, especially when spatially integrated data sets are used.

Resumé of chapters 9.2 and 9.3 – results of including spatial information in the classification through texture channels and spatial integration of high resolution data

On the whole, it can be said that a pure conventional per-pixel classification of the 4 m multispectral IKONOS data is not a suitable approach for forest type and land cover mapping with this kind of high resolution data. The tested approaches for the integration of spatial information – through different kinds of spatial integration of the multispectral data, through the inclusion of texture channels in the classification or through the spatial integration of the classification results (mode filtering) – all lead to significantly improved classification results. The best results were achieved when several methods for the inclusion of spatial information were combined – e.g. a classification including texture data followed by mode filtering of the results. This leads to overall accuracies of around 70 % (Kappa ~0.653) when mapping 13 land cover classes in the heterogeneous and mostly forested eastern test area. Overall accuracies of over 65 % were only achieved for mode-filtered classification results of data sets containing texture data.

9.4 Combining Landsat ETM+ and IKONOS Data

Having explored the possibilities to extract information from IKONOS data alone, additional available data sets were integrated with the IKONOS data to test whether these data can contribute any additional useful information for mapping the land cover categories of interest.

Landsat ETM+ data has a lower spatial resolution but a higher spectral resolution than IKONOS data. While the first four Landsat multispectral channels have almost exactly the same spectral range as the four IKONOS multispectral channels in the visible and near infrared part of the electromagnetic spectrum, Landsat data contains three further multispectral channels. These contain information about the spectral response of objects in the mid infrared (channels 5 and 7) and thermal infrared (channel 6) and thus provide additional features for the discrimination of land cover classes which are lacking in the high resolution satellite data (Goetz et al. 2003). In the following, multispectral Landsat data is combined with high resolution IKONOS data.

Landsat data alone for comparison

The Landsat classification discussed here is not a subset of the map for the whole UCRYN but a classification conducted only for the eastern test area using the same 13 classes and the same training areas which were also used with the IKONOS data.

The seven channel classification (using Landsat multispectral channels 1-6 and the panchromatic channel, all resampled to 15 m resolution) resulted in an overall accuracy of 37.6 %, which could be increased to 46 % through 5×5 mode filtering. The Landsat classification accuracy is similar to the

accuracy achieved only with the multispectral IKONOS data without texture or spatial integration (41 %). The latter can, however, be increased to 56 % through mode filtering, which is significantly more than the accuracy achieved for the mode-filtered Landsat classification. The classification accuracy for the Landsat data is constricted by the low spatial resolution of these data, (which is originally only 30 m for most of the Landsat channels) in combination with the high spatial heterogeneity of the study area. Most core class areas are rendered correctly (figure 37) but the overall classification accuracy is still below 50 %. By contrast, the spatial resolution of the IKONOS multispectral data is certainly sufficient or even unnecessarily high (see chapter 9.2), but the class separability with these data may suffer from a lack of spectral resolution.
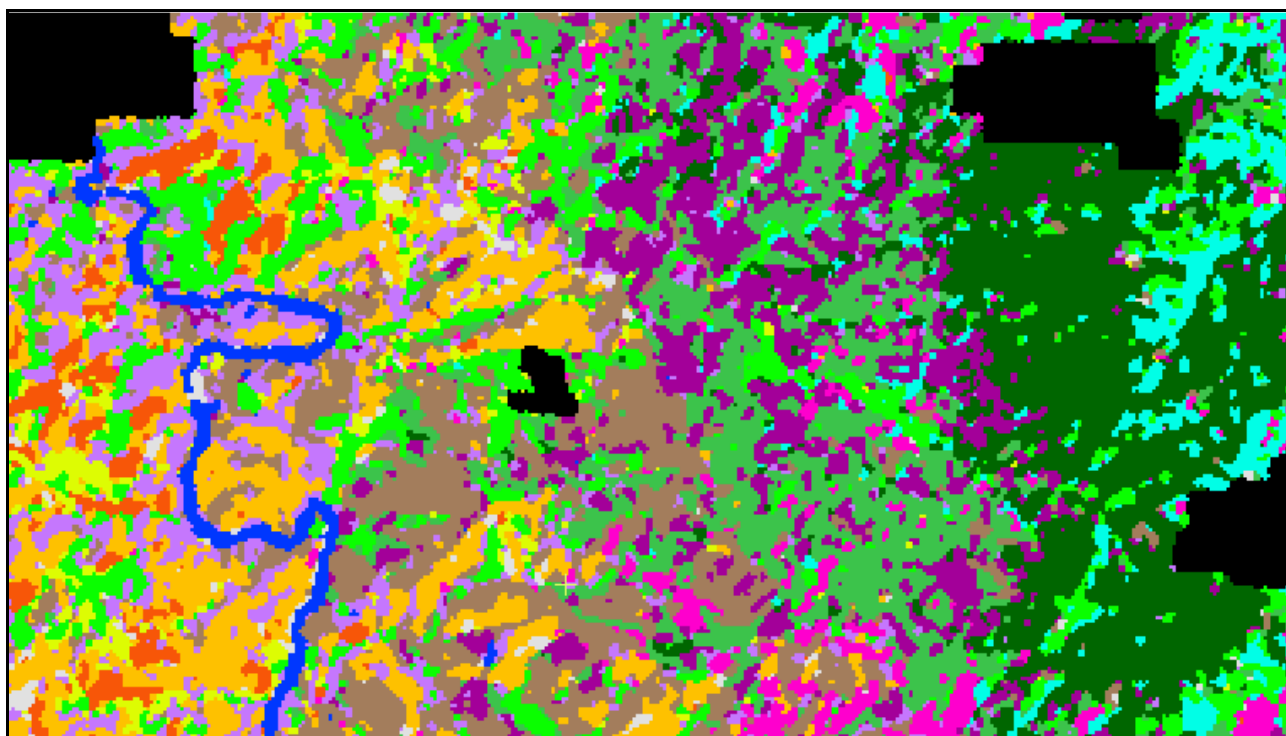
Figure 37: Landsat ETM+ classification of the eastern test area, 3×3 mode filtered. For the legend see plate 44, appendix 2.

IKONOS and Landsat multispectral channel combination

In order to add spectral information from beyond the near infrared to the IKONOS data, two or three Landsat multispectral channels (without or with the thermal infrared) were added to the multispectral data at 8 m resolution. The resulting accuracy measures in table 24 show that there is no significant difference between the classification accuracies achieved with the four IKONOS multispectral channels only and with the 6 or 7 combined multispectral channels. The advantage of the additional spectral information is probably cancelled by the low spatial resolution of the additional Landsat channels, introducing more mixed pixel effects in the classification.

Table 24: Classification accuracy (13 classes) for multispectral data sets at 8 m resolution consisting of IKONOS data or IKONOS data combined with Landsat data.

Data Set	Post-classification mode filter			
	No filter	3×3	5×5	7×7
IKONOS ms channels 1-4	45.6 (0.387)	55.9 (0.499)	61.7 (0.561)	61.0 (0.554)
IKONOS ms channels 1-4, Landsat ms channels 5 & 7	46.5 (0.395)	54.9 (0.488)	59.5 (0.537)	59.8 (0.540)
IKONOS ms channels 1-4, Landsat ms channels 5-7	45.8 (0.385)	55.0 (0.486)	58.2 (0.522)	58.9 (0.529)

Combining Landsat multispectral data and IKONOS texture data

The Landsat channels 2, 4, 6 and 7 and the IKONOS-derived GLCM texture features *Entropy*, *Standard Deviation* and *Contrast* were combined for a classification. This is the optimal seven channel combination out of all Landsat bands and five texture features according to the average transformed divergence. The overall classification accuracy for this data set was 41 % when the results were not mode filtered. The maximum classification accuracy achieved with mode filtering was 56 % (5×5 mode filter). These are significantly higher values than those achieved with Landsat data alone, but they do not come close to the overall accuracies of around 70 % achieved with the combination of IKONOS spectral and textural data (see also Brötje 2003).

On the whole, Landsat data do not seem to provide useful additional information for the combination with IKONOS data for a detailed classification of the test area. The advantage of their higher spectral resolution is outweighed by the disadvantage of their lower spatial resolution, which is insufficient for a detailed classification of the eastern test area.

9.5 Use of Non-Parametric Classification Methods and Integration of Ancillary Data

The IKONOS data used for the combination with ancillary (DEM-derived) data and for the comparison of MLC and non-parametric classification methods were the 8 m resolution data (block-averaged multispectral data set 2 and spectral-textural data set 14).

9.5.1 Using Non-Parametric Classifiers to Classify Spectral-Textural Data Sets

The maximum likelihood classification method is based on the assumption of normal distribution of the class data. As could be seen in table 15, this assumption is valid for the multispectral and textural channels in most of the cases, so MLC should be a good classifier for multispectral or

spectral-textural classifications of the eastern test area and was exclusively used for most of these classifications. Only the spectral-textural data set 14 was also classified using the non-parametric classifiers k-NN and ANN to verify whether MLC really is the superior classifier for such data sets. The results of the k-NN and ANN classifications of data set 14 are also intended as a basis of comparison for the cases where these non-parametric classifiers are used to classify data sets including DEM-derived data.

For the classification of data set 14, MLC does result in higher overall accuracies than the non-parametric ANN and k-NN classifications (table 25), but the overall accuracies of the mode-filtered k-NN and ANN results are only insignificantly lower than that of the MLC result at the 95 % confidence interval. With its easy implementation, the k-NN classifier (using the parameters described in chapter 8.8.2) could be regarded as a viable alternative to MLC.

The comparison shows that of the three tested classifiers, none is more suitable than MLC for the classification of a data set consisting of multispectral and texture channels.

Table 25: Overall accuracy [%] and Kappa index of agreement (in brackets) for classifications of data set 14 with different classifiers (13 classes).

	MLC	k-NN	ANN
Unfiltered result	53.7 (0.471)	48.9 (0.411)	49.2 (0.428)
Result 3 x 3 mode filtered	63.0 (0.572)	60.4 (0.542)	59.3 (0.539)
Result 5 x 5 mode filtered	66.0 (0.607)	65.8 (0.602)	63.7 (0.588)

9.5.2 Integration of Ancillary (DEM-Derived) Data as Additional Channels in MLC

In spite of the fact that of the topographic variables, only the slope data show a normal distribution for most of the classes (table 15), some data sets containing DEM-derived data were classified using MLC. This serves as a basis for comparison with the non-parametric classifiers. Elevation, slope and incidence from 60° azimuth and 20° elevation ('incidence60') had been integrated as additional channels with the 8 m resolution spectral and texture data. The three DEM-derived data channels were combined with the four multispectral channels for a spectral-topographic data set. This improved the classification result compared to the data set consisting only of multispectral data, but after mode filtering, the overall accuracies were not significantly different from each other with or without the DEM-derived data (table 24). The main positive effect of the addition of three topographic channels to the multispectral data is that the unfiltered classification result is less 'noisy' than that of the classification based only on the multispectral channels (figure 38). However, this effect is also achieved by post-classification mode filtering.

When the classification is based on the data set including the three DEM-derived data channels (and no texture channels), areas along the western margin of the cloud forest are misclassified as open pine forest (figure 38). These areas are in reality mostly dense pine plantations with some cloud forest regeneration. The misclassification can be explained by the fact that dense pine forest is a relatively homogeneous class, and has an accordingly narrow probability density function G_i (as calculated for MLC, see chapter 8.8.1). This means that there is only a small part of the feature space in which the probability of membership to the dense pine forest class is high. Open pine forest, on the other hand, is a high variance class in the multispectral as well as in the DEM-derived data channels. This means that it has a very wide probability density function with a lower peak. In other words, there are large parts of the feature space for which the calculation of the probability of membership to this class results in moderate values. In the misclassified area, the probability density function calculated from the dense pine forest training sample is unrealistically low because the training sample is not fully representative of all topographic positions of the dense pine forest (the training areas are located mostly in areas of lower elevations). In these marginal areas of dense pine forest, its probability density function is then no longer higher than that of the open pine forest (figure 39). In the absence of other classes for which the probability density function is high in this part of the feature space, the pixels are thus assigned to the pine forest class.
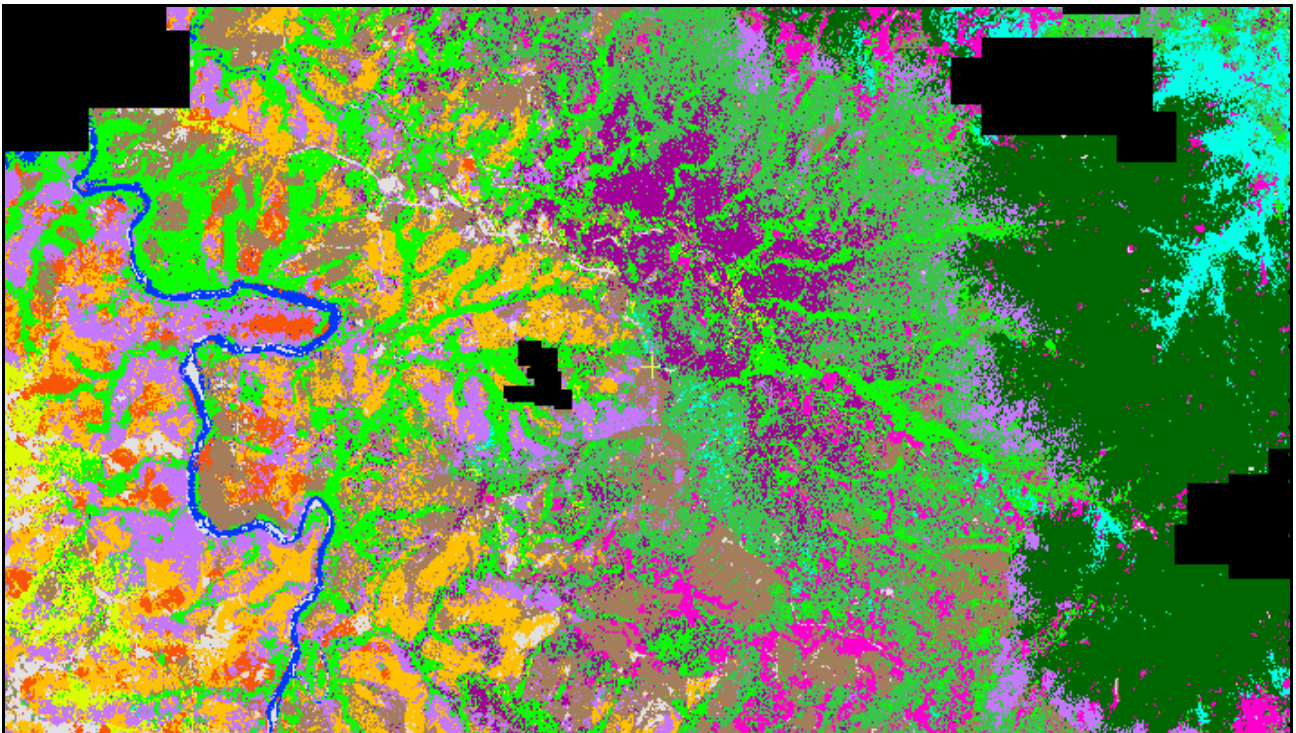
Figure 38: MLC result for the spectral-topographic data set 27, 8 m resolution, no mode filter. For the legend see plate 44, appendix 2.
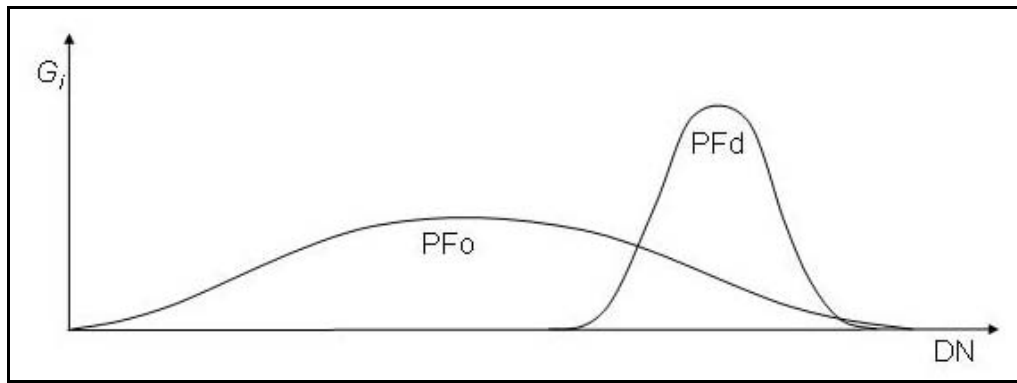
Figure 39: Sketch of probability density functions of two classes, shown for a one-dimensional feature space.

The maximum likelihood classification of the seven channel spectral-topographic data set resulted in lower overall accuracies than that of the seven channel spectral-textural data set. The difference increased with post-classification mode filtering, and the overall accuracy of data set 14 after 5×5 mode filtering is significantly higher than that of data set 27 after the same post-processing (table 26).

Table 26: Results of maximum likelihood classifications for 8 m resolution data sets with different combinations of spectral, textural and topographic channels.

Data Set	Post-classification mode filter		
	No filter	3×3	5×5
No. 2 (IKONOS ms channels 1-4)	45.6 (0.387)	55.9 (0.499)	61.7 (0.561)
No. 27 (IKONOS ms channels 1-4, DEM-based elevation, slope and incidence60)	51.5 (0.447)	57.1 (0.507)	58.4 (0.522)
No. 14 (IKONOS ms channels 1-4, GLCM texture *ENT*, *SD*, *CONT*)	53.7 (0.471)	63.0 (0.572)	66.0 (0.607)
No. 28 (IKONOS ms channels 1,2,4, GLCM texture *ENT*, *SD*, *CONT*, elevation)	55.6 (0.492)	64.8 (0.594)	67.2 (0.622)
No. 29 (IKONOS ms channels 1,2,4, GLCM texture *ENT*, *SD*, *CONT*, slope)	51.8 (0.448)	59.0 (0.528)	61.0 (0.550)
No. 30 (IKONOS ms channels 1,2,4, GLCM texture *ENT*, *SD*, *CONT*, incidence60)	54.2 (0.474)	62.3 (0.564)	65.2 (0.597)

Spectral, textural *and* DEM-derived data were also combined in stacked vectors as input for MLC. In order to keep the number of input channels at seven for the maximum likelihood classification, the multispectral channel 3 (which is highly correlated with channels 1 and 2) was left out of the data set and replaced by one of the DEM-derived data channels (table 24).

The inclusion of elevation in the maximum likelihood classification improved the overall accuracy somewhat (though not significantly at the 95 % confidence interval) compared to the spectral-textural data set 14. It leads to a more homogeneous classification of the classes which occur only in the higher areas (cloud forest and palm dominated forest) but also produces some unwanted results, like the misclassification of some of the broadleaved riparian forest at high elevations as palm dominated forest.

The overall accuracy for the data set containing 'incidence60' is very similar to that of the spectral-textural data set. The inclusion of the 'incidence60' parameter has the main effect that the broadleaved riparian forest on leeward slopes is less likely to be misclassified as palm dominated forest, leading to an improved user's accuracy for palm dominated forest. The incidence is only a very rough approximation of exposure to the east-north-easterly winds, however, and does not take account of rain shadow effects. Consequently, some small areas of broadleaved forest on slopes facing east, but situated in the rain shadow of the main mountain range (Loma La Sal / Loma La Golondrina), are misclassified as palm dominated forest.

In spite of the fact that the slope angles were normally distributed for a larger number of classes than the two other topographic variables (table 15), the inclusion of slope in the classification fails to improve the MLC results. The fact that the slope values are rather inaccurate, because of the low resolution of the DEM on which their calculation was based, is at least partly responsible for these poor results. It could also be that slope is not a very relevant factor for the distribution of most of the land cover classes in the study area.

Elevation was the only DEM-derived data channel which improved the classification results consistently (although not significantly) for unfiltered and mode-filtered results, compared to the classification of the spectral-textural data set 14. It is also the most reliable of the three topographic data channels. Spot-checks of the elevation values of the 8 m kriged DEM showed that they differed less than ±25 m from values derived directly from the 1:50000 topographic maps. In relation to the 765 m of elevation difference within the eastern test area, this does provide an acceptable 'signal to noise ratio'. In other words, there is real information about the approximate elevation of a pixel which will differ for different altitudinal zones in the image. But of course this interpolated DEM is a lot smoother than the real relief. Additionally, ridge lines and drainage lines are often misplaced by some tens of metres because of the low resolution of the input data. This can be expected to introduce significant errors into the slope and aspect or incidence models which are derived from such a DEM, so that it is questionable whether these derived topographic channels contain much useful information.

As the elevation channel did seem to contain some information which could be utilised by a maximum likelihood classifier, it was also resampled to 4 m resolution and used to replace the

multispectral channel 3 in data set 18 (3×3 mean filtered multispectral channels and three texture channels). This is the spectral-textural data set the maximum likelihood classification of which had resulted in the highest overall accuracy so far (70.4 % after 7×7 mode filtering). The classification of the data set including the elevation data was assessed to be 64.0 % correct without post-classification processing and 71.9 % correct after 7×7 mode filtering. This is a slight improvement, but it is again not significant at the 95 % confidence level.

9.5.3 Non-Parametric Classification of Data Sets Including DEM-Derived Data

In contrast to MLC, the non-parametric k-NN and ANN classifiers should not be adversely affected by the lack of normal distribution in some of the DEM-derived data channels. When the 8 m spectral-topographic data set is classified with non-parametric classifiers, however, the results are not more accurate than those achieved with MLC (table 27). With all three classifiers, the resulting accuracies for the spectral-topographic seven channel combination are either similar to the accuracies achieved with the spectral-textural seven channel combination, or lower (compare table 25). For some of the mode-filtered results, the overall accuracies are significantly lower at the 95 % confidence level. In other words, for the classification of the eastern test area, the spectral-textural channel combination is a better classification input than the spectral-topographic channel combination even when using non-parametric classifiers.

Table 27: Overall accuracy [%] and Kappa index of agreement (in brackets) for classifications of data set 27 (Ikonos ms channels 1-4, DEM-based elevation, slope and incidence60, at 8 m resolution) with different classifiers (13 classes).

	MLC	k-NN	ANN
Unfiltered result	51.5 (0.447)	51.3 (0.442)	50.8 (0.443)
Result 3 × 3 mode filtered	57.1 (0.507)	53.3 (0.464)	53.0 (0.467)
Result 5 × 5 mode filtered	58.4 (0.522)	56.4 (0.499)	54.0 (0.476)

In all cases of spectral-topographic classification, and especially in the ANN classification, artefacts in the resulting maps point out that the influence of the topographic variables was too strong and/or the training samples were not fully representative of the ranges of elevations, slopes and incidence angles of the respective classes. This resulted in the creation of phenomena like an 'agroforestry altitudinal belt' in the ANN result, where areas of broadleaved riparian forest and even of grassland were misclassified as agroforestry because the pixel elevations (and in part also slope and incidence angles) matched those of the agroforestry training samples. In the ANN as well as in the k-NN classifications, broadleaved riparian forest at high elevations was classified as palm dominated forest. The positive effect that the cloud forest in the high mountains is classified more homogeneously is offset by the introduction of a false lower boundary of occurrence which leads to

cloud forest in the north-eastern corner of the image being misclassified as secondary forest. Again this is due to a lack of training samples representing the lower areas of cloud forest. This highlights the difficulty of ensuring that the training data of all classes are really representative of the full ranges of all channel values, even of ancillary data channels which are included in a classification.

k-NN and ANN classifications were also conducted with more than seven channels. In these classifications, DEM-derived data channels were used in addition to the four multispectral and three textural channels. The resulting data sets had up to ten channels.

Table 28: Overall accuracy [%] and Kappa index of agreement (in brackets) for non-parametric classifications of spectral-textural-topographic data sets.

Data Set	Classifier	Post-classification mode filter		
		No filter	3x3	5x5
No. 14 (IKONOS ms channels 1-4, GLCM texture *ENT*, *SD*, *CONT*)	k-NN	48.9 (0.411)	60.4 (0.542)	65.8 (0.602)
	ANN	49.2 (0.428)	59.3 (0.539)	63.7 (0.588)
No. 32 (IKONOS ms channels 1-4, GLCM texture *ENT*, *SD*, *CONT*, elevation)	k-NN	53.7 (0.468)	61.9 (0.560)	62.7 (0.569)
	ANN	50.4 (0.439)	53.0 (0.466)	56.4 (0.505)
No. 33 (IKONOS ms channels 1-4, GLCM texture *ENT*, *SD*, *CONT*, slope)	k-NN	50.3 (0.426)	61.1 (0.547)	65.1 (0.593)
	ANN	49.9 (0.432)	58.1 (0.523)	63.4 (0.581)
No. 34 (IKONOS ms channels 1-4, GLCM texture *ENT*, *SD*, *CONT*, incidence60)	k-NN	49.1 (0.414)	60.4 (0.540)	63.9 (0.580)
	ANN	48.7 (0.421)	57.1 (0.515)	61.7 (0.564)
No. 35 (IKONOS ms channels 1-4, GLCM texture *ENT*, *SD*, *CONT*, elevation, slope, incidence60)	k-NN	54.9 (0.480)	60.5 (0.544)	62.1 (0.561)
	ANN	49.7 (0.429)	54.7 (0.483)	58.0 (0.519)

Table 28 shows that in most cases, the two non-parametric classifiers perform similarly with regard to the overall accuracy. For data sets including DEM-derived data, the overall accuracies resulting from ANN tend to be slightly lower than those resulting from k-NN. When data sets containing an elevation channel were classified, the disadvantage of ANN compared to k-NN was most pronounced. In ANN classifications, the elevation always became too dominant, producing altitudinal belts of classes in the map to an extent which does not exist in reality (figure 40).

On the whole, it can be said that the inclusion of the available ancillary data in the classification and the use of non-parametric classifiers did not manage to improve the classification results for the eastern test area significantly beyond what had already been achieved with MLC and IKONOS-derived data (using a combination of multispectral and textural data and spatial integration). No classification of the 8 m resolution data sets containing DEM-derived data achieved an overall

accuracy above 55.6 % without post-classification mode filtering. With 5×5 mode filtering, the best result was 67.2 % accuracy. These best results were achieved with MLC for data set 28, which contains elevation data, in spite of the fact that the elevation data is not normally distributed for most training classes. This demonstrates the robustness of MLC towards moderate violations of its underlying assumptions. The best results achieved with non-parametric classifiers were insignificantly lower at 54.9 % without post-classification filtering (k-NN classification of 10 channel data set 35) and 65.1 % for 5×5 mode filtered results (k-NN classification of data set 33, including slope data).
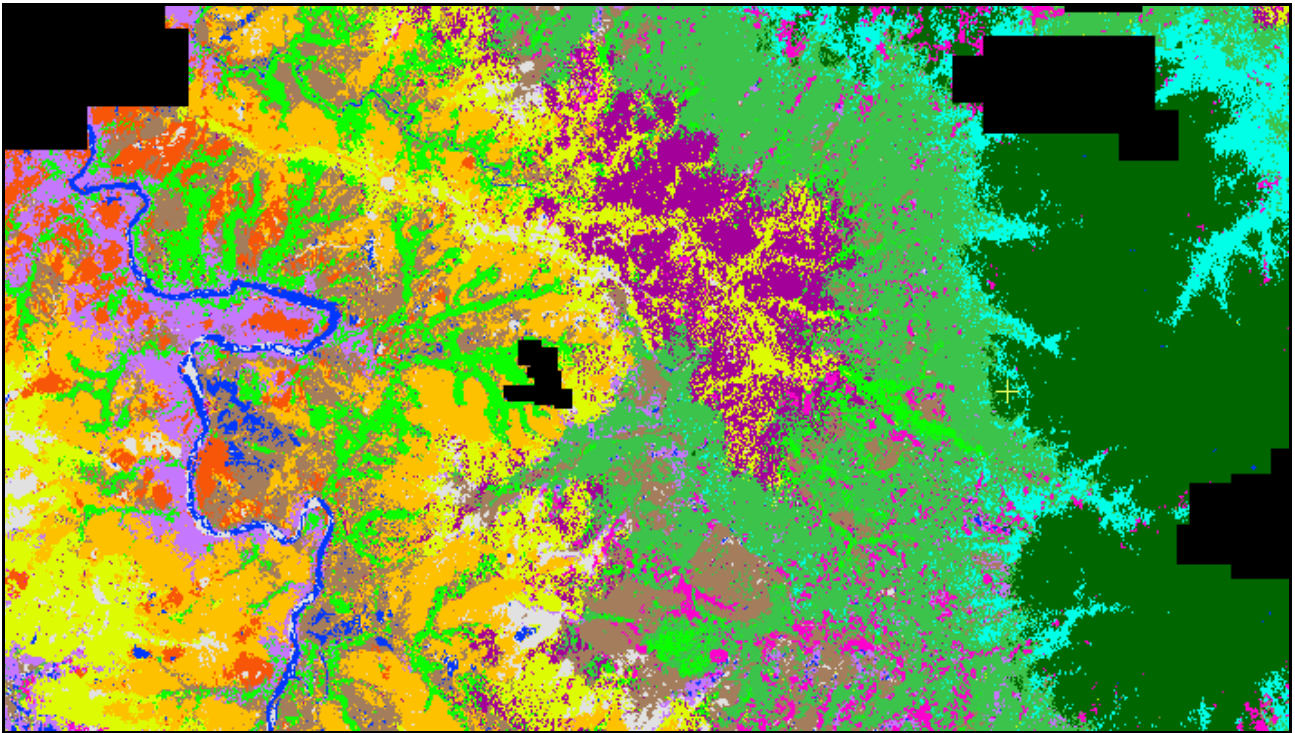
Figure 40: ANN classification result of data set 32 (IKONOS ms channels 1-4, GLCM Texture *ENT*, *SD*, *CONT*, elevation), demonstrating how this classifier confines classes like pine forest, palm dominated forest, cloud forest, secondary forest and agroforestry to certain ranges of elevations which they then dominate to an unrealistic extent. For the legend see plate 44, appendix 2.

The lack of significant improvements of classification results when DEM-derived data are used as additional input channels is partly due to the low resolution of the available DEM, leading to inaccuracies in the DEM-derived data channels. If a better DEM were available, it might still be worth experimenting with the inclusion of more DEM-derived variables in the classifications. Successful inclusion of DEM-derived data would also require that the training samples are carefully chosen with regard to the ancillary data channels from the outset. To make sure that the training samples are representative not only of the spectral and textural characteristics of the classes, but also of their elevations and other topographic characteristics, would require the establishment of a larger number of separate training areas for each class.

9.5.4   Use of DEM-Derived Data in Post-Classification Sorting

Post-classification processing with elevation was not successful in this test area either, because the land cover classes did not follow a clear vertical zonation in this area, which was also quite small and had a maximum elevation difference of only 765 m. The altitudinal zonation of vegetation is not the dominant factor determining the land cover pattern here. There are land cover classes which do have upper or lower limits of occurrence in the eastern test area, like cloud forest. However, these classes were hardly ever misclassified in a way which made these classes appear in the map in areas outside of their elevation range in the better classifications. This means that post-classification sorting with elevation data could not be effective in significantly improving classification results. The use of digital elevation data for post-classification sorting could make sense for larger areas, though.

A slope threshold could theoretically be used to correct the areas of bare ground misclassified as water. However, the resolution of the available DEM is not high enough to produce low slope values for all areas which were correctly classified as water.

Resumé of chapters 9.2 to 9.5 – use of IKONOS, Landsat and DEM-derived data for classifications of the eastern test area

Using information extracted only from IKONOS multispectral and panchromatic data for maximum likelihood classifications of 13 land cover classes led to classification accuracies of up to 65 % without post-classification processing, and up to 70 % for mode-filtered results. This is significantly more than could be achieved with Landsat data. Multi-source data integration and the use of non-parametric classifiers did not lead to any significantly improved classification results. In fact, they led to lower overall accuracies in most cases.

9.6 Discussion of the Classification Results and Accuracy Assessment Methods

9.6.1   Validity of the Calculated Accuracy Measures

Stratified random sampling was used to create an unbiased sample for accuracy assessment. However, a third of the initial sample points had to be dropped from the sample because their true land cover class was not ascertainable. This has probably led to a slightly biased testing sample with an under-representation of ambiguous land cover types in remote (unvisited) areas. Accordingly, a slight over-estimation of classification accuracy compared to a complete random sample can be expected. On the other hand, the sampling and assessment method was rigid in that it did not from the outset exclude ambiguous or transitional areas or areas close to land cover class borders. Also,

the accuracy measures reported so far in this chapter are the result of 'hard' accuracy assessments, with only one of the land cover classes being assigned as 'true' for each of the reference points. It can be argued that it would be justified to allow more than one class to count as correct in transitional and mixed areas, so that the hard accuracy measures used so far may actually lead to an under-estimation of accuracy.

Rarely are two accuracy assessments by different authors conducted with exactly the same methods and the same rigidity (see chapter 2.7). However, the method used here was explained in detail so that it should be reproducible. In any case, as the same testing set was used to assess the accuracy of all the classifications of the eastern test area, the resulting accuracy values are at the very least comparable among each other.

The sample size of 583 is large enough to produce overall accuracy estimates with 95 % confidence intervals of approximately ± 4 %. This means that the differences between many of the reported classification results can be rated as significant. The confidence intervals for the individual class accuracies are much larger, however, so these values give only vague indications about the relative accuracies and have to be interpreted with restraint.

9.6.2 Success and Limitations in Mapping Detailed Forest and Land Cover Classes with IKONOS Data, Considering Land Cover Fuzziness

In the following, I am going to take a closer look at the results of the maximum likelihood classification of data set 18 (consisting of four 3×3 mean filtered multispectral channels and three GLCM texture channels). This data set belongs to the group of data sets with which the best classification results were achieved. The single highest overall accuracy estimate for classifications based exclusively on IKONOS data was calculated for a 7×7 mode filtered MLC result based on this data set (OA: 70.4 %, KIA: 0.659). Table 29 contains the confusion matrix for these 7×7 mode filtered results. Figure 35 shows the corresponding map.

The forest classes, except for open pine forest, all have user's as well as producer's accuracies between 65.6 % and 85.7 % (as estimated with the reference sample). Cloud forest was the most accurately classified land cover class of all, which is encouraging because of the importance of cloud forest as the protected ecosystem in the Scientific Reserve Ebano Verde. Using the product of user's and producer's accuracy as the basis for comparison, grassland and *matorral* are the non-forest classes with the highest class-specific accuracies. This is in spite of the fact that they are often confused with each other (which is understandable because of the many areas of fern-rich 'rough grassland' in transition to *matorral* in the buffer zone of the reserve). Agroforestry and broadleaved riparian forest are another class pair which is often confused. This could already be expected because of the low separability of these two classes.

Table 29: Confusion matrix for the IKONOS classification, MLC of data set 18, 7×7 mode filtered, 13 classes. For class abbreviations see table 10. RD: Reference Data, CD: Classified Data, UA: User's Accuracy, PA: Producer's Accuracy, OA: Overall Accuracy.

RD CD	PFd	PFo	CF	SF	PmF	BRF	Mat	Cal	AF	GL	Cr	BG	W	Sum	UA (%)
PFd	**21**		5	6										32	65.6
PFo	2	**12**	1			5	3	1	1		4			30	40.0
CF	1		**78**	14	3	2		1						99	78.8
SF	2	3	4	**93**		11	4	9				1		127	73.2
PmF			1		**16**	5								22	72.7
BRF	2		2	4	1	**71**	2	1	7	1				91	78.0
Mat		4		1		5	**51**	2	2	13				78	65.4
Cal				4			2	**11**						17	64.7
AF						4	2		**6**			1		13	46.2
GL		2				1	6	1		**35**				45	77.8
Cr						1				5	**10**			16	62.5
BG										1	1	**2**		4	50.0
W												4	**4**	8	50.0
Sum	28	21	91	123	20	105	70	26	16	55	15	8	4	582	
PA (%)	75.0	57.1	85.7	75.6	80.0	67.6	72.9	42.3	37.5	63.6	66.7	25.0	100		**OA: 70.4**

The classes with the lowest class-specific accuracies are bare ground, agroforestry, open pine forest and calimetal. These are all minor classes with regard to the total area which they cover in the eastern test area and with regard to the contiguous areas which are occupied by these land cover types. (There are also only few reference samples per class for these classes leading to low confidence in the class-specific accuracy values.) The bare ground occurs along narrow roads and in small patches of landslide scars and single bare fields. *Calimetal* occurs in patches many of which are smaller than 0.1 ha. Agroforestry is conducted on a small scale in the eastern test area, often in the form of house gardens or very small plantations. Open pine forest usually consists of relatively small groups or stands of pine trees surrounded mostly by non-forested areas. These small contiguous class areas entail a large proportion of border pixels, leading to an increased likelihood of misclassifications. In the case of agroforestry, there is the additional problem that the class is spectrally very similar to the broadleaved riparian forest class. Both have an upper canopy cover of broadleaved trees with similar spectral characteristics (partly even the same species). The inclusion of texture in the classification has increased the class separability somewhat, probably because agroforestry tends to have a canopy cover which is not as closed as that of broadleaved riparian

forest. However, the classification accuracy remains low for agroforestry, due to confusions with broadleaved riparian forest and also with *matorral*.

In spite of its similarity to agroforestry and in spite of its occurrence in often narrow bands along the streams, broadleaved riparian forest belongs to the classes with the highest class-specific accuracies. Most misclassifications as agroforestry could be prevented by reducing the *a priori* probability for the agroforestry class. And the spatial resolution of the IKONOS data is high enough to produce good classifications of this class in spite of its linear occurrence – in contrast to the Landsat classification of the eastern test area, where broadleaved riparian forest was often confused with *matorral*, cloud forest and secondary forest, among others.

Although it is not apparent in the confusion matrix in table 27, too many areas in the western half of the image tend to be classified as open pine forest, especially when data sets containing texture channels are classified. This is also the case for the classification of data set 18. The areas which are given as open pine forest in the map are usually related to pines, but they do not all conform to the definition given in table 10 (pines with 25-60 % crown cover). Instead, they also represent areas of pine woodland or pines in the agricultural landscape with less than 25 % crown cover, including single pine trees and small groups of pines outside forest with their surrounding pixels.

Many of these 'problem classes' can also be expected to play a role in detailed high resolution classifications of other sub-areas of the UCRYN, although the composition of land cover classes varies somewhat across the catchment area. In the western UCRYN (Manabao area) for example, there are many pine plantations of different ages, large areas of pine forests with different degrees of crown cover and some transitions to *matorral*, and coffee plantations with gradual transitions to agroforestry (sporadic open coverage of shade trees). This constellation can be expected to lead to challenges in a detailed land cover classification, including difficulties to differentiate between open and closed pine forest, between *matorral* and coffee, or between coffee without shade trees and agroforestry.

Class transitions and ambiguity

The classes in the classification scheme for the eastern test area are defined in a way that should theoretically make them mutually exclusive, provided that there is perfect knowledge about the percentage canopy cover of the species or life forms in a specified area (table 10).

In reality, however, the land cover classes do not necessarily have crisp boundaries, and there are many image primitive areas for which the land cover type is ambiguous. Besides mixed pixels occurring along class area boundaries (which is possible for most class pairs), gradual spatial and temporal transitions can occur between many of the defined classes, as well as cases of small-scale land cover heterogeneity. These phenomena result in pixels (image primitives) for which a definite

assignment to one of the classes is not possible. This ambiguity can be caused by a mixture of land cover types within the area of the classified image primitive, by a border between land cover types running through the pixel area or by a transitional land cover type in the pixel area which is approximately half-way between the defined classes. Types of transition and other causes of ambiguity between the land cover classes of the eastern test area are shown in the diagram in figure 41. Examples of borderline cases are for example areas covered by grasses and ferns with approximately 25 % shrubs (halfway between the defined classes grassland and *matorral*) or a riparian forest where about half of the trees are *Prestoea Montana* (halfway between broadleaved riparian forest and palm dominated forest). These ambiguities entail boundary uncertainties.
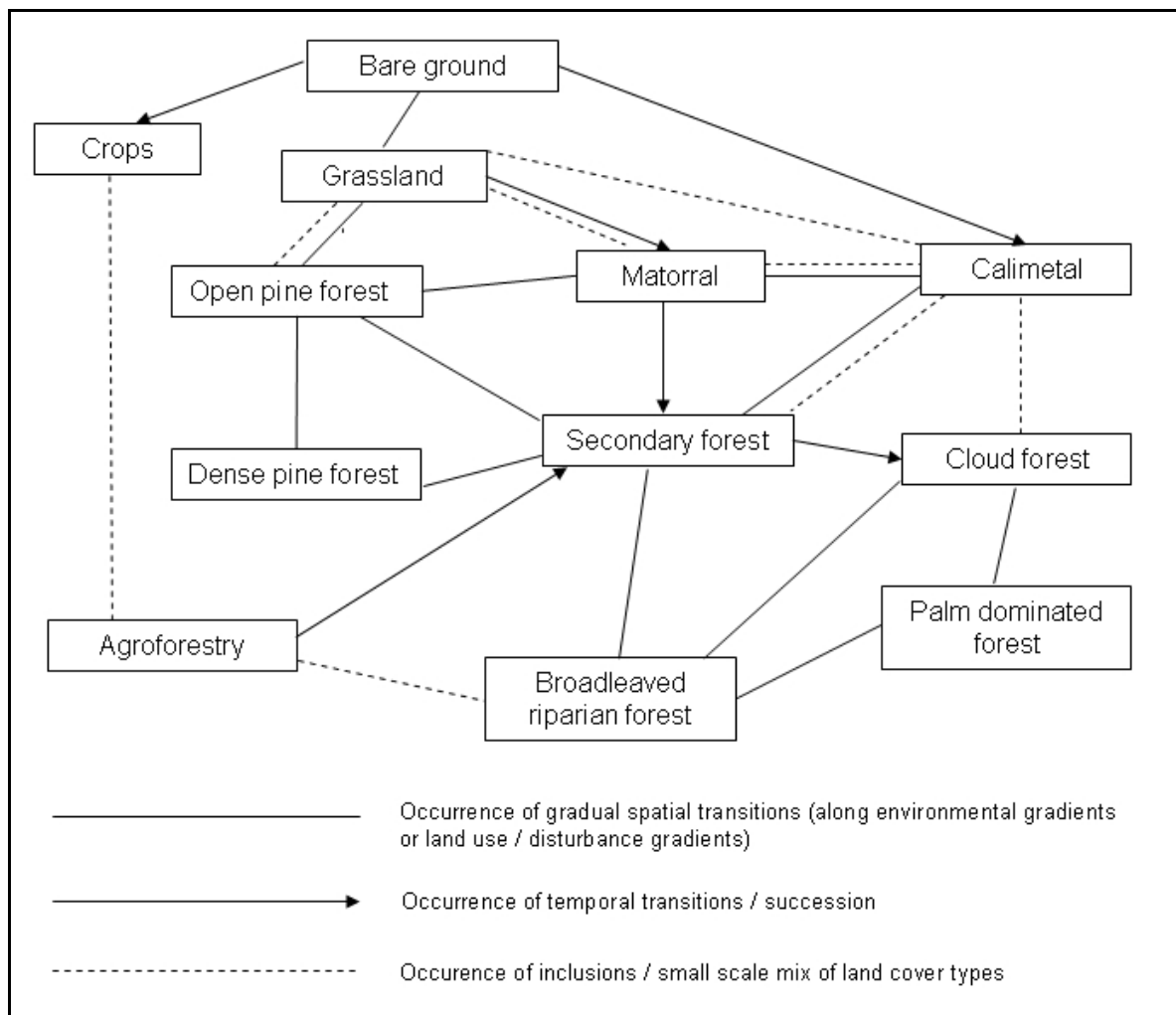
Figure 41: Diagram of causes of ambiguities between class pairs (beyond mixed boundary pixels) in the eastern test area.

One example of a class pair with high boundary uncertainty is open pine forest and grassland. Where is the correct boundary between open pine forest and grassland when a group of pine trees, with an average crown cover of ca. 40 % and a grassy herbaceous layer, is surrounded by grassland? In figure 42, both classifications could be called justified for many of the pixels. Some

of these ambiguous pixels are marked with an x. Some pixels which should be classified as open pine forest, but for which a classification as grassland or dense pine forest would be understandable in a per-pixel classification of 4 m resolution pixels, are marked with plus signs (+). Classification of these pixels as grassland or dense pine forest would not be optimal, but would still transport some information about the real land cover of that area. Such classifications would certainly be less incorrect than a classification as cloud forest or water, for example. The dashed squares mark two 15 m × 15 m areas which are used for the calculation of the texture parameters assigned to the central pixels. The central pixels would probably be classified as grassland in a per-pixel multispectral classification without spatial integration. The texture values, however, would indicate that these are not homogeneous grassland areas. Consequently, in a classification including texture, even the right central pixel (•) might be classified as open pine forest.
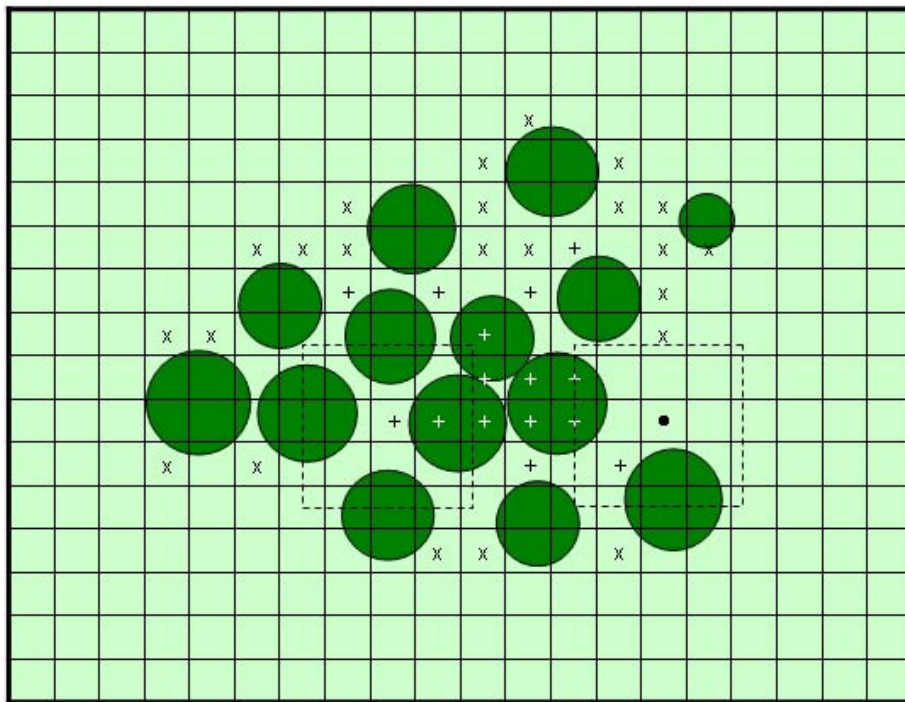
Figure 42: Schematic representation of pines (omitting shadows) on a grass background with a 4 m raster, illustrating the boundary uncertainty between grassland and the open pine forest class.

Similar points could be made for the cases of (open) secondary forest or disturbed cloud forest with a fern (*Dicranopteris pectinata*) undergrowth, bordering on pure *calimetal* areas (plate 7) – or for open pine or secondary forest with a shrub layer bordering on *matorral* areas.

Another factor which limits the preciseness of the class definitions is the fact that there can be no explicit uniform minimum mapping units in the classifications. The minimum mapping units in the classifications themselves depend on the image primitives used (between 16 m² for single multispectral pixels and 256 m² for the 16 m resolution data sets). Post-classification mode filtering leaves hardly any single pixels of one class. A minimum mapping area, depending on the desired

scale of the output map, could be standardised after a classification by sieve filtering the classification result, eliminating image value polygons containing less than a specified number of pixels. But during the classification itself (without post-processing), the minimum mapping unit is equivalent to the size of the image primitives which are classified, so that e.g. a 16 m² pixel can end up being assigned to a forest class even if it represents the only tree in the neighbourhood.

Off-diagonal entries in the confusion matrix need not all be errors of the same severity but may be the unavoidable outcome of ambiguities ('fuzziness') in the land cover, leading to pixels being assigned to different classes in two independent classifications. As usual, the reference sample has to be regarded as another classification, which should be on the whole more accurate than the automated classification of a satellite image but which can also contain errors and uncertainties. The reference data cannot be assumed to represent the absolute truth. To come close to that, it would have been necessary to visit each reference point at the time of the image acquisition, to classify the main species and to measure the canopy cover of all relevant species and live forms. Instead, what I have available as 'ground truth' for the reference data is based mostly on the visual interpretation of high resolution satellite data and ground and aerial photographs in connection with field data acquired one and two years after the image acquisition – and not every reference point could be visited on the ground.

Considering the many unavoidable cases of uncertainty (given the characteristics of the land cover patterns in the study area, the classification scheme, and the available data), the overall agreement between a 'hard' classification result and a 'hard' reference data set cannot be expected come close to 100 % even with optimal processing and classification methods.

9.6.3 *A Posteriori* Probabilities and the Spatial Distribution of Errors

The maximum likelihood classification of data set 18 was 'softened' by outputting not only the most likely class but also the second and third most likely class and the *a posteriori* probabilities for these three classes in six channels. The *a posteriori* probabilitiy for the most likely class (PP1, figure 43) has a mean value of 0.77. It is above 0.5 for 86.3 % of the classified pixels, above 0.66 for 68.6 % of the pixels and above 0.9 for 37.2 % of the pixels. The largest contiguous areas with *a posteriori* probabilities of at least 0.98 are the cores of the cloud forest area.

Figure 44 shows a map where the land cover class is only specified if the *a posteriori* class probability is above 0.66, while areas where the *a posteriori* probability is lower are left white. As can be seen, low *a posteriori* probabilities occur mostly along class borders (mixed pixel phenomenon) or in highly diverse areas or areas of transition between chosen information classes (for example in the area of transition between pine plantations and mixed secondary forest; or in the transitional zone between palm forest and cloud forest).

175

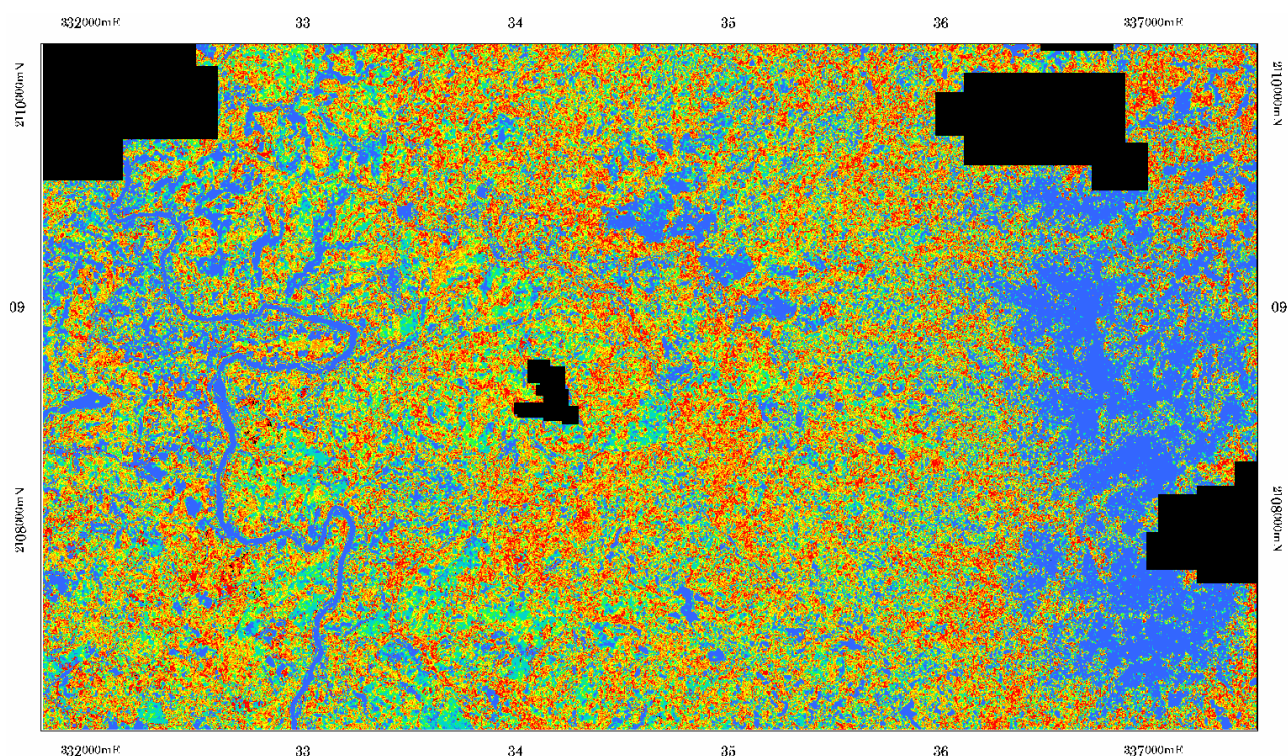Figure 43: *A posteriori* probabilities for the class assigned in a maximum likelihood classification of data set 18. Red: 0.00-0.50, orange: 0.51-0.66, yellow: 0.67-0.80, light green: 0.81-0.90, bluish green: 0.91-0.97, blue: 0.98-1.00.
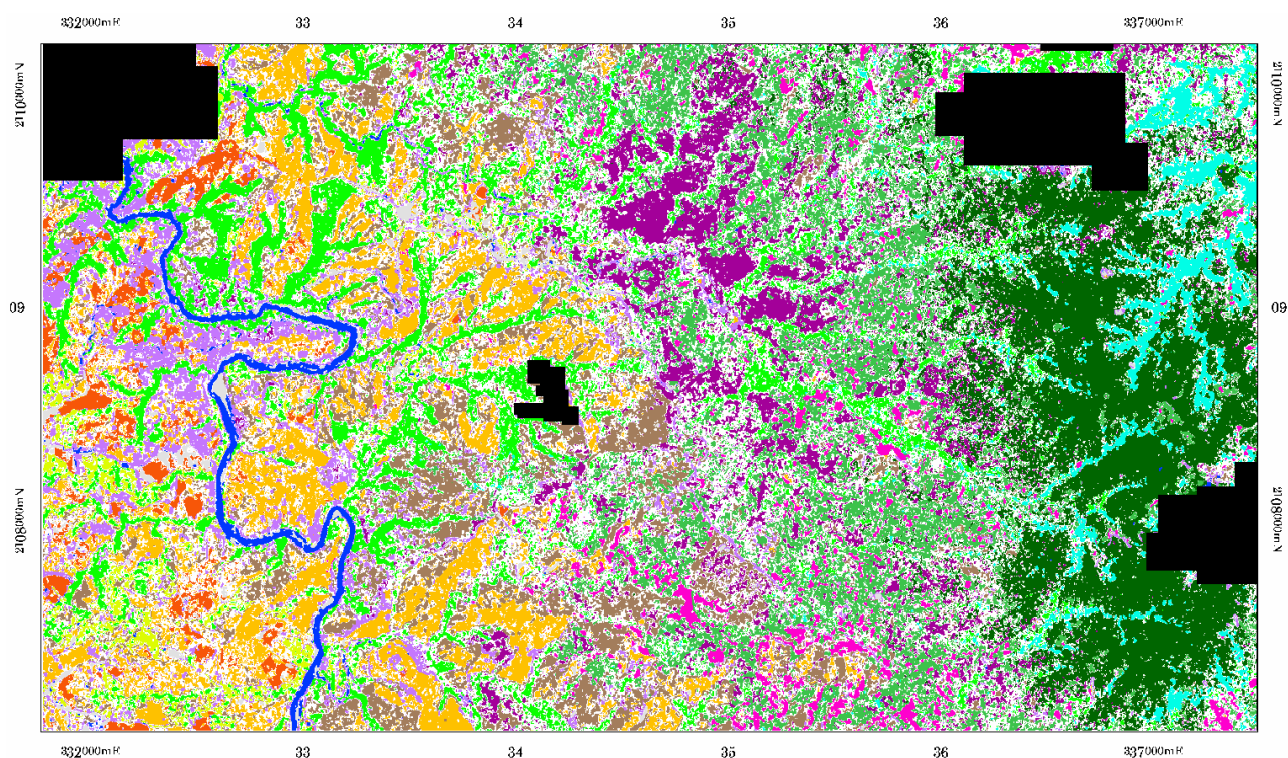

Figure 44: Unfiltered MLC result of data set 18 with classes depicted only if PP1 > 0.66, and white areas where PP1 is lower. For the legend see plate 44, appendix 2.

The mean *a posteriori* probability for the second most likely class (PP2) is 0.15. When the *a posteriori* probabilities of the two most likely classes are summed up, the resulting values are larger than 0.90 in 70 % of the cases. The mean *a posteriori* probability for the third most likely class (PP3) is only 0.04. This indicates that, from the standpoint of *a posteriori* probabilities, there are usually no more than two classes for which assignments would be probable to a substantial degree.

As the *a posteriori* probability is not directly proportional to the Gaussian density function (see chapter 8.8.1), there are a few cases (3 % of the pixels) where the PP2 is higher than PP1, so that the class to which a pixel was assigned by MLC does not in all cases have the highest *a posteriori* probability. The difference between the *a posteriori* probabilities of the two most likely classes could be used as another indicator of classification certainty. In a digital classification output (e.g. in a GIS), areas where 'PP1 minus PP2' is below a specified value could be annotated with a warning, offering information about the second most likely class (according to MLC) as an alternative class assignment.

9.6.4 Elimination of Reference Points Close to Land Cover Class Boundaries from the Accuracy Assessment

When only testing points located more than 12 m from a land cover class boundary are retained while the others are eliminated from the accuracy assessment, only 57 % of the original reference points (333 of 583) are left. The fact that almost half of the 583 reference points are located within 12 m buffers around the land cover class boundaries is an indicator of the high land cover diversity and heterogeneity of the landscape of the study area. Eliminating testing points close to boundaries leads to markedly higher overall accuracies for all data sets (table 30). The smallest improvement was 5.5 % for data set 1 (the 4 m resolution multispectral data without any form of spatial integration). For spatially integrated data sets and data sets including texture channels (the values of which are based on 15 m × 15 m areas), the improvements were bigger. In most cases of spatially integrated data sets, the difference to the overall accuracy values estimated with the full set of reference points was above 8 %. The overall accuracies estimated with the reduced set of reference points reached values of up to 79.6 % (MLC of data set 13, 7×7 mode filtered). The overall accuracy estimated for the 5×5 mode filtered MLC result of data set 18 was 79.0 %.

The fact that a disproportionate part of the errors occurs close to class boundaries demonstrates the detrimental effect of mixed pixels and other edge effects (particularly between-class texture) on classification accuracies. The results also indicate that such edge effects are relatively minor in the multispectral 4 m resolution data without spatial integration, while spatial integration and the inclusion of texture data augment the proportion of errors caused by edge effects. However, the benefits of the inclusion of spatial information outweigh the disadvantage of increased edge effects

considerably. So it is in spite of increased edge effects that significantly better results could be observed for classification results after the inclusion of spatial information (chapters 9.2 and 9.3).

Table 30: Improvement (in %) of the overall accuracy values when using the testing sample without points close to boundaries, compared to the values achieved with the complete testing sample.

Post-classification mode filter	Data Set			
	1 (Ikonos ms channels 1-4, 4 m)	13 (Ikonos ms channels 1-4, GLCM *ENT, SD, CONT*, 4 m)	18 (Ikonos ms channels 1-4, GLCM *ENT, SD, CONT*, 3×3 mean)	15 (Ikonos ms channels 1-4, GLCM *ENT, SD, CONT*, 12 m)
No filter	5.5	8.4	7.3	8.5
3×3	6.1	8.0	9.3	9.4
5×5	7.8	9.6	9.7	9.7

9.6.5 Fuzzy Accuracy Assessment

For the data set 18 MLC result, the fuzzy overall classification accuracy ('right' value according to Woodcock & Gopal 2000) was estimated for the unfiltered and the 7×7 mode filtered classification result. The linguistic ratings – what constitutes a 'good answer' and what is a 'reasonable or acceptable answer' – are of course rather subjective, but so is the assignment of a 'best' class as reference class for the 'hard' reference sample in some cases (see chapter 9.6.2).

So instead of determining one 'best' class to every reference point, the fuzzy accuracy assessment makes it possible to count several classes as acceptable, e.g. both grassland and *matorral* in the rough grassland areas where small shrubs are starting to appear among the ferns and grasses, or both secondary forest and *calimetal*, if the testing point is located near the border of a *calimetal* patch within a secondary forest area. The fuzzy accuracy ('right' value) was estimated to be 76 % for the unfiltered classification result (compared to 61.2 % as estimated with the hard accuracy assessment) and 85 % for the 7×7 mode filtered result (compared to 70.4 % as estimated with the hard accuracy assessment). So in the best IKONOS-based map, about 85 % of the class assignments are at least acceptable (carrying useful information about the real land cover in the pixel area and its immediate neighbourhood).

9.6.6 Class Aggregation

The confusion matrix used for the conventional accuracy assessment of the best IKONOS classification (table 27) was used as a basis for class aggregation (reducing the classification detail by aggregating similar informational classes). The overall two class forest - non-forest classification

accuracy is 89.0 % if agroforestry is not counted as a forest class. If agroforestry *is* counted as a forest class, it is 91.4 %. Aggregating the classes to four broad classes results in an overall classification accuracy of 83.7 %. The pixels can be assigned to six broad classes with an overall accuracy of 78.7 % (table 31).

Table 31: Class aggregation and corresponding overall accuracies, based on the 7x7 mode filtered MLC result for data set 18.

13 class scheme, OA=70.4 %	6 class scheme, OA=78.7 %	4 class scheme, OA=83.7 %	2 class scheme, OA=89.0 %
Dense Pine forest	Coniferous forest	Forest	Forest
Open Pine forest	Coniferous forest	Forest	Forest
Cloud forest	Broadleaved (<50% coniferous) and palm forest	Forest	Forest
Secondary forest	Broadleaved (<50% coniferous) and palm forest	Forest	Forest
Palm dominated forest	Broadleaved (<50% coniferous) and palm forest	Forest	Forest
Broadleaved riparian forest	Broadleaved (<50% coniferous) and palm forest	Forest	Forest
Matorral	Shrub and herb dominated semi-natural vegetation	Shrub and herb dominated semi-natural vegetation	Non-Forest
Calimetal	Shrub and herb dominated semi-natural vegetation	Shrub and herb dominated semi-natural vegetation	Non-Forest
Agroforestry	Agricultural land use	Agricultural land use	Non-Forest
Grassland	Agricultural land use	Agricultural land use	Non-Forest
Crops	Agricultural land use	Agricultural land use	Non-Forest
Bare ground	Bare ground	No vegetation	Non-Forest
Water	Water	No vegetation	Non-Forest

10 Conclusions and Perspectives

The aim of this study was to find optimised methods for the automated digital classification of satellite images − including high resolution satellite data – of heterogeneous tropical mountain areas and to produce forest and land cover maps of areas for which there was a lack of detailed spatial land cover information.

Landsat ETM+ and IKONOS-2 data were used as examples of conventional medium resolution satellite data on the one hand and of data of the new generation of high spatial resolution satellites on the other hand. A Landsat ETM+ classification was conducted for the mountainous upper catchment area of the Río Yaque del Norte (785 km²) in the Cordillera Central of the Dominican Republic. IKONOS data were analysed and processed for smaller subsets of this region.

Most of the analyses regarding the processing of high resolution IKONOS data were conducted for one test area only, using a subset of one IKONOS image. The eastern test area was chosen as an example of a heterogeneous tropical mountain area, containing protected forest areas as well as semi-natural vegetation and small-scale farming. A one-to-one transfer of the data processing results to other IKONOS images of other areas will not be feasible, because of the varying (geometric) aquisition paramters of IKONOS data, among other things. On the other hand, the data of the eastern test area were analysed in great detail. The qualified results and conclusions drawn from the analysis of this image area contribute to the body of experience which exists about the use of high resolution satellite data for tropical forest and land cover mapping, and which is up to now quite limited.

The results of the Landsat and IKONOS classifications which were carried out indicate that, for mapping the heterogeneous land cover of tropical mountain areas, the use of high spatial resolution data does indeed lead to higher accuracies, compared to a conventional classification of medium resolution data (as stated in the central hypothesis). It can also be confirmed that the spatial characteristics of high resolution data have to be taken into account in order to make good use of such data.

For the eastern test area, a conventional per-pixel classification of the four multispectral IKONOS channels did not lead to a significantly higher overall accuracy than the classification of seven Landsat channels. As a source of multispectral data for land cover and particularly forest classifications, the spatial resolution of IKONOS data is unnecessarily high, so that some kind of spatial integration (decreasing the resolution, low pass filtering or image segmentation) is needed in order to achieve optimal classification results. Similar accuracy improvements can also be achieved when mode filtering is used as a technique for post-classification spatial integration.

180

The higher resolution information, particularly of the panchromatic channel, should also be exploited and can be used through the derivation of texture parameters. GLCM texture features, calculated from the panchromatic channel in 15 m × 15 m windows, proved to be a useful addition to the limited number of multispectral IKONOS channels, increasing class separabilities and classification accuracies. The inclusion of texture data increased the classification accuracies for all forest classes and was especially useful for the discrimination of palm dominated forest, secondary forest and open pine forest. Among the non-forest classes, *matorral* benefits a lot from the inclusion of texture, with better separabilites between open forest and its 'background class' *matorral* on the one hand and between *matorral* and the more 'smooth' grassland on the other hand.

The best IKONOS based classification results were achieved when the integration of textural features and multispectral channels to spectral-textural data sets was combined with spatial integration methods, e.g. 3×3 or 5×5 mean filtering of the multispectral channels and post-classification mode filtering. Similar results (overall accuracy around 70 %) were also achieved without pre-classification spatial integration of the 4 m multispectral data, when information about larger areas was only introduced through the texture data (calculated in 15 m × 15 m windows) and post-classification mode filtering. The best classification results before post-processing (mode filtering) were achieved with the combination of mean filtered multispectral data and three texture features. Classifications of the segmented data (with object-oriented standard nearest neighbour classification in eCognition and MLC as tested classification methods) were less successful with overall accuracies not exceeding 60 %.

A basic factor limiting the accuracy of automated classifications of high resolution remotely sensed data is the trade-off between using either high resolution data with few mixed pixels, but with pixels which are often not representative of their classes, or data incorporating spatial information, where the pixels are more representative of their classes but edge effects play a larger role. The eastern test area and most of the UCRYN are areas of high land cover heterogeneity and fragmentation, which is typical for partly farmed tropical mountain areas. This entails that the threshold of homogeneity and the threshold of heterogeneity (in the terminology of Puech 1994) for detailed target land cover classes are quite close to one another. In other words, when the pixels become large enough (or there is enough spatial integration in another form) to aggregate the class elements in a representative pixel, many of the pixels are already so large (or contain so much information from neighbouring areas) that they represent several target land cover classes. In areas where the land cover classes exhibit a high within-class heterogeneity (e.g. open forest classes consisting of many different elements) while at the same time the contiguous areas of the individual classes are very small, the thresholds of homogeneity and of heterogeneity of the target classes can become very close to each other. This may entail that information about the separate target classes in such areas cannot be extracted from the data in an automated per-pixel classification.

When using medium resolution (Landsat ETM+) satellite data to classify the eastern test area, the threshold of heterogeneity is already reached for parts of some of the target classes (e.g. narrow riparian forest, the smaller patches of *calimetal* and *matorral*), meaning they are integrated with their neighbouring classes in the spectral response, and the percentage of mixed pixels is very high. The 4 m resolution of the IKONOS data, on the other hand, is below the threshold of homogeneity for many target classes, meaning that the elements of many of the target classes are still resolved separately. Spatial integration of this high resolution data leads to better classification results until the amount of mixed pixels and the detrimental edge effects become so large that they cannot be compensated by improvements through spatial integration any longer.

When Landsat and IKONOS data were integrated, the classification results were degraded compared to optimised classifications of IKONOS data alone. Even though a higher spectral resolution is provided with the Landsat data, their spatial resolution is too low to effectively improve the class separabilities in the heterogeneous test area compared to IKONOS data alone.

The fundamental trade-off between trying to reduce edge effects or trying to reduce the within-class variability in the choice of a spatial resolution (degree of spatial integration) does not seem to be avoidable in automated per-pixel classifications. It becomes more relevant with increasing land cover heterogeneity and increasing within-class heterogeneity. While for the purpose of detailed classifications of areas of high land cover heterogeneity, high resolution data are clearly preferable to medium resolution data, processing them in a way that uses their advantages but cancels their disadvantages does pose some challenges. The methods of spatial integration and use of texture tested in this study go some way in that direction, but some problems of misclassifications, caused among other things by edge effects in the texture data, remain. With this in mind, a more thorough look at image segmentation of high resolution data and especially at optimising the classification methods for segmented data might still be worthwhile.

The low resolution of the available DEM (50 m grid spacing) limited its usefulness in connection with the high resolution IKONOS data. The DEM was useful for a post-classification sorting of the Landsat classification of the whole UCRYN, but the integration of DEM-derived topographic variables in the IKONOS classifications of the eastern test area did not manage to enhance the classification results significantly.

The high resolution data sets were classified better (or at least equally well) with the maximum likelihood classification method than with the tested non-parametric classification techniques (k-nearest neighbour classification, artificial neural network classification and object-oriented nearest neighbour classification). The MLC method, which is well proven for the classification of medium resolution multispectral data, was shown to be suitable for the classification of the spectral-textural IKONOS data sets, which were mostly Gaussian and exhibited only moderate violations of the

Gaussian assumption for a minority of the classes and channels. It would have to be replaced or complemented by other classification methods only if more non-Gaussian ancillary data were used as variables during the classification.

An overall classification accuracy of around 70 % was the maximum that could be achieved for a 'hard' classification of the Ebano Verde test area with its 13 classes, no matter how much information was extracted or added. Edge effects (mixed pixels) boosted by a high landscape heterogeneity, the many occurrences of gradual transitions between the defined classes and the (usual) lack of 'absolutely true' reference data limit the agreement which can be achieved between the automated classification of high resolution satellite data and the reference data (which represents essentially an independent classification). A consideration of the land cover as fuzzy helps to differentiate between serious errors and less serious disagreements between the map and the reference data. 'Softening' the output of a maximum likelihood classification yields complimentary information about the spatial distribution of the map reliability and about possible alternative class assignments.

In spite of the above mentioned uncertainties, IKONOS data offer good possibilities to differentiate a number of land cover classes in the heterogeneous study area. Cloud forest, which is a particularly important forest type from a biodiversity and conservation standpoint, could be differentiated reliably from other forest types with the IKONOS data. It was sometimes confused with secondary forest, which represents a successional stage on the way towards cloud forest. Apart from that, the only significant number of confusions occurred with dense pine forest, with which cloud forest shares a more similar spectral signature (with relatively low reflection in the NIR) than with other broadleaved forest classes. Satisfactory classification accuracies could also be achieved for the other forest classes except open pine forest. The classification of agroforestry remains challenging even with high resolution and textural data.

For the small test area, IKONOS was clearly a better data source for a detailed classification than Landsat. Having said that, the choice of data is of course also a question of the desired scale of the map output, the size of the area to be classified and of the costs. IKONOS has a swath width of just 11 km and single IKONOS images cover accordingly much smaller areas than e.g. Landsat images. This and their high resolution make it more difficult to map larger regions.

For an extension of the areas mapped with IKONOS so far in this study, the next step would be to transfer the methods which were successful in the eastern test area (mean filtering of multispectral channels, inclusion of texture channels, mode filtering) to other areas of interest within the UCRYN, e.g. to the western area around Manabao. To classify the complete UCRYN with high resolution data and the appropriate methods would be very expensive and time-consuming. It would involve the pre-processing of about 12 separate IKONOS images (maybe more because of the cloud

cover in many images), most of which come with different acquisition geometry, different acquisition dates and varying atmospheric effects. A high resolution DEM would be needed to geometrically correct the images with lower collection angles and strong topographic effects. Even after thorough pre-processing, the images would probably still have to be classified separately because their different acquisition dates would not allow the use of training data derived from one image to represent the same class in an image acquired in a different season. This would require the collection of a sufficiently large amount of field data in every IKONOS-image-area of the catchment.

Classifying medium resolution data like Landsat may be the best solution for the production of a coarse base map, providing an overview of the spatial distribution of a limited number of broad land cover or land use classes for a larger region like a catchment area. However, the accuracy and / or detail of maps based on 30 m resolution satellite data can always be expected to be rather limited in heterogeneous tropical mountain areas. High resolution satellite data would be a suitable source of more detailed spatial information about smaller areas of special ecological or economical interest (e.g. protected areas).

The methods of high resolution data processing which were shown to be successful in this study could be implemented for example to monitor protected areas, or to gain information about the area and extent of threatened ecosystems in order to be able to make informed decisions about the boundaries for protected areas. The methods presented here do not produce information which could replace a detailed forest inventory as a basis for specific economic forest management decisions. It can be said, however, that maps produced for areas of interest with these methods, using high resolution satellite data, would certainly be more detailed and accurate than the land cover information which has been available for most parts of the Dominican Republic until now.

11 Zusammenfassung

Die vorliegende Arbeit beschäftigt sich mit Methoden zur automatisierten Kartierung von tropischen Bergwäldern und anderen Landoberflächen unter Ausnutzung der räumlichen Information in Satellitendaten hoher räumlicher Auflösung. Die mit hochauflösenden Satellitendaten (IKONOS) erzielten Ergebnisse werden dabei mit den Möglichkeiten und Grenzen einer konventionellen Landsat-Klassifizierung verglichen. Die verschiedenen Satellitendaten und weitere zur Verfügung stehende Geodaten werden teilweise integriert verarbeitet.

Tropische Bergwälder spielen eine wichtige Rolle für die nachhaltige Entwicklung tropischer Ökosysteme. Ihre Zerstörung oder Erhaltung bzw. Regenerierung und Aufforstung hat Auswirkungen auf den Bodenschutz, die Landschaftsdegradierung, die Wasserversorgung, das Klima und die Biodiversität. Außerdem sind sie eine Quelle von Holz und anderen Produkten des Waldes (Price & Butt 2000). Die Karibischen Inseln sind ein 'Hotspot' der Biodiversität mit vielen endemischen Pflanzenarten. Obwohl nur in 11 % dieses Gebietes noch die Primärvegetation erhalten ist, kommen 2,3 % der Gefäßpflanzenarten der Welt nur hier vor (Myers et al. 2000). Dabei sind die Gebirge mit ihren vielfältigen klimatischen und edaphischen Bedingungen (und einer im Vergleich zum Tiefland in der Regel eher erhaltenen natürlichen Vegetation) besonders artenreich und auch besonders reich an endemischen Arten.

Die Zentralkordillere (Cordillera Central) der Dominikanischen Republik ist ein randtropisches Gebirge, das Höhen bis zu 3175 m erreicht. Hier sind noch einige großflächige Waldgebiete erhalten. Dies ist eine ökologisch relativ günstige Situation im Vergleich zu vielen anderen karibischen Inselstaaten (z.B. dem fast völlig entwaldeten und stark degradierten angrenzenden Haiti). Das obere Einzugsgebiet des Río Yaque del Norte liegt in der nordöstlichen Cordillera Central (18°55' bis 19°18' N und 70°30' bis 70°58' W) in Meereshöhen zwischen 320 m und 3038 m und nimmt eine Fläche von ca. 785 km² ein (siehe *figure 5*). Das Gebiet ist gebirgig und weist überwiegend Hangneigungen über 40 % auf.

Die natürliche Vegetation dieses Gebietes besteht fast ausschließlich aus Wäldern. In Höhen über 2200 m herrschen natürliche Kiefernwälder vor, die von *Pinus occidentalis* dominiert werden. Reine Kiefernwälder kommen auch auf tiefer gelegenen Mangelstandorten vor. Außerdem fördern Waldbrände die Verbreitung der Kiefern in niedrigeren Lagen, wo sie teilweise in Form von Mischwäldern mit Laubgehölzen vorkommen. In Höhen zwischen 1100 und 2200 m liegen natürliche Verbreitungsgebiete von Nebelwäldern, von denen im Untersuchungsgebiet noch einige Reste vorhanden sind. Nebelwälder zeichnen sich dadurch aus, dass der Nebeleintrag hier einen wesentlichen Anteil an der Wasserversorgung hat. Entsprechend ändern sich die lokalen klimatischen und hydrologischen Verhältnisse, sobald die natürliche Vegetation fehlt. In Nebelwäldern findet man in der Regel viele Epiphyten und eine hohe Zahl endemischer Arten. Sie gehören zu den

weltweit am stärksten bedrohten Ökosystemen. Am Ostrand der Cordillera Central kommt der *Magnolia*-Nebelwaldtyp (Hager & Zanoni 1993) vor. Nach Störungen (natürlicherweise z.B. Hurricanschäden) entstehen in diesen Bereichen oft Flächen mit dichtem Farnbewuchs, wo hauptsächlich die Art *Dicranopteris pectinata* die Vegetation dominiert und die Regeneration von anderen Pflanzen behindert. Diese Flächen werden lokal *calimetales* genannt. Ein Palmenwald, der von *Prestoea montana* dominiert wird, wächst als edaphischer Vegetationstyp hauptsächlich auf nassen und skelettreichen Böden unter ähnlichen klimatischen Bedingungen wie die Nebelwälder.

Humide immergrüne Laubwälder wachsen bei Jahresniederschlägen um 2000 mm in Höhen bis zu 1500 m, manchmal auch bis zu 1800 m. Mit abnehmenden Niederschlägen (in niedrigeren Lagen) geht dieser immergrüne Waldtyp in einen teilweise laubabwerfenden Wald über, von dem aber heute kaum noch Reste erhalten sind. Laubtragende immergrüne Uferwälder, die in oft sehr schmalen Streifen entlang der Flüsse und Bäche des Untersuchungsgebiets vorkommen, sind heute meist die einzigen Waldreste innerhalb landwirtschaftlich genutzter Gebiete. Sie kommen aber auch innerhalb von Laub- und Kiefernwaldgebieten vor und zeichnen sich in ihrem natürlichen Zustand durch eine große Artenvielfalt aus.

Das obere Einzugsgebiet des Río Yaque del Norte war bis zum 19. Jahrhundert weitgehend unbesiedelt. Im frühen 20. Jahrhundert wurde nur im breiten Tal um Jarabacoa bereits Landwirtschaft betrieben. Seit den 1930er Jahren, als die Tieflandbereiche schon weitgehend entwaldet waren, wurden die Kiefernwälder in den leichter zugänglichen Gebieten der Cordillera Central dann verstärkt abgeholzt und das Holz in Sägemühlen verarbeitet. Das Land wurde langfristig in der Regel in Weideland umgewandelt, wobei in den ersten Jahren nach der Abholzung Ackerbau betrieben wurde. Heute ist nur noch etwa ein Drittel des oberen Einzugsgebiets des Río Yaque del Norte bewaldet, während der Rest hauptsächlich als extensives Weideland für Rinder genutzt wird. Außerdem wird in Lagen bis 1500 m Höhe Kaffee angebaut, teilweise mit Schattenbäumen. Die sonstige Landwirtschaft ist überwiegend kleinbäuerlich. Dabei werden (oft auf sehr steilen Hängen) Bohnen und anderes Gemüse sowie Mais und Tabak angebaut. Lokal existieren auch kleinbäuerliche Agroforst-Systeme.

Die Reduktion der Primärvegetation und die Fragmentierung der verbliebenen Waldgebiete reduzieren die Lebensräume der einheimischen Tier- und Pflanzenarten und machen die Ökosysteme anfälliger für Störungen. Die Reduktion der Waldflächen beeinflusst auch die lokalen klimatischen und hydrologischen Verhältnisse. Der Río Yaque del Norte ist die bedeutendste Wasserquelle der Dominikanischen Republik (Vicioso 2002) und wird seit 1973 am unteren Ende des oberen Einzugsgebietes aufgestaut, um Strom zu erzeugen und die Wasserversorgung des unterhalb liegenden Cibao-Tals (mit der Großstadt Santiago und verbreiteter Bewässerungsland-wirtschaft) zu regulieren. Die Entwaldung der steilen Hänge des oberen Einzugsgebietes hat zu einer verstärkten Erosionsrate und einer größeren Häufigkeit von Erdrutschen bei Starkregen-ereignissen geführt.

Dies wiederum führt zu einer starken Sedimentation in den Gewässern und hohen Kosten für die Instandhaltung des Stausees, dessen Kapazität durch die Sedimentation bereits signifikant reduziert wurde. Außerdem kommt es zu einer Degradierung der landwirtschaftlich unangepasst genutzten Flächen, wobei einige Gebiete bereits so stark degradiert sind, dass noch nicht einmal mehr eine Nutzung als extensives Weideland wirtschaftlich ist (SEMARENA 2002).

Die Dominikanische Regierung hat in der zweiten Hälfte des 20. Jahrhunderts versucht, die Entwaldung des Landes durch gesetzliche Maßnahmen aufzuhalten. 1967 wurde ein Gesetz erlassen, das die Sägemühlen schloss und jegliche Holzernte verbot. Das führte allerding auch dazu, dass Landbesitzer und -nutzer Bäumen gegenüber feindlich eingestellt waren, weil sie sie nicht nutzen durften, und eine Waldregeneration auf ihrem Land in der Regel aktiv verhinderten. Seit den 1980er Jahren wird versucht, Aufforstungen zu fördern, aber es bestehen immer noch bürokratische Hürden für die private Forstwirtschaft. Im oberen Einzugsgebiet des Río Yaque del Norte wurden staatlicherseits seit den 1970er Jahren einige Flächen mit Kiefern (hauptsächlich *Pinus caribaea*) aufgeforstet. Es gibt auch einige jüngere und z.T. private Aufforstungsflächen. Das dominikanisch-deutsche Enwicklungshilfe-Projekt PROCARYN (GTZ, KfW, DED) war zwischen 2001 und 2004 im oberen Einzugsgebiet aktiv darum bemüht, die nachhaltige Landnutzung und den Bodenschutz zu fördern, und hat dabei besonders kleinere Landbesitzer bei Aufforstungsprojekten und der Erstellung von Plänen für die Waldnutzung unterstützt.

Das westliche Ende des oberen Einzugsgebiets des Río Yaque del Norte gehört zum Nationalpark Armando Bermúdez. Das 29 km² große Reservat Ebano Verde (Reserva Científica Ebano Verde) liegt am Ostrand der Cordillera Central, an der östlichen Wasserscheide des Yaque del Norte-Einzugsgebiets. Es wurde 1989 eingerichtet, um zusammen mit dem dortigen Nebelwald (*Didymopanax tremulus*-*Magnolia pallescens*-Nebelwald-Gesellschaft) die bedrohte endemische Baumart *Magnolia pallescens* zu schützen. Außerhalb des Primärwald-Restes sind in den 1970er Jahren einige Flächen mit Kiefern aufgeforstet worden. Auf ehemals landwirtschaftlich genutzten Flächen und durch natürliche Verjüngung in nicht gepflegten Kiefernplantagen ist inzwischen in Teilen des Reservats ein vorwiegend laubtragender Sekundärwald (Sukzessionsstadium) entstanden. Außerdem kommen im Reservat Uferwälder und Palmenwald vor.

Wie in vielen tropischen Entwicklungsländern herrscht auch in der Dominikanischen Republik ein Mangel an zuverlässigen Daten über die vorhandenen Waldresourcen, sowohl für die Forstwirtschaft also auch für Naturschutzzwecke. May (1997) beklagt die ungenügende Qualität der biologischen und kartographischen Informationen, die oft zu einer recht willkürlichen Abgrenzung von Schutzgebieten führt. Gerade auch bessere räumliche Informationen (z.B. in Form von Vegetationskarten) wären von großem Nutzen für Fragestellungen des Schutzes der Biodiversität sowie für die Entwicklung von Strategien für eine möglichst nachhaltige Land- und Waldnutzung. Fernerkundung ist eine unersetzliche Quelle für flächendeckende räumliche Informationen. Dabei wurden

automatisierte Klassifizierungen von Satellitendaten für die Gewinnung von aktuellen Landbe-deckungsinformationen bisher hauptsächlich für relativ großflächige und kleinmaßstäbliche Kartierungen angewendet.

IKONOS-2 gehört zu einer neuen Generation kommerzieller räumlich hochauflösender Satelliten. Er wurde als erster dieser Satelliten 1999 in seine Umlaufbahn gebracht und liefert seit dem Jahr 2000 panchromatische Bilddaten mit 1 m Auflösung und vier multispektrale Kanäle mit 4 m Auf-lösung. Landsat ETM+, auch im Umlauf seit 1999, führt die Tradition der Landsat-Serie fort, die seit 1972 Satellitendaten mittlerer räumlicher Auflösung liefert.

Die Methoden zur automatisierten Klassifizierung von Satellitendaten, die sich seit den 1970er Jahren etabliert haben, wurden hauptsächlich für Daten mittlerer Auflösung entwickelt. Bei der pixelweisen Klassifizierung von Multispektraldaten kann man bei Landsat-Daten (30 m Auflösung) davon ausgehen, dass die Elemente der meisten Zielklassen (etwa Baumkronen und Unterwuchs mit Licht- und Schattenbereichen eines zu klassifizierenden Waldtyps) in dem pro Pixel gemessenen spektralen Signal weitgehend integriert sind. Das erhöht die Homogenität innerhalb der Klassen, wodurch ihre Trennbarkeit verbessert wird. Andererseits entstehen in den Grenzbereichen zwischen verschiedenen Klassenarealen Mischpixel, was zu Fehlklassifizierungen führen kann. In heteroge-nen, stark fragmentierten Landschaften, wie man sie typischerweise in kleinbäuerlich genutzten tro-pischen Gebirgen findet, ist der Anteil der Mischpixel so hoch, dass die Möglichkeiten zu einer detaillierten Klassifizierung sehr beschränkt sind bzw. die Klassifizierungsgenauigkeit sehr gering wird.

Für das obere Einzugsgebiet des Río Yaque del Norte wurde eine 'klassische' Maximum-Likeli-hood-Klassifizierung durchgeführt, bei der die multispektrale Information von sechs Spektral-kanälen genutzt wurde, um jedes Pixel einer von 14 Landbedeckungsklassen (davon vier Wald-klassen und eine Agroforst-Klasse) zuzuordnen. Das Maximum-Likelihood-Verfahren ist eine überwachte Klassifizierung. Die dafür verwendeten Trainingsgebiete beruhten auf vor Ort aufge-nommenen Geländedaten ('*ground truth*'). Das Klassifizierungsergebnis wurde durch eine 3×3 Modalfilterung und die Reklassifizierung einiger Pixel mit Hilfe der Höheninformation aus einem digitalen Geländemodell nachbearbeitet. Dies führte zwar zu einer Karte, in der die Hauptver-breitungsgebiete der Landbedeckungstypen weitgehend richtig wiedergegeben werden (*plate 43*), aber die Klassifizierungsgenauigkeit, die mit Hilfe eines Referenzdatensatzes aus 304 Punkten abgeschätzt wurde, lag nur bei 40 %. Nach Aggregierung der Landbedeckungsklassen in fünf Gruppen (davon nur eine allgemeine Waldklasse) lag die Genauigkeit bei 61 %.

Für genauere und detailliertere Klassifizierungen ist also die Verwendung anderer Daten und/oder anderer Methoden notwendig. Hierzu wurden die Nutzungsmöglichkeiten von IKONOS-Daten für Teile des Einzugsgebietes analysiert. Das Haupttestgebiet für die Verarbeitung der hochauflösenden

Satellitendaten umfasst das zentrale und westliche Reservat Ebano Verde und das Río Jimenoa-Tal in der westliche Pufferzone des Reservats (*figure 9*). Es ist ein Beispiel für eine heterogene, kleinräumig strukturierte tropische Berglandschaft mit natürlichen Waldflächen, Aufforstungsbereichen, verbuschten Flächen (*Matorral*) und kleinbäuerlicher Landwirtschaft.

Die hohe räumliche Auflösung der IKONOS-Daten führt zu einem geringeren Anteil an Mischpixeln. Andererseits führt sie auch zu einer mangelnden Integrierung der konstituierenden Elemente vieler Zielklassen. Dadurch entsteht eine hohe Variabilität der Spektralwerte innerhalb der Klassen. Dies ist ein Nachteil für die automatisierte pixelweise Klassifizierung, da sich die Klassenbereiche im Merkmalsraum dadurch stärker überschneiden. Für Transekte durch einige Klassenausschnitte in den panchromatischen Daten wurden experimentelle Variogramme erstellt, um Informationen über die räumliche Beziehung zwischen den Grauwerten zu gewinnen. Für die Waldklassen wurde die maximale Semivarianz bei einer Entfernung (*lag*) von durchschnittlich 8 m (4 bis 14 m) erreicht. Mindestens so grob sollte also die räumliche Auflösung sein, damit die Pixelwerte repräsentativ für ihre Klassen werden.

Eine pixelweise Maximum-Likelihood-Klassifizierung der vier IKONOS-Multispektralkanäle (4 m Auflösung) für das östliche Testgebiet mit 13 Klassen (Nebelwald, Sekundärwald, offener und geschlossener Kiefernwald, Uferwald, Palmenwald, Agroforst, *Matorral*, *Calimetal*, Grasland, Ackerfrüchte, bloßer Boden/Gestein, Wasser) resultierte in einer anhand einer Referenz-Stichprobe geschätzten Klassifizierungsgenauigkeit von nur 41 %. Dieses ohne eine räumliche Integrierung der Multispektraldaten erzielte Ergebnis ist nicht signifikant besser als das einer Landsat-Klassifizierung für das gleiche Gebiet.

Um die Spektralwerte der Pixel repräsentativer für die Klassen, denen sie angehören, zu machen, wurden drei Methoden zur räumlichen Integrierung der Multispektraldaten getestet:
- Reduktion der räumlichen Auflösung auf 8, 12 und 16 m durch Mittelwertbildung in Gruppen von 2 × 2, 3 × 3 und 4 × 4 Pixeln (Block-Aggregierung);
- Bildung gleitender Mittelwerte durch Tiefpassfilterung (3×3, 5×5 und 7×7 Mittelwert-filter);
- Bildsegmentierung (Gruppierung zusammenhängender Pixel nach Einheitlichkeitskriterien) und Mittelwertbildung innerhalb der generierten Bildsegmente.

Die so bearbeiteten Multispektraldaten wurden dann als Eingangskanäle für Klassifizierungen benutzt. Die Klassifizierungsergebnisse (außer denen der segmentweisen Klassifizierungen) wurden anschließend zusätzlich modalgefiltert. Das heißt, dass die in einer Pixelnachbarschaft (3×3, 5×5 und 7×7 Pixel große Filtermatrizen) am häufigsten vorkommende Klasse dem zentralen Pixel als Ergebnisklasse zugewiesen wurde. Dadurch kommt es zu einer weiteren räumlichen Integrierung der pixelweisen Information.

Diese räumliche Integrierung führte zu einer Verringerung der spektralen Variabilität innerhalb der Klassen. Alle getesteten Arten der räumlichen Integration führten auch zu erhöhten Klassifizierungsgenauigkeiten. Am erfolgreichsten war die 3×3 Tiefpassfilterung in Kombination mit einer 7×7 Modalfilterung der Klassifizierungsergebnisse. Dies führte zu einer Gesamtgenauigkeit von 64 % für die Klassifizierung der vier IKONOS-Multispektralkanäle mit 13 Klassen.

Die räumliche Integrierung verringert aber natürlich die detaillierte räumliche Information, die dank der hohen räumlichen Auflösung in IKONOS-Daten enthalten ist. Diese Information sollte jedoch auch in einer automatisierten Klassifizierung nicht ungenutzt bleiben. Wenn die Auflösung der Fernerkundungsdaten so hoch ist, dass die Elemente der Zielklassen nicht in einzelnen Pixeln integriert werden (während gleichzeitig die zu klassifizierenden Objekte wesentlich größer sind als die Pixel), bedeutet das auch, dass sich innerhalb der Zielkassen im Bild Texturen (strukturelle Eigenschaften der Oberflächen) erkennen lassen. Bei der visuellen Interpretation hochauflösender Fernerkundungsdaten (z.B. Luftbildinterpretation) spielt neben der spektralen Information (Grau- und Farbtöne) auch die Textur der Flächen eine wichtige Rolle, d.h. Eigenschaften wie Kontrast, Grobkörnigkeit und Rauhigkeit oder Homogenität.

Um die Textur in einer automatisierten Klassifizierung digitaler Bilddaten zu nutzen, müssen Textur-Parameter anhand der Grauwerte im Bild errechnet werden. Dies geschieht in der fernerkundlichen Bildverarbeitung in der Regel über die Berechnung von statistischen Werten, die etwas über die räumliche Grauwertverteilung und die Beziehungen zwischen Grauwerten in quadratischen Pixelnachbarschaften aussagen. Der innerhalb einer Nachbarschaft (in einer Filtermatrix) errechnete Wert wird dann jeweils dem zentralen Pixel zugewiesen. Die GLCM (*Grey-Level Co-Occurrence Matrix*) Textur-Parameter sind statistische Texturmaße zweiter Ordnung. Sie basieren auf einer Matrix, die die relative Häufigkeit von Grauwertkombinationen für benachbarte Pixel wiedergibt (Haralick, Shanmugam & Dinstein 1973). Auf der Basis des panchromatischen IKONOS-Kanals wurden (mit einer Filtergröße von 15×15 Pixeln) acht GLCM-Texturparameter errechnet. Außerdem wurde die 'lokale Varianz' als statistisches Texturmaß erster Ordnung errechnet, indem die Varianz innerhalb von 9×9 und 15×15 Pixel großen Filter-Matrizen errechnet wurde. Die resultierenden zehn Texturbilder mit 1 m Auflösung wurden einer Korrelationsanalyse unterzogen und auf fünf relativ gering korrelierende Textur-Bildkanäle reduziert. Die räumliche Auflösung dieser Texturdaten wurde durch *Resampling* an die der Multispektraldaten angeglichen und die Daten in gemeinsamen Dateien integriert.

Die Anzahl der Eingangskanäle für die Maximum-Likelihood-Klassifizierung wurde auf sieben begrenzt. Anhand einer Maximierung der durchschnittlichen ‚Transformed Divergence' zwischen Klassenpaaren wurde eine Kombination von sieben der neun Bildkanäle (vier spektrale und fünf Texturkanäle) ausgewählt. Die resultierenden Datensätze bestanden aus vier Multispektralkanälen

unterschiedlicher räumlicher Integrierung und drei GLCM-Texturkanälen (GLCM Entropie, GLCM Standard-abweichung und GLCM Kontrast).

Die Trennbarkeit der Klassen mit Hilfe der integrierten Datensätze wurde mit der Trennbarkeit ohne Textur (nur über die Multispektralkanäle) verglichen. Als Maß für die Trennbarkeit von Klassenpaaren wurde die ‚Bhattacharyya-Distanz' errechnet. Die Trennbarkeit erhöhte sich durch die Einbeziehung der Texturkanäle für alle Klassenpaare. Besonders stark erhöhte sich die Bhattacharyya-Distanz zwischen offenem Kiefernwald und Grasland bzw. *Matorral* (da die krautige oder Strauchvegetation, die den Unterwuchs zwischen den Kiefern bildet, das rein spektrale Signal bei offenem Kiefernwald oft dominiert), zwischen *Matorral* und weiteren Waldklassen sowie zwischen Palmenwald und laubtragendem Uferwald (aufgrund der unterschiedlichen Struktur der Kronendächer) (*tables 19* und *20*). Die Klassifizierungsgenauigkeit erhöhte sich erwartungsgemäß ebenfalls durch Einbeziehung der Texturkanäle in die Klassifizierungen. Palmenwald, Sekundärwald und *Matorral* gehören zu den Klassen, deren Klassifizierungsgenauigkeit davon am meisten profitierte.

Das beste Klassifizierungsergebnis, das für 13 Klassen nur unter Verwendung von IKONOS-Daten und aus ihnen abgeleiteten Informationen für das Testgebiet erzielt wurde, stimmte zu 70,4 % mit den Referenzdaten überein. Es war das Ergebnis einer Maximum-Likelihood-Klassifizierung eines Datensatzes aus vier 3×3 mittelwertgefilterten Multispektralkanälen und drei GLCM-Textur-kanälen mit 4 m Auflösung, mit anschließender 7×7 Modalfilterung. Aber auch die Klassifizierung des Datensatzes aus Texturdaten und nicht räumlich integrierten Multispektraldaten führte bei anschließender 7×7 Modalfilterung zu einer Klassifizierungsgenauigkeit von 70 %. Hier wurde die nötige räumliche Integrierung der hochaufgelösten Daten offensichtlich durch die Texturparameter (errechnet in 15 m × 15 m großen Filtermatritzen) und die Modalfilterung erreicht.

Wegen der geringen spektralen Auflösung der IKONOS-Daten, die keine spektrale Information von jenseits des nahen Infrarots beinhalten, wurden die IKONOS-Daten mit zusätzlichen Landsat-Multispektralkanälen integriert. Außerdem wurde die räumliche Information aus den IKONOS-Daten (in Form der Texturkanäle) mit den Landsat-Daten kombiniert. Mit diesen beiden integrierten Datensätzen konnten aber die Ergebnisse, die nur mit den IKONOS-Daten erzielt worden waren, nicht übertroffen werden. Die Klassifizierungsgenauigkeiten für Datensätze, die Landsat-Multi-spektraldaten beinhalteten, lagen immer unter 60 %. Die geringere räumliche Auflösung der Landsat-Daten führte im räumlich sehr heterogenen Testgebiet zu einem großen Anteil von Mischpixeln und begrenzte so, trotz der besseren spektralen Auflösung, die Klassifizierungsgenauigkeit.

An zusätzlichen Geodaten stand ein digitales Geländemodell (DGM) mit einer Rasterweite von 50 m zur Verfügung. Durch *Kriging* wurde ein Höhenmodell mit 8 m Rasterweite erstellt. Drei

daraus abgeleitete topographische Modelle wurden als zusätzliche Bildkanäle mit den IKONOS-Daten bei 8 m räumlicher Auflösung integriert. Die Verwendung dieser Modelle als zusätzliche Variablen in den Klassifizierungen führte aber nicht zu einer signifikanten Verbesserung der Klassifizierungsgenauigkeiten, was unter anderem mit der mangelnden Genauigkeit des verfügbaren DGMs zu begründen ist. Im relativ kleinen Testgebiet konnten die ungenauen Höhen- und Hangneigungsdaten auch nicht sinnvoll für eine Nachbearbeitung der Klassifizierungs-ergebnisse eingesetzt werden (im Gegensatz zum Einsatz des Höhenmodells für die Nachbearbeitung der Landsat-Klassifizierung für das gesamte obere Einzugsgebiet).

Das Maximum-Likelihood-Verfahren ist die optimale überwachte Klassifizierungsmethode unter der Voraussetzung, dass die zu klassifizierenden Daten für die definierten Klassen normalverteilt sind. Dies traf bei den meisten Klassen im Testgebiet sowohl für die Multispektraldaten als auch für die Texturdaten zu, für die topographischen Modelle (abgesehen von der Hangneigung) allerdings nicht. Deshalb wurden neben dem Maximum-Likelihood-Verfahren auch nicht-parametrische Klassifizierungsmethoden (die nicht auf Annahmen über die Verteilung der Daten basieren) angewendet, um die kombinierten Datensätze zu klassifizieren. Es konnten aber weder mit einem *k-Nearest-Neighbour*-Verfahren noch mit ,künstlichen Neuronalen Netzen' bessere Ergebnisse erzielt werden als mit dem Maximum-Likelihood-Verfahren.

Insgesamt war für eine detaillierte Klassifizierung des Testgebiets eine Klassifizierungsgenauigkeit (im Sinne einer Übereinstimmung mit den Klassen, die 583 Referenzpunkten zugewiesen worden waren) von wesentlich über 70 % nicht zu erreichen. Bei der Bewertung dieser 'harten' Genauigkeit muss beachtet werden, dass der Referenzdatensatz eine Stichprobe von Punkten darstellt, die über das gesamte Gebiet verteilt wurden, ohne Grenzbereiche zwischen Klassenarealen auszuschließen. Den Testpunkten wurden Referenzklassen zugewiesen, die bei einem Teil der Punkte durch die Feldarbeit im dortigen Gelände bekannt waren und die ansonsten hauptsächlich über die visuelle Interpretation von Luftbildern und von den IKONOS-Bildern selbst bestimmt wurden. Die Refe-renzdaten stellen also eine unabhängige Klassifizierung dar, die auch nicht hundertprozentig fehlerfrei sein kann. Dies ist bei Genauigkeitsanalysen generell zu beachten. Dazu kommen im Testgebiet viele graduelle Klassenübergänge und kleinräumige Vermischungen oder Einschlüsse (*figure 41*), die dazu führen, dass es (nicht nur entlang linearer Grenzen) Gebiete gibt, die nicht eindeutig zu einer bestimmten Klasse gehören, bzw. deren Zuordnung zu mehreren Vegetations-typen 'nicht ganz falsch' wäre. Diese Unschärfe (*fuzziness*) in den Vegetationsklassen lässt sich durch eine unscharfe (*fuzzy*) Genauigkeitsanalyse berücksichtigen (Woodcock & Gopal 2000). Dies wurde anhand einer Klassifizierung getestet, mit dem Ergebnis, dass 85 % der Klassenzuweisungen 'absolut richtig', 'gut' oder zumindest 'akzeptabel' waren. Das 'harte' Ergebnis einer Maximum-Likelihood-Klassifizierung lässt sich auch ,aufweichen', indem z.B. die *A-Posteriori*-Wahrschein-lichkeit für die zugewiesenen Klassen berechnet wird. So lassen sich weitere Informationen und Interpretationshilfen (über eine ,harte' thematischen Karte hinaus) gewinnen.

Es konnte gezeigt werden, dass Klassifizierungsfehler und -unsicherheiten überproportional in Bereichen in der Nähe von Grenzen zwischen Landbedeckungsklassen auftreten. Die Grenzeffekte spielen eine größere Rolle bei Datensätzen mit stärkerer räumlicher Integrierung (mehr Mischpixel) und mit Texturmerkmalen (da die 15 m × 15 m große Filtermatrix mehrere Klassenareale einschließen kann, so dass z.T. nicht die Textur innerhalb einer Klasse, sondern die zwischen mehreren Klassen berechnet wird). Die Verstärkung der Grenzeffekte durch räumliche Integrierung und Einbeziehung von Texturdaten setzt den positiven Effekten dieser Methoden Grenzen.

Gute Ergebnisse wurden bei der Kartierung des Nebelwaldes erzielt, und auch die meisten anderen Waldtypen ließen sich mit relativ hohen Genauigkeiten klassifizieren. Eine Ausnahme bildet der 'offene Kiefernwald'. Diese Klasse tritt im östlichen Testgebiet hauptsächlich in Form von lockeren Kieferngruppen auf, die schwer genau von ihrer Umgebung (die ihrem Unterwuchs entspricht, z.B. Gräser und Farne) abzugrenzen sind. Problematisch ist auch die Trennbarkeit von Agroforst und Wald, obwohl die Einbeziehung von Textur die Trennbarkeit (ebenso wie beim offenen Kiefernwald) verbessern konnte.

Insgesamt konnte mit Hilfe der hochauflösenden IKONOS-Daten, sofern bei ihrer Verarbeitung ihre räumlichen Eigenschaften berücksichtigt und genutzt wurden, eine wesentlich genauere und detailliertere Kartierung der Wald- und sonstigen Landbedeckungsklassen erreicht werden als mit den Landsat-Daten. Allerdings sind diese für das Testgebiet analysierten Methoden nicht ohne weiteres auf wesentlich größere Regionen übertragbar. Eine detaillierte Klassifizierung des gesamten oberen Einzugsgebietes des Río Yaque del Norte mit IKONOS-Daten würde u.a. eine aufwändige Vorverarbeitung von mindestens zwölf IKONOS-Bildern und auch die Existenz einer großen Menge an Geländedaten aus dem gesamten Einzugsbereich voraussetzen. Für regionale Kartierungen können also Satellitendaten mittlerer Auflösung weiterhin die einzige praktikable Datenquelle sein, auch wenn damit in heterogenen tropischen Gebirgsbereichen nur relativ grobe und ungenaue Karten erstellt werden können. Hochauflösende Satellitendaten bieten sich in erster Linie für die Kartierung kleinerer Gebiete an, in denen ein spezielles Interesse an detaillierten Landbedeckungsinformationen besteht, z.B. zur Kartierung und Überwachung bedrohter bzw. geschützter Vegetationstypen.

References

Literature and Internet Sources

ACHARD, F., H.D. EVA, H.-J. STIBIG, P. MAYAUX, J. GALLEGO, T. RICHARDS & J.-P. MALINGREAU (2002): Determination of deforestation rates of the world's humid tropical forests. – Science 297 (5583): 999-1002.

ACQWEATHER.COM: Meteorologia, Clima y Desastres. Santo Domingo, Dominican Republic. URL (1.2.2005): http://www.acqweather.com

AHLQUIST, O., J. KEUKELAAR & K. OUKBIR (2000): Rough classification and accuracy assessment. – International Journal of Geographical Information Science 14 (5): 475-496.

AHMAD, R., F.N. SCATENA & A. GUPTA (1993): Morphology and sedimentation in Caribbean montane streams: examples from Jamaica and Puerto Rico. – Sedimentary Geology 85: 157-169.

ALDRICH, M. (2000): Tropical montane cloud forests. In: Price, M.F. & N. Butt (eds.): Forests in sustainable mountain development: a state of knowledge report for 2000. – IUFRP research series 5. CABI Publishing, Wallingford, UK. Pp. 390-397.

ALLEN, T.R. (2000): Topographic normalization of Landsat Thematic Mapper data in three mountain environments. – Geocarto International 15 (2): 13-19.

ALVES, D.S., J.L.G. PEREIRA, C.L. DE SOUSA, J.V. SOARES & F. YAMAGUCHI (1999): Characterizing landscape changes in central Rondônia using Landsat TM imagery. – International Journal of Remote Sensing 20 (14): 2877-2882.

AMARSAIKHAN, D. & T. DOUGLAS (2004): Data fusion and multisource image classification. – International Journal of Remote Sensing 25 (17): 3529-3539.

ANYS, H. & D-C. HE (1995): Evaluation of textural and multipolarization radar features for crop classification. – IEEE Transactions on Geoscience and Remote Sensing 33 (5): 1170-1181.

APLIN, P., P.M. ATKINSON & P.J. CURRAN (1999): Fine spatial resolution simulated satellite sensor imagery for land cover mapping in the United Kingdom. – Remote Sensing of Environment 68: 206-216.

ARAI, K. (1992): TM classification using local spectral variability. – Geocarto International 7 (4): 37-45.

ARECES-MALLEA, A.E., et al. (1999): Caribbean Vegetation Mapping Report. The Nature Conservancy, Washington, D.C., 166 p. URL (16.03.2004): http://edcintl.cr.usgs.gov/tnc/products/report/table.html

ARMENTEROS RIUS, E. (1989): Forestry's Zero Hour in the Dominican Republic. PROGRESSIO Series, No. 9, Santo Domingo.

ARORA, M.K. & S. MATHUR (2001): Multi-source classification using artificial neural network in a rugged terrain. – Geocarto International 16 (3): 37-44.

ASNER, G.P., M. KELLER, R. PEREIRA & J.C. ZWEEDE (2002): Remote Sensing of selective logging in Amazonia. Assessing limitations based on detailed field observations, Landsat ETM+, and textural analysis. – Remote Sensing of Environment 80: 483-496.

ASNER, G.P., M.M.C. BUSTAMANTE, A.R. TOWNSEND (2003): Scale dependence of biophysical structure in deforested area bordering the Tapajós National Forest, Central Amazon. – Remote Sensing of Environment 87 (4): 507-520.

ATKINSON, P.M. & P. APLIN (2004): Spatial variation in land cover and choice of spatial resolution for remote sensing. International Journal of Remote Sensing 25 (18): 3687-3702.

ATKINSON, P.M., G.M. FOODY, P.J. CURRAN & D.S. BOYD (2000): Assessing the ground data requirements for regional scale remote sensing of tropical forest biophysical properties. – International Journal of Remote Sensing 21 (13&14): 2571-2587.

ATTA-KRAH, K. & TANG YA (2000): Agroforestry in sustainable mountain development. In: Price, M.F. & N. Butt (eds.): Forests in sustainable mountain development: a state of knowledge report for 2000. – IUFRP research series 5. CABI Publishing, Wallingford, UK. Pp. 270-284.

ATZBERGER, C. & M. SCHLERF (2002): Automatisierte Bestimmung der Bestockungsdichte in Nadelwäldern aus räumlich hochauflösenden Ortholuftbildern. – Photogrammetrie – Fernerkundung – Geoinformation 2002 (3): 171-180.

BAATZ, M. & A. SCHÄPE (2000): Multiresolution segmentation: an optimization approach for high quality multi-scale image segmentation. – PCI technical papers.
URL (1.12.2003): http://www.agit.at/papers/2000/baatz_FP_12.pdf

BAATZ, M., U. BENZ, S. DEHGHANI, M. HEYNEN, A. HÖLTJE, P. HOFFMANN, I. LINGENFELDER, M. MIMLER, M. SOHLBACH, M. WEBER & G. WILLHAUCK (2002): eCognition User Guide 3. Definiens. Publisher: PCI Geomatics, Toronto.

BAULIES, X. & X. PONS (1995): Approach to forestry inventory and mapping by means of multi-spectral airborne data. – International Journal of Remote Sensing 16 (1): 61-80.

BEAULIEU, J.-M. (2004): Utilisation of contour criteria in micro-segmentation of SAR images. – International Journal of Remote Sensing 25 (17): 3497-3512.

BEER, J., C. HARVEY, M. IBRAHIM, J.M. HARMAND, E. SOMARRIBA & F. JIMÉNEZ (2003): Servicios ambientales de los sistemas agroforestales. – Agroforestería en las Americas 10 (37-38): 80-87.

BEHERA, M.D., S.P.S. KUSHWAHA & P.S. ROY (2001): Forest vegetation characterization and mapping using IRS-1C satellite images in Eastern Himalaya region. – Geocarto International 16 (3): 53-62.

BENEDIKTSON, J.A., P.H. SWAIN & O.K. ERSOY (1990): Neural network approaches versus statistical methods in classification of multisource remote sensing data. – IEEE Transactions on Geoscience and Remote Sensing 28 (4): 540-552.

BIGGS, P. (1996): Application of modern inventory techniques in the jarrah forests of Western Australia. New thrusts in forest inventory. *In* Proceedings of the Subject Group S4.02-00 "Forest Resource Inventory and Monitoring" and Subject Group S4.12-00 "Remote Sensing Technology" : IUFRO XX World Congress, 6-12 August 1995, Tampere, Finland. Vol. I. EFI Proceedings No. 7, pp. 105-109.

BØCHER, P.K., K.R. MCCLOY & A.S. BARFOD (2003): Average local variance - revisited. *In* Proceedings of the Annual Conference of the Remote Sensing and Photogrammetric Society. Scales and Dynamics in Observing the Environment. 10-12 September 2003. Nottingham, UK. Unpaginated CD-ROM.

BOLAY, E. (1997): The Dominican Republic – A country between rain forest and desert. Bonn.

BROGAARD, S. & R. ÓLAFSDÓTTIR (1997): Ground-truths or ground-lies? – Lund Electronic Reports in Physical Geography No. 1, Oct. 1997.
URL (20.03.2005): http://www.natgeo.lu.se/Publikationer/Lerpg/1/1Article.htm

BRONDOZIO, E., E. MORAN. P. MAUSEL & Y. WU (1996): Land cover in the Amazon estuary: Linking of the Thematic Mapper with botanical and historical data. – Photogrammetric Engineering & Remote Sensing 62 (8): 921-929.

BRÖTJE, A. (2003): Combining multiscale spectral and textural data for tropical mountain forest classification. *In* Proceedings of the Annual Conference of the Remote Sensing and Photogrammetry Society. Scales and Dynamics in Observing the Environment. 10-12 September 2003. Nottingham, UK. Unpaginated CD-ROM.

BROWN, D.G. (1998): Classification and boundary vagueness in mapping presettlement forest types. – International Journal of Geographical Information Science 12 (2): 105-129.

BRUNIQUEL-PINEL, V. & J.P. GASTELLU-ETCHEGORRY (1998): Sensitivity of texture of high resolution images of forest to biophysical and acquisition parameters. – Remote Sensing of Environment 65: 61-85.

BUBB, P., M. ALDRICH & J. SAYER (2002): Tropical montane cloud forests – time for action. – Unasylva 53 (208): 36-37.

CAMPBELL (1996): Introduction to Remote Sensing. Second Edition. Taylor & Francis, London.

CAO, C. & N.S. LAM (1997): Understanding the scale and resolution effects in remote sensing and GIS. *In*: D.A. Quattrochi & M.F. Goodchild (eds.): Scale in remote sensing and GIS. CRC Press, Boca Raton. Pp. 57-72.

CARR, J.R. & F.P. MIRANDA (1998): The semivariogram in comparison to the co-occurrence matrix for classification of image texture. – IEEE Transactions on Geoscience and Remote Sensing 36 (6): 1945-1952.

CASTRO, K.L., G.A. SANCHEZ-AZOFEIFA & B. RIVARD (2003): Review article. Monitoring secondary tropical forests using space-borne data: implications for Central America. – International Journal of Remote Sensing 24 (9): 1853-1894.

CHARDÓN, C.E. (1941): Los pinares de la República Dominicana. – The Caribbean Forester 2 (3): 120-131.

CHEN, D., D.A. STOW & P. GONG (2004): Examining the effect of spatial resolution and texture window size on classification accuracy: an urban environment case. – International Journal of Remote Sensing 25 (11): 2177-2192.

CHENG, T. (2002): Fuzzy Objects: Their Changes and Uncertainties. – Photogrammetric Engineering & Remote Sensing 68 (1): 41-49.

CHENG, T, M. MOLENAAR & H. LIN (2001): Formalizing fuzzy objects from uncertain classification results. – International Journal of Geographical Information Science 15 (1): 27-42.

CIFERRI, R. (1936): Studio geobotanico dell'Isola Hispaniola (Antille). – Atti dell'Istituto Botanico "Giovanni Briosi" e Laboratorio Crittogramico Italiano, Vol. VIII, Serie IV^a: 1-336.

CINGOLANI, A.M., D. RENISON, M.R. ZAK & M.R. CABIDO (2004): Mapping vegetation in a heterogeneous mountain rangeland: an alternative method to define and classify land-cover units. – Remote Sensing of Environment 92: 84-97.

CLARK, D.B., J.M. READ, M.L. CLARK, A. MURILLO CRUZ, M. FALLAS DOTTI & D.A. CLARK (2004): Application of 1-m and 4-m resolution satellite data to ecological studies of tropical rain forest. – Ecological Applications 14 (1): 61-74.

COBURN, C.A. & A.C.B. ROBERTS (2004): A multiscale texture analysis procedure for improved forest stand classification. – International Journal of Remote Sensing 25 (20): 4287-4308.

COHEN, J. (1960): A coefficient of agreement for nominal scales. – Educational and Psychological Measurement 20 (1): 37-46.

COLBY, J.D. & P.L. KEATING (1998): Land cover classification using Landsat TM imagery in the tropical highlands: the influence of anisotropic reflectance. – International Journal of Remote Sensing 19 (8): 1479-1500.

COLLINS, M.J., C. DYMOND & E.A. JOHNSON (2004): Mapping subalpine forest types using networks of nearest neighbour classifiers. – International Journal of Remote Sensing 25 (9): 1701-1721.

COLOMBO, R., D. BELLINGERI, D. FASOLINI & C.M. MARINO (2003): Retrieval of leaf area index in different vegetation types using high resolution data. – Remote Sensing of Environment 86: 120-131.

CONGALTON, R.G. (1991): A review of assessing the accuracy of classifications of remotely sensed data. – Remote Sensing of Environment 37: 35-46.

CONSORCIO INGENIERÍA CAURA - ESRI - DESAGRO (2002): Plan de Accion Territiorial. - Secretariado Técnico de la Presidencia, unidad Ejecutora Sectorial del Sub-Programa de Prevención de Desastres (UES del PMR), Componente 2: Instrumentos de Gestión Territorial y de Recursos Naturales.
URL (16.02.2005):
http://www.uespmr.gov.do/comp_2/doctos_2/Plan%20de%20accion/plan%20de%20accion.pdf

COOPS, N. & D. CULVENOR (2000): Utilizing local variance of simulated high spatial resolution imagery to predict spatial pattern of forest stands. – Remote Sensing of Environment 71: 248-260.

COSMOPOULOS, P. & D.J. KING (2004): Temporal analysis of forest structural condition at an acid mine site using multispectral digital camera imagery. – International Journal of Remote Sensing 25 (12): 2259-2275.

COSTA, M.P.F. (2004): Use of SAR satellites for mapping zonation of vegetation communities in the Amazon floodplain. – International Journal of Remote Sensing 25 (10): 1817-1835.

COULTER, L., D. STOW, A. HOPE, J. O'LEARY, D. TURNER, P. LONGMIRE, S. PETERSON & J. KAISER (2000): Comparison of high spatial resolution imagery for efficient generation of GIS vegetation layers. – Photogrammetric Engineering & Remote Sensing 66 (11): 1329-1335.

CURRAN, P.J. (1988): The semivariogram in remote sensing: an introduction. – Remote Sensing of Environment 24: 493-507.

CUSHNIE, J.L. (1987): The interactive effect of spatial resolution and degree of internal variability within land-cover types on classification results. – International Journal of Remote Sensing 8 (1): 15-29.

DARROW, W.K. & T. ZANONI (1991): Hispaniolan Pine (*Pinus occidentalis* Swartz) a little known sub-tropical pine of economic potential. – Commonwealth Forestry Review 69 (2): 133-146.

DAVIS, B.A. & J.R. JENSEN (1998): Remote sensing of mangrove biophysical characteristics. – Geocarto International 13 (4): 55-64.

DAVIS, C.H. & X. WANG (2003): Planimetric accuracy of IKONOS 1 m panchromatic orthoimage products and their utility for local government GIS basemap applications. – International Journal of Remote Sensing 24 (22): 4267-4288.

DEBEIR, O., I. VAN DEN STEEN, P. LATINNE, P. VAN HAM & E. WOLFF (2002): Textural and Contextual Land-Cover Classification Using Single and Multiple Classifier Systems. – Photogrammetric Engineering & Remote Sensing 68 (6): 597-605.

DIAL, G., H. BOWEN, F. GERLACH, J. GRODECKI & R. OLESZCZUK (2003): IKONOS satellite, imagery, and products. – Remote Sensing of Environment 88 (1): 23-36.

DIKSHIT, O. & D.P. ROY (1996): An empirical investigation of image resampling effects upon the spectral and textural supervised classification of a high spatial resolution multispectral image. – Photogrammetric Engineering & Remote Sensing 62 (9): 1085-1092.

DOBSON, M.C., F.T. ULABY, L.E. PIERCE, T.L. SHARIK, K.M. BERGEN, J. KELLNDORFER, J.R. KENDRA, E. LI, Y.C. LIN, A. NASHASHIBI, K. SARABANDI & P. SIQUEIRA (1995): Estimation of forest biophysical characteristics in northern Michigan with SIR-C/X-SAR. – IEEE Transactions on Geoscience and Remote Sensing 33 (4): 877-895.

DOBSON, M.C., L.E. PIERCE & F.T. ULABY (1996): Knowledge-based land-cover classification using ERS-1/JERS-1 SAR composites. – IEEE Transactions on Geoscience and Remote Sensing 34 (1): 83-99.

DOLAN, J., P. MANN, R. DE ZOETEN, C. HEUBECK & J. SHIROMA (1991): Sedimentologic, stratigraphic, and tectonic synthesis of Eocene-Miocene sedimentary basins, Hispaniola and Puerto Rico. In: Mann, P., G. Draper & J.F. Lewis (eds.): Geologic and tectonic development of the North America-Caribbean plate boundary in Hispaniola. – Geological Society of America Special Paper 262, Boulder, Colorado. Pp. 217-240.

DOTZAUER, H. (1993): The political and socio-economic factors causing forest degradation in the Dominican Republic. Rural Development Forestry Network Paper 16d.
URL (1.10.03): http://www.odifpeg.org.uk/publications/rdfn/16/rdfn-16d.pdf

DRAPER, G. & J.F. LEWIS (1991): Metamorphic belts in central Hispaniola. In: Mann, P., G. Draper & J.F. Lewis (eds.): Geologic and tectonic development of the North America-Caribbean plate boundary in Hispaniola. – Geological Society of America Special Paper 262, Boulder, Colorado. Pp. 29-45.

DUBAYA, R.O. & J.B. DRAKE (2000): Lidar remote sensing for forestry. – Journal of Forestry, June 2000: 44-46.

DURLAND, W.D. (1922): The forests of the Dominican Republic. – The Geographical Review 12: 206-222.

DYMOND, C.C. & E.A. JOHNSON (2002): Mapping vegetation spatial patterns from modelled water, temperature and solar radiation gradients. – ISPRS Journal of Photogrammetry and Remote Sensing 57: 69-85.

EHLERS, M, M. GÄHLER & R. JANOWSKY (2003): Automated analysis of ultra high resolution remote sensing data for biotope type mapping: new possibilities and challenges. – ISPRS Journal of Photogrammetry and Remote Sensing 57: 315-326.

ERHART, M. (1995): Tropenwaldschutz durch Bodenbesitzreform und nachhaltige Bewirtschaftung: der Fall Dominikanische Republik. Metropolis-Verlag, Marburg, Hochschulschriften Bd. 19.

ERICKSON, T. (1940): El servicio forestal en la República Dominicana. – The Caribbean Forester 1 (2): 13-16.

ERIKSON, J.P., J.L. PINDELL, G.D. KARNER, L.J. SONDER, E. FULLER & L. DENT (1998): Neogene sedimentation and tectonics in the Cibao Basin and Northern Hispaniola: An example of basin evolution near a strike-slip-dominated plate boundary. – The Journal of Geology 106: 473-494.

ERLER, N. (2004): GIS- und fernerkundungsgestützte Bewertung von „Natural Hazards" im oberen Einzugsgebiet des Río Yaque del Norte (Dominikanische Republik). – Reihe Erdsicht - Einblicke in geographische und geoinformationstechnische Arbeitsweisen Vol. 3 (ed. M. Kappas), ibidem-Verlag, Stuttgart.

EVELYN, O.B. & R. CAMIRAND (2003): Forest cover and deforestation in Jamaica: an analysis of forest cover estimates over time. – International Forestry Review 5 (4): 354-363.

FAO (2001): Global Forest Resources Assessment 2000 Main Report. FAO Forestry Paper 140. Rome.
(URL: (02.02.2004): http://www.fao.org/forestry/foris/webview/forestry2/index.jsp?siteId=2921&sitetreeId=7947&langId=1&geoId=0)

FAO (31.12.2000): Forestry, Dominican Republic.
URL: http://www.fao.org/forestry/fo/country/index.jsp?lang_id=1&geo_id=187

FAOSTAT DATA (2004): FAO on-line statistical databases. URL (30.01.2005): http://apps.fao.org/faostat/

FAO-UNESCO (1975): Soil map of the world. Volume III, Mexico and Central America. Unesco, Paris.

FAO-UNESCO (1990): Soil map of the world. Revised Legend. Reprinted with corrections. FAO, Rome.

FEIDEN, K. (2004): GIS-gestützte Analyse der zeitlichen und räumlichen Verteilung der Niederschlagsjahressummen (1961-1990) in der Dominikanischen Republik. – Reihe Erdsicht - Einblicke in geographische und geoinformationstechnische Arbeitsweisen Vol. 2 (ed. M. Kappas), ibidem-Verlag, Stuttgart.

FELICÍSIMO, A.M., E. FRANCÉS, J.M. FERNÁNDEZ, A. GONZÁLEZ-DIEZ & J. VARAS (2002): Modeling the Potential Distribution of Forests with a GIS. – Photogrammetric Engineering & Remote Sensing 68 (5): 455-461.

FERREIRA, L.G. & A.R. HUETE (2004): Assessing the seasonal dynamics of the Brazilian Cerrado vegetation through the use of spectral vegetation indices. – International Journal of Remote Sensing 25 (10): 1837-1860.

FERRO, C.J.S. & T.A. WARNER (2002): Scale and Texture in Digital Image Classification. – Photogrammetric Engineering & Remote Sensing 68 (1): 51-63.

FLORINSKY, I.V. (1998): Combined analysis of digital terrain models and remotely sensed data in landscape investigations. – Progress in Physical Geography 22 (1): 33-60.

FOODY, G.M. (2004): Supervised image classification by MLP and RBF neural networks with and without an exhaustively defined set of classes. – International Journal of Remote Sensing 25 (15): 3091-3104.

FOODY, G.M. & R.A. HILL (1996): Classification of tropical forest classes from Landsat TM data. – International Journal of Remote Sensing 17 (12): 2353-2367.

FOODY, G.M., G. PALUBINSKAS, R.M. LUCAS, P.J. CURRAN & M. HONZAK (1996): Identifying terrestrial carbon sinks: Classification of successional stages in regenerating tropical forest from Landsat TM data. – Remote Sensing of Environment 55: 205-216.

FOODY, G.M., D.S. BOYD & M.E.J. CUTLER (2003): Predictive relations of tropical forest biomass from Landsat TM data and their transferability between regions. – Remote Sensing of Environment 85: 463-474.

FRANKLIN, J. (1995): Predictive vegetation mapping: geographic modelling of biospatial patterns in relation to environmental gradients. – Progress in Physical Geography 19 (4): 474-499.

FRANKLIN, S.E. (1992): Satellite remote sensing for forest type and landcover in the subalpine forest region, Kananaskis Valley, Alberta. – Geocarto International 7 (4): 25-35.

FRANKLIN, S.E. & D.R. PEDDLE (1990): Classification of SPOT HRV imagery and texture features. – International Journal of Remote Sensing 11 (3): 551-556.

FRANKLIN, S.E., R.J. HALL, L.M. MOSKAL, A.J. MAUDIE & M.B. LAVIGNE (2000): Incorporating texture into classification of forest species composition from airborne multispectral images. – International Journal of Remote Sensing 21 (1): 61-79.

FRANKLIN, S.E., A.J. MAUDIE & M.B. LAVIGNE (2001a): Using Spatial Co-Occurrence Texture to Increase Forest Structure and Species Composition Classification Accuracy. – Photogrammetric Engineering & Remote Sensing 67 (7): 849-855.

FRANKLIN, S.E., M.A. WULDER & G.R. GERYLO (2001b): Texture analysis of IKONOS panchromatic data for Douglas-fir forest age separability in British Columbia. – International Journal of Remote Sensing 22 (13): 2627-2632.

FRANKLIN, S.E., R.J. HALL, L. SMITH & G.R. GERYLO (2003): Discrimination of conifer height, age and crown closure classes using Landsat-5 TM imagery in the Canadian Northwest Territories. – International Journal of Remote Sensing 24 (9): 1823-1834.

FRANSSON, J.E.S., F. WALTER & H. OLSSON (1999): Identification of clear felled areas using SPOT P and Almaz-1 SAR data. – International Journal of Remote Sensing 20 (18): 3583-3593.

FUKUNAGA, K. (1990): Introduction to statistical pattern recognition. 2nd edition. Academic Press, Boston.

FULLER, D.O. & M. FULK (2001): Burned area in Kalimantan, Indonesia mapped with NOAA-AVHRR and Landsat TM imagery. – International Journal of Remote Sensing 22 (4): 691-697.

GARCÍA, M.C. & R. ALVAREZ (1994): TM digital processing of a tropical forest region in southeastern Mexico. – International Journal of Remote Sensing 15 (8): 1611-1632.

GARCÍA, R., M. MEJÍA & T. ZANONI (1994): Composición floristica y principales asociaciones vegetales en la Reserva Científica Ebano Verde, Cordillera Central, República Dominicana. – Moscosoa 10: 86-130.

GEMMELL, F.M. (1995): Effects of forest cover, terrain, and scale on timber volume estimation with Thematic Mapper data in a Rocky Mountain site. – Remote Sensing of Environment 51: 291-305.

GEMMELL, F. (1999): Estimating conifer forest cover with Thematic Mapper data using reflectance model inversion and two spectral indices in a site with variable background characteristics. – Remote Sensing of Environment 69: 105-121.

GIADA, S., T. DE GROEVE, D. EHRLICH & P. SOILLE (2003): Information extraction from very high resolution satellite imagery over Lukole refugee camp, Tanzania. – International Journal of Remote Sensing 24 (22): 4251-4266.

GLEITSMANN, A. & M. KAPPAS (2005): Use of high spatial resolution satellite data in tropical forest mapping. In: Kleinn, C., J. Nieschulze & B. Sloboda (eds.): Remote Sensing & GIS for Environmental Studies: Applications in Forestry. Schriften aus der Forstlichen Fakultät der Universität Göttingen und der Niedersächsischen Forstlichen Versuchsanstalt 138, pp. 167-175.

GOETZ, S.J., R.K. WRIGHT, A.J. SMITH, E. ZINECKER & E. SCHAUB (2003): IKONOS imagery for resource management: Tree cover, impervious surfacs, and riparian buffer analyses in the mid-Atlantic region. – Remote Sensing of Environment 88 (1): 195-208.

GONG, P., G.J. MARCEAU & P.J. HOWARTH (1992): A comparison of spatial feature extraction algorithms for land-use classification with SPOT HRV data. – Remote Sensing of Environment 40: 137-151.

GRAY, C.R. (1993): Regional meteorology and hurricanes. In: G.E. Maul (ed.): Climatic Change in the Intra-Americas Sea. United Nations Environment Programme. Edward Arnold, London. Pp. 87-99.

GREEN, K. (2000): Selecting and interpreting high-resolution images. – Journal of Forestry, June 2000: 37-39.

GWB / GFA-AGRAR (1998): Estudio de factibilidad. Unpublished pilot study for the PROCARY project, 150 pp.

HAGER, J. & T.A. ZANONI (1993): La vegetación natural de la República Dominicana: una nueva clasificación. – Moscosoa 7: 39-81.

HALL-BEYER, M. (2002): GLCM Texture: A Tutorial. National Council on Geographic Information and Analysis Remote Sensing Core Curriculum.
URL (15.04.2004): http://www.cla.sc.edu/geog/rslab/rsccnew/rscc?frames.html
and http://www.ucalgary.ca/~mhallbey/texture/texture_tutorial.html

HAMILTON, L.S., J.O. JUVIK & F.N. SCATENA (1995): The Puerto Rico Tropical Cloud Forest Symposium: Introduction and Workshop Synthsis. In: Hamilton, L.S., J.O. Juvik & F.N. Scatena (eds.): Tropical Montane Cloud Forests. – Ecological Studies, Vol. 110. Springer, New York. Pp. 1-23.

HARALICK, R.M. 1979. Statistical and structural approaches to texture. Proceedings of the IEEE, 67: 786-804.

HARALICK, R.M., K. SHANMUGAM & I. DINSTEIN (1973): Textural Features for Image Classification. – IEEE Transactions on Systems, Man and Cybernetics. SMC-3 (6): 610-620.

HARALICK, R.M. & L.G. SHAPIRO (1985): Image segmentation techniques. – Computer Vision, Graphics, and Image Processing 29: 100-132.

HARCOURT, C.S. & J. OTTENWALDER (1996): Hispaniola. In: C.S. Harcourt & J.A. Sayer (eds.): The Conservation Atlas of Tropical Forests: The Americas. Simon & Schuster, New York. Pp. 102-111.

HAY, G.J. & K.O. NIEMANN (1994): Visualizing 3-D texture: A three-dimensional structural approach to model forest texture. – Canadian Journal of Remote Sensing 20 (2): 90-101.

HAY, G.J., K.O. NIEMANN & G.F. MCLEAN (1996): An object-specific image-texture analysis of H-resolution forest imagery. – Remote Sensing of Environment 55: 108-122.

HAY, G.J., K.O. NIEMANN & D.G. GOODENOUGH (1997): Spatial thresholds, image-objects, and upscaling: A multiscale evaluation. – Remote Sensing of Environment 62: 1-19.

HAY, G.J., T. BLASCHKE, D.J. MARCEAU & A. BOUCHARD (2003): A comparison of three image-object methods for the multiscale analysis of landscape structure. – ISPRS Journal of Photogrammetry & Remote Sensing 57: 327-345.

HE, D-C. & L. WANG (1990): Texture Unit, Texture Spectrum and Texture Analysis. – IEEE Transactions on Geoscience and Remote Sensing 28 (4): 509-512.

HEINDRICHS, T. (2004): Pagos pro servicios ambientales (PSA) en PROCARYN – Concertar fondos nacionales e internacionales para la conservación de los resursos hídricos de la República Dominicana. *In*: FAO (2004): Sistemas de pago por servicios ambientales en cuencas hidrográficas. Informe del Foro celebrado en Arequipa, Junio 2003. Documento de Debate de Tierras y Aguas 3. FAO, Rome.
(URL (14.12.2004): http://www.rlc.fao.org/foro/psa/pdf/heindrichs2.pdf)

HELMER, E.H., S. BROWN & W.B. COHEN (2000): Mapping montane tropical forest successional stage and land use with multi-date Landsat imagery. – International Journal of Remote Sensing 21 (11): 2163-2183.

HELMER, E.H., O. RAMOS, T. DEL M. LÓPEZ, M. QUIÑONES & W. DIAZ (2002): Mapping the forest type and land cover of Puerto Rico, a component of the Caribbean biodiversity hotspot. – Caribbean Journal of Science 38 (3-4): 165-183.

HERNÁNDEZ, A. (1995): Economic and institutional analysis of agroforestry projects in the Dominican Republic. *In*: D. Current, E. Lutz & S. Scherr (eds): Costs, benefits and farmer adoption of agroforestry. Washington.

HERRERA, B., C. KLEINN, B. KOCH & M. DEES (2004): Automatic classification of trees outside forest using an object-driven approach: an application in a Costa Rican landscape. – Photogrammetrie – Fernerkundung – Geoinformation 2004 (2): 111-119.

HESE, S. (2001): Segmentation of forest stands in very high resolution stereo data. *In* Proceedings of the Geoscience and Remote Sensing Symposium, 2001. IGARSS '01, Sydney, Australia, Vol. 4, pp. 1654-1656. URL (20.05.2005): http://solarsystem.dlr.de/FE/abteilung/pdfs/igarss2001-hese.pdf

HILL, R.A. (1999): Image segmentation for humid tropical forest classification in Landsat TM data. – International Journal of Remote Sensing 20 (5): 1039-1044.

HILL, R.A. & G.M. FOODY (1994): Separability of tropical rain-forest types in the Tambopata-Candamo Reserved Zone, Peru. – International Journal of Remote Sensing 15 (13): 2687-2693.

HIRATA, Y., T. ENOKI, A. MIYAMOTO, M. FUKUDA & T. NISHIZONO (2002): Estimation of forest stand parameters from IKONOS panchromatic data. *In* Proceedings of the ForestSAT 2002 conference – Operational tools in forestry using remote sensing techniques, August 5th - 9th 2002, Edinburgh.

HOLDRIDGE, L.R., W.C. GRENKE, W.H. HATHEWAY, T. LIAND & J.A. TOSI JR. (1971): Forest Environments in Tropical Life Zones: A Pilot Study. Pergamon Press, Oxford. (Chapter 2, pp. 4-17).

HOLMGREN, P. & T. THURESSON (1998): Satellite remote sensing for forestry planning – a review. – Scandinavian Journal of Forest Research 13: 90-110.

HOLOPAINEN, M. & G. WANG (1998): The calibration of digitized aerial photographs for forest stratification. – International Journal of Remote Sensing 19 (4): 677-696.

HORN, S.P., K.H. ORVIS, L.M. KENNEDY & G.M. CLARK (2000): Prehistoric fires in the highlands of the Dominican Republic: Evidence from charcoal in soils and sediments. – Caribbean Journal of Science 36 (1-2): 1-18.

HORST, O.H. (1992): Climate and the "Encounter" in the Dominican Republic. – Journal of Geography 91 (5): 205-210.

HUDAK, A.T., M.A. LEFSKY, W.B. COHEN & M. BERTERRETCHE (2002): Integration of lidar and Landsat ETM+ for estimating and mapping forest canopy height.

HUDSON, W.D. (1991): Photo interpretation of montane forests in the Dominican Republic. – Photogrammetric Engineering & Remote Sensing 57 (1): 79-84.

HURTT, G., X. XIAO, M. KELLER, M. PALACE, G.P. ASNER, R. BRASWELL, E.S. BRONDÍZIO, M. CARDOSO, C.J.R. CARVALHO, M. G. FEARON, L. GUILD, S. HAGEN, S. HETRICK, B. MOORE III, C. NOBRE, J.M. READ, T. SÁ, A. SCHLOSS, G. VOURLITIS & A.J. WICKEL (2003): IKONOS imagery for the Large Scale Biosphere-Atmosphere Experiment in Amazonia (LBA). – Remote Sensing of Environment 88 (1): 111-127.

HUTCHINSON, C.F. (1982): Techniques for combining Landsat and ancillary data for digital classification improvement. – Photogrammetric Engineering & Remote Sensing 48 (1): 123-130.

ICHII, K., M. MARUYAMA & Y. YAMAGUCHI (2003): Multi-temporal analysis of deforestation in Rondônia state in Brazil using Landsat MSS, TM, ETM+ and NOAA AVHRR imgery and its relationship to changes in the local hydrological environment. – International Journal of Remote Sensing 24 (22): 4467-4479.

JAKUBAUSKAS, M.E. & K. PRICE (2000): Regression-based estimation of Lodgepole Pine forest age from Landsat Thematic Mapper data. – Geocarto International 15 (1): 19-24.

JULESZ, B. (1962): Visual pattern discrimination. – IRE Transactions on Information Theory 8 (2): 84-92.

KADMON, R. & R. HARARI-KREMER (1999): Studying long-term vegetation dynamics using digital processing of historical aerial photographs. – Remote Sensing of Environment 68: 164-176.

KALÁCSKA, M., G.A. SÁNCHEZ-AZOFEIFA, B. RIVARD, J.C. CALVO-ALVARADO, A.R.P. JOURNET, J.P. ARROYO-MORA & D. ORTIZ-ORTIZ (2004): Leaf area index measurements in a tropical moist forest: A case study from Costa Rica. – Remote Sensing of Environment 91: 134-152.

KAPPAS, M. (1999): Klimaökologische Aspekte eines Bergwaldgebietes in der Dominikanischen Republik. – Geographische Rundschau 51 (9): 462-468.

KAPPAS, M. & F. SCHÖGGL (2005): Bodenerosion in der Dominikanischen Republik. – Reihe Erdsicht - Einblicke in geographische und geoinformationstechnische Arbeitsweisen Vol. 4 (ed. M. Kappas), ibidem-Verlag, Stuttgart.

KAYITAKIRE, F., C. FARCY & P. DEFOURNY (2002): IKONOS-2 imagery potential for forest stands mapping. *In* Proceedings of the ForestSAT 2002 conference – Operational tools in forestry using remote sensing techniques, August 5th - 9th 2002, Edinburgh.

KELLNDORFER J.M., L.E. PIERCE, M.C. DOBSON & F.T. Ulaby (1998): Toward consistent regional-to-global-scale vegetation characterization using orbital SAR systems. – IEEE Transactions on Geoscience and Remote Sensing 36 (5): 1396-1411.

KELLNDORFER, J.M., M.C. DOBSON, J.D. VONA & M. CLUTTER (2003): Toward precision forestry: plot-level parameter retrieval for slash pine plantations with JPL AIRSAR. – IEEE Transactions on Geoscience and Remote Sensing 41 (7): 1571-1582.

KESLER, S.E., J.F. SUTTER, J.M. BARTON & R.C. SPECK (1991): Age of intrusive rocks in northern Hispaniola. *In*: Mann, P., G. Draper & J.F. Lewis (eds.): Geologic and tectonic development of the North America-Caribbean plate boundary in Hispaniola. – Geological Society of America Special Paper 262, Boulder, Colorado. Pp. 165-172.

KIEMA, J.B.K. (2002): Texture analysis and data fusion in the extraction of topographic objects from satellite imagery. – International Journal of Remote Sensing 23 (4): 767-776.

KIMES, D.S., R.F. NELSON, W.A. SALAS & D.L. SKOLES (1999): Mapping secondary tropical forest and forest age from SPOT HRV. – International Journal of Remote Sensing 20 (18): 3625-3640.

KLEINHANS, A. (2003): Einfluss der Waldkonversion auf den Wasserhaushalt eines tropischen Regenwaldeinzugsgebietes in Zentral Sulawesi (Indonesien): Experimentelle Analyse und Modellierung unter Berücksichtigung von Landnutzungsszenarien. – Elektronische Dissertation der Georg-August-Universität Göttingen. URL: http://webdoc.sub.gwdg.de/diss/2004/kleinhans/index.html

KLEINN, C. (2002): New technologies and methodologies for national forest inventories. – Unasylva 53 (210): 10-15.

KOCH, B., J. KRÜGER, H. SAGISCHEWSKI & S. CHMARA (2002): Large area forest mapping using segmentation based image classification. *In* Proceedings of the ForestSAT 2002 conference – Operational tools in forestry using remote sensing techniques, August 5th - 9th 2002, Edinburgh.

KOCH, B., M. JOCHUM, E. IVITS & M. DEES (2003): Pixelbasierte Klassifizierung im Vergleich und zur Ergänzung zum objektbasierten Verfahren. – Photogrammetrie, Fernerkundung, Geoinformation 2003 (3): 195-204.

KÖHL, M. (1996): Multi-phase sampling schemes for extensive surveys in tropical forests. *In*: R. Päivinen, J. Vanclay & S. Miina (eds.): New thrusts in forest inventory. Proceedings of the Subject Group S4.02-00 "Forest Resource Inventory and Monitoring" and Subject Group S4.12-00 "Remote Sensing Technology" : IUFRO XX World Congress, 6-12 August 1995, Tampere, Finland. Vol. I. EFI Proceedings No. 7, pp. 27-41.

KOK, R. DE, A. BUCK, T. SCHNEIDER & U. AMMER (2000): Analysis of image objects from VHR imagery for forest GIS updating in the Bavarian Alps. – ISPRS, Vol. XXXIII, Amsterdam, 2000.
(URL: http://www.pcigeomatics.com/tech-papers/paper814tcvii-51.pdf)

References

LABA, M., S.D. SMITH & S.D. DEGLORIA (1997): Landsat-based land cover mapping in the lower Yuna River watershed in the Dominican Republic. – International Journal of Remote Sensing 18 (14): 3011-3025.

LABA, M., S.K. GREGORY, J. BRADEN, D. OGURCAK, E. HILL, E. FEGRAUS, J. FIORE & S.D. DEGLORIA (2002): Conventional and fuzzy accuracy assessment of the New York Gap Analysis Project land cover map. – Remote Sensing of Environment 81: 443-455.

LANDGREBE, D.A. (2003): Signal theory methods in multispectral remote sensing. Wiley, New Jersey.

LANGFORD, M. & W. BELL (1997): Land cover mapping in a tropical hillsides environment: a case study in the Cauca region of Colombia. – International Journal of Remote Sensing 18 (6): 1289-1306.

LATIFOVIC, R., Z. ZHU, J. CIHLAR, C. GIRI & I. OLTHOF (2004): Land cover mapping of North and Central America – Global Land Cover 2000. – Remote Sensing of Environment 89: 116-127.

LAUER, W., M.D. RAFIQPOOR & J. BENDIX (2003): Vergleichende Geoökologie der Hochgebirge der nördlichen (Mexiko) und südlichen (Bolivien) Randtropen sowie der inneren Tropen (Ecuador). Akademie der Wissenschaften und der Literatur, Mainz.

LECKIE, D.G., F.A. GOUGEON, N. WALSWORTH & D. PARADINE (2003): Stand delineation and composition estimation using semi-automated individual tree crown analysis. – Remote Sensing of Environment 85: 335-369.

LEWIS, J.F. & G. DRAPER (1990): Geology and tectonic evolution of the northern Caribbean margin. In: Dengo, G. & J.E. Case (eds): The Caribbean region. Geological Society of America, The Geology of North America, Vol. H. Boulder, Colorado.

LEWIS, J.F., A. AMARANTE, G. BLOISE, J.G. JIMÉNEZ G. & H.D. DOMINGUEZ (1991): Lithology and stratigraphy of upper Cretaceous volcanic and volcaniclastic rocks of the Tireo Group, Dominican Republic, and correlations with the Massif du Nord in Haiti. In: Mann, P., G. Draper & J.F. Lewis (eds.): Geologic and tectonic development of the North America-Caribbean plate boundary in Hispaniola. – Geological Society of America Special Paper 262, Boulder, Colorado.

LI, Z. (1994): A comparative study of the accuracy of digital terrain models (DTMs) based on various data models. – ISPRS Journal of Photogrammetry and Remote Sensing 49 (1): 2-11.

LISTÍN DIARIO (12.02.2005): Puig dice presentará un nuevo proyecto ley áreas protegidas. – Article in Domincan daily newspaper, Santo Domingo. URL: http://listin.com.do/

LISTÍN DIARIO (19.03., 20.03., 22.03, 24.03. & 30.03.2005): Las FFAA tratan de rescatar 70 técnicos atrapados en fuego; Intensifican lucha contra fuegos forestales en la cordillera Central; Los EEUU enviará avión para apagar los incendios en la Cordillera Central; Fuegos en la cordillera Central afectan 80 mil tareas de bosques; Sigue incendio forestal en Loma de Macutico. – Articles in Domincan daily newspaper. URL: http://listin.com.do/

LIU, Q.J., T. TAKAMURA & N. TAKEUCHI (2002a): Mapping of boreal vegetation of a temperate mountain in China by multitemporal Landsat TM imagery. – International Journal of Remote Sensing 23 (17): 3385-3405.

LIU, X.-H., A.K. SKIDMORE & H. VAN OOSTEN (2002b): Integration of classification methods for improvement of land-cover map accuracy. – ISPRS Journal of Photogrammetry & Remote Sensing 56: 257-268.

LLOYD, C.D., S. BERBEROGLU, P.J. CURRAN & P.M. ATKINSON (2004): A comparison of texture measures for the per-field classification of Mediterranean land cover. – International Journal of Remote Sensing 25 (19): 3943-3965.

LOBO, A. (1997): Image segmentation and discriminant analysis for the identification of land cover units in ecology. – IEEE Transactions on Geoscience and Remote Sensing 35 (5): 1136-1145.

LUGO, A.E. (1995): Tropical Forests: Their future and our future. *In*: Lugo, A.E. & C. Lowe (eds.): Tropical forests: management and ecology. – Ecological Studies, Vol. 112. Springer, New York. Pp. 3-17.

LUND, H.G. (1996): Global resource assessments beyond 2001: An introduction to the panel. *In*: R. Päivinen, J. Vanclay & S. Miina (eds.): New thrusts in forest inventory. Proceedings of the Subject Group S4.02-00 "Forest Resource Inventory and Monitoring" and Subject Group S4.12-00 "Remote Sensing Technology" : IUFRO XX World Congress, 6-12 August 1995, Tampere, Finland. Vol. I. EFI Proceedings No. 7, pp. 231-238.

LUNDBERG, E. (1997): Background for the teaching of Caribbean prehistory.
URL (04.11.04): http://web.archive.org/web/20020615125245/http://www.friendsvinp.org/archeol/lesson/back.htm

MA, Z., M.M. HART & R.L. REDMOND (2001): Mapping vegetation across large geographic areas: Integration of remote sensing and GIS to classify multisource data. – Photogrammetric Engineering & Remote Sensing 67 (3): 295-307.

MAGNUSSEN, S. (1997): A method for enhancing tree species proportions from aerial photos. – The Forestry Chronicle 73 (4): 479-487.

MANN, P., G. DRAPER & J.F. LEWIS (1991a): An overview of the geologic and tectonic development of Hispaniola. *In*: Mann, P., G. Draper & J.F. Lewis (eds.): Geologic and tectonic development of the North America-Caribbean plate boundary in Hispaniola. – Geological Society of America Special Paper 262, Boulder, Colorado. Pp. 1-28.

MANN, P., P.P. MCLAUGHLIN & C. COOPER (1991b): Geology of the Azua and Enriquillo basins, Dominican Republic; 2, Structure and tectonics. *In*: Mann, P., G. Draper & J.F. Lewis (eds.): Geologic and tectonic development of the North America-Caribbean plate boundary in Hispaniola. – Geological Society of America Special Paper 262, Boulder, Colorado. Pp. 367-390.

MARCEAU, D.J., P.J. HOWARTH, J.-M.M. DUBOIS & D.J. GRATTON (1990): Evaluation of the Grey-Level Co-occurence Matrix method for land-cover classification using SPOT imagery. – IEEE Transactions on Geoscience and Remote Sensing 28 (4): 513-519.

MARCEAU, D.J., P.J. HOWARTH & D.J. GRATTON (1994a): Remote sensing and the measurement of geographic entities in a forested environment. 1. The scale and spatial aggregation problem. – Remote Sensing of Environment 49: 93-104.

MARCEAU, D.J., P.J. HOWARTH & D.J. GRATTON (1994b): Remote sensing and the measurement of geographic entities in a forested environment. 2. The optimal spatial resolution. – Remote Sensing of Environment 49: 105-117.

MARKHAM. B.L. & J.R.G. TOWNSHEND (1981): Land cover classification accuracy as a function of sensor spatial resolution. *In* Proceedings of the 15th International Symposium on Remote Sensing of Environment, Ann Arbor, MI, pp. 1075-1090.

MARTIN, M.E., S.D. NEWMAN, J.D. ABER & R.G. CONGALTON (1998): Determining forest species composition using high spectral resolution remote sensing data. – Remote Sensing of Environment 65: 249-254.

MAS, J.-F., A. VELÁZQUEZ, J.L. PALACIO-PRIETO, G. BOCCO, A. PERALTA & J. PRADO (2002): Assessing forest ressources in Mexico: Wall-to-wall land use / cover mapping. – Photogrammetric Engineering & Remote Sensing 68 (10): 966-973.

MASUOKA, P.M., D.M. CLABORN, R.G. ANDRE, J. NIGRO, S.W. GORDON, T.A. KLEIN, H.-C. KIM (2003): Use of IKONOS and Landsat for malaria control in the Republic of Korea. – Remote Sensing of Environment 88 (1): 187-194.

MATTHEWS, E. & A. GRAINGER (2002): Evaluacion of FAO's Global Forest Resources Assessment from the user perspective. – Unasylva 53 (210): 42-50.

MAY, T. (1994): Regeneración de la vegetación arbórea y arbustiva en un terreno de cultivos abandonado durante 12 años en la zona de bosques húmedos montanos (Reserva Científica Ebano Verde, Cordillera Central, República Dominicana). – Moscosoa 8: 131-149.

MAY, T. (1997): Bergwälder in der Dominikanischen Republik. – Geographische Rundschau 49 (11): 662-667.

MAY, T. (2000): Respuestas de la vegetación en un calimetal de Dicranopteris pectinata después de un fuego, en la parte oriental de la Cordillera Central, República Dominicana. – Moscosoa 11: 113-132.

MAY, T. (2001): El endemismo de especies de plantas vasculares en República Dominicana, en relación con condiciones ambientales y factores biogeográficos. – Moscosoa 12: 60-78.

MAY, T. & B. PEGUERO (2000): Vegetación y flora de la Loma El Mogote, Jarabacoa, Cordillera Central, República Dominicana. – Moscosoa 11: 11-37.

MEANS, J.E., S.A. ACKER, B.J. FITT, M. RENSLOW, L. EMERSON & C. HENDRIX (2000): Predicting Forest Stand Characteristics with Airborne Scanning Lidar. – Photogrammetric Engineering & Remote Sensing 66 (11): 1367-1371.

MEINEL, G., M. NEUBERT & J. REDER (2001): Pixelorientierte versus segmentorientierte Klassifikation von IKONOS-Satellitenbilddaten – ein Methodenvergleich. – Photogrammetrie, Fernerkundung, Geoinformation 2001 (3): 157-170.

MEJÍA, M., R. GARCÍA & F. JIMÉNEZ (2000): Sub-región fitogeográfica Barbacoa-Casabito: Riqueza florística y su importancia en la conservación de la flora de la Isla Española. – Moscosoa 11: 57-106.

MILLINGTON, A.C., X.M. VELEZ-LIENDO & A.V. BRADLEY (2003): Scale dependence in multitemporal mapping of forest fragmentation in Bolivia: implications for explaining temporal trends in landscape ecology and applications to biodiversity conservation. – ISPRS Journal of Photogrammetry & Remote Sensing 57: 281-299.

MITRI, G.H. & I.Z. GITAS (2004): A performance evaluation of a burned area object-based classification model when applied to topographically and non-topographically corrected TM imagery. – International Journal of Remote Sensing 25 (14): 2863-2870.

MORISETTE, J.T., J.E. NICKESON, P. DAVIS, Y. WANG, Y. TIAN, C.E. WOODCOCK, N. SHABANOV, M. HANSEN, W.B. COHEN, D.R. OETTER & R.E. KENNEDY (2003): High spatial resolution satellite observations for validation of MODIS land products: IKONOS observations acquired under the NASA Scientific Data Purchase. – Remote Sensing of Environment 88 (1): 100-110.

MOSKAL, L.M. & S.E. FRANKLIN (2004): Relationship between airborne multispectral image texture and aspen defoliation. – International Journal of Remote Sensing 25 (14): 2701-2711.

MOYA PONS, F. (1994): Historia y Medio Ambiente en la Isla de Santo Domingo.
URL (27.03.2004): http://www.ceiba.gov.do/2004/aprendiendo_naturaleza/esp/natura_esp.html

MUMBY, P.J. & A.J. EDWARDS (2002): Mapping marine environments with IKONOS imagery: enhanced spatial resolution can deliver greater thematic accuracy. – Remote Sensing of Environment 82: 248-257.

MURPHY, P.G., A.E. LUGO, A.J. MURPHY & D.C. NEPSTAD (1995): The dry forests of Puerto Rico's south coast. *In*: Lugo, A.E. & C. Lowe (eds.): Tropical forests: management and ecology. – Ecological Studies, Vol. 112. Springer, New York. Pp. 178-209.

MYERS, N., R.A. MITTERMEIER, C.G. MITTERMEIER, G.A.B. DA FONSECA & J. KENT (2000): Biodiversity hotspots for conservation priorities. – Nature 403: 853-858.

MYINT, S.W. (2001): A robust texture analysis and classification approach for urban land-use and land-cover feature discrimination. – Geocarto International 16 (4): 27-38.

NÆSSET, E. (1996): Use of the weighted Kappa coefficient in classification error assessment of thematic maps. – International Journal of Geographical Information Systems 10 (5): 591-604.

NARASIMHA RAO, P.V., M.V.R. SESHA SAI, K. SREENIVAS, M.V. KRISHNA RAO, B.R.M. RAO, R.S. DWIVEDI & L. VENKATARATNAM (2002): Textural analysis of IRS-1D panchromatic data for land cover classification. – International Journal of Remote Sensing 23 (17): 3327-3345.

OAS (1984): Planificación del Desarrollo Regional Integrado: Directrices y Estudios de Casos Extraídos de la Experiencia de la OEA. Estudio de casos 1 - Recursos naturales y desarrollo regional en la República Dominicana. – Departamento de Desarrollo Regional, Secretaria Ejecutiva para Asuntos Economicos y Sociales, Organizacion de los Estados Americanos, en colaboración con: Servicio de Parques Nacionales de los EE.UU., Agencia de los EE.UU. para el Desarrollo Internacional, Washington, D.C.
URL (16.02.2005): http://www.oas.org/usde/publications/Unit/oea72s/begin.htm#Contents

ORVIS, K.H., G.M. CLARK, S.P. HORN & L.M. KENNEDY (1997): Geomorphic traces of quarternary climates in the Cordillera Central, Dominican Republic. – Mountain Research and Development 17 (4): 323-331.

PAL, N.R. & S.K. PAL (1993): A review of image segmentation techniques. – Pattern Recognition 26 (9): 1277-1294.

PALUBINSKAS, G., R.M. LUCAS, G.M. FOODY & P.J. CURRAN (1995): An evaluation of fuzzy and texture-based classification approaches for mapping tropical forest classes from Landsat-TM data. – International Journal of Remote Sensing 16 (4): 747-759.

PAOLA, J.D. & R.A. SCHOWENGERDT (1995): A detailed comparison of backpropagation neural network and maximum-likelihood classifiers for urban land use classification. – IEEE Transactions on Geoscience and Remote Sensing 33 (4): 981-995.

PARADELLA, W.R., M.F.F. DA SILVA, N. DE LA ROSA & C.A. KUSHIGBOR (1994): A geobotanical approach to the tropical rain forest environment of the Carajás Mineral Province (Amozon Region, Brazil), based on digital TM-Landsat and DEM data. – International Journal of Remote Sensing 15 (8): 1633-1648.

PCI GEOMATICS (2003): Geomatica Version 9.0 User Guide. Richmond Hill, Ontario.

PCI GEOMATICS (2001): OrthoEngine Reference Manual Version 8.2. Richmond Hill, Ontario.

PCI (2001): Xpace help system (softcopy), Version 9.1. Richmond Hill, Ontario.

PEDDLE, D.R. (1993): An empirical comparison of evidential reasoning, linear discriminant analysis, and maximum likelihood algorithms for alpine land cover classification. – Canadian Journal of Remote Sensing 19 (1): 31-44.

PEKKARINEN, A. (2002): A method for the segmentation of very high spatial resolution images of forested landscapes. – International Journal of Remote Sensing 23 (14): 2817-2836.

PERALTA, P. & P. MATHER (2000): An analysis of deforestation patterns in the extractive reserves of Acre, Amazonia from satellite imagery: a landscape ecological approach. – International Journal of Remote Sensing 21 (13&14): 2555-2570.

PETER, H. (2003): Pine forests in the Dominican Republic – A unique resource between all fronts. - ETFRN News 38: 47-49.
(URL (01.04.2004): http://www.etfrn.org/etfrn/newsletter/pdf/etfrnnews38.pdf)

References

PETER, H. (2004): Disillusion and hope of smallholders in Cordillera Central, Dominican Republic: Is PROCARYN the right way to change the trend of forest deterioration? *In*: Baumgartner D.M. (ed.): Proceedings of Human Dimensions of Family, Farm and Community Forestry International Symposium, March 29-April 1, 2004, Washington. Pp. 193-198.

PITT, D.G., R.G. WAGNER, R.J. HALL, D.J. KING, D.G. LECKIE & U. RUNESSON (1997): Use of remote sensing for forest vegetation management: A problem analysis. – The Forestry Chronicle 73 (4): 459-477.

PIZZOLATO ANGELO, N. & V. HAERTEL (2003): On the application of Gabor filtering in supervised classification. – International Journal of Remote Sensing 24 (10): 2167-2189.

POHL, C. & J.L. VAN GENDEREN (1998): Multisensor image fusion in remote sensing: concepts, methods and applications. – International Journal of Remote Sensing 19 (5): 823-854.

POULIOT, D.A., D.J. KING, F.W. BELL & D.G. PITT (2002): Automated tree crown detection and delineation in high-resolution digital camera imagery of coniferous forest regeneration. – Remote Sensing of Environment 82: 322-334.

PRESUTTI, M.E., S.E. FRANKLIN, L.M. MOSKAL & E.E. DICKSON (2001): Supervised classification of multisource satellite image spectral and texture data for agricultural crop mapping in Buenos Aires province, Argentina. – Canadian Journal of Remote Sensing 27 (6): 679-684.

PRICE, M.F. & N. BUTT (eds.) (2000): Forests in sustainable mountain development: a state of knowledge report for 2000. IUFRP research series 5. CABI Publishing, Wallingford, UK.

PUECH, C. (1994): Thresholds of homogeneity in targets in the landscape. Relationship with remote sensing. – International Journal of Remote Sensing 15 (12): 2421-2435.

QIU, F. & J.R. JENSEN (2004): Opening the black box of neural networks for remote sensing image classification. – International Journal of Remote Sensing 25 (9): 1749-1768.

QUACKENBUSH, L.J., P.F. HOPKINS & G.J. KINN (2000): Developing Forestry Products from High Resolution Digital Aerial Imagery. – Photogrammetric Engineering & Remote Sensing 66 (11): 1337-1346.

READ, J.M. (2003): Spatial analyses of logging impacts in Amazonia using remotely sensed data. – Photogrammetric Engineering & Remote Sensing 69 (3): 275-282.

REPÚBLICA DOMINICANA (2000): Ley General Sobre Medio Ambiente y Recursos Naturales (64-00). Publicación Oficial. Santo Domingo, Dominican Republic.
URL (20.03.2004): http://www.usaid.gov/dr/docs/resources/ley_medio_ambiente.pdf

RIAZA, A., M.L. MARTINEZ-TORREZ, R. RAMON-LLUCH, J. ALONSO & P. HERAS (1998): Evolution of equatorial vegetation communities mapped using Thematic Mapper images through a geographical information system (Guinea, Equatorial Africa). – International Journal of Remote Sensing 19 (1): 43-54.

RICOTTA, C. (2004): Evaluation the classification accuracy of fuzzy thematic maps with a simple parametric measure. – International Journal of Remote Sensing 25 (11): 2169-2176.

RIOU, R. & F. SEYLER (1997): Texture analysis of tropical rain forest infrared satellite images. – Photogrammetric Engineering & Remote Sensing 63 (5): 515-521.

ROBINSON, G.J. (1994): The accuracy of digital elevation models derived from digitised contour data. – Photogrammetric Record 14 (83): 805-814.

RODRÍGUEZ, A.R. (2004): Informe Nacional, República Dominicana. *In* FAO: Estudio de tendencias y persperctivas del sector forestal en América Latina, Documento de Trabajo - ESFAL/N/11.
URL (16.02.2005): http://www.fao.org/documents/show_cdr.asp?url_file=/docrep/007/j3268s/j3268s06.htm

ROTH, L.C. (1999): Anthropogenic change in subtropical dry forest during a century of settlement in Jaiquí Picado, Santiago Province, Dominican Republic. – Journal of Biogeography 26: 739-759.

RUSSELL, F.A. & L. FOURNIER (1992): Análisis de los cambios de la cobertura del suelo en la zona occidental de la República Dominicana. – Eme eme: estudios dominicanos 18: 53-62. Santiago de los Caballeros.

RYHERD, S. & C. WOODCOCK (1996): Combining spectral and texture data in the segmentation of remotely sensed images. – Photogrammetric Engineering & Remote Sensing 62 (2): 181-194.

SADER, S.A., D. AHL & WEN-SHU LIOU (1995): Accuracy of Landsat-TM and GIS rule-based methods for forest wetland classification in Maine. – Remote Sensing of Environment 43: 133-144.

SAKET, M. (2002): Gaps in national-level information on forests and trees in developing countries. – Unasylva 53 (210): 24-27.

SAMBROOK, R.A., B.W. PIGOZZI & R.N. THOMAS (1999): Population pressure, deforestation, and land degradation: A case study from the Dominican Republic. – Professional Geographer 51 (1): 25-40.

SAMPSON, P.H., P.M. TREITZ & G.H. MOHAMMED (2001): Remote sensing of forest condition in tolerant hardwods: An examination of spatial scale, structure and function. – Canadian Journal of Remote Sensing 27 (3): 232-246.

SANCHEZ-AZOFEIFA, G.A., B. RIVARD, J. CALVO & I. MOORTHY (2002): Dynamics of tropical deforestation around national parks: Remote sensing of forest change on the Osa Peninsula of Costa Rica. – Mountain Research and Development 22 (4): 352-358.

SCARFF, J.G. (1940): Forestry and forest legislation in the Dominican Republic. – The Caribbean Forester 1 (3): 4-9.

SCARTH, P., S.R. PHINN & C. MCALPINE (2001): Integrating high and moderate spatial resolution image data to estimate forest age structure. – Canadian Journal of Remote Sensing 27 (2): 129-142.

SCHLERF, M., J. HILL, S. BÄRISCH & C. ATZBERGER (2003): Einfluss der spektralen und räumlichen Auflösung von Fernerkundungsdaten bei der Nadelwaldklassifikation. – Photogrammetrie, Fernerkundung, Geoinformation 2003 (1): 27-34.

SCHUBERT, A. (1993): Conservation of biological diversity in the Dominican Republic. – Oryx 27 (2): 115-121.

SCHUBERT, C. & E. MEDINA (1982): Evidence of Quarternary glaciation in the Dominican Republic: Some implications for the Caribbean paleoclimatology. – Palaeogeography, Palaeoclimatology, Palaeoecology 39 (3-4): 281-294.

SCHUBERT, W.H., P.E. CIESIELSKI, C. LU & R.H. JOHNSON (1995): Dynamical adjustment of the trade wind inversion layer. – Journal of the Atmospheric Sciences 52 (16): 2941-2952.

SEA/DVS (1994): Reconocimiento y Evaluación de los Recursos Naturales de la Sierra de Baoruco. Secretaría de Estado de Agricultura, Departamento de Vida Silvestre. Santo Domingo, República Dominicana.

SEMARENA (2001a): Inventario de Cobertura Forestal en la República Dominicana. Santo Domingo, Dominican Republic.
URL (23.03.2004): http://www.ceiba.gov.do/2004/downloads/Inventario.pdf

SEMARENA (2001b): Normas Técnicas Forestales. Normas Técnicas para Planes de Manejo Forestal. Santo Domingo, Dominican Republic.
URL (23.03.2004): http://www.ceiba.gov.do/2004/downloads/Manejo.pdf

SEMARENA (2001c): Normas Técnicas Forestales. Normas y procedimientos para los permisos forestales. Santo Domingo, Dominican Republic.
URL (23.03.2004): http://www.ceiba.gov.do/2004/downloads/Permisos.pdf

SEMARENA (2001d): Normas Técnicas Forestales. Normas técnicas para el establecimiento y certificación de plantaciones forestales. Santo Domingo, Dominican Republic.
URL (23.03.2003): http://www.ceiba.gov.do/2004/downloads/Plantaciones.pdf

SEMARENA (2001e): Reglamento Forestal. Santo Domingo, Dominican Republic.
URL (23.03.2003): http://www.ceiba.gov.do/2004/downloads/Reglamento.pdf

SEMARENA (2002): Publicación Especial Sobre el Proyecto de Reforma de las Políticas Nacionales de Medio Ambiente. Santo Domingo, Dominican Republic.
URL (18.03.2004): http://www.ambiente.org.do/PDF_finales/publicacion_especial.pdf

SIMARD, M., S.S. SAATCHI & G. DE GRANDI (2000): The use of decision tree and multiscale texture for classification of JERS-1 SAR data over tropical forest. – IEEE Transactions on Geoscience and Remote Sensing 38 (5): 2310-2321.

SINGH, A. (1987): Spectral separability of tropical forest cover classes. – International Journal of Remote Sensing 8 (7): 971-979.

SKOLE, D. & C.J. TUCKER (1993): Tropical deforestation and habitat fragmentation in the Amazon: satellite data from 1978 to 1988. – Science 260: 1905-1910.

SLOCUM, M., T.M. AIDE, J.K. ZIMMERMAN & L. NAVARRO (2000): La vegetación leñosa en helechales y bosques de ribera en la Reserva Científica Ebano Verde, República Dominicana. – Moscosoa 11: 38-56.

SMITH, J.H., J.D. WICKHAM, S.V. STEHMAN & L. YANG (2002): Impacts of Patch Size and Land-Cover Heterogeneity on Thematic Image Classification Accuracy. – Photogrammetric Engineering & Remote Sensing 68 (1): 65-70.

SONG, C. & C.E. WOODCOCK (2002): The spatial manifestation of forest succession in optical imagery. The potential of multiresolution imagery. – Remote Sensing of Environment 82: 271-284.

SONG, C., C.E. WOODCOCK, K.C. SETO, M.P. LENNEY & S.A. MACOMBER (2001): Classification and change detection using Landsat TM data: When and how to correct atmospheric effects? – Remote Sensing of Environment 75 (2): 230-244.

SPACE IMAGING (2004): IKONOS product guide, Version 1.4. Space Imaging, LLC, Thornton, Colorado.
URL (10.05.2005): www.spaceimaging.com

STATISTISCHES BUNDESAMT (1996): Länderbericht Karibische AKP-Staaten. Wiesbaden.

STATISTISCHES BUNDESAMT (2002): Statistisches Jahrbuch 2002 für das Ausland. Wiesbaden.

STIBIG, H.-J., J.P. MALINGREAU & R. BEUCHLE (2001): New possibilities of regional assessment of tropical forest cover in insular Southeast Asia using SPOT-VEGETATION satellite image mosaics. – International Journal of Remote Sensing 22 (4): 503-505.

ST-ONGE, B.A. (1999): Topographic effects on the texture of high-resolution forest-stand images measured by the semivariogram. – Photogrammetric Engineering & Remote Sensing 65 (8): 923-935.

ST-ONGE, B.A. & F. CAVAYAS (1995): Estimating forest stand structure from high resolution imagery using the directional variogram. – International Journal of Remote Sensing 16 (11): 1999-2021.

St-Onge, B.A. & F. Cavayas (1997): Automated forest structure mapping from high resolution imagery based on directional semivariogram estimates. – Remote Sensing of Environment 61: 82-95.

Strahler, A.H., T.L. Logan & N.A. Bryant (1978): Improving forest cover classification accuracy from Landsat by incorporating topographic information. *In* Proceedings of the 12th International Symposium on Remote Sensing of Environment, Ann Arbor, MI, pp. 927-942.

Strahler, A.H. (1980): The use of prior probabilities in maximum likelihood classification of remotely sensed data. – Remote Sensing of Environment 10: 135-163.

Strahler, A.H., C.E. Woodcock & J.A. Smith (1986): On the nature of models in remote sensing. – Remote Sensing of Environment 20: 121-139.

Sugumaran, R. (2001): Forest land cover classification using statistical and artificial neural network approaches applied to IRS LISS-III sensor. – Geocarto International 16 (2): 37-42.

Sunar Erbek, F., C. Özkan & M. Taberner (2004): Comparison of maximum likelihood classification method with supervised artificial neural network algorithms for land use activities. – International Journal of Remote Sensing 25 (9): 1733-1748.

Sutter, R. (1990): Increasing efficiency in volume estimation by the combination of aerial and terrestrial samples in the Swiss NFI. *In* Proceedings from SNS/IUFRO workshop "The usability of remote sensing for forest inventory and planning", Umeå 26-28 February 1990, pp. 67-75.

Thenkabail, P.S., E.A. Enclona, M.S. Ashton, C. Legg & M.J. De Dieu (2004a): Hyperion, IKONOS, ALI, and ETM+ sensors in the study of African rainforests. – Remote Sensing of Environment 90: 23-43.

Thenkabail, P.S., N. Stucky, B.W. Griscom, M.S. Ashton, J. Diels, B. van der Meer & E. Enclona (2004b): Biomass estimations and carbon stock calculations in the oil palm plantations of African derived savannas using IKONOS data. – International Journal of Remote Sensing 25 (23): 5447-5472.

Thomas, R.W. (1990): Some thoughts on the development of remote sensing-aided national forest inventory in Sweden. *In* Proceedings from SNS/IUFRO workshop "The usability of remote sensing for forest inventory and planning", Umeå 26-28 February 1990, pp. 48-66.

Tickle P., C. Witte, T. Danaher & K. Jones (1998): The application of large-scale video and laser altimetry to forest inventory. *In* Proceedings of the 9th Australasian Remote Sensing and Photogrammetry Conference, Sydney, Australia, July 1998.

Tolentino, L. & M. Peña (1998): Inventario de la vegetación y uso de la tierra en la República Dominicana. – Moscosoa 10: 179-203.

Tomczak, M. & J.S. Godfrey (2003): Regional Oceanography: an Introduction. 2nd edition, Daya Publishing House, Delhi.
URL (1.2.2005): http://www.cmima.csic.es/mirror/mattom/regoc/index.html

Tomppo, E. (1996): Multi-source national forest inventory of Finland. *In*: R. Päivinen, J. Vanclay & S. Miina (eds.): New thrusts in forest inventory. Proceedings of the Subject Group S4.02-00 "Forest Resource Inventory and Monitoring" and Subject Group S4.12-00 "Remote Sensing Technology" : IUFRO XX World Congress, 6-12 August 1995, Tampere, Finland. Vol. I. EFI Proceedings No. 7, pp. 27-41.

Toutin, T. (2004): Review article: Geometric processing of remote sensing images: models, algorithms and methods. – International Journal of Remote Sensing 25 (10): 1893-1924.

TOUTIN, T. & P. CHENG (2001): Entmystifizierung von IKONOS. – Photogrammetrie, Fernerkundung, Geoinformation 2001 (3): 171-176.

TREITZ, P. (2001): Variogram analysis of high spatial resolution remote sensing data: An examination of boreal forest ecosystems. – International Journal of Remote Sensing 22 (18): 3895-3900.

TREITZ, P. & P. HOWARTH (2000a): High spatial resolution remote sensing data for forest ecosystem classification: An examination of spatial scale. – Remote Sensing of Environment 72: 268-289.

TREITZ, P. & P. HOWARTH (2000b): Integrating Spectral, Spatial, and Terrain Variables for Forest Ecosystem Classification. – Photogrammetric Engineering & Remote Sensing 66 (3): 305-317.

TUFTE, L. (2003): Automatisierte Bestimmung von Bearbeitungsskalen für die multiskalige Auswertung von hoch auflösenden Fernerkundungsdaten. – Photogrammetrie, Fernerkundung, Geoinformation 2003 (5): 383-394.

TUOMINEN, S. & A. PEKKARINEN (2005): Selecting the combination of aerial photograph features for multi-source foreset inventory. *In*: Kleinn, C., J. Nieschulze & B. Sloboda (eds.): Remote Sensing & GIS for Environmental Studies: Applications in Forestry. Schriften aus der Forstlichen Fakultät der Universität Göttingen und der Niedersächsischen Forstlichen Versuchsanstalt 138, pp. 214-223.

TUOMISTO, H., A. LINNA & R. KALLIOLA (1994): Use of digitally processed satellite images in studies of tropical rain forest vegetation. – International Journal of Remote Sensing 15 (8): 1595-1610.

ULBERT, V. (1999): Partizipative Gender-Forschung: Umweltprobleme und Strategien der Ressourcennutzung in der Dominikanischen Republik. Verlag für Entwicklungspolitik, Saarbrücken.

USGS (01.03.2005): Landsat Project Website. URL: http://landsat.usgs.gov/index.php

USTIN, S.L. & A. TRABUCCO (2000): Using hyperspectral data to assess forest structure. – Journal of Forestry, June 2000: 47-49.

VAN DER MEER, F., K.S. SCHMIDT, W. BAKKER & W. BIJKER (2002): New environmental remote sensing systems. *In*: Skidmore, A. (ed.): Environmental modelling with GIS and remote sensing. Taylor & Francis, London.

VERBEKE, L.P.C., F.M.B. VANCOILLIE & R.R. DE WULF (2004): Reusing back-propagation neural networks for land cover classification in tropical savannahs. – International Journal of Remote Sensing 25 (14): 2747-2771.

VICIOSO, F. (2002): Situación de los recursos hidricos en la cuenca del Río Yaque del Norte. Proyecto manejo de recursos naturales cuenca alta del Río Yaque del Norte -PROCARYN-. Santo Domingo (unpublished).

VOGELMANN, J.E., T. SOHL & S.M. HOWARD (1998): Regional characterization of land cover using multiple sources of data. – Photogrammetric Engineering & Remote Sensing 64 (1): 45-57.

WALKER, L.R., D.J. LODGE, N.V.L. BROKAW & R.B. WAIDE (1991): An introduction to hurricanes in the Caribbean. – Biotropica 23 (4a): 313-316.

WANG, C., J. QI, D.L. SKOLE, M.A. COCHRANE & E.A.T. MATRICARDI (2003): Tropical forest degradation and recovery: Estimation and validation of canopy cover with Landsat and IKONOS imagery. CGCEO/RA01-03/w. Michigan State University, East Lansing, Michigan.

WANG, G., G. GERTNER & A.B. ANDERSON (2004a): Up-scaling methods based on variability-weighting and simultation for inferring spatial information across scales. – International Journal of Remote Sensing 25 (20): 4961-4979.

WANG, L., W.P SOUSA, P. GONG & G.S. BIGING (2004b): Comparison of IKONOS and QuickBird images for mapping mangrove species on the Caribbean coast of Panama. – Remote Sensing of Environment 91: 432-440.

WANG, L., W.P SOUSA, P. & P. GONG (2004c): Integration of object-based and pixel-based classification for mapping mangroves with IKONOS imagery. – International Journal of Remote Sensing 25 (24): 5655-5668.

WATTS, D. (1987): The West Indies: Patterns of development, culture and environmental changes since 1492. – Cambridge Studies in Historical Geography 8. Cambridge.

WEISCHET, W. (1996): Regionale Klimatologie. Teil 1. Die Neue Welt: Amerika, Neuseeland, Australien. Teubner, Stuttgart.

WOODCOCK, C.E. & S. GOPAL (2000): Fuzzy set theory and thematic maps: accuracy assessment and area estimation. – International Journal of Geographical Information Science 14 (2): 153-172.

WOODCOCK, C.E. & S.L. RYHERD (1989): Generation of texture images using adaptive windows. *In*: Image data processing. ASPRS/ACSM Annual Meeting 1989, Falls Church, Va., Vol. 2, pp. 11-22.

WOODCOCK, C.E. & A.H. STRAHLER (1987): The factor of scale in remote sensing. – Remote Sensing of Environment 21: 311-332.

WOODCOCK, C.E., S.A. MACOMBER & L. KUMAR (2002): Vegetation mapping and monitoring. *In*: Skidmore, A. (ed): Environmental modelling with GIS and remote sensing. Taylor & Francis, London.

WULDER, M.A., E.F. LEDREW, S.E. FRANKLIN & M.B. LAVIGNE (1998): Aerial image texture information in the estimation of northern deciduous and mixed wood forest leaf area index (LAI). – Remote Sensing of Environment 64: 64-76.

XU, B., P. GONG & R. PU (2003): Crown closure estimation of oak savannah in a dry season with Landsat TM imagery: comparison of various indices through correlation analysis. – International Journal of Remote Sensing 24 (9): 1811-1822.

ZANONI, T. (1989): Hispaniola. *In*: D.G. Campbell & H.D. Hammond (eds.): Floristic inventory of tropical forests: the status of plant systematics, collections, and vegetation, plus recommendations for the future. New York Botanical Garden, New York. Pp. 336-340.

ZHANG, J. & N. STUART (2001): Fuzzy methods for categorical mapping with image-based land cover data. – International Journal of Geographical Information Science 15 (2): 175-195.

ZHANG, Y. (2001): Texture-Integrated Classification of Urban Treed Areas in High-Resolution Color-Infrared Imagery. – Photogrammetric Engineering & Remote Sensing 67 (12): 1359-1365.

ZHANG, Y. (2003): Spatial Autocorrelation in Remote Sensing Image Analysis. A Report. Environmental Remote Sensing Laboratory, Electrical Engineering Department, University of Nebrasca, Lincoln. 43 pp. (URL: http://doppler.unl.edu/~rockee/Image_Report.pdf)

Maps

BGR (1991): Mapa Geológico de la República Dominicana 1:250,000, Hannover.

PROGRESSIO (1995): Cobertura y uso de la tierra, Reserva Científica Ebano Verde, 1:25,000, DIRENA/Progressio, based on 1984 aerial photographs.

República Dominicana 1:50,000 (Topographic Maps), Instituto Cartográfico Militar (ICM), Santo Domingo, in collaboration with the U.S. Defence Mapping Agency Interamerican Geodetic Survey, varying editions 1968-1988.

Appendix 1

Plates – Land Cover Types of the Study Area

Plate 1: Natural open pine forest at 2700 m elevation in the Cordillera Central, 28 February 2002.

Plate 2: Natural pine forest at 2300 m elevation, with fire scars on the right side, 28 February 2002.

Plate 3: Remainder of native *Pinus occidentalis* in an agricultural area at 900 m a.s.l. (eastern test area), March 2002.

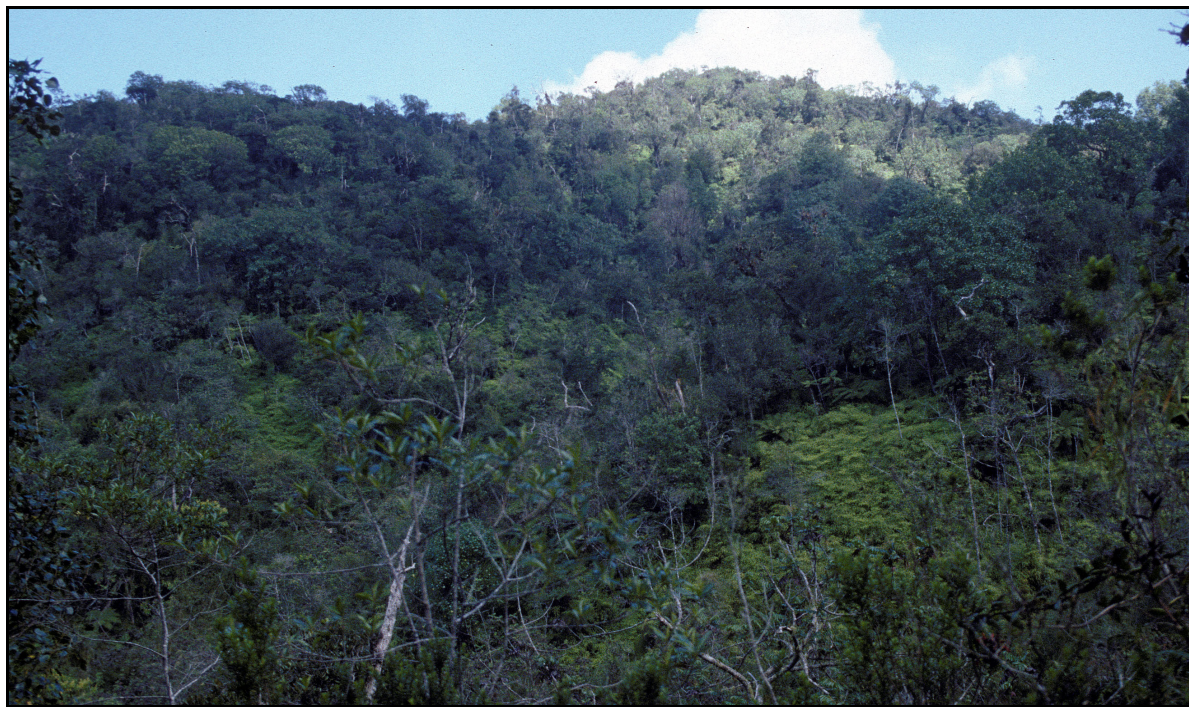Plate 4: Mixed pine and humid broadleaved forest at 900 m elevation, above the Río Jimenoa, 27 March 2003.

Plate 5: *Didymopanax tremulus - Magnolia pallescens* cloud forest, Reserva Científica Ebano Verde, 1400-1500 m a.s.l., 10 March 2003.

Plate 6: Cloud forest, Reserva Científica Ebano Verde, 1400 m a.s.l., 19 March 2002.

Plate 7: Cloud forest with *Dicranopteris pectinata* ground cover, Reserva Científica Ebano Verde, approximately 1300 m a.s.l., 19 March 2002.

Plate 8: *Magnolia pallescens* (Ebano verde), Reserva Científica Ebano Verde, 10 March 2003.

Plate 9: Calimetal (*Dicranopteris pectinata*), Reserva Científica Ebano Verde, 1150 m a.s.l., 10 March 2003.

Plate 10: Aerial view of palm dominated forest (light green areas are fern / *calimetal*, large crowns are broadleaved and pine trees), 23 March 2003.

Plate 11: Broadleaved riparian forest with *Prestoea montana* as a subdominant species, eastern test area, Scientific Reserve Ebano Verde, 10 March 2003.

Plate 12: Humid evergreen broadleaved forest (Salto de Jimenoa, 650 m a.s.l.), March 2003.

Plate 13: Humid evergreen broadleaved forest in the National Park Armando Bermúdez, 1200 m a.s.l., 2 March 2002. (Presence of bamboo indicates secondary forest/past disturbances at least along the path.)

Plate 14: Riparian forest in forest surroundings, Scientific Reserve Ebano Verde, 1200 m a.s.l., 19 March 2002.

Plate 15: Riparian forest bordered by pasture area, 1100 m a.s.l., March 2003.

Plate 16: Aerial view of broadleaved riparian forest in between grassland (pasture) areas just outside of the Scientific Reserve Ebano Verde, eastern test area, 23 March 2003.

Plate 17: Degraded remains of broadleaved semi-deciduous forest in the area of the Tavera reservoir, March 2003.
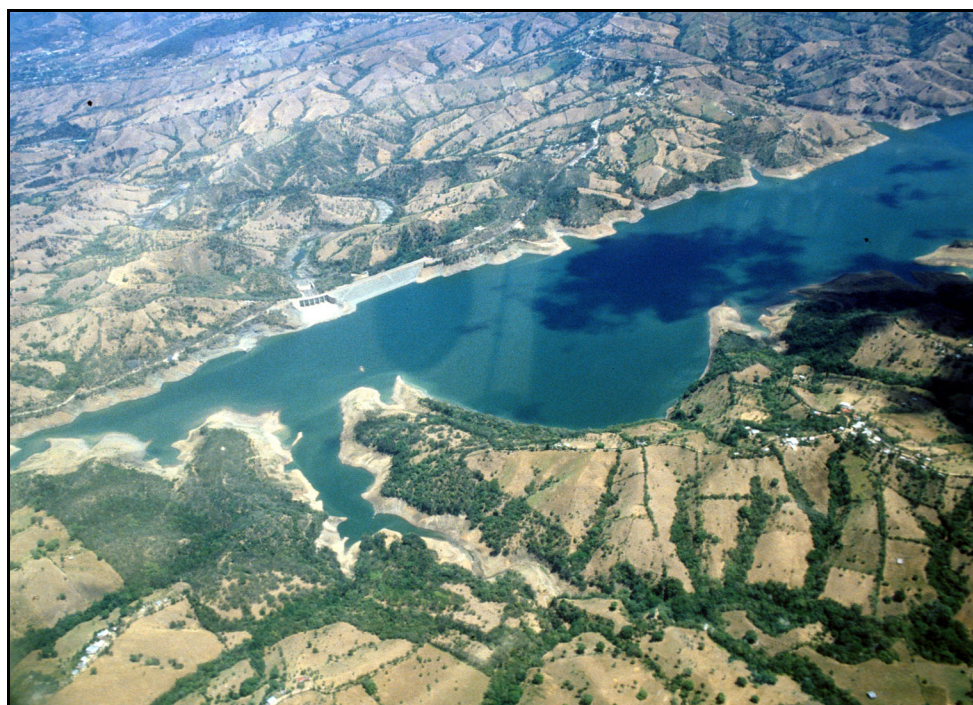
Plate 18: Aerial view of the Presa de Tavera, 23 March 2003.

Plate 19: A slope with young pine trees after a probably deliberate fire, western UCRYN, March 2003.

Plate 20: Young pine plantation with older pine stands in the background, western UCRYN, 1000 m a.s.l., March 2003.

Plate 21: *Pinus caribaea* plantation, Scientific Reserve Ebano Verde, eastern test area, March 2003.

Plate 22: *Acacia mangium* plantation, southern UCRYN, March 2003.

Plate 23: Grassland, eastern test area, March 2003.

Plate 24: Grassland (pasture) with trees in the northern UCRYN, March 2003.

Plate 25: Intensive agriculture including Chayote fields in the alluvial plain of La Ciénaga, March 2003.

Plate 26: Chayote field, western UCRYN, 22 March 2002.

Plate 27: Bean field, March 2002.

Plate 28: Bean fields, March 2003.

Plate 30: Coffee without shade, low ground coverage, western UCRYN, 1300 m a.s.l., March 2002

Plate 31: Coffee with high ground coverage and some trees, western UCRYN, 1300 m a.s.l., March 2002.

Plate 32: Agroforestry: medium-sized coffee plantation with *Inga vera* and banana plants, southern UCRYN, March 2002.

Plate. 33: Small area of mixed agroforestry, eastern test area, March 2003.

Plate 34: Agroforestry: coffee under pine trees, 31 March 2003.

Plate 35: Two views of open (degraded) lower montane pine forest, with bracken dominating the herbaceous layer, southern UCRYN, between 1200 and 1300 m a.s.l., March 2002.

Plate 36: Eastern test area (buffer zone of Reserva Cientifica Ebano Verde), around 900 m a.s.l. Land cover mix of crops and grassland, *matorral*, broadleaved riparian forest along the river, pines in the form of small closed stands, single pines and groups of pines / open pine forest with a transition to grassland, some landslide scars, March 2003 (photo looking south-westward and down to the Río Jimenoa).

Plate 37: Secondary forest, Scientific Reserve Ebano Verde (agricultural use before 1989, photographed 19 March 2002).

Plate 38: Secondary forest with pines. Eastern test area, March 2003.

Plate 39: Secondary forest in the Scientific Reserve Ebano Verde, eastern test area, March 2003.

Plate 40: Hurricane damaged pine plantation, regeneration mostly broadleaved. Eastern test area, 1200 m a.s.l., March 2003.

Plate 41: *Matorral*. Eastern test area, March 2003.

Plate 42: Transition from rough grassland to *matorral*. Eastern test area, March 2003.

Appendix 2

Plates – Land Cover Maps and Legends
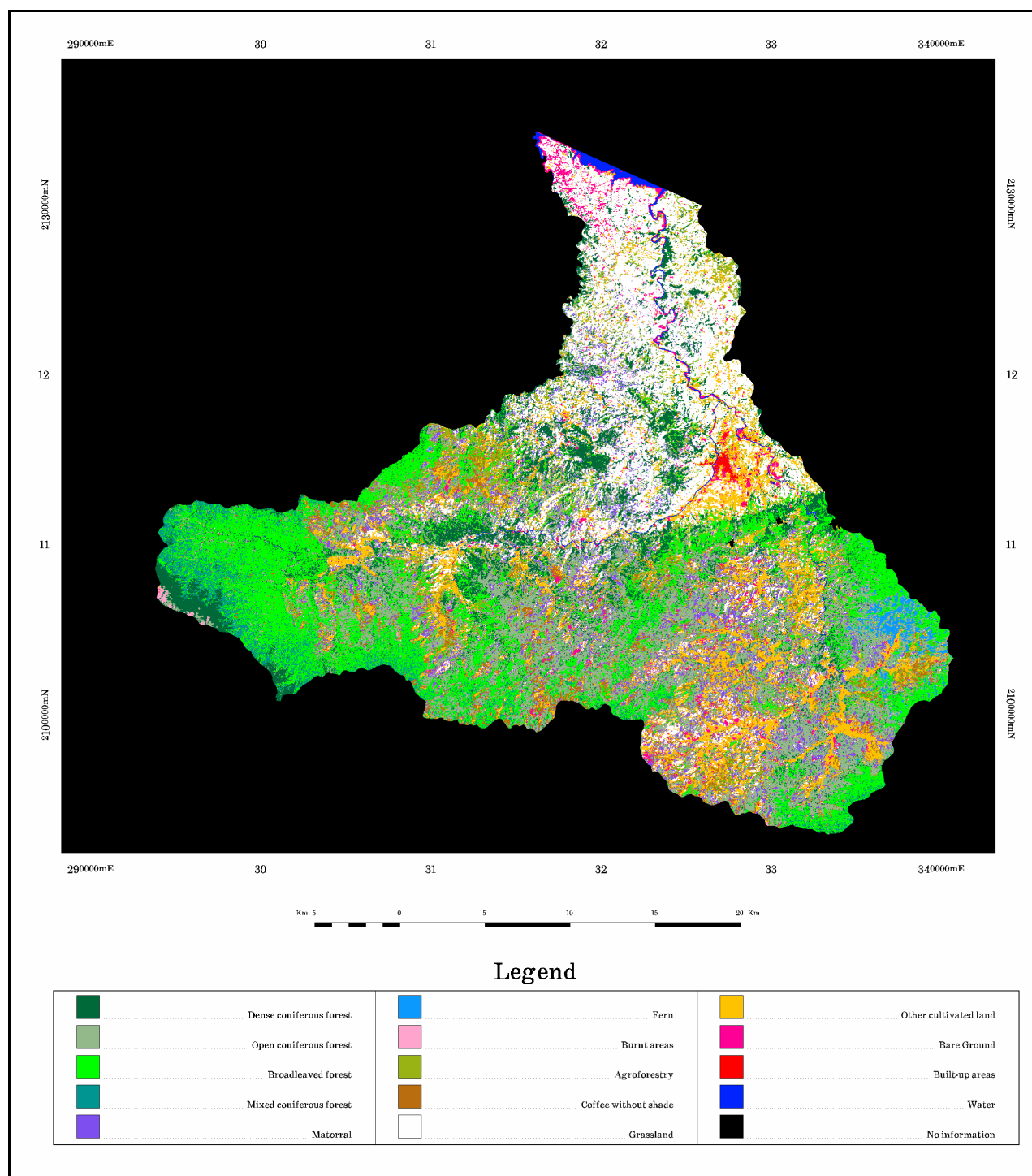
Plate 43: Landsat ETM+ classification of the upper catchment area of the Río Yaque del Norte.

Legend

Dense pine forest (PFd)

Open pine forest (PFo)

Cloud forest (CF)

Secondary forest (SF)

Palm dominated forest (PmF)

Broadleaved riparian forest (BRF)

Matorral (Mat)

Calimetal (Cal)

Agroforestry (AF)

Grassland (GL)

Crops without trees (Cr)

Bare Ground (BG)

Water (W)

No information

Plate 44: Legend for classifications of the eastern test area.

Appendix 3

Metadata and Scripts

Metadata of the Landsat-7 scene used

```
GROUP = METADATA_SCENE_02

  GROUP = WRS_SCENE_02
    WRS_SCENE_NO = 2
    FULL_OR_PARTIAL_SCENE = "F"
    BROWSE_FILE_NAME = "L72EDC140026001020.R02"
    WRS_PATH = 008
    WRS_ROW = 047
    SCENE_CENTER_SCAN_NO = 237
    SCENE_CENTER_SCAN_TIME = 2000-259T14:59:20.6004739Z
    SCENE_CENTER_LAT =   18.7880
    SCENE_CENTER_LON =  -71.3301
    HORIZONTAL_DISPLAY_SHIFT = -119
    SCENE_UL_CORNER_LAT =   19.7284
    SCENE_UL_CORNER_LON =  -72.0424
    SCENE_UR_CORNER_LAT =   19.4693
    SCENE_UR_CORNER_LON =  -70.2465
    SCENE_LL_CORNER_LAT =   18.0936
    SCENE_LL_CORNER_LON =  -72.4071
    SCENE_LR_CORNER_LAT =   17.8369
    SCENE_LR_CORNER_LON =  -70.6283
    SUN_AZIMUTH_ANGLE =  119.9528961
    SUN_ELEVATION_ANGLE =   60.5478325
    SCENE_CCA = 1
    UL_QUAD_CCA = 1
    UR_QUAD_CCA = 0
    LL_QUAD_CCA = 3
    LR_QUAD_CCA = 1
    ACCA_ALGORITHM_ID_VER = "ACCA_21JUN00_LSO31.ALG"

    BAND6_SL_GAIN_CHANGE = 0
    FULL_APERTURE_CAL_FLAG = "N"
    DAY_NIGHT_FLAG = "D"
  END_GROUP = WRS_SCENE_02

  GROUP = ETM_QA_02
    SCENE_QUALITY = 99
    CADUS_VCDUS_RECEIVED = 243013
    FLY_WHEEL_CADUS = 0
    CADUS_SYNC_ERR = 0
    CADUS_MISSING = 0
    RS_ERR_VCDUS = 0
    BCH_CORRECTED_VCDUS = 0
    BCH_UNCORRECTED_VCDUS = 0
    BCH_CORRECTED_BITS = 0
    BIT_ERROR_RATE = 0
    ETM_TIMECODE_ERRORS = 0
    ENTIRELY_FILLED_SCANS = 0
    PARTIALLY_FILLED_SCANS = 0
  END_GROUP = ETM_QA_02

  GROUP = PCD_QA_02
```

A15

```
      PCD_WORDS_RECEIVED = 114688
      PCD_BYTE_VOTING_ERR = 0
      TOTAL_PCD_MINOR_FRAMES = 896
      PCD_MINOR_FRAME_ERR = 0
      FILLED_PCD_MINOR_FRAMES = 0
      FILLED_PCD_MAJOR_FRAMES = 0
   END_GROUP = PCD_QA_02

   GROUP = PROCESSED_PCD_QA_02
      TOTAL_ATTITUDE_POINTS = 7
      REJECTED_ATTITUDE_POINTS = 0
      MISSING_ATTITUDE_POINTS = 0
      TOTAL_EPHEMERIS_POINTS = 7
      REJECTED_EPHEMERIS_POINTS = 0
      MISSING_EPHEMERIS_POINTS = 0
   END_GROUP = PROCESSED_PCD_QA_02

 END_GROUP = METADATA_SCENE_02
```

Ikonos Metadata

Eastern image (Ebano Verde)

Product Order Metadata
…
Processing Level: Standard Geometrically Corrected
Image Type: PAN/MSI
Interpolator Method: Bicubic
Multispectral Algorithm: None
Stereo: Mono
Mosaic: No
Map Projection: Universal Transverse Mercator
   UTM Specific Parameters
      Hemisphere: N
      Zone Number: 19
Datum: WGS84
Product Order Pixel Size: 1.00 meters
Product Order Map Units: meters
MTFC Applied: Yes
DRA Applied: No
Media: CD
File Format: GeoTIFF
   TIFF Tiled: No
   Bits per Pixel per Band: 11 bits per pixel
Multispectral Files: Separate Files
Special Instructions: NA
==

Source Image Metadata

Number of Source Images: 1
Source Image ID: 2001041615193490000011622370
Product Image ID: 000
Sensor: IKONOS-2
Acquired Nominal GSD
   Cross Scan: 0.83 meters
   Along Scan: 0.83 meters
Scan Direction: 0 degrees
Nominal Collection Azimuth: 220.2470 degrees
Nominal Collection Elevation: 81.33666 degrees
Sun Angle Azimuth: 109.8652 degrees
Sun Angle Elevation: 68.33561 degrees
Acquisition Date/Time: 2001-04-16 15:19
===

Product Component Metadata

Number of Components: 1
Tile ID: 0000000
Product Image ID: 000
Tile File Name: po_75581_pan_0000000.tif   po_75581_red_0000000.tif   po_75581_grn_0000000.tif
po_75581_blu_0000000.tif po_75581_nir_0000000.tif
Tile Geographic Corner Coordinates
  Number of Coordinates: 4
  Coordinate: 1
    Latitude: 19.08007470 degrees
    Longitude: -70.60417356 degrees
  Coordinate: 2
    Latitude: 19.08086933 degrees
    Longitude: -70.51012032 degrees
  Coordinate: 3
    Latitude: 18.95650021 degrees
    Longitude: -70.50899736 degrees
  Coordinate: 4
    Latitude: 18.95571115 degrees
    Longitude: -70.60298072 degrees
Tile Map Coordinates (in Map Units)
  UL Map X (Easting): 331224.38 meters
  UL Map Y (Northing): 2110460.06 meters
Pixel Size X: 1.00 meters
Pixel Size Y: 1.00 meters
Product Order Map Units: meters
Columns: 9899 pixels
Rows: 13767 pixels

Western image (Manabao)

Product Order Metadata
…
Processing Level: Standard Geometrically Corrected
Image Type: PAN/MSI
Interpolation Method: Cubic Convolution
Multispectral Algorithm: None
Stereo: Mono
Mosaic: No
Map Projection: Universal Transverse Mercator
  UTM Specific Parameters
    Hemisphere: N
    Zone Number: 19

Datum: WGS84
Product Order Pixel Size: 1.00 meters
Product Order Map Units: meters
MTFC Applied: Yes
DRA Applied: No
Media: CD
File Format: GeoTIFF
  TIFF Tiled: No
  Bits per Pixel per Band: 11 bits per pixel
Multispectral Files: Separate Files
==

Source Image Metadata

Source Image ID: 2002052215372320000011617649
Product Image ID: 002
Sensor: IKONOS-2
Acquired Nominal GSD
  Cross Scan: 0.91 meters
  Along Scan: 0.93 meters
Scan Azimuth: 0.00 degrees
Scan Direction: Forward
Panchromatic TDI Mode: 13
Nominal Collection Azimuth: 322.0301 degrees
Nominal Collection Elevation: 66.89434 degrees
Sun Angle Azimuth: 81.5937 degrees
Sun Angle Elevation: 75.11806 degrees
Acquisition Date/Time: 2002-05-22 15:37 GMT
==

Product Component Metadata

Component ID: 0020000
Product Image ID: 002
Component File Name: po_92198_pan_0020000.tif   po_92198_red_0020000.tif   po_92198_grn_0020000.tif
po_92198_blu_0020000.tif po_92198_nir_0020000.tif
Component Geographic Corner Coordinates
  Number of Coordinates: 4
  Coordinate: 1
    Latitude: 19.15357304 degrees
    Longitude: -70.88673515 degrees
  Coordinate: 2
    Latitude: 19.15477904 degrees
    Longitude: -70.76542113 degrees
  Coordinate: 3
    Latitude: 19.06459993 degrees

Longitude: -70.76446413 degrees
  Coordinate: 4
    Latitude: 19.06340003 degrees
    Longitude: -70.88571247 degrees
Component Map Coordinates (in Map Units)
  UL Map X (Easting): 301575.88 meters
  UL Map Y (Northing): 2118892.30 meters
Pixel Size X: 1.00 meters
Pixel Size Y: 1.00 meters
Product Order Map Units: meters
Columns: 12764 pixels
Rows: 9984 pixels

Component ID: 0020001
Product Image ID: 002
Component File Name: po_92198_pan_0020001.tif po_92198_red_0020001.tif po_92198_grn_0020001.tif po_92198_blu_0020001.tif po_92198_nir_0020001.tif
Component Geographic Corner Coordinates
  Number of Coordinates: 4
  Coordinate: 1
    Latitude: 19.06338050 degrees
    Longitude: -70.88673833 degrees
  Coordinate: 2
    Latitude: 19.06457853 degrees
    Longitude: -70.76575608 degrees
  Coordinate: 3
    Latitude: 18.97414561 degrees
    Longitude: -70.76480109 degrees
  Coordinate: 4
    Latitude: 18.97295369 degrees
    Longitude: -70.88571800 degrees
Component Map Coordinates (in Map Units)
  UL Map X (Easting): 301467.88 meters
  UL Map Y (Northing): 2108908.30 meters
Pixel Size X: 1.00 meters
Pixel Size Y: 1.00 meters
Product Order Map Units: meters
Columns: 12736 pixels
Rows: 10012 pixels

Sripts

```
! Korrektur des Linienversatzes bei Landsat7-L0R-Daten inkl. Pan

local i

fili="e:\abroetj\DomRep\Landsat7\L7CAY.pix
filo="e:\abroetj\DomRep\Landsat7\L7CAYv.pix
dbic=1, 2, 3, 4, 5, 6, 7, 8
dboc=1, 2, 3, 4, 5, 6, 7, 8

for i=0 to 125

DBIW=0,i*32,2550,32
DBOW=250-(2*i),i*32,2550,32

r iii

endfor
```

```
! Calculation of local variance in a moving window
! First, a channel containing the mean is calculated, then the variance itself
local integer i, j
%10 = 0
for i = -7 to 7
for j = -7 to 7
%10 = %10 + (%1[@x+i,@y+j])/225
endfor
endfor
%11 = 0
for i = -7 to 7
for j = -7 to 7
%11 = %11 + ((%1[@x+i,@y+j]-%10)^2)/225
endfor
endfor
```

Name: Anke Gleitsmann, geb. Brötje

Geburtsdatum: 9. Januar 1974

Geburtsort: Braunschweig

Familienstand: verheiratet

Staatsangehörigkeit: deutsch

Studium:

1994 bis 1997	Studium der Geographie an der Georg-August-Universität in Göttingen mit den Nebenfächern Botanik und Geologie; Studienschwerpunkte: Physische Geographie und Fernerkundung
Oktober 1996	Vordiplom
1997 bis 1998	M.Sc.-Kurs in *Environmental Remote Sensing* an der University of Aberdeen, Schottland (DAAD-Jahresstipendium); Thema der Abschlussarbeit: 'Land Cover Classification in Mountainous Terrain Using Multi-Source Remotely Sensed Data'; Abschluss *Master of Science* im Oktober 1998
10/1998 bis 02/2001	Fortsetzung des Geographiestudiums in Göttingen
November 2000	Abgabe der Diplomarbeit zum Thema: ‚Vergleich rezenter Vegetations- und Niederschlagsdynamik im Gansu-Korridor (China) unter Verwendung von NOAA-AVHRR-Daten' (Note sehr gut)
Februar 2001	Diplomprüfung in Geographie, Botanik und Geologie (Gesamtnote sehr gut)

Promotionsstudium:

Seit Juli 2001:	Promotion zum Thema ‚Exploiting the Spatial Information in High Resolution Satellite Data and Utilising Multi-Source Data for Tropical Mountain Forest and Land Cover Mapping', gefördert durch ein Graduiertenstipendium des Landes Niedersachsen 07/01 bis 02/04, einschließlich zweier 5-wöchiger DAAD-geförderter Forschungsaufenthalte im Untersuchungsgebiet

Studienbegleitende Tätigkeiten/Praktische Erfahrung:

1996	8-wöchiges Praktikum bei der Gesellschaft für bedrohte Völker
1999	10-wöchiges Praktikum beim Deutschen Fernerkundungsdatenzentrum
2000 bis 2001	Tätigkeit als studentische / wissenschaftliche Hilfskraft am Institut für Geographie in Göttingen (Fernerkundungsarbeiten zur Landschaftsökologie in Ost-Ecuador)
SS2001, 2003, 2005	Mitarbeit in der Lehre (Leitung der Übung ‚Fernerkundung I')